**DOT/FAA/AR-06/48**

Office of Aviation Research
and Development
Washington, DC 20591

# Investigations of Performance of Pneumatic Deicing Boots, Surface Ice Detectors, and Scaling of Intercycle Ice

November 2006

Final Report

This document is available to the U.S. public through the National Technical Information Service (NTIS), Springfield, Virginia 22161.

U.S. Department of Transportation
**Federal Aviation Administration**

## NOTICE



This report is available at the Federal Aviation Administration William J. Hughes Technical Center's Full-Text Technical Reports page: actlibrary.tc.faa.gov in Adobe Acrobat portable document format (PDF).

**Technical Report Documentation Page**

| 1. Report No. | 2. Government Accession No. | 3. Recipient's Catalog No. |
|---|---|---|
| DOT/FAA/AR-06/48 | | |

**4. Title and Subtitle**

INVESTIGATIONS OF PERFORMANCE OF PNEUMATIC DEICING BOOTS, SURFACE ICE DETECTORS, AND SCALING OF INTERCYCLE ICE

**5. Report Date**

November 2006

**6. Performing Organization Code**

**7. Author(s)**

Eugene Hill[1], Manny Rios[3] Galdemir Botura[2], James T. Riley[3], Christopher J. Dumont[3], Decio Pullin[4], Sudhindra Uppuluri[5], Andrew Broeren[5], Michael S. Selig[5], and David N. Anderson[6]

**8. Performing Organization Report No.**

**9. Performing Organization Name and Address**

[1]FAA
601 Lind Ave., SW
Renton, WA 98055-4056

[2]Goodrich De-icing and Specialty Systems
1555 Corporate Woods Parkway
Uniontown, Ohio

[3]FAA William J. Hughes Technical Center Atlantic City International Airport, NJ 08405

[4]EMBRAER
Sao Jose Dos Campos
Brazil

[5]University of Illinois at Urbana-Champaign
Champaign, IL 60201

[6]Ohio Aerospace Institute
Cleveland, Ohio

**10. Work Unit No. (TRAIS)**

**11. Contract or Grant No.**

**12. Sponsoring Agency Name and Address**

U.S. Department of Transportation
Federal Aviation Administration
Office of Aviation Research and Development
Washington, DC 20591

**13. Type of Report and Period Covered**

Final Report

**14. Sponsoring Agency Code**

AIR-100

**15. Supplementary Notes**

The Federal Aviation Administration Airport and Aircraft Safety R&D Division Technical Monitor was James T. Riley.

**16. Abstract**

This report represents the results from collaborative icing wind tunnel and flight test investigations of pneumatic deicing boot deicing performance. Also presented are the results of icing wind tunnel investigations into ice accumulations prior to activation of an ice protection system, scaling of intercycle ice accretions, and detection of ice accretion aft of the deicing boots using commercially available surface ice detectors.

A 36-inch chord hybrid model of the National Advisory Committee for Aeronautics 23012 airfoil, with leading-edge ordinates of a 72-inch, full-scale airfoil, was used for the investigations. The tests were part of a collaborative icing research program of the Federal Aviation Administration, the National Aeronautics and Space Administration, Goodrich Aerospace Corporation, the University of Illinois at Urbana-Champaign, Empresa Brasileira de Aeronautica S.A (EMBRAER), and other airplane manufacturers.

Ice shapes were documented with photographs, video recordings, tracings, and ice thickness measurements. Selected cases of special interest were documented with molds from which ice castings were made. These castings are available for subsequent aerodynamic testing and other purposes.

Icing wind tunnel tests were performed at a true airspeed of 170 knots (195 miles per hour), which is representative of maneuvering and holding airspeeds used by turbopropeller regional air transports. Flight testing of the deicing boots intercycle ice using a fully instrumented EMBRAER EMB-120 aircraft showed lift losses of 25 to 27 percent at the airplane angle of attack for the control column pusher. The lift losses are greater at the aerodynamic stall angles of attack.

Using the Ruff method for scaling test conditions, intercycle ice roughness obtained on a model that was one-half the scale of the hybrid model compared well with that obtained on the hybrid model. However, tests with the smaller model tended to produce ice that was less rough than of the hybrid model and often did not reproduce the large-scale roughness elements seen during the hybrid model tests. These differences may have occurred because the models' pneumatic deicers were not scaled from what would have been installed on the full-scale airfoil.

The surface ice detector test results indicated the potential for use of a local surface ice detector for detecting ice accretion aft of a lifting surface's leading-edge ice protection system.

| 17. Key Words | 18. Distribution Statement |
|---|---|
| Pneumatic deicing boot, Intercycle ice, Residual ice, Preactivation ice, Hybrid airfoil, Surface ice detector | This document is available to the public through the National Technical Information Service (NTIS) Springfield, Virginia 22161. |

| 19. Security Classif. (of this report) | 20. Security Classif. (of this page) | 21. No. of Pages | 22. Price |
|---|---|---|---|
| Unclassified | Unclassified | 158 | |

ACKNOWLEDGEMENTS

Several organizations contributed to the implementation of the testing and reporting of the test results in this document. Without their dedicated efforts, the value of the test program would not have been fully realized.

Empresa Brasileria de Aeronautica S.A. contributed significantly to the test objectives by flight testing simulated intercycle ice shapes on their EMB-120 prototype aircraft. Messrs. Acir Padilha, Jr., and Paulo Stolf provided guidance on the development of the icing wind tunnel test plan and support during the wind tunnel tests. The results of the EMB-120 flight tests contained in this document were provided by Mr. Decio Pullin.

The National Aeronautical and Space Administration (NASA) Glenn Research Center (GRC) developed training for making molds of the model ice accretions. This process is unique and provided a means of documenting the ice accretion characteristics for future reference. Mr. Eugene Addy of NASA GRC was instrumental in providing the training and making the casting material available.

The model design information was provided by Messrs. Sudhindra Uppuluri, Andrew Broeren, and Michael S. Selig of the University of Illinois at Champaign-Urbana. Use of the hybrid model testing technique was critical to the success of the test program.

Mr. David Anderson of the Ohio Aerospace Institute performed and documented the intercycle ice accretion scaling investigation. Since Mr. Anderson is among the few experts on ice accretion scaling, this document benefited greatly from the depth of knowledge he contributed in his reporting of the scaling investigation results.

Mr. David Sweet of Goodrich was instrumental in ensuring the outstanding support and resources provided by Goodrich for the testing, which contributed greatly to its success. Mr. Jerry Hansard of Goodrich did an outstanding job throughout the testing and was chiefly responsible for the high quality of the ice molds.

The investigation of the ability of surface ice detectors to detect ice accretion aft of the deicer would not have been possible without the contributions of Mr. Mark Koosmann and Mr. Gary Williams of the Aircraft Sensors Division of the Goodrich Corporation. In addition to providing and installing the ice detectors on the model's upper surface plate, they supported execution of the testing.

TABLE OF CONTENTS

LIST OF FIGURES

LIST OF TABLES

LIST OF SYMBOLS AND ACRONYMS

| | |
|---|---|
| $\alpha$ | Angle of attack relative to the chord line |
| $\propto$ | Upper design angle of attack distribution |
| $\beta$ | Water collection efficiency |
| $\beta_0$ | Collection efficiency at stagnation line, dimensionless |
| θ | Air energy transfer parameter B-2 |
| $A_c$ | Accumulation parameter, dimensionless |
| $b$ | Relative heat factor, dimensionless |
| $c$ | Model chord, m |
| $c_1$ | Coefficient of lift |
| $c_{p,ws}$ | Specific heat of water at the surface temperature, cal/g K |
| g | Grams |
| G | Gravitational acceleration, 9.807 m/sec$^2$ |
| $h_c$ | Convective heat transfer coefficient, cal/s m² K |
| $K_0$ | Modified inertia parameter, dimensionless |
| kgf | kilograms force |
| kt/sec | knots per second |
| kts | knots |
| M | Mach number, dimensionless |
| $n$ | Freezing fraction, dimensionless |
| $p$ | Static pressure, nt/m² |
| $pw$ | Vapor pressure of water in the atmosphere, nt/m² |
| $Re$ | Reynolds number |
| $r_{le}$ | Leading-edge radius of airfoil |
| $T_{model}$ | Measured temperature of model |
| $t_{st}$ | Static temperature |
| $T_{tot}$ | Total temperature |
| $V$ | Air velocity |
| $We$ | Weber Number |
| AOA | Angle of attack |
| ATA | Air Transport Association of America |
| CFR | Code of Federal Regulations |
| DSSD | Deicing and Specialty Systems Division |
| EFCV | Ejector flow controls valves |
| EMB | Embraer |
| EMBRAER | Empresa Brasileira de Aeronautica |
| FAA | Federal Aviation Administration |
| FTI | Flight Test Instrumentation |
| GRC | Glenn Research Center |
| HE | Horizontal event |
| IWT | Icing Wind Tunnel |
| LTPT | Low Turbulence Pressure Tunnel |
| LWC | Liquid water content |
| mph | Miles per hour |
| MVD | Median volume diameter |

| | |
|---|---|
| NACA | National Advisory Committee for Aeronautics |
| NASA | National Aeronautical and Space Administration |
| nmi | Nautical miles |
| P/N | Part number |
| psig | Pound per square inch |
| SCFM | Standard cubic feet per minute |

# EXECUTIVE SUMMARY

This document presents the results from collaborative icing wind tunnel and flight test investigations of pneumatic deicing boot deicing performance. Also presented are the results of icing wind tunnel investigations into ice accumulations prior to activation of an ice protection system, scaling of intercycle ice accretions, and detection of ice accretion aft of the deicing boots using commercially available surface ice detectors.

A 36-inch chord hybrid model of the National Advisory Committee for Aeronautics (NACA) 23012 airfoil, with leading-edge ordinates of a 72-inch, full-scale airfoil, was used for these investigations. The tests were part of a collaborative icing research program of the Federal Aviation Administration, the National Aeronautics and Space Administration (NASA), Goodrich Corporation, the University of Illinois at Urbana-Champaign, Empresa Brasileira de Aeronautica S.A. (EMBRAER), and other airplane manufacturers.

Ice shapes were documented with photographs, video recordings, tracings, and ice thickness measurements. Selected cases of special interest were documented with molds from which ice castings were made. These castings are available for subsequent aerodynamic testing and other purposes.

Wind tunnel tests were performed at a true airspeed of 170 knots (kts) (195 miles per hour), which is representative of maneuvering and holding airspeeds used by turbopropeller regional air transports. Since the ice shedding performance of pneumatic deicing boots may vary with airspeed, the deicing performance results from this investigation are questionable for the many general aviation and utility aircraft that operate at lower airspeeds. There are a large number of general aviation and utility airplanes that operate at lower airspeeds. Therefore, a second test of the model used for this investigation at an airspeed of about 100 kts is recommended. The ice shedding shear force at 170 kts is 290 percent higher than at 100 kts. In addition, an atmospheric icing wind tunnel was used to test the model to determine performance of the deicing boots at the ice shedding shearing forces that occur at operational altitudes and airspeeds.

Flight testing of the deicing boots intercycle ice using a fully instrumented EMBRAER EMB-120 aircraft showed lift losses of 25 to 27 percent at the airplane angle of attack for the control column pusher. The lift losses were greater at the aerodynamic stall angles of attack. At the recommended icing conditions maneuvering speed of 160 kts, the increase in drag was 0.0089.

Using the Ruff method for scaling test conditions, intercycle ice roughness obtained on a model that was one-half the scale of the hybrid model compared well with the hybrid model. However, the tests with the smaller model tended to produce ice that was less rough than the hybrid model and often did not reproduce the large-scale roughness elements seen during the hybrid model tests. These differences may have occurred because the models' pneumatic deicers were not scaled from what would have been installed on the full-scale airfoil.

The results for the ice detectors tested indicated the potential for use of a local surface ice detector for detecting ice aft of a lifting surface's leading-edge ice protection system. However, further testing is needed for different angles of attack and airspeeds.

This collaborative research program also included a December 1999 icing wind tunnel test of a 36-inch chord NACA 23012 model. Castings of intercycle ice accretions obtained during that test were used during a subsequent aerodynamic test in the low turbulence pressure tunnel at the NASA Langley Research Center. An ice shape scaling study was conducted using the results of paired runs from the December 1999 and hybrid model tests.

The results of these investigations and other tests performed under this program underscore the need to carefully consider the effects of intercycle and preactivation ice accretions during the certification of aircraft that use pneumatic deicing boots. The test results also provide information that supports the activation of lifting surfaces' deicers at the first detection of ice formation on the aircraft's lifting surfaces and for the operation of pneumatic deicers in the automatic cycling mode.

## 1. INTRODUCTION.

This document presents the results of airfoil icing wind tunnel tests performed to investigate the following:

- Leading-edge surface roughness resulting from ice accretion prior to activation of an ice protection system.
- Intercycle ice accretions resulting from periodic cycling of a typical leading-edge pneumatic deicer.
- Scaling of full-scale, leading-edge deicer intercycle ice accretion using a smaller-scale model.
- Detection of ice accretion aft of the airfoil's leading-edge ice protection using commercially available surface ice detectors.

The results of Empresa Brasileira de Aeronautica S.A. (EMBRAER) EMB-120 flight tests with and without the intercycle ice accretions are also provided to document the aerodynamic effects of ice accretions at the full-scale Reynolds number (*Re*) for a typical regional air transport.

The icing wind tunnel tests were conducted at the Goodrich Corporation Deicing and Specialty Systems Division (DSSD) Icing Wind Tunnel (IWT) located in Uniontown, Ohio, during March 2000. The tests were part of a collaborative icing research program to investigate intercycle ice and preactivation ice and their aerodynamic effects on a representative airplane airfoil. Participants in the collaborative research included the Federal Aviation Administration (FAA), the National Aeronautics and Space Administration (NASA) Glenn Research Center (GRC), the Goodrich Corporation, the University of Illinois at Urbana-Champaign, EMBRAER, and other airplane manufacturers.

The model used was a hybrid National Advisory Committee for Aeronautics (NACA) 23012 airfoil. The NACA 23012 airfoil is considered representative of airfoils used for the wing designs of a significant portion of the current turbopropeller airplane fleet, as well as some general aviation airplanes. To obtain ice accretion data at full-scale with a typical deicer in a 22- by 44-inch IWT test section, hybrid scaling methods were used to design the model. The model's leading-edge ordinates simulated those of a 72-inch chord NACA 23012 airfoil. The simulated 72-inch chord airfoil leading edge was considered representative of the outboard wing panel of a regional air transport. The hybrid model had a leading edge of a 72-inch chord NACA 23012 airfoil, but had an actual chord of 36 inches. The aft portion of the model was designed using hybrid scaling methods so that the flow and impingement characteristics about the leading edge of the model would closely match those for a 72-inch chord model at the conditions tested. See appendix A for a detailed description of the hybrid model design process.

The deicer was designed to produce ice protection equivalent to current deicers installed on airplanes. The hybrid airfoil model deicer used the same fabrication procedure and materials of current neoprene deicers. The deicer inflation rate, inflated dwell time and pressure, deflation rate, and deflated suction pressure were representative of current deicer designs. During the

tests, the deicer could be operated manually or automatically based on interval time. The initial activation of the deicer varied according to test objectives; however, for many tests, the initial activation of the deicer was predicated on an algorithm that predicted, for the test icing conditions and ice detector type, the ice detection response time for a Goodrich Model 871 ice detector.

Ice shapes were documented with photographs, video recordings, tracings, and ice thickness measurements. Ice accretions of special interest were documented with ice molds from which ice castings were made. These castings are available from the Airport and Aircraft Safety Research and Development Division at the FAA William J. Hughes Technical Center for fabrication of simulated ice shapes that are used for aerodynamic flight tests and other purposes.

Application of the investigation results to full-scale airplanes is limited. Use of the hybrid model allowed the testing of a full-scale leading edge and deicer ice protection system, and the Goodrich IWT provided appropriate atmospheric icing cloud temperatures, drop size, and liquid water content (LWC). However, the IWT is an atmospheric tunnel whose test section static pressure is limited to the local atmospheric air pressure; hence, the tunnel air pressure could not be varied to simulate operational air pressures and densities.

Full-scale *Re* and Weber (*We*) numbers could not be simultaneously achieved in the IWT. For example, to duplicate the full-scale *Re* at a typical operational equivalent airspeed of 170 knots (kts), 15,000 ft altitude, and at an outside temperature of 14°F, an IWT true airspeed of only 140 mph is required. (This is because of the higher IWT air density relative to air density at 15,000 feet.) However, an IWT true airspeed of 249 mph would be required to match the full-scale *We* (assuming that water density and surface tension are invariant with air pressure). An airspeed of 249 mph is not achievable in the IWT with the hybrid model installed.

The inability to match the *Re* and *We* simultaneously is a common problem since most icing wind tunnels are atmospheric test facilities. However, information obtained in these atmospheric icing wind tunnels has proven to be useful and comparable to flight test results. See appendix B for further information concerning scaling considerations for icing tests.

Application of the preactivation ice accretion test results to metallic airfoil leading edges may be questioned since the model's leading edge was a neoprene deicer. Previous investigations indicate that variations in surface materials insignificantly affect leading-edge ice accretion shapes.

Flight tests of a representative deicer intercycle ice shape were performed by EMBRAER using an EMB-120 test airplane during the summer of 2002. The results are discussed in section 4.2.

The collaborative program also included a December 1999 IWT test of a 36-inch chord NACA 23012 model [1]. Casting of intercycle ice accretions obtained during the December 1999 test were used during a subsequent aerodynamic test in the Low Turbulence Pressure Tunnel (LTPT) at the NASA Langley Research Center [2].

Relative to investigating the possibility of using small-scale models to obtain intercycle ice accretion shapes, results from the December 1999 IWT half-scale model test were compared to

test results from the hybrid model that were performed with scaled test conditions, using the Ruff ice scaling method. The results are presented in appendix B and in reference 3.

Use of local area ice detectors has been proposed as a means to alert flight crews of hazardous ice accretion, such as a ridge of ice aft of the wing's leading-edge ice protection. A cursory investigation of the capability of three commercially available local area ice detectors to perform this function was made by exposing the detectors to large droplet icing conditions and by rotating the wind tunnel model to negative angles of attack [4]. Although the ice detectors' installations in the wind tunnel model did not address the issue of installing ice detectors in a production airplane wing, the test results are indicative of whether or not the ice detectors could perform the intended ice detection function.

## 2. BACKGROUND.

Intercycle ice accretions of normal operating deicers and the surface roughness prior to the activation of ice protection systems are considered during the certification of ice protection systems. Also, icing-related accident investigations may be hampered without some knowledge of the wing's leading-edge surface during the normal operation of deicers and the resulting aerodynamic effects of the ice accretion. There is limited published information characterizing intercycle and preactivation types of ice accretions [5-9]. Also, questions have been raised concerning the effects of these ice accretions and the operation of deicers relative to possible ice-bridging of the deicing system [10 and 11]. Information developed by airframe manufacturers for their aircraft is typically proprietary and not available for public guidance. Therefore, a collaborative research program was proposed to respond to these issues.

The resulting research program is intended to produce information that is representative and broadly applicable to aircraft that are equipped with deicers on the leading edges of lifting surfaces. Accordingly, the testing was planned not as a detailed study of ice accretions for a specific deicer design or aircraft, but rather as a study of ice accretions for a generic, representative deicer that is representative of those used on current turbopropeller and piston engine airplanes. This investigation focuses on the physical attributes of those ice accretions and observable trends in the ice accretions, as conditions and operation of the deicer are varied.

The key questions addressed by this research program concern possible effects of ice accretions on aircraft aerodynamics. Aerodynamic results from the LTPT for intercycle ice shapes obtained during the December 1999 test on the 36-inch NACA 23012 model are presented in reference 2, while the flight test results are discussed in section 4.2.

## 3. TEST DESCRIPTION.

### 3.1 ICING WIND TUNNEL TESTS.

#### 3.1.1 Test Facility.

Tests were performed in the Goodrich DSSD IWT. The IWT is a closed-loop refrigerated tunnel, measuring 40 by 70 ft overall. The test section is 22 inches wide, 44 inches high, and 60 inches long. Models are normally mounted horizontally between automated, 1-inch-thick

aluminum turning planes 30 inches in diameter. Seven heated spray bars equipped with NASA-type nozzles, located in the tunnel bell mouth, produce the icing cloud. A honeycomb array installed immediately upstream of the spray bars promotes flow uniformity in the test section. Figures 1 and 2 show the IWT schematic and test section overview, respectively.

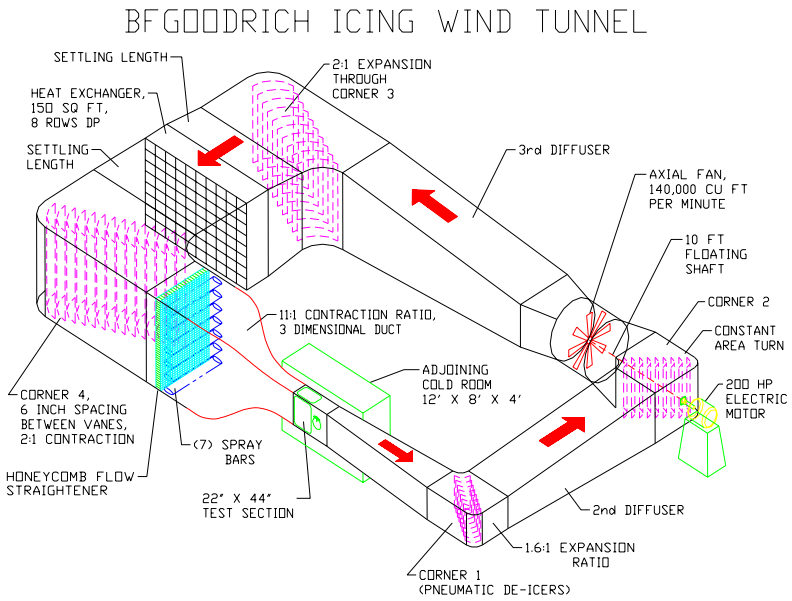


Figure 1. Icing Wind Tunnel Schematic

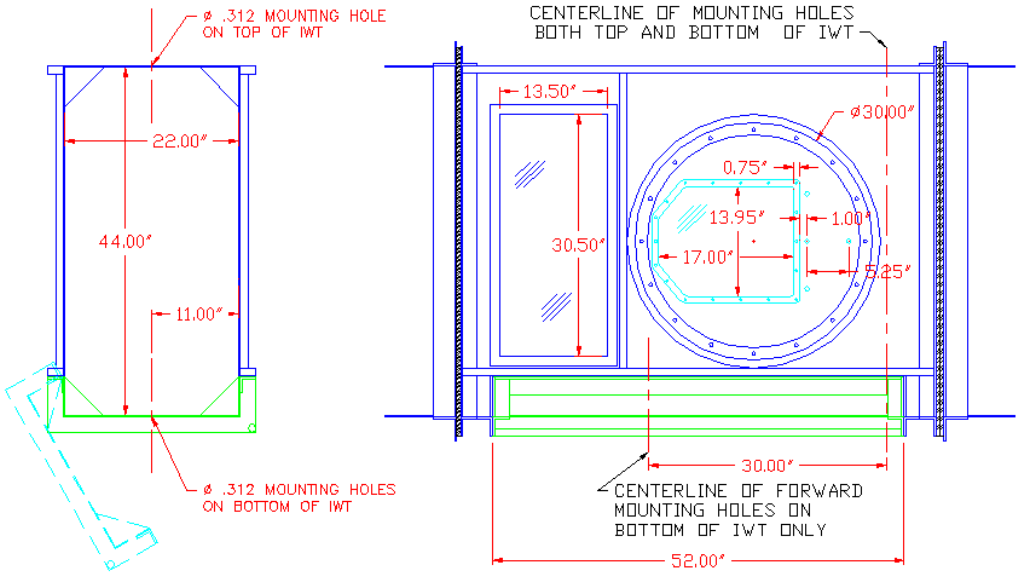


Figure 2. Test Section Details

The IWT test section airspeed capability ranges from 30 to 230 mph. The test section temperature is microprocessor-controlled from -22° to +32°F. It can be held within ±1°F of set

point through most of this range. Spray conditions can be varied from about 0.1 g/m$^3$ to over 3.0 g/m$^3$, with droplet sizes from 14 to over 40 μm, limited by velocity and nozzle pattern density. The IWT is capable of simulating almost all of Title 14 Code of Federal Regulations (CFR) Part 25, Appendix C intermittent maximum icing conditions and most of Appendix C continuous maximum icing conditions. Test conditions may be limited by temperature, spray time, and model blockage.

A single operator controls all IWT functions from a central location. The icing cloud parameters are microprocessor-controlled and can be programmed from the IWT control computer. The computer continuously displays and records all test conditions. The IWT operator can also control the closed-circuit video and test data acquisition systems, which are located adjacent to the operator's station.

A 4- by 12- by 8-ft cold room (adjacent to the test section) is available for casting ice structures and determining ice adhesion values. The cold room can provide temperatures as low as -65°F.

3.1.2 Instrumentation and Data Acquisition.

Photographic equipment included 35-mm still cameras, digital still cameras, and a closed-circuit video system with two remotely operated cameras. Tracings of the ice accretions were accomplished by first inserting a hot ice knife into the ice accretions to melt a chordwise slot to insert a template of the model's leading edge and then using a pencil to trace the adjacent ice accretion contour. Tracings were made at the model's midspan and, when deemed appropriate, off-center.

Molds of ice accretions were made using methods developed at NASA GRC. (The molds were subsequently used to produce castings of the ice accretions for documenting specific preactivation and intercycle ice accretions.) Boxes for producing the molds were manufactured by Goodrich DSSD and molding materials were purchased from NASA GRC. NASA GRC also trained Goodrich DSSD IWT personnel to make the molds. Figure 3 illustrates the mold-making process, with the removable leading edge and ice accretion inserted into the mold box after the uncured mold material had been poured into the container. Figure 4 shows a typical mold.

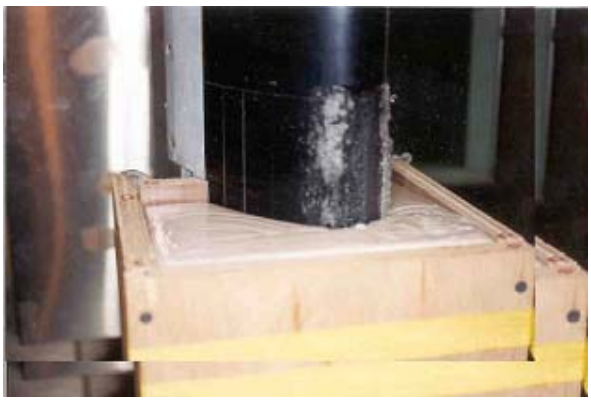

Figure 3. Mold-Making Process

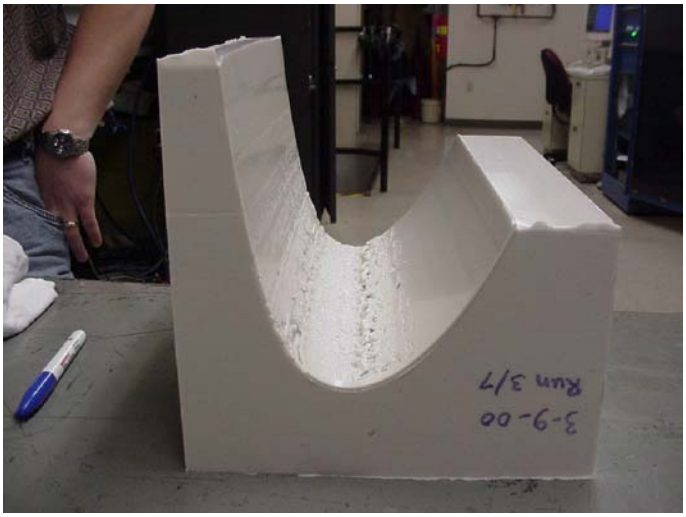


Figure 4. Typical Hybrid Model Mold

Three thermocouples were installed on the model, two internally on the machined model spar and one externally on the model spar. The temperatures provided by these thermocouples were used to determine when the model temperature had stabilized prior to beginning ice accumulation on the model.

Special instrumentation used during the test included a Model 5600 OPTRON biaxial displacement follower, which allowed remote monitoring of the model's leading-edge ice thickness.

Tunnel test conditions were set and recorded using the IWT instrumentation and control computer, respectively.

3.1.3 Model.

3.1.3.1 Airfoil.

The two-dimensional model consisted of a 36-inch chord, 22-inch span NACA 23012 hybrid airfoil equipped with a pneumatic deicing boot ice protection system. The model was mounted horizontally at the center of the IWT test section. (The ice protection system is described in section 3.1.3.2.) Local area ice detectors were installed aft of the ice protection system during the later phase of the testing. (These ice detectors are described in section 4.1.4.) The leading edge of the model was constructed of prepreg fiberglass and three internal ribs were used for stiffness and contour control of the model's leading edge. The afterbody was machined from a block of aluminum alloy, with a hinged trailing-edge flap attached to allow control of the model's leading-edge flow conditions, surface pressures, and resulting icing cloud droplet impingement. A schematic of the model is shown in figure 5. Figure 6 shows the model installed in the IWT, as viewed looking downstream from the IWT's bell mouth.

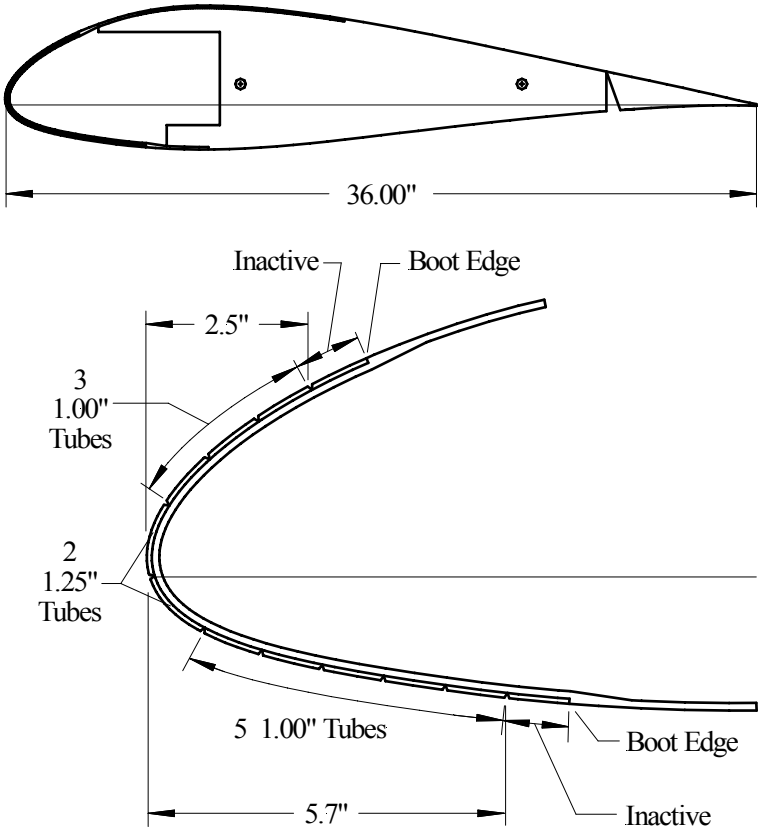


Figure 5. Diagram of the Model

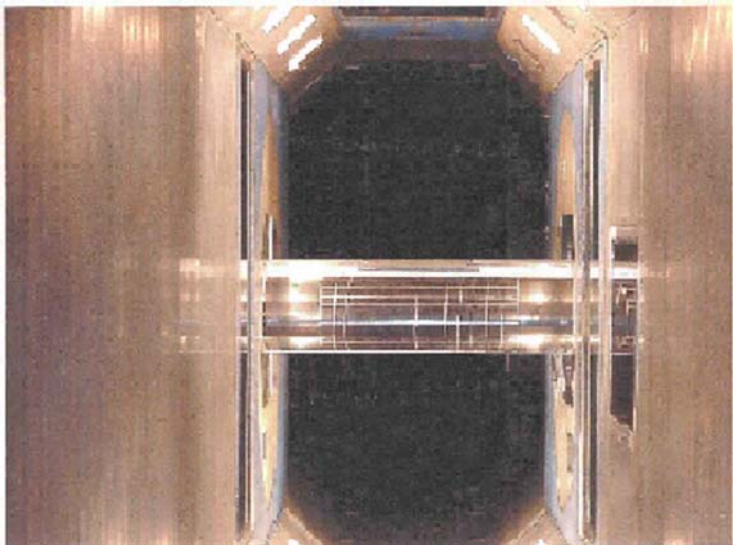

Figure 6. Hybrid Model Installed in the IWT

The NACA 23012 hybrid model was designed at the University of Illinois at Urbana-Champaign by S. Uppuluri, A. Broeren, and M. Selig. (Appendix A describes the hybrid model design process.) The model design conditions included the following:

- Full-scale airfoil: NACA 23012
- Full-scale airfoil chord: 72 inches
- Model scale chord: 36 inches
- Angle of attack (AOA): 2 degrees (0° and 4° off-design)
- Airspeed: 200 mph
- Icing ambient (static) temperature: -4° to 21°F
- Icing cloud drop medium volume diameter (MVD): 20 and 40 μm

The design objective was to duplicate the impingement limits and water collection efficiency of the full-scale NACA 23012 airfoil with a 36-inch chord hybrid airfoil at an AOA of 4° and 0°. The airfoil's AOA of 4° and 0° were selected as being representative of holding and descent phases of flight.

Ordinates of the resulting SU 1030 airfoil are tabulated in table 1. The airfoil designed to best match the full-scale NACA 23012 impingement limits and water catch efficiency at 2° AOA was optimized. Then a 20 percent chord hinged flap was added to the model to control the flow circulation around the model and droplet impingement at 4° and 0° AOA. To best achieve the design objectives at a 4° AOA , the optimum flap setting was 2º, for a 0° AOA, the optimum flap setting was -3.5°.

Figures 7 and 8 show the 4° AOA velocity distribution and water collection efficiency (β) of the full-scale NACA 23012 and the hybrid NACA 23012 (SU 1030 with a flap setting of 2°) airfoils. Figures 9 and 10 show the 0° AOA velocity distribution and water collection efficiency (β) of the full-scale NACA 23012 and the hybrid NACA 23012 (SU 1030 with a flap setting of -3.5°) airfoils. Note that at 4° AOA, the water catch efficiency agreement is very good everywhere except at the lower-surface impingement limit. The lower-surface impingement limit could have been moved further aft, but this would have resulted in a much thicker airfoil, which was considered undesirable. This difference in lower-surface catch efficiency and impingement limit were not considered critical relative to the test objectives, but should be considered when viewing the lower-surface ice accretions obtained during the test at 4° AOA. The water collection efficiency and impingement limits matches at 0° were considered satisfactory.

Table 1. SU 1030 Hybrid Airfoil Coordinates

| x/c | y/c | x/c | y/c | x/c | y/c | x/c | y/c |
|---|---|---|---|---|---|---|---|
| 0.500066 | 0.000620 | 0.119336 | 0.065572 | -0.000628 | 0.003528 | 0.159223 | -0.028826 |
| 0.495649 | 0.001404 | 0.111441 | 0.064992 | -0.000490 | 0.002179 | 0.169751 | -0.028227 |
| 0.488418 | 0.002930 | 0.103762 | 0.064119 | -0.000224 | 0.000814 | 0.180477 | -0.027456 |
| 0.480282 | 0.004783 | 0.096268 | 0.062970 | 0.000181 | -0.000554 | 0.191414 | -0.026523 |
| 0.471279 | 0.006870 | 0.088950 | 0.061560 | 0.000730 | -0.001915 | 0.202580 | -0.025440 |
| 0.461543 | 0.009091 | 0.081814 | 0.059903 | 0.001427 | -0.003258 | 0.214002 | -0.024205 |
| 0.451185 | 0.011368 | 0.074877 | 0.058015 | 0.002277 | -0.004572 | 0.225791 | -0.022853 |
| 0.440233 | 0.013692 | 0.068154 | 0.055924 | 0.003278 | -0.005847 | 0.237826 | -0.021455 |
| 0.428759 | 0.016097 | 0.061684 | 0.053699 | 0.004431 | -0.007079 | 0.250027 | -0.020017 |
| 0.416939 | 0.018579 | 0.055553 | 0.051410 | 0.005733 | -0.008266 | 0.262338 | -0.018558 |
| 0.404915 | 0.021113 | 0.049825 | 0.049083 | 0.007185 | -0.009407 | 0.274688 | -0.017097 |
| 0.392777 | 0.023684 | 0.044525 | 0.046748 | 0.008787 | -0.010505 | 0.287033 | -0.015645 |
| 0.380573 | 0.026279 | 0.039661 | 0.044432 | 0.010545 | -0.011562 | 0.299339 | -0.014214 |
| 0.368344 | 0.028887 | 0.035224 | 0.042155 | 0.012468 | -0.012583 | 0.311591 | -0.012813 |
| 0.356123 | 0.031492 | 0.031194 | 0.039933 | 0.014567 | -0.013573 | 0.323790 | -0.011450 |
| 0.343939 | 0.034082 | 0.027543 | 0.037773 | 0.016858 | -0.014537 | 0.335923 | -0.010129 |
| 0.331813 | 0.036646 | 0.024240 | 0.035679 | 0.019362 | -0.015479 | 0.347988 | -0.008861 |
| 0.319757 | 0.039173 | 0.021252 | 0.033654 | 0.022106 | -0.016403 | 0.359986 | -0.007649 |
| 0.307785 | 0.041654 | 0.018550 | 0.031694 | 0.025123 | -0.017318 | 0.371904 | -0.006499 |
| 0.295902 | 0.044075 | 0.016106 | 0.029798 | 0.028455 | -0.018227 | 0.383735 | -0.005421 |
| 0.284116 | 0.046429 | 0.013894 | 0.027961 | 0.032151 | -0.019138 | 0.395468 | -0.004421 |
| 0.272438 | 0.048704 | 0.011893 | 0.026178 | 0.036271 | -0.020058 | 0.407074 | -0.003505 |
| 0.260869 | 0.050889 | 0.010082 | 0.024446 | 0.040885 | -0.020989 | 0.418523 | -0.002686 |
| 0.249427 | 0.052974 | 0.008445 | 0.022759 | 0.046068 | -0.021945 | 0.429768 | -0.001970 |
| 0.238118 | 0.054946 | 0.006969 | 0.021112 | 0.051894 | -0.022927 | 0.440742 | -0.001368 |
| 0.226954 | 0.056792 | 0.005643 | 0.019503 | 0.058414 | -0.023941 | 0.451359 | -0.000889 |
| 0.215948 | 0.058503 | 0.004457 | 0.017925 | 0.065644 | -0.024988 | 0.461514 | -0.000540 |
| 0.205120 | 0.060064 | 0.003404 | 0.016376 | 0.073454 | -0.026053 | 0.471095 | -0.000321 |
| 0.194485 | 0.061463 | 0.002478 | 0.014853 | 0.081758 | -0.026993 | 0.479985 | -0.000226 |
| 0.184065 | 0.062689 | 0.001675 | 0.013354 | 0.090546 | -0.027810 | 0.488106 | -0.000256 |
| 0.173887 | 0.063730 | 0.000993 | 0.011878 | 0.099705 | -0.028488 | 0.495445 | -0.000423 |
| 0.163972 | 0.064575 | 0.000430 | 0.010423 | 0.109155 | -0.029007 | 0.499934 | -0.000620 |
| 0.154352 | 0.065216 | -0.000014 | 0.008992 | 0.118827 | -0.029350 | | |
| 0.145058 | 0.065642 | -0.000341 | 0.007586 | 0.128681 | -0.029507 | | |
| 0.136102 | 0.065850 | -0.000551 | 0.006207 | 0.138697 | -0.029471 | | |
| 0.127520 | 0.065844 | -0.000646 | 0.004862 | 0.148876 | -0.029242 | | |

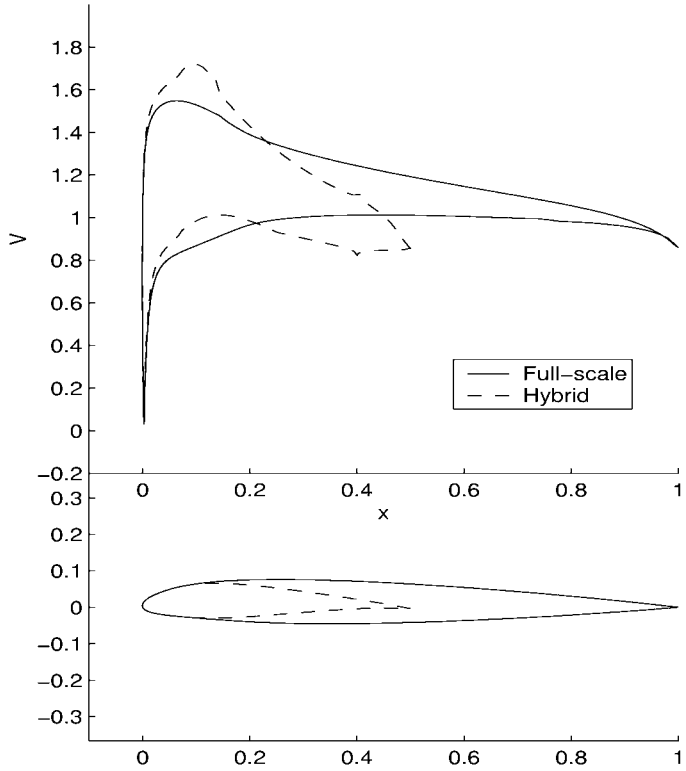


Figure 7. Full-Scale and Hybrid Airfoil Velocity Distributions at 4° AOA, 2° Flap Setting, and 12.8 $\times 10^6$ *Re*

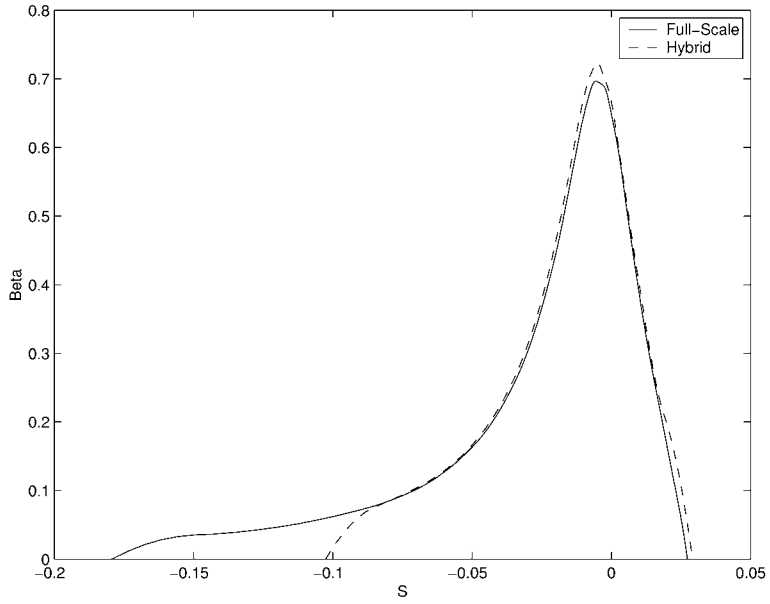


Figure 8. Full-Scale and Hybrid Airfoil Water Collection Efficiency ($\beta$) Curves at 4° AOA, 2° Flap Setting, and 12.8 $\times$ $10^6$ *Re*

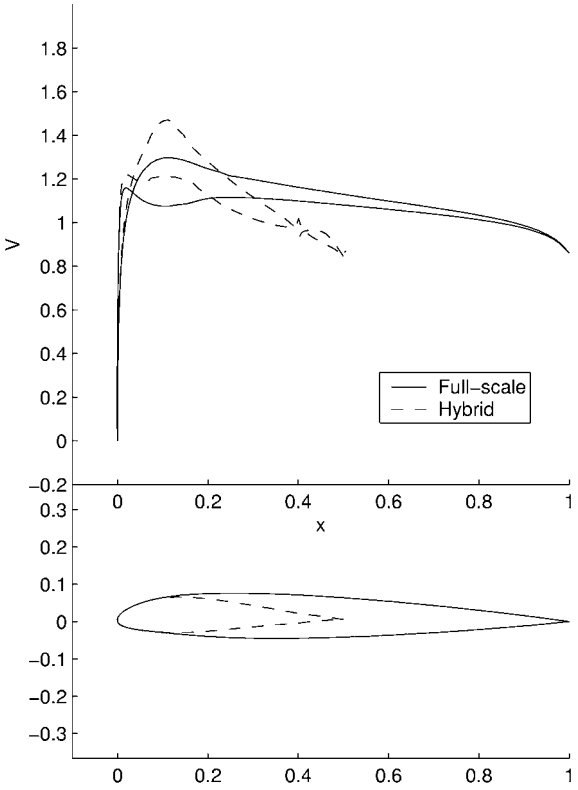


Figure 9. Full-Scale and Hybrid Airfoil Velocity Distributions at 0° AOA, -3.5° Flap Setting, and 12.8 $\times 10^6$ *Re*

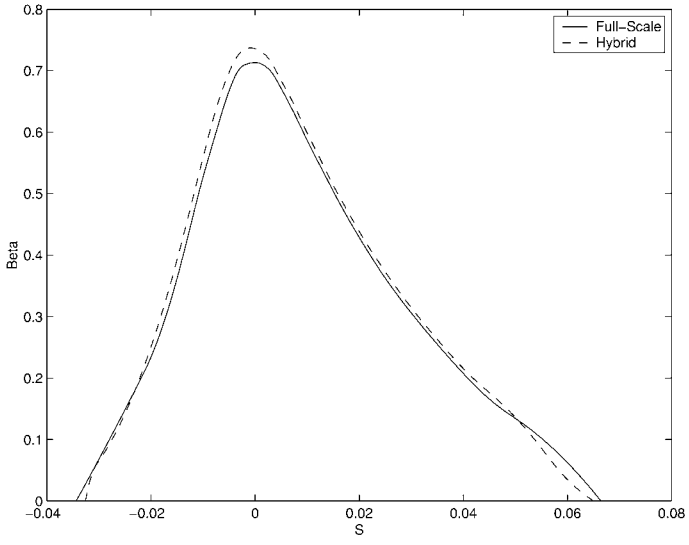


Figure 10. Full-Scale and Hybrid Airfoil Water Collection Efficiency ($\beta$) Curves at 0° AOA, -3.5° Flap Setting, and 12.8 $\times 10^6$ *Re*

3.1.3.2 Deicer.

The deicer was designed to produce ice protection equivalent to current deicers installed on airplanes. The hybrid airfoil model deicer used the same fabrication procedure and materials as an ordinary neoprene deicer.

The ice protection system consisted of two deicers (one installed on the hybrid model and the other installed outside the tunnel), one laboratory timer, one pressure regulator/reliever valve, and two ejector flow control valves. The purpose of the outside deicer was to reduce the inflation rate of the deicer inside the IWT. In this way, an attempt could be made to reproduce the equivalent airplane deicer inflation rate on the deicer inside the IWT. Figure 11 shows the hybrid model IWT deicer system schematic.

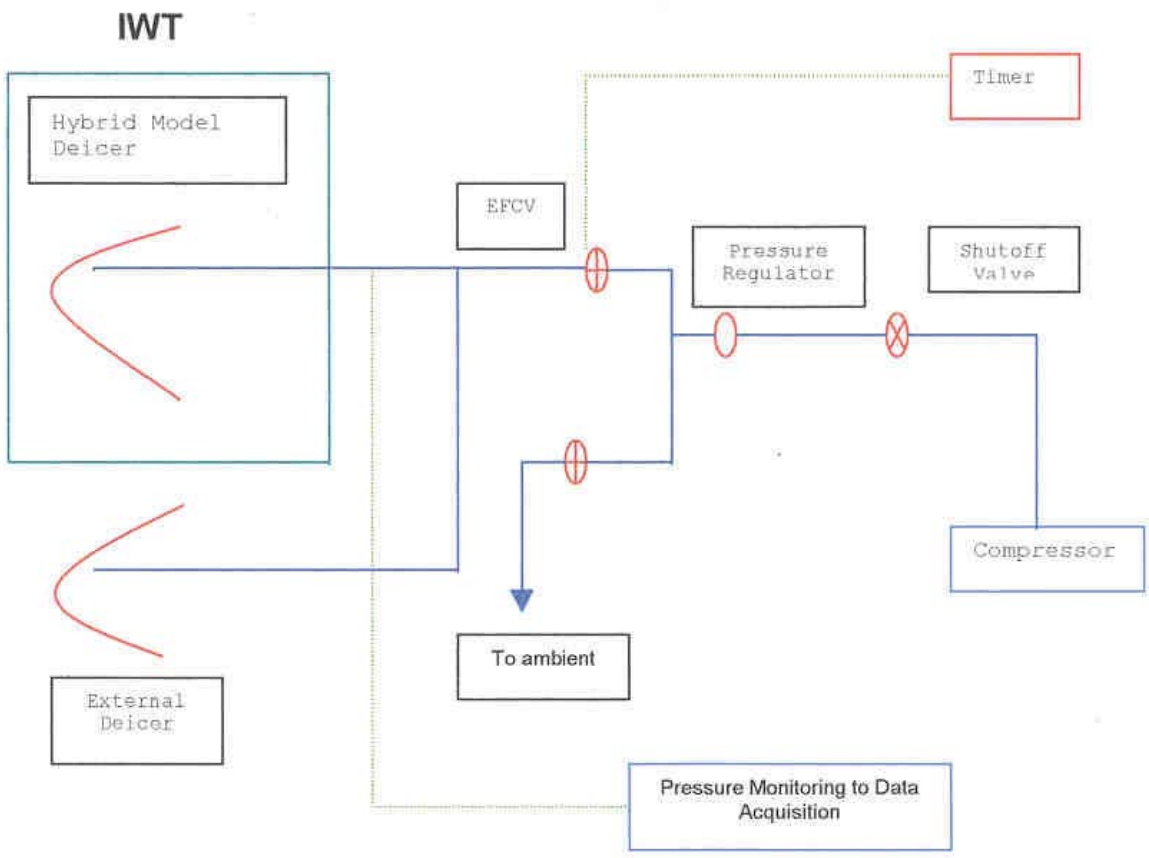


Figure 11. Hybrid Airfoil Model Deicer System Schematic

System supply pressure for the deicers was obtained from the IWT facility compressors, and the pressurized air was routed through the pressure regulator/reliever valve. There, it was reduced to the pneumatic deicing system operating pressure of 20 ±1 psig for distribution to the deicers through the ejector flow control valve. A pressure sensor was installed close to the hybrid model deicer air connection to provide continuous monitoring of the inlet deicer pressure.

The deicer installed on the hybrid NACA 23012 model was a Goodrich DSSD Part Number (P/N) XA 520-012, Revision A 29 S type, which is constructed of a 0.085-inch-thick material and is designed to be installed on a recessed leading edge. The deicer surface is black neoprene compounded to provide resistance to weathering, erosion, fuel, and oil. The deicer surfaces are conductive and will bleed off static charges. An edge sealer was used during deicer installation to provide a smooth transition from the boot to the leading edge. The deicer contains spanwise deicing tubes that inflate during activation. The deicer has a 3/8-inch air connection through which all tubes are inflated simultaneously. Figure 12 shows the deicer layout, as well as the inflatable tubes.

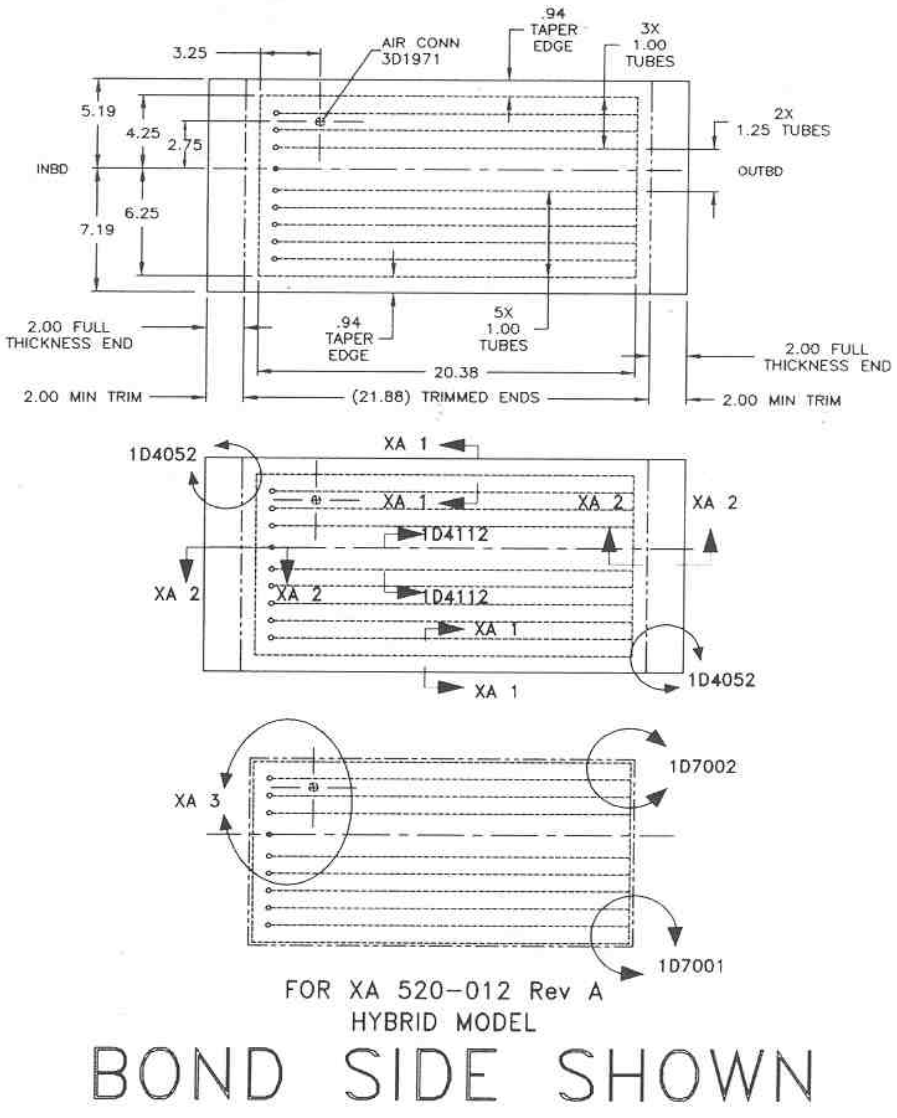


Figure 12. Deicer Installed on the Hybrid Model

The deicer spanwise dimension was limited by the 22-inch span of the IWT. The inactive portion of the deicer between the end of the inflatable tubes and the IWT walls minimized ice formation between the IWT walls and the model.

The deicer chordwise coverage was based on an impingement analysis performed by the University of Illinois. An effort was made to ensure that the chordwise extent of the deicer coverage was consistent with the NACA 23012 airfoil impingement analysis. The droplet trajectory analysis showed that all 20-μm droplets and the majority of 40-μm droplets impinged within the upper surface of the deicer. For the airfoil's lower surface, a few more 40-μm droplets impinged aft of the deicer area than would have occurred on a typical airplane deicer. The lower surface impingement aft of the deicer was considered acceptable for the purpose of the test.

The deicer was manufactured with spanwise inflatable tubes typical of aerospace applications. Photographs of the deicing system, uninflated and inflated, are shown in figures 13 and 14.

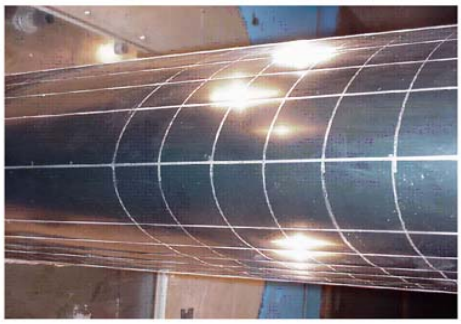

Figure 13. Uninflated Hybrid Model Deicer

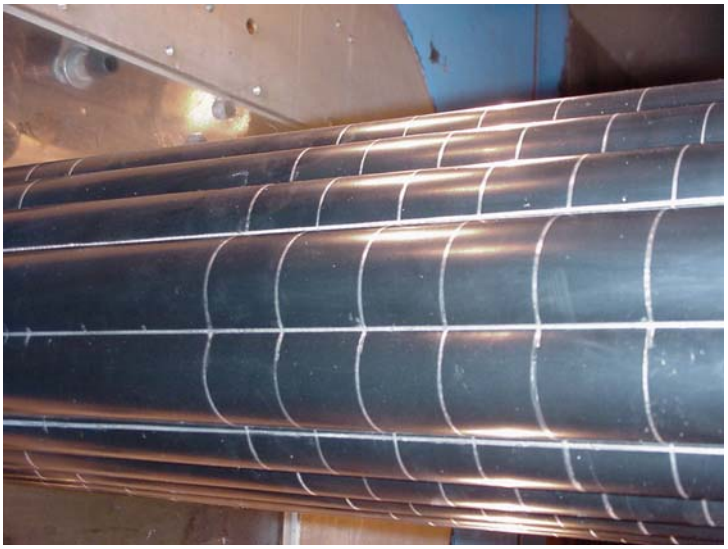

Figure 14. Inflated Hybrid Model Deicer

A nominal pressure regulation of 20 psig, similar to that used on some airplanes' deicing systems, was selected for the hybrid model deicer.

Based on Goodrich experience, a deicer inflation rate reflective of a generic airplane deicing system design was selected. The hybrid model deicer was designed to pressurize to 18 psig in approximately 3 seconds and deflate from 20 psig to partial vacuum in approximately 10 seconds. Due to the small size of the hybrid model deicer, a parallel deicer was connected to reduce the inflation rate in the tested deicer. A laboratory deicer with a volume of 0.5 $ft^3$ was installed outside the IWT to ensure a suitable inflation rate on the hybrid model deicer. A pressure transducer was installed close to the hybrid model air connection to verify the pressure rate and ensure that the equivalent pressure was present for all test conditions. (The pressure transducer used for the hybrid model deicer was a Gpi50, Model 211D, with 0.1% (0.05 psig) accuracy.) Figures 15, 16, and 17 show the inflation rate for three icing conditions.

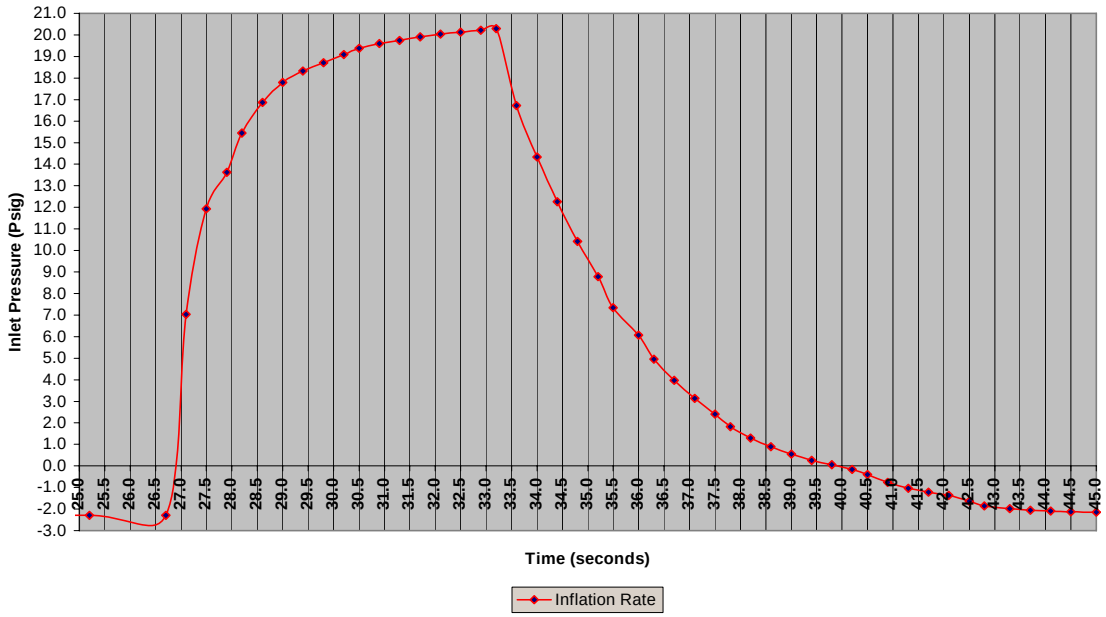


Figure 15. Pneumatic Inflation Rate at 21°F for Condition 4-1A

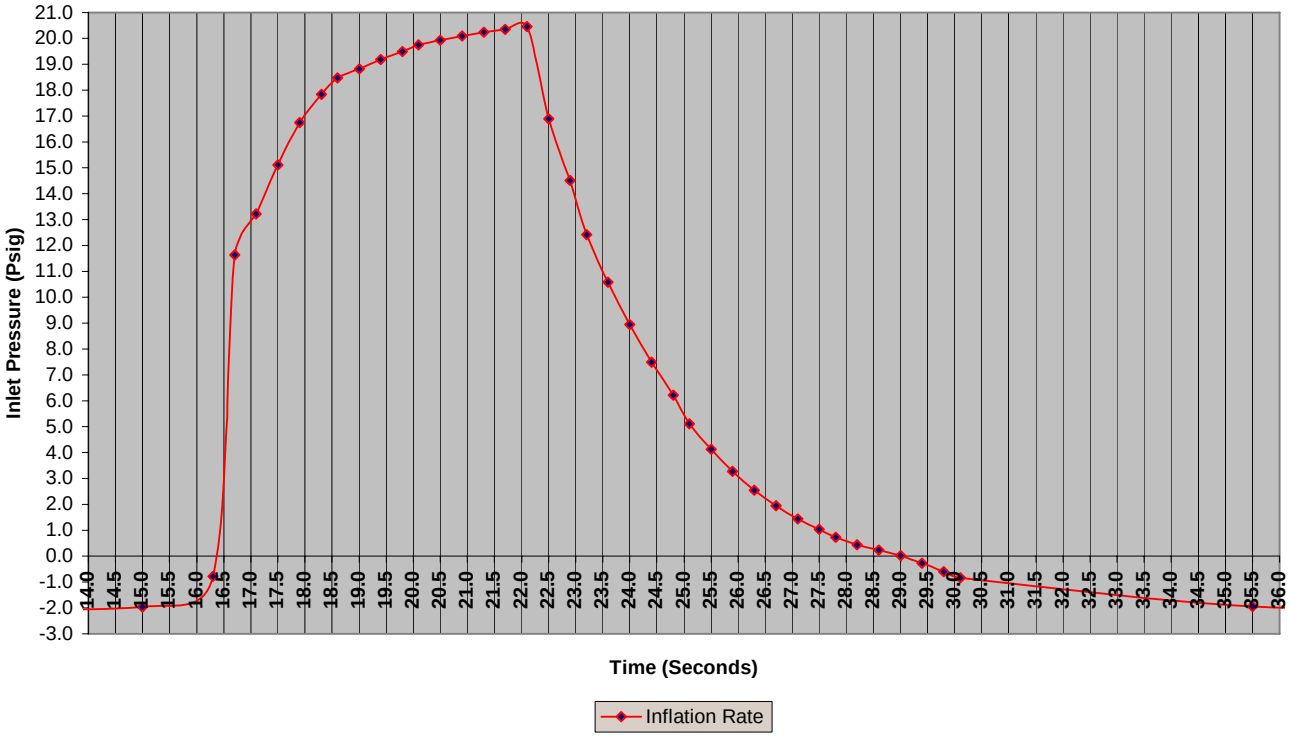


Figure 16. Pneumatic Inflation Rate at 14°F for Condition 2-2

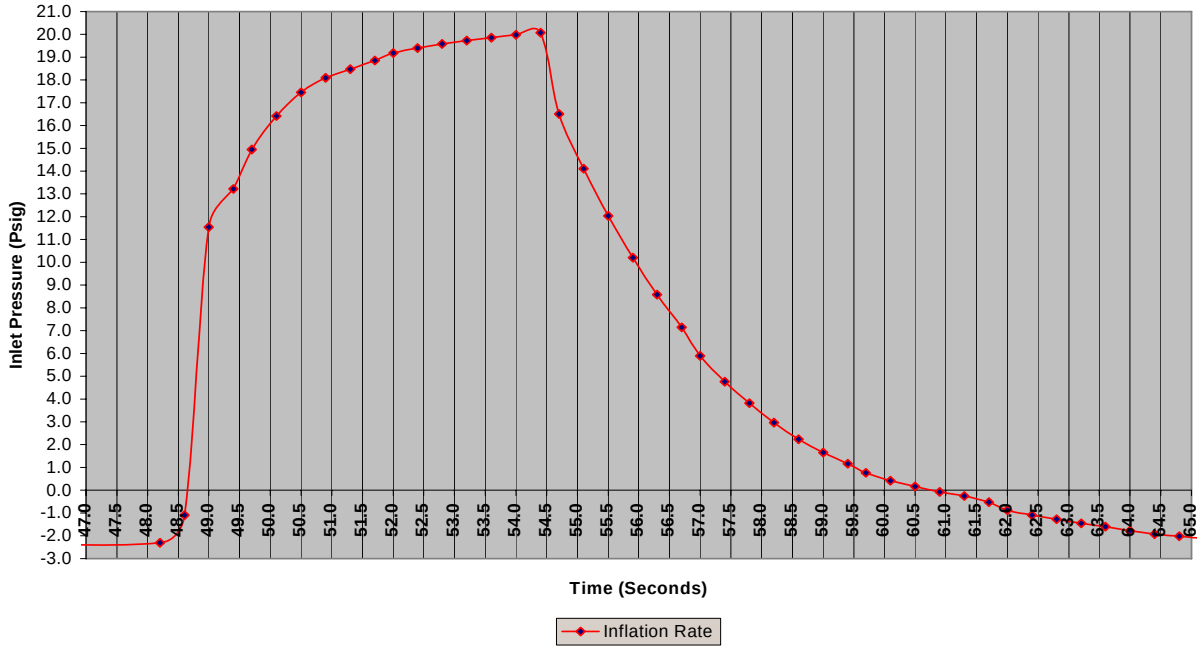


Figure 17. Pneumatic Inflation Rate at -22°F for Condition 5-1

A Goodrich DSSD P/N 4D2095-201 hybrid model deicer system pressure regulator/reliever valve was used. It contains a spring-loaded diaphragm that is balanced by downstream pressure. The balancing of the diaphragm mechanically controls the flow area to adjust and maintain the required regulated pressure. The pressure regulator reduces the compressed bleed air pressure to a normal system operating pressure of 20 ±1 psig. The pressure regulator contains an integral reliever that reduces the outlet pressure to an acceptable level for deicer operation in the event the regulating mechanism fails. Reliever cracking (opening) pressure is 26.0 ±0.5 psig.

The ejector flow control valve (EFCV), Goodrich DSSD P/N 3D3556-01, controls the flow of air to and from the deicers. The EFCV is a two-position, solenoid-operated poppet valve that provides system pressure (when in the energized position) or a vacuum (when de-energized) to the deicers. When the valve solenoid is in the de-energized condition, the ejector section of the valve provides the vacuum necessary to maintain the deicing tubes in a deflated condition using a minimum amount of air flow (1.5 scfm).

The deicer timer provides single or automatic repeat deicer cycle operation. The inflatable deicer time and dwell times were adjusted to comply with the ice conditions defined for the test. The timer, Goodrich DSSD P/N CA100A6, operates the ejector flow control valve, which controls the flow of air or vacuum to the deicers. When the timer is actuated through the control switch, the solenoid in the valve is immediately energized for 6 seconds. At the end of the 6-second deicer inflation period, the solenoid is de-energized and the deicers are deflated under vacuum produced by the valve.

The deicer was installed according to the Air Transport Association of America (ATA) report ATA 30-10-31, “Installation, Maintenance and Repair Manual for Pneumatic De-icers.” The

deicer was visually inspected and tested for leakage before and after installation on the hybrid model's leading edge.

3.1.3.3 Surface Ice Detectors.

Three surface ice detectors were installed on the model aft of the deicing system:

- Goodrich Ultrasonic Ice Detector (HALO®)
- Goodrich magneostrictive surface sensor
- Goodrich SMARTboot®-type ice detector

The HALO and SMARTboot detectors were adjusted to detect ice of thickness as small as 0.010″ to 0.020″, and the magnetostrictive detector was adjusted to detect ice of thickness as small as 0.0005″ to 0.015″. Installation of the ice detectors is shown in figures 18 and 19.

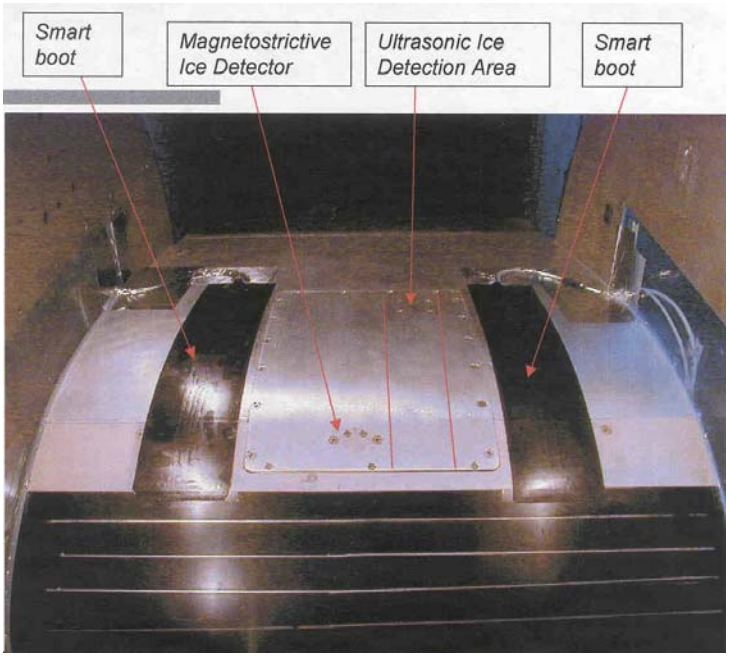


Figure 18. Hybrid Model Surface Ice Detector Installation


Figure 19. Goodrich Ultrasonic Local Area and Magnetostrictive Spot Ice Detector Installations on the UnderSurfAce of the Hybrid Model Upper Skin

3.1.4 Test Procedures.

For each run, a video of the entire run was taken. By pausing the video, the residual ice and intercycle ice for each of the deicing cycles can be observed.

The Goodrich OPTRON ice measurement device, which provides a valuable time-dependent record of leading-edge ice thickness at a single point on the model, was employed during part of the test.

Photographs were taken at the end of each run. These photographs provide a good representation of the ice accretion texture and features. To aid in determining the size and thickness of the ice accretions, longitudinal grid lines were added to the models along the stitch lines of the deicing boot tubes and at 1-inch intervals, chordwise, at the center of the models. These gridlines are shown in figures 13 and 14. Also, a scale was included in many of the ice accretion photographs.

Tracings were taken at the end of each run for which a mold was not made. One or more spanwise locations were identified as being typical or having particularly pronounced features. One of these positions was always at or near the center position. A thin aluminum plate was heated and used as an ice knife. The ice knife was applied normal to the model surface at selected locations to melt a chordwise groove into the ice down to the airfoil surface. A cardboard template from which the shape of the airfoil leading-edge region was cut was then placed into this groove to fit snugly against the clean surface of the wing. The two-dimensional profiles of the ice shape features were traced onto these templates with a no. 2 pencil. The tracings provided a good depiction of a spanwise cross section, including quantitative data.

However, typically there is a substantial variation along the span, which could only be depicted with many tracings.

Local ice depth measurements were made using a depth gauge to measure from the top of the ice roughness to the model's surface at the spanwise positions where the tracings were made.

Molds were made for only a few selected runs that were of special interest to the experimenters. Castings were subsequently made of the molds. The castings provide extremely valuable information, but since the molding process is very time-consuming and expensive (as is the process by which castings are made from the molds), castings could only be generated for selected runs.

3.1.5 Test Conditions.

Conditions were selected to achieve test objectives by simulating flight in the icing conditions of 14 CFR Part 25, Appendix C using common aircraft ice protection system operating procedures. Testing was performed in icing tunnel conditions conducive to glaze, mixed, and rime ice accretions. These test conditions were defined by specifying eight parameters. The icing condition variables, MVD, static temperature ($t_{st}$), LWC, and tunnel velocity (V), are discussed below.

The aerodynamic configuration variable was angle of attack, $\alpha$, which was either 0° or 4°, to be representative of flight during descent or holding, respectively, for all test runs. Setting $\alpha$ also required deflection of the flap to achieve the proper flow and impingement characteristics in the leading-edge region. Finally, the deicing system variables were preactivation time, number of cycles, and cycle duration.

Normally, the preactivation time was based on a calculation as to how long it would take a Goodrich Aircraft Sensors Division probe-type ice detector to acquire sufficient ice buildup to annunciate. However, the preactivation time was determined in other ways for some runs to evaluate the effect of this variable. The cycle duration was either 1 minute or 3 minutes for the runs discussed in this report. The 1-minute cycle was ordinarily used for intermittent maximum conditions, which generally had higher LWC values, and the 3-minute cycle was ordinarily used for continuous maximum conditions, which generally had lower LWC values. Based on previous testing, it was expected that approximately steady-state deicing performance could be expected after three deicing cycles. (Steady-state deicing performance reflects not the effectiveness of the deicing system, but the general features of residual and intercycle ice observed by the experimenters.) A slightly more conservative approach, employing three cycles for the 1-minute cycles (higher LWC) and four cycles for the 3-minute cycles (lower LWC), was followed during the test to the extent possible, but there was another criterion also considered. Run duration or LWC were sometimes adjusted to obtain icing conditions for which both the LWC and the horizontal extent (HE) (velocity times duration) strictly conformed to the appropriate 14 CFR Part 25, Appendix C icing envelope.

The MVD was either 20 or 40 μm for all runs. The static temperatures generally corresponded to the temperature curves in the 14 CFR Part 25, Appendix C icing envelopes: 32°, 14°, -4°, and -22°F. However, 32°F was replaced with 21°F because 32°F would have resulted in a total

temperature well above freezing and because, based on past icing tunnel experience, the 21°F temperature would ensure highly repeatable conditions, which was particularly important in view of the time and expense involved in producing the molds. The LWC was then selected from the appropriate icing envelope, interpolating between the temperature curves as necessary. If the HE exceeded the standard distance, either the run time was reduced (resulting in fewer deicing cycles) or the LWC was adjusted using the appropriate F factor based on HE from figures 4 or 6 in 14 CFR Part 25, Appendix C.

A true airspeed of 195 mph was considered a compromise test condition relative to matching the scaling parameters of *Re* and *We* and providing data representative of recommended turbopropeller air transport minimum maneuver airspeeds during in-flight icing operations.

A minimum LWC of 0.25 g/m$^3$ was used for the continuous maximum conditions at 40 μm. These conditions were outside the 14 CFR Part 25, Appendix C icing envelopes, but 0.25 g/m$^3$ was the minimum possible LWC the tunnel could produce at the high speeds and with the considerable model blockage of these tests.

## 3.2 FLIGHT TESTS.

### 3.2.1 Test Airplane.

All tests were performed using the EMBRAER EMB-120 prototype aircraft, serial number 120-001, Brazilian Registration PT-ZBA. The aircraft represented the production standard for items relevant to the tests. Artificial intercycle ice shapes were added to the protected areas and 45-minute, double-horn ice shapes were added to the unprotected areas, as described in section 3.2.3.

The side, top, and front views and dimensions of the EMB-120 aircraft are shown in figure 20.

### 3.2.2 Instrumentation and Data Acquisition.

During the tests, the aircraft was fully instrumented and the data analysis performed was based on data gathered by a Herley Metraplex onboard data acquisition system and recorded on a Hein D3 recorder. The aircraft was also equipped with a safety tailchute for low-speed tests. The parameter list is given in table 2.

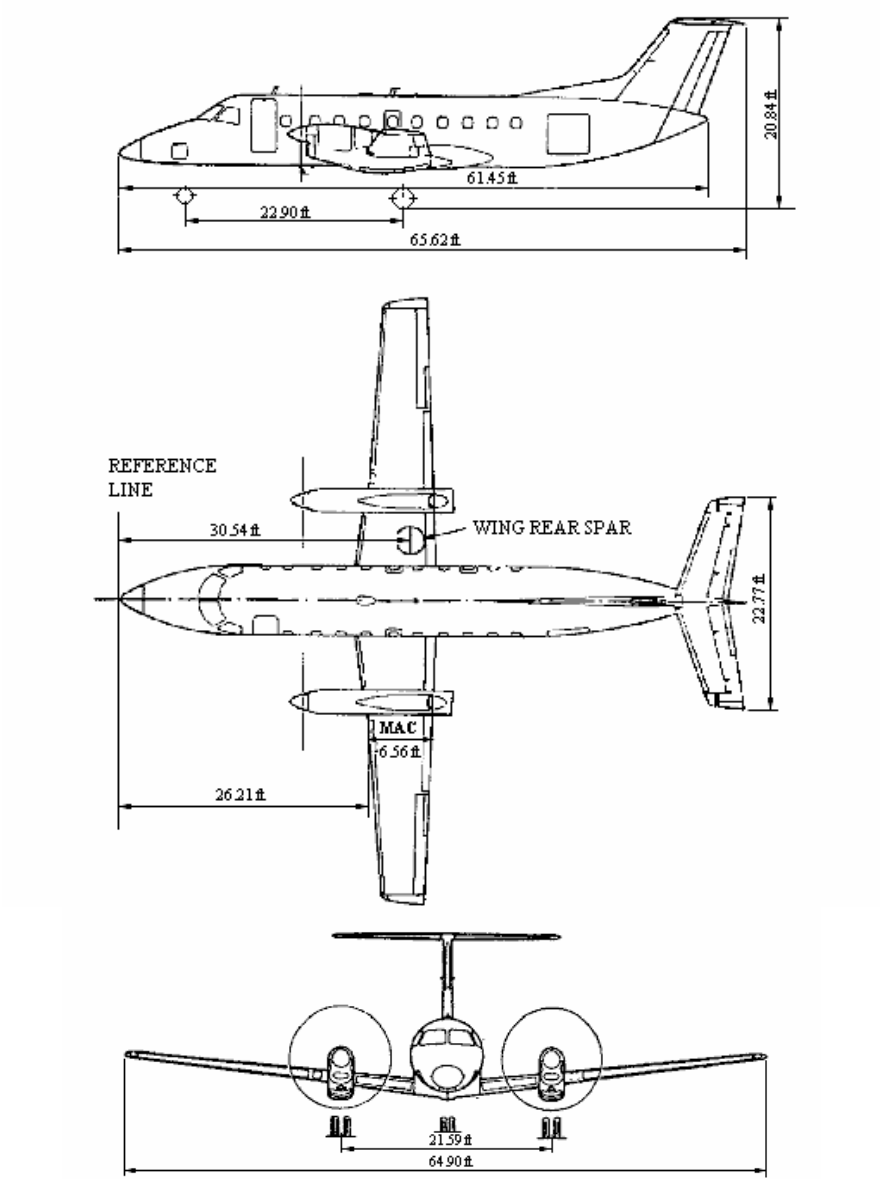


Figure 20. EMB-120 Three View (Side, Top, and Front Views)

Table 2. Flight Test Instrument Parameters List

| Parameter Code | Description |
|---|---|
| A200030 | AOA Right |
| A200040 | AOA Left |
| A200050 | Angle of Sideslip |
| A200060 | Nz |
| A201000 | Airspeed 1P |
| A201001 | Airspeed TC x Kiel |
| A201040 | Altitude 1P |
| A201045 | Altitude TC |
| A201080 | Difference Static 1P x TC |
| A227000 | Stick Force Elevator 1P |
| A227010 | Stick Force Aileron Left 1P |
| A227011 | Stick Force Aileron Right 1P |
| A227020 | Rudder Pedal Force 1P |
| A227060 | Left Elevator Position |
| A227065 | Right Elevator Position |
| A227100 | Rudder Position |
| A227150 | Left Aileron Position |
| A227160 | Right Aileron Position |
| A227320 | Flap Indication |
| A234010 | Pitch Angle (AHRS 1) |
| A234020 | Roll Angle (AHRS 1) |
| A234030 | True Heading (AHRS 1) |
| A234040 | Pitch Rate (AHRS 1) |
| A234050 | Roll Rate (AHRS 1) |
| A234060 | Yaw Rate (AHRS 1) |
| A234070 | Acceleration Nx (AHRS 1) |
| A234080 | Acceleration Ny (AHRS 1) |
| A234090 | Acceleration Nz (AHRS 1) |
| A301071 | TAT |
| A327131 | Shaker 1 |
| A327132 | Shaker 2 |
| A327141 | Pusher 1 |
| A327142 | Pusher 2 |
| A477030 | Left Engine Torque |
| A477035 | Right Engine Torque |
| A477050 | Left Np |
| A477055 | Right Np |
| A728010 | Left Fuel Totalizer |
| A728020 | Right Fuel Totalizer |
| A732170 | Cond. Main Land. Gear |

3.2.3 Simulated Ice Shapes.

The intercycle ice shape configurations used on the flight tests resulted from a joint research program with the participation of the FAA, NASA, EMBRAER, and others. The ice shape configurations were discussed during a technical meeting in Atlanta, Georgia, on July 13, 1999, where it was agreed to represent the most critical intercycle ice accretion that might occur during normal operation of the deicing boots.

These ice shapes were attached to the entire wing protected surfaces (boots). In all unprotected areas that were susceptible to ice accretion, a 14 CFR Part 25, Appendix C holding double-horn shape was attached (same as used for the original EMB-120 certification). On the horizontal and vertical tail protected surfaces (boots), sandpaper grit #40 was attached to simulate some kind of intercycle ice.

Figures 21 through 23 show the ice shapes installed on the test airplane, and figures 24 and 25 show the comparison between the ice mold from the icing tunnel tests and the simulated ice shape to be installed on the airplane.

Figure 21. Left Wing Outboard Leading Edge

Figure 22. Left Wing Inboard Leading Edge


Figure 23. Aircraft Tail

Figure 24. Ice Shape Comparison on Upper Surface: Mold (Right) and Simulated (Left)

Figure 25. Ice Shape Comparison on Under Surface: Mold (Right) and Simulated (Left)

Figures 26, 27, and 28 show the roughness comparison between the mold and the simulated ice shape, as well as the ice shape's general dimensions.

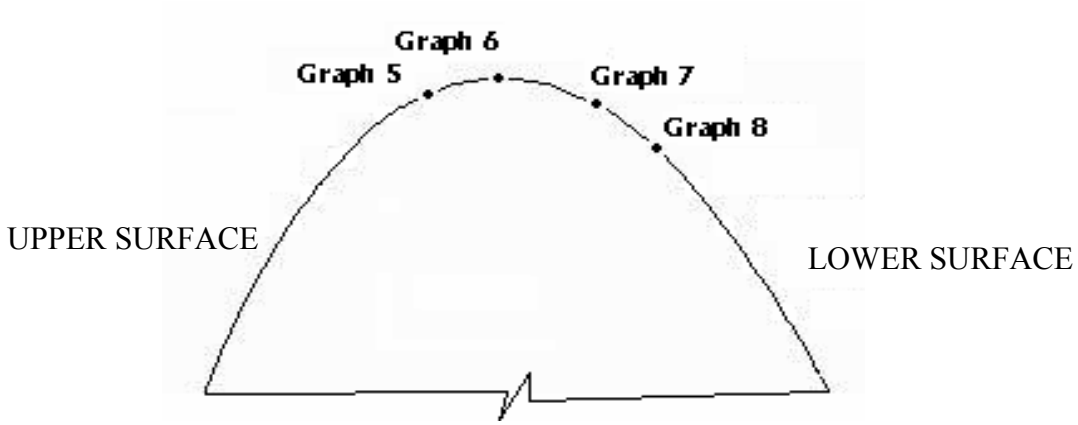


Figure 26. Locations of Graphs of Spanwise Roughness Measurements

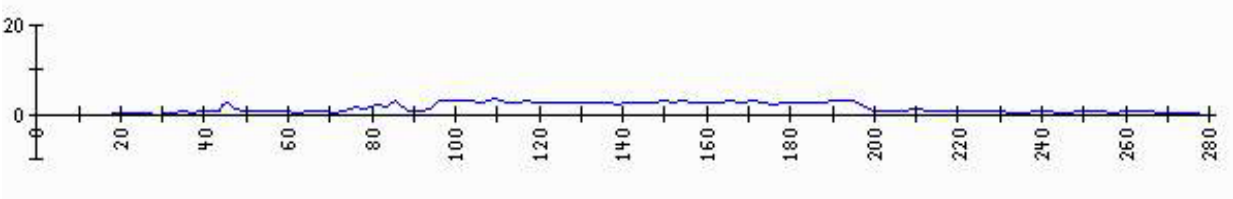


➢ GRAPH 7 – FAA MOLD

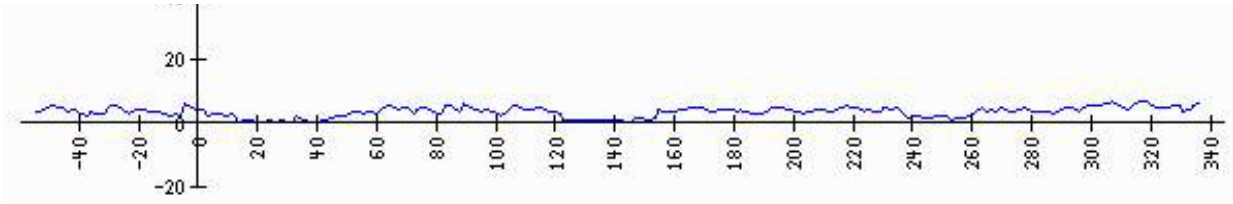


➢ GRAPH 7 – EMBRAER MOLD

Figure 27. Graphs of Roughness Measurements at Location 7 on FAA and EMBRAER Molds

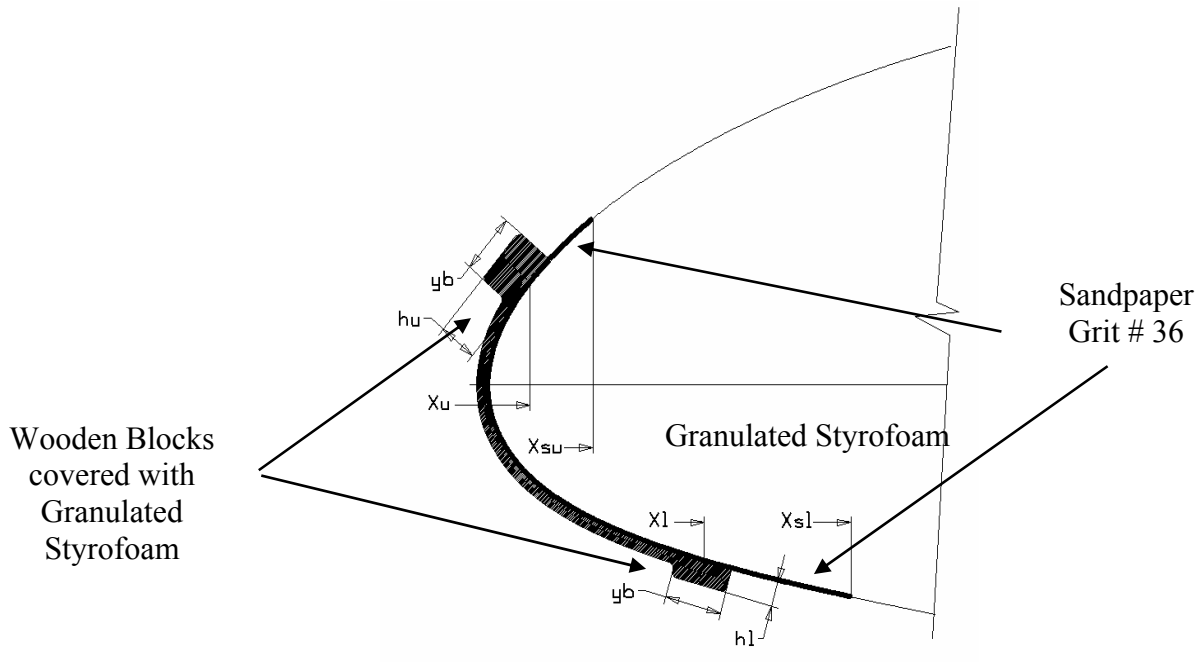


Figure 28. Impingement Limits for Roughness Comparison Results

3.2.4 Test Plans.

To obtain the most accurate aerodynamic influence of intercycle ice shapes, a baseline flight was performed without any ice on the airplane. Slow downs up to the shaker and pusher were performed with forward center of gravity (c.g.) to obtain the lift curve, drag polars, and maximum $C_l$ for the gear up flaps up, gear up flap 15° , and gear down flap 45° configurations.

Table 3 presents the flight test proposal to check the handling characteristics of the airplane subject to the intercycle ice shapes.

Table 3. Handling Tests With Simulated Intercycle Ice Shapes

| No. | Test | Gear/Flap | Weight | c.g. | Power | Speed | Test Procedure |
|---|---|---|---|---|---|---|---|
| 1 | Stall characteristics | UP/0, UP/15, DN/15, DN/25, DN/45 | High | AFT | Idle | Vtrim = 1.3 Vs | Perform wings level stalls at an entry rate of 1 kt/sec. Tests to be carried out at idle power. |
| 2 | Stall characteristics | UP/0, UP/15, DN/15, DN/25, DN/45 | Low, HIGH | AFT | Power On (see note 2) | Vtrim = 1.3 Vs | Perform wings level stalls at an entry rate of 1 kt/sec. Tests to be carried out with power on. |
| 3 | Stall characteristics | UP/0, UP/15, DN/15, DN/25, DN/45 | High | AFT | IDLE | Vtrim = 1.3 Vs | Perform stalls from 30° banked turns (left and right) at an entry rate of 1 kt/sec. Tests to be carried out at idle power. |
| 4 | Stall characteristics | UP/0, UP/15, DN/15, DN/25, DN/45 | Low, High | AFT | Power On (see note 2) | Vtrim = 1.3 Vs | Perform stalls from 30° banked turns (left and right) at an entry rate of 1 kt/sec. Tests to be carried out with power on. |
| 5 | Maneuver margin, all engines | UP/0 | MLW | FWD | MCP Np = 85% | 160 KIAS | Perform 40° banked turns for left and right. Demonstrate that aircraft is free of buffeting or stall warning at the specified conditions. |
| 6 | Maneuver margin, all engines | UP/0 | MLW | FWD | MCP Np = 85% | As required | Determine the minimum airspeed at which a 40° coordinated turn can be flown without aerodynamic buffeting, stick shaker firing, or any other adverse characteristics. |
| 7 | Maneuver margin all engines | UP/15 | MLW | FWD | MCP Np = 100% | 140 KIAS | Perform 40° banked turns for left and right. Demonstrate that aircraft is free of buffeting or stall warning at the specified conditions. |

Table 3. Handling Tests With Simulated Intercycle Ice Shapes (Continued)

| No. | Test | Gear/Flap | Weight | c.g. | Power | Speed | Test Procedure |
|---|---|---|---|---|---|---|---|
| 8 | Maneuver margin, all engines | UP/15 | MLW | FWD | MCP Np = 100% | As required | Determine the minimum airspeed at which a 40° coordinated turn can be flown without aerodynamic buffeting, stick shaker firing, or any other adverse characteristics. |
| 9 | Maneuver margin, all engines | DN/25, DN/45 | MLW | FWD | As required for $\gamma$ = -3° | $V_{REF}$ | Perform 40° banked turns for left and right. Demonstrate that aircraft is free of buffeting or stall warning at the specified conditions. |
| 10 | Maneuver margin, all engines | DN/25, DN/45 | MLW | FWD | As required for $\gamma$ = -3° | As required | Determine the minimum airspeed at which a 40° coordinated turn can be flown without aerodynamic buffeting, stick shaker firing, or any other adverse characteristics. |
| 11 | Maneuver margin, critical engine Inoperative go around | UP/15 | MLW | FWD | ASYM. - Approach climb WAT limited | $V_2$ + 10 (Approach climb speed) | Perform 30° banked turns for left and right. Demonstrate the aircraft is free of buffeting or stall warning at the specified conditions. |
| 12 | Maneuver margin, critical engine inoperative go around | UP/15 | MLW | FWD | ASYM. - Approach climb WAT limited | As required | Determine the minimum airspeed at which a 30° coordinated turn can be flown without aerodynamic buffeting, stick shaker firing, or any other adverse characteristics. |

MLW = Maximum landing weight
FWD = Forward
WAT = Weight/altitude/temperature

# 4. TEST RESULTS.

## 4.1 ICING WIND TUNNEL.

### 4.1.1 Preactivation Ice Accretion.

The objective of the ice protection system preactivation ice accretion investigation was to characterize the surface roughness that would represent the time required to detect icing conditions and the time for the flight crew to activate the ice protection system. Also, 1/4-inch ice shapes, gauged visually from outside the tunnel and by the OPTRON, were documented. For later reference, a mold was made of the preactivation surface roughness in maximum continuous mixed icing conditions (run 3/3R).

Each test run included in this section is documented by a table, an ice tracing (provided the run was not a mold run), and an ice photograph. Table 4 provides summary information about the conditions for each run and the table and figure numbers by which the run is documented.

Table 4. Preactivation Ice Accretion Investigation Summary

| Scenario Prior to Ice Protection System Activation | | | Test Conditions | | Icing Conditions | | | | | | |
|---|---|---|---|---|---|---|---|---|---|---|---|
| Ice Detection Response Time (sec) | Pilot Reaction Time (sec) | Total (sec) | AOA (degrees) | Velocity (mph) | Type | $t_{st}$ (°F) | MVD (µm) | LWC ($g/m^3$) | Run | Figure | Table |
| 11 (Ice Detector) | 30 | 41 | 4 | 195 | MC | 14 | 20 | 0.45 | 3/3R | 29, 30 | 5 |
| 3 (Ice Detector) | 30 | 60 | 4 | 195 | IM | 14 | 20 | 1.95 | 6/3 | 31, 32 | 6 |
| 30 (Visual) | 30 | 33 | 4 | 195 | MC | 14 | 20 | 0.45 | 3/3 | 33 | 7 |
| 1/4 inch (Measured) | - | 324 | 4 | 195 | MC | 14 | 20 | 0.45 | 3/2 | 34, 35 | 8 |
| 1/4 inch (Visual) | 30 | 107 | 4 | 195 | IM | 14 | 20 | 1.95 | 6/2 | 36, 37 | 9 |

For an ice protection system that included an advisory Ice detector, figure 29 characterizes the ice accretion that resulted from an exposure to 14 CFR Part 25, Appendix C continuous maximum icing conditions for 41 seconds. The results from a repeat run for the same icing conditions, but a 60-second duration, are shown in figure 33. The 41 seconds allowed an 11-second ice detector response time and 30 seconds for the flight crew to activate the ice protection system. The impinged surface was characterized by a thin distributed roughness with pebble-like, rounded particle texture. (The impinging water droplets appeared to coagulate into larger drops on the surface and then freeze prior to being sheared aft as the drop height grew beyond the boundary layer thickness and began to be influenced by the free-stream airflow.) The 1-inch chordwise lines scribed on the model can be used to gauge the particle density, and the 1-inch scale shown on the ice shape tracing can be used to gauge the ice accretion thickness.

Table 5. Run 3/3R Test Parameters

| Date 3/17/00 | | Run 3/3R | | AOA: +4° | | No Mold | Flap Angle: +2° | | | |
|---|---|---|---|---|---|---|---|---|---|---|
| | | | | | | | Boot Settings | | | Spray Start and Spray Off Time |
| $T_{model}$ (°F) | $t_{st}$ (°F) | $T_{tot}$ (°F) | V (mph) | MVD (μm) | LWC ($g/m^3$) | Time (min:sec) | Initial Fire | Cycle | Activation | |
| 21.18 | 14 (14.4) | 21.50 | 195 | 20 | 0.45 | 0:41 | No boot fire | - | ID 0: | 11:32:22 11:33:03 |
| 21.07 | | | | | | | | | | |
| 24.54 | | | | | | | | | | |
| 25.05 | | | | | | | | | | |
| 22.64 | | | | | | | | | | |

| Tracing Location |
|---|
| Center |

| Ice Thickness Measurements | |
|---|---|
| Location | Thickness |
| 0.5″ up | 0.0″8 |
| Stagnation | 0.0″8 |
| 1″ Down | 0.07″ |

Notes:

$T_{model}$ – the reading of three thermocouples installed on the model

$T_1$ – After body outside

$T_2$ – After body inside

$T_3$ – IB

$T_4$ – CB

$T_5$ – CT

Description/comments: Preactivation ice with a ice detector response time of 11 seconds and pilot reaction time of 30 seconds to activate the ice protection system. Ice accretion surface texture was pebble-like.

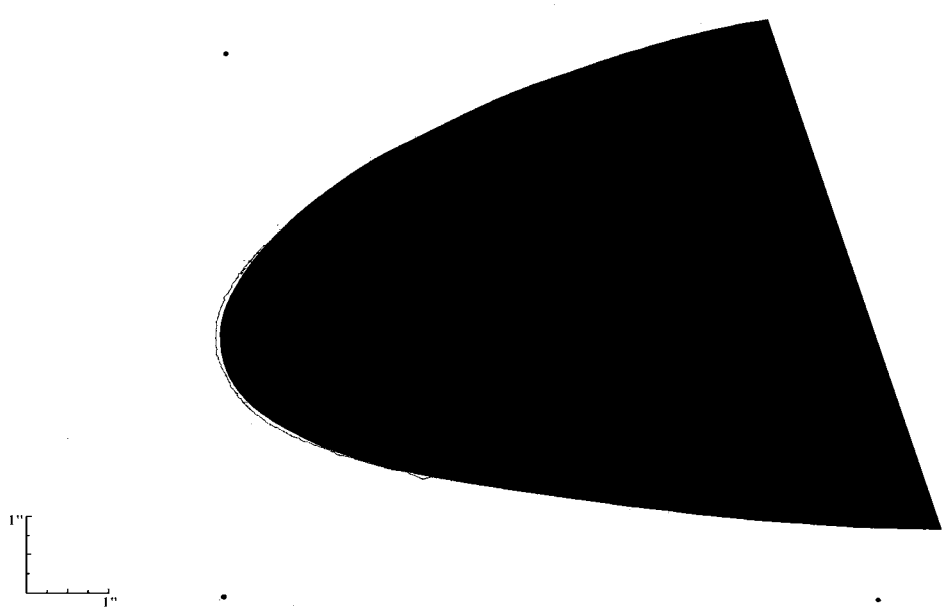


Figure 29. Tracing of Run 3/3R

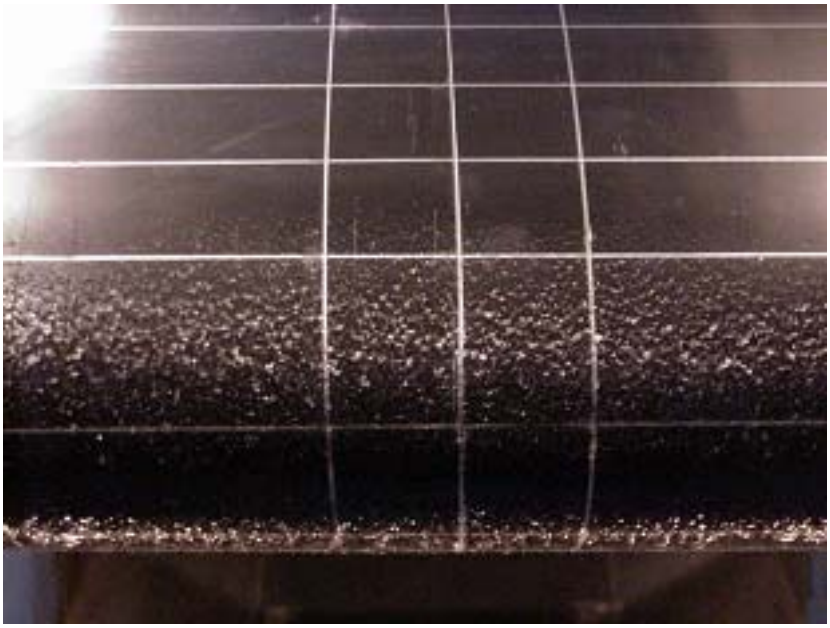

Figure 30. Photograph of Run 3/3R (Upper Surface Leading Edge)

Table 6. Run 6/3 Test Parameters

| Date 3/13/00 | | Run 6/3R | | AOA: +4° | | No Mold | Flap Angle: +2° | | | |
|---|---|---|---|---|---|---|---|---|---|---|
| | | | | | | | Boot Settings | | | Spray Start and Spray Off Time |
| $T_{model}$ (°F) | $t_{st}$ (°F) | $T_{tot}$ (°F) | V (mph) | MVD (μm) | LWC ($g/m^3$) | Time (min:sec) | Initial Fire | Cycle | Activation | |
| 20.5 | 14 (13.9) | 20.7 | 195 | 20 | 1.95 | 0:33 | No boot fire | - | ID 0: | 14:14:31 14:15:05 |
| 20.2 | | | | | | | | | | |
| 22.0 | | | | | | | | | | |

| Tracing Location |
|---|
| Center |

| Ice Thickness Measurements | |
|---|---|
| Location | Thickness |
| 1.25″ up | 0.07″ |
| Stagnation | 0.07″ |
| 1.25″ down | 0.07″ |

Notes:
$T_{model}$ – The reading of three thermocouples installed on the model
$T_1$ – On the surface of the hybrid model aft-body
$T_2$ – Inside the hybrid model aft-body massive aluminum body
$T_3$ – Embedded inside the pneumatic boot of the hybrid model leading edge

Description/comments: Preactivation ice within Appendix C intermittent maximum icing conditions, as limited by the IWT, with a 3-second ice detector response time and a 30-second pilot reaction time.

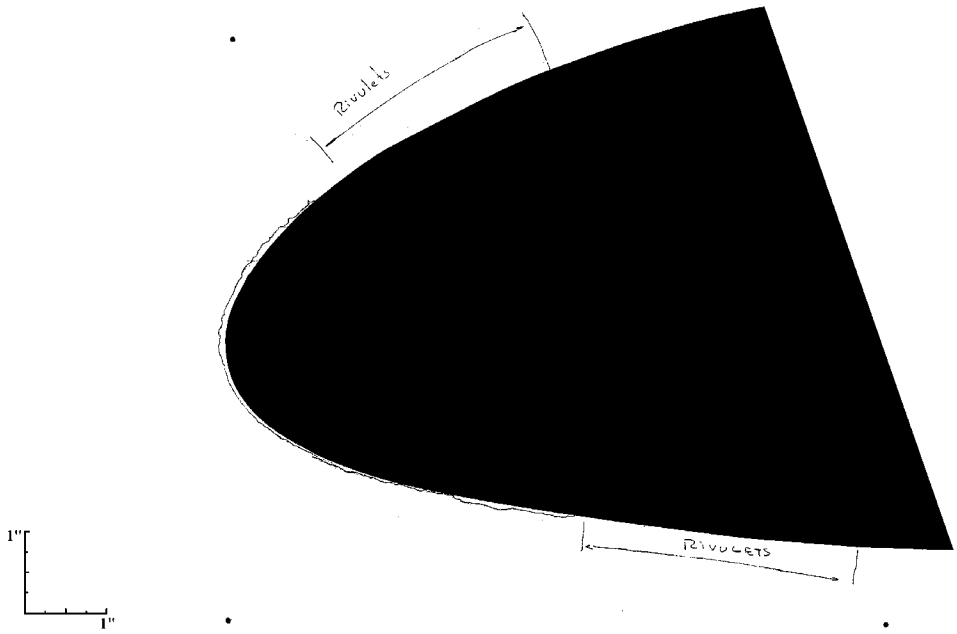


Figure 31. Tracing of Run 6/3

Figure 32. Photograph of Run 6/3 (Upper Surface Leading Edge)

Table 7. Run 3/3 Test Parameters

| Date 3/9/00 | | Run 3/3R | | AOA: +4° | | No Mold | Flap Angle: +2° | | | |
|---|---|---|---|---|---|---|---|---|---|---|
| | | | | | | | Boot Settings | | | |
| $T_{model}$ (°F) | $t_{st}$ (°F) | $T_{tot}$ (°F) | V (mph) | MVD (μm) | LWC ($g/m^3$) | Time (min:sec) | Initial Fire | Cycle | Activation | Spray Off Time |
| 22.6 | 14(14.4) | 21.4 | 195 | 20 | 0.45 | 1:00 | - | None | - | 13:52:44 |
| 22.7 | | | | | | | | | | |
| 21.2 | | | | | | | | | | |

| Tracing Location |
|---|
| Center |

| Ice Thickness Measurements | |
|---|---|
| Location | Thickness |
| Upper | 0.04 inch |
| Stagnation | 0.05 inch |
| Lower | 0.09 inch |

Notes:
$T_{model}$ – The reading of three thermocouples installed on the model
$T_1$ – On the surface of the hybrid model aft-body
$T_2$ – Inside the hybrid model aft-body massive aluminum body
$T_3$ – Embedded inside the pneumatic boot of the hybrid model leading edge

Description/comments: Preactivation ice — a thin layer of glaze ice over the entire pneumatic boot area inside the impingement limits. A tracing was attempted, but the accretion was too thin. To the touch, this ice felt roughly similar to 60-grit sandpaper.

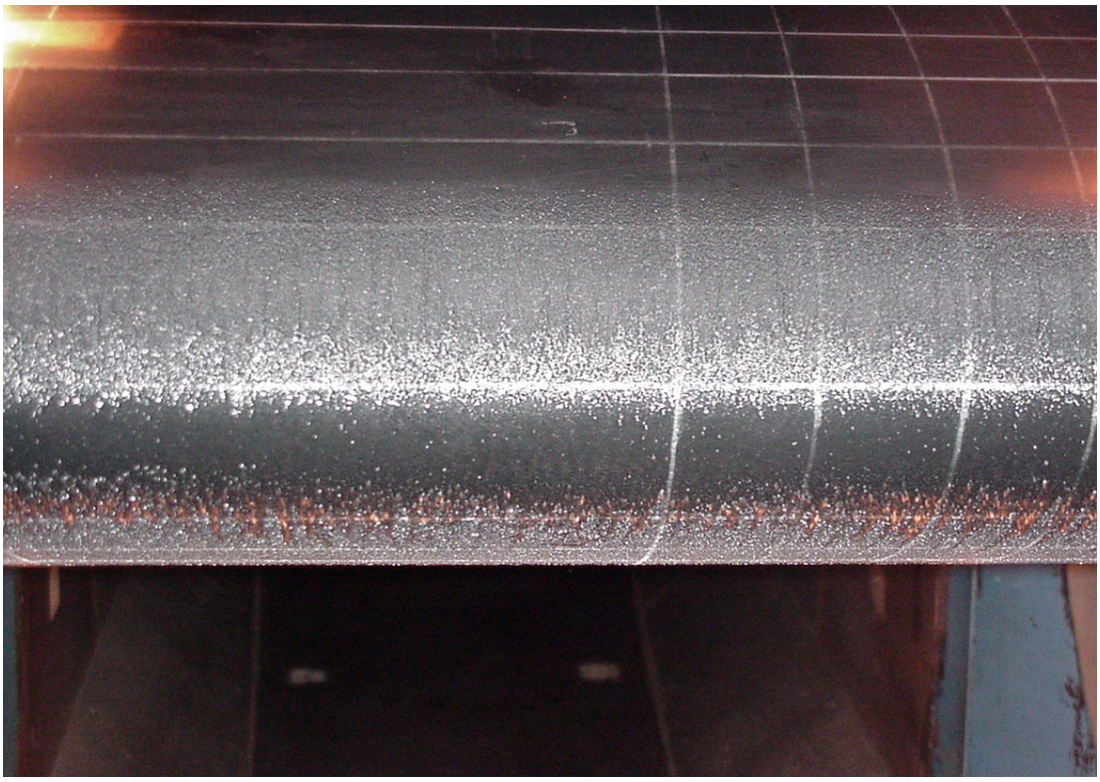

Figure 33. Photograph of Run 3/3 (Upper Surface Leading Edge)

Table 8. Run 3/2 Test Parameters

| Date 3/9/00 | | Run 3/2 | | AOA: +4° | | No Mold | Flap Angle: +2° | | | |
|---|---|---|---|---|---|---|---|---|---|---|
| | | | | | | | Boot Settings | | | |
| $T_{model}$ (°F) | $T_{stat}$ (°F) | $T_{tot}$ (°F) | V (mph) | MVD (μm) | LWC ($g/m^3$) | Time (min:sec) | Initial Fire | Cycle | Activation | Spray Off Time |
| 21.2 | 14(14.4) | 21.4 | 195 | 20 | 0.45 | 5:24 | - | - | - | N/A |
| 21.3 | | | | | | | | | | |
| 20.4 | | | | | | | | | | |

| Tracing Location |
|---|
| |
| Center |
| |

| Ice Thickness Measurements | |
|---|---|
| Location | Thickness |
| Upper 1.25″ | 0.55 inch |
| Stagnation | 0.26 inch |
| Lower 1.25″ | 0.32 inch |

Notes:
$T_{model}$ – The reading of three thermocouples installed on the model
$T_1$ – On the surface of the hybrid model aft-body
$T_2$ – Inside the hybrid model aft-body massive aluminum body
$T_3$ – Embedded inside the pneumatic boot of the hybrid model leading edge

Description/comments: Preactivation ice. The OPTRON was used to define when a 1/4 inch of ice had accumulated on the model's leading edge. The spray-on time required for the 1/4 inch of leading-edge ice was 2:30 minutes. The spray was continued for an additional 30 seconds to simulate pilot reaction time to activate an ice protection system. The front leading edge collected rough glaze ice, while the lower leading edge had horn feathers of a height greater than a 1/4 inch, and the upper leading edge had horn feathers of a height much greater than a 1/4 inch. This run can be regarded as simulating preactivation ice.

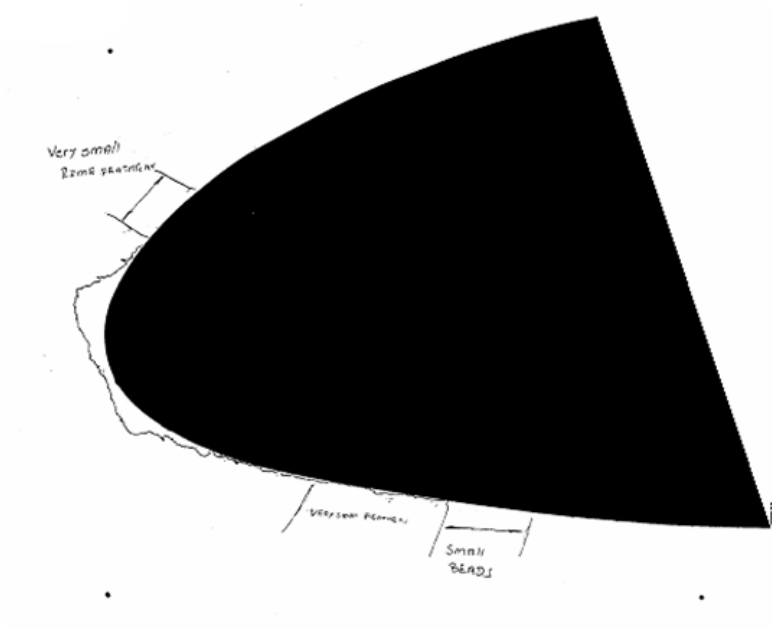


Figure 34. Tracing of Run 3/2

Figure 35. Photograph of Run 3/2

Table 9. Run 6/2 Test Parameters

| Date 3/13/00 | | Run 6/2 | | AOA: +4° | | No Mold | Flap Angle: +2° | | | |
|---|---|---|---|---|---|---|---|---|---|---|
| | | | | | | | Boot Settings | | | Spray Start and Spray Off Time |
| $T_{model}$ (°F) | $t_{st}$ (°F) | $T_{tot}$ (°F) | V (mph) | MVD (μm) | LWC ($g/m^3$) | Time (min:sec) | Initial Fire | Cycle | Activation | |
| 20.6 | 14 (13.7) | 20.5 | 195 | 20 | 1.95 | Est. 1/4″ | No boot fire | - | ID 0: | 13:43:08 13:44:25 |
| 20.0 | | | | | | | | | | |
| 21.3 | | | | | | | | | | |

| Ice Thickness Measurements | |
|---|---|
| Max thickness | 0.24″ |

Notes:

$T_{model}$

$T_1$ – On the surface of the hybrid model aft-body

$T_2$ – Inside the hybrid model aft-body massive aluminum body

$T_3$ – Embedded inside the pneumatic boot of the hybrid model leading edge

Description/comments: This run was an experiment to investigate how accurately a 1/4 inch of ice could be visually estimated. Thickness of the ice accretion was made from the IWT test section side window as a rough simulation of a pilot's view of ice accretion on a wing. The test was run until the observer determined that the maximum thickness of the ice was a 1/4 inch. The tunnel was stopped and the maximum ice thickness was measured. Since the measurement was 0.24 inch, the visual estimate was remarkably accurate in this case. No photograph was taken at this time.

Table 9. Run 6/2 Test Parameters (Continued)

| Date 3/13/00 | | Run 6/2 | | AOA: +4° | | No Mold | Flap Angle: +2° | | | |
|---|---|---|---|---|---|---|---|---|---|---|
| | | | | | | | Boot Settings | | | Spray Start and Spray Off Time |
| $T_{model}$ (°F) | $T_{stat}$ (°F) | $T_{tot}$ (°F) | V (mph) | MVD (μm) | LWC ($g/m^3$) | Time (min:sec) | Initial Fire | Cycle | Activation | |
| 22.4 | 14 (14.1) | 20.9 | 195 | 20 | 1.95 | Est.1/4″ +0:30 | No boot fire | - | ID 0: | 13:53:29 13:53:59 |
| 22.3 | | | | | | | | | | |
| 23.1 | | | | | | | | | | |

| Tracing Location |
|---|
| Center |

| Ice Thickness Measurements | |
|---|---|
| Location | Thickness |
| 2″ up | 0.50″ |
| Stagnation | 0.15″ |
| 1.25″down | 0.21″ |

Notes:
$T_{model}$ – The reading of three thermocouples installed on the model
$T_1$ – On the surface of the hybrid model aft-body
$T_2$ – Inside the hybrid model aft-body massive aluminum body
$T_3$ – Embedded inside the pneumatic boot of the hybrid model leading edge

Description/comments: The tunnel was restarted and ice accretion was continued for an additional 30 seconds from the time that the observer estimated that a 1/4 inch of ice had accreted. This simulated a delay by the pilot in activating the ice protection system. A tracing and a photograph were made of the final ice shape.

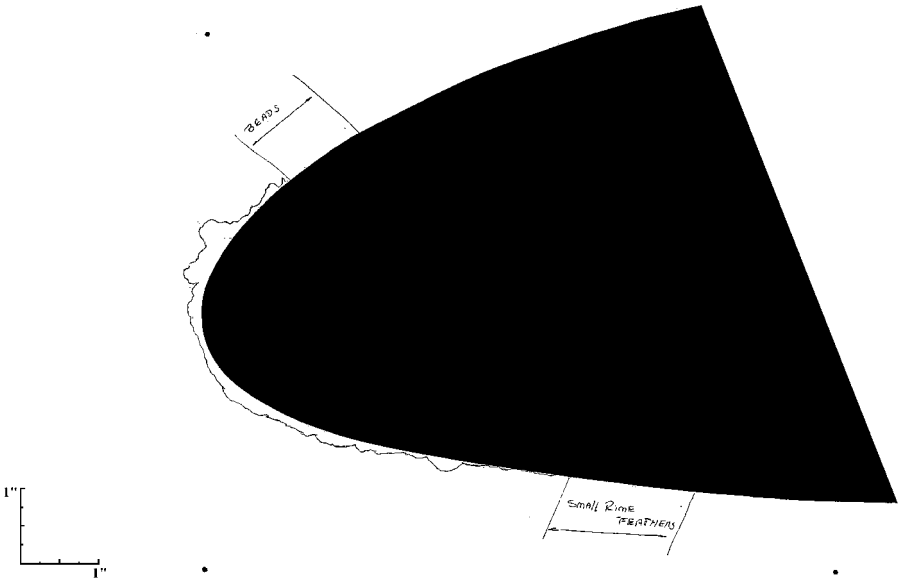


Figure 36. Tracing of Run 6/2

Figure 37. Photograph of Run 6/2 (Upper Surface Leading Edge)

For conditions within 14 CFR Part 25, Appendix C intermittent icing conditions, the model's water catch is higher, the resulting ice accretion texture is rougher, and the ice thickness is slightly greater, as shown in figure 32.

Preactivation ice accretion for ice protection systems that operate sequentially with delayed activation of local elements of the ice protection system was not investigated.

For ice protection systems where the recommended procedure is to delay activation of the system until 1/4 inch of ice has accreted, the resulting preactivation ice accretion is characterized in table 8 and figures 34 and 35, as well as in table 9 and figures 36 and 37 for conditions within 14 CFR Part 25, Appendix C continuous maximum and intermittent maximum icing conditions. The character of the resulting surface roughness is significant as is evident in figures 35 and 37. Note that for an airplane flying at 195 mph true airspeed (133 kts at 15,000 feet altitude and temperature of 14°F), the time required to accrete 1/4 inch of ice is longer than the time required to traverse standard maximum continuous and intermittent cloud extents (14.7 and 2.6 nmi., respectively). Preactivation ice accretion for ice protection systems that operate sequentially with delayed activation of local elements of the ice protection system was not investigated for this ice protection system activation procedure.

4.1.2 Deicer Intercycle Ice Accretion.

The objective of the deicer residual and intercycle ice accretion investigation was to characterize residual and intercycle ice accretions that result from normal operation of a pneumatic deicing ice protection system. The December 2001 IWT test [2] indicated that residual ice is more adverse, relative to surface roughness and ice mass, than intercycle ice. Therefore, the following only addresses deicer intercycle ice accretion.

The character of the intercycle ice accretion may be influenced by the following considerations:

- Design of the deicer (tube size and orientation relative to the free-stream airflow, air pressure and inflation/deflation rate, material characteristics, etc.).
- The shearing forces of local airflow.
- Airplane configuration, deicer installation, and flight conditions.
- Ice thickness prior to cycling of the deicer or ice accumulated during the deicer rest periods following an initial deicer cycling at the first detection of ice accretion.
- The icing cloud horizontal extent and, subsequently, the number of deicer cycles.
- Icing conditions/intensity (temperature, LWC, drop size, and airspeed).

As discussed earlier, the deicer design is reflective of typical deicer systems installed on turbopropeller-powered regional air transports and general aviation airplanes. Test results are not considered applicable for early, large tube, low-pressure deicer designs, such as those installed on the DC-3, C-47, and other earlier propeller-powered air transports. The deicer tubes were oriented spanwise on the model. The investigation did not address chordwise oriented deicers.

The two-dimensional test model was installed normal to the IWT airflow; therefore, the test results are considered applicable to the mid and outer wing panels of straight or moderately swept wings that are not characterized by significant span-flow or three-dimensional configuration influences. The NACA 23012 airfoil was selected because NACA 230xx airfoils, with varying thickness ratios, have been used for a number of airplane designs that use pneumatic deicer ice protection systems. The investigation was performed at the maximum IWT airspeed, as limited by model blockage. The 195 mph true airspeed is a compromise test condition relative to matching the scaling parameters of *Re* and *We* and provides data representative of recommended turbopropeller air transport minimum maneuver airspeeds during in-flight icing operations. A model AOA of 4° was considered representative of recommended turbopropeller air transport holding and minimum maneuver airspeeds while an AOA of 0° was considered representative of approach descent operations. The following discusses the test results relative to these three considerations.

Each test run included in this section is documented by a table, an ice tracing (provided the run was not a mold run), and an ice photograph. Table 10 provides summary information about the conditions for each run and the table and figure numbers by which the run is documented.

Table 10. Deicer Intercycle Ice Accretion Investigation 195 mph (2.82 nmi/min) True Airspeed

| | Icing Conditions Description | | | | | Deicer Operation | | | | | | | |
|---|---|---|---|---|---|---|---|---|---|---|---|---|---|
| AOA (deg) | Type Icing Cond. | Type Ice | $t_{st}$ (°F) | MVD (μm) | LWC ($g/m^3$) | Initial Activ. (sec) | Cycle Period (Min) | No. Cycles | Icing Cloud Extent (nmi) | Comments | Run | Figure | Table |
| 4 | CM | Mixed | 14 | 20 | 0.45 | 11 | 3 | 2 | 14.7 | Appendix C LWC | 2/1R | 42, 43 | 13 |
| | | | | " | " | " | " | 4 | Contin | " | 2/1A | 40, 41 | 8 |
| | | | | " | " | " | 1 | 5 | 14.7 | " | 2/2 | 44, 45 | 14 |
| | | | | " | " | 1/4 in. | 3 | 4 | Contin | " | 3/1 | 38, 39 | 11 |
| | | | | 40 | 0.25 | 19 | " | " | Contin | App. C LWC = 0.1 | 3/6A | 78, 79 | 31 |
| | | Glaze | 21 | 20 | 0.51 | 11 | 3 | 2 | 14.7 | App. C LWC = 0.52 | 4/1 | 46, 47 | 15 |
| | | | | | | | " | 4 | Contin | | 4/1A | 58, 59 | 21 |
| | | | | | | | 1 | 5 | 14.7 | | 4/1.5 | 48, 49 | 16 |
| | | Rime | -22 | 20 | 0.15 | 34 | 3 | 4 | Contin | App. C LWC = 0.14 | 5/1 | 74, 75 | 29 |
| | IM | Mixed | 14 | 20 | 1.87 | 3 | 3 | 4 | Contin | App. C LWC = 2.21 but | 6/1B | 50, 51 | 17 |
| | IM | | | " | " | " | 1 | 2 | Contin | IWT max. LWC = 1.95 | 6/1 | 64, 69 | 26 |
| | IM | | | " | " | " | " | 4 | Contin | | 6/1A | 52, 53 | 18 |
| | IM(s) | | | 40 | 0.25 | 19 | - | 1 | 2.6(s) | 2 min. to sim. 0.52 LWC | 3/6 | 62, 63 | 23 |
| | IM | | | " | 0.44 | 9 | 1 | 2 | Contin | App. C LWC = 0.52 | 6/6 | 64, 65 | 24 |
| | IM | | | " | 0.52 | " | " | 4 | Contin | " | 6/5 | 66, 67 | 25 |
| | IM(s) | Glaze | 21 | 40 | 0.25 | 19 | - | 1 | 2.6(s) | 2 min. to sim. 0.52 LWC | 4/4 | 80, 81 | 32 |
| | IM | | | | | | | | | 3 min. to sim. 0.52 LWC | 4/4.5 | 82, 83 | 33 |
| | | Rime | -22 | 20 | 0.85 | 6 | 1 | 2 | Contin | App. C LWC = 0.99 | 5/5 | 76, 77 | 30 |
| 0 | CM | Mixed | 14 | 20 | 0.45 | 11 | 3 | 2 | 14.7 | Appendix C LWC | 3/4 | 60, 61 | 22 |
| | | | | | | | " | 4 | Contin | | 3/4A | 54, 55 | 19 |
| | | | | | | | 1 | 5 | 14.7 | | 3/4.5 | 56, 57 | 20 |
| | | Glaze | 21 | 20 | 0.51 | 11 | 3 | 2 | 14.7 | App. C LWC = 0.52 | 4/2 | 84, 85 | 34 |
| | IM | Mixed | 14 | 20 | 1.87 | 3 | 1 | 2 | Contin | App. C LWC = 2.21 but | 6/4 | 70, 71 | 27 |
| | IM | | | " | " | 3 | " | 4 | Contin | IWT max. LWC = 1.95 | 6/4A | 72, 73 | 28 |
| | IM(s) | | | 40 | 0.25 | 19 | - | 1 | 2.6(s) | 2 min. to sim. 0.52 LWC | 3/5 | 86, 87 | 35 |
| | IM(s) | | | " | " | " | - | " | 2.6(s) | 3 min. to sim. 0.52 LWC | 4/3 | 88, 89 | 36 |

4.1.2.1 Delayed or Immediate Deicer Activation.

To achieve efficient shedding of ice from deicers and avoid ice bridging across the pneumatic deicer's tubes, airframe manufacturers recommended delayed initiation of each deicer cycle until after ice accretions of 1/4 to 1 1/2 inches have been observed. Based on the 3-minute exposure required to accrete the 1/4 inch of leading-edge ice shown in figure 35, figure 39 illustrates the intercycle ice accretion resulting from 3-minute periodic cycling (four cycles) of the model's deicer following an initial deicer cycle with 1/4 inch (3 minutes of icing cloud exposure) of ice accumulation. The test icing conditions were representative of 14 CFR Part 25, Appendix C continuous maximum, mixed ice icing conditions with the model attitude set at the 4° holding AOA. These results are comparable with those shown in figure 41, for which the initial deicer activation was based on the 11-second ice detection response time of a commonly used ice detector. These results suggest that, following repeated cycling of the deicer after using the two deicer initial activation procedures, there were no significant differences between the intercycle ice accretion characteristics.

Note that the 3-minute deicer rest period allows approximately 1/4 inch of leading-edge ice to accumulate and allows 30 seconds for the pilot to activate the deicer; the same icing cloud exposure time required to accumulate 1/4 inch preactivation shown in figures 35 and 37. However, comparing the preactivation ice accretions shown in figures 35 and 36 with the intercycle ice accretions shown in figures 41 and 43 reveals that even though the leading-edge ice thicknesses are similar, the intercycle ice roughness is more random and less organized than that of the preactivation ice accretions. The random and less organized intercycle ice roughness was observed to result from further ice accumulation on random residual ice that remained after cycling the deicer.

Using the 1-minute automatic deicer cycling mode resulted in the intercycle ice accretion shown in figure 45. The shorter deicer rest interval reduced the intervening ice thickness accumulated to less than the 3-minute rest, interval 1/4-inch ice thickness, and the intervening ice thickness would be representative of preactivation and pilot reaction time ice thickness. Comparing figures 43 and 45 illustrates the effect of reducing the deicer rest interval/ice accumulation from 3 minutes to 1 minute for 14 CFR Part 25, Appendix C continuous maximum mixed icing conditions. Similar comparisons are shown between figures 47 and 49 for 14 CFR Part 25, Appendix C continuous maximum glaze ice icing conditions at the 4° hold AOA.

For 14 CFR Part 25, Appendix C intermittent maximum, mixed icing conditions, similar comparisons are shown in figures 51 and 53. These data show that for the icing intensity and rapid ice accretion associated with 14 CFR Part 25, Appendix C intermittent icing conditions, flight crews would probably select the 1-minute deicer rest interval (without contrary recommendations), even though the larger 3-minute ice accretion resulted in a more efficient ice shed. For the 0° descent AOA, similar 3-minute versus 1-minute cycling interval comparisons are shown between figures 55 and 57 for 14 CFR Part 25, Appendix C continuous maximum mixed ice icing conditions.

Visual observation of the ice accretions suggested that the shorter 1-minute cycle interval generally resulted in less smaller-scale intercycle ice roughness. This investigation indicated that

the intercycle ice accretion tended to increase in thickness until the minimum thickness needed for shedding to occur.

Pneumatic deicer systems that automatically cycle the deicer following an initial activation typically perform that function on the basis of time, based on the flight crew's judgement of icing intensity. Using 3- and 1-minute time intervals for light and moderate icing intensities, respectively, is common. Further insight of the effect of ice accretion thickness on the ice shedding efficiency of the pneumatic deicer resulted from varying the deicer rest period between cycles.

Observations of deicer performance during the inflated dwell time suggested that the shear force of the local airflow tended to shed ice efficiently from the forward portion of each inflated deicer tube. Ice did not tend to accrete on the forward portion of the inflated deicer, perhaps because the smaller cloud droplets were diverted from impingement by the direction of the local airflow. However, residual ice tended to remain on the aft portion of each tube (the region of flow deceleration and pressure recovery). Also, a thin coating of ice tended to accrete on the aft portion of the inflated deicer tubes, perhaps caused by entrainment and impingement of cloud droplets in the turbulent local airflow that would occur aft of the apex and maximum local airspeed of the inflated deicer tube. This local behavior is similar to the airflow characteristics around a cylinder. The reduced ice shedding efficiency, remaining residual ice, and the light accumulation of ice of the aft portion of the inflated deicer tube resulted in local nuclei for more rapid accumulation of intercycle ice during the subsequent deflated tube portion of the deicer cycle interval. The more rapid accumulation of intercycle ice resulted in ridges of ice forward of and along the stitch lines between the deicer tubes. This intercycle ice accretion phenomenon appears to be inherent for current pneumatic tube deicer designs that are installed normal to the free-stream airflow.

The intercycle ice accretion tended to be highly three-dimensional and granular, yet definitive by major coherent features. The three-dimensional texture appeared to be caused by random residual ice and, depending on temperature and cloud drop size, the coalescence of small cloud droplets into larger droplets on the surface before freezing. The bead-like texture of the intercycle ice accretion is very apparent in the following photographs for glaze and mixed ice temperatures. Accumulation of ice forward and along the deicer tube stitch lines dominated the major coherent feature of the intercycle ice accretion.

The ice shedding efficiency of the deicer's initial cycle improved with increased ice thickness. However, the value of the cleaner shedding of the initial deicer cycle tended to deteriorate during subsequent cycling of the deicer, with the deicer shedding efficiency being equivalent after a few cycles to an initial deicer cycle with a thin layer of ice. The intercycle ice accretion phenomena described above may explain this observation.

Throughout the investigation, with initial deicer activation predicated on the ice detection reaction time of a commonly used ice detector or on a predetermined initial ice thickness and a 30-second flight crew reaction time, no ice bridging across the deicer tubes was observed. Residual ice that remained on the deicer following its cycling remained until sufficient thickness accumulated for the ice to be shed during a subsequent cycling of the deicer.

Table 11. Run 3/1 Test Parameters

| Date 3/9/00 | | Run 3/1 | | AOA: +4° | | No Mold | Flap Angle: +2° | | | |
|---|---|---|---|---|---|---|---|---|---|---|
| | | | | | | | Boot Settings | | | |
| $T_{model}$ (°F) | $t_{st}$ (°F) | $T_{tot}$ (°F) | V (mph) | MVD (μm) | LWC ($g/m^3$) | Time (min:sec) | Initial Fire | Cycle | Activation | Spray Off Time |
| 20.6 | 14(13.3) | 20.1 | 195 | 20 | 0.45 | 15:00 | 09:34:27 | 3:00 | Manual 3:00 | 09:46:27 |
| 20.5 | | | | | | | | | | |
| 19.4 | | | | | | | | | | |

| Tracing Location |
|---|
| Center |

| Ice Thickness Measurements | |
|---|---|
| Location | Thickness |
| Maximum | 0.53 inch |
| Stagnation | 0.21 inch |
| Lower Surface | 0.42 inch |

Notes:
$T_{model}$ – The reading of three thermocouples installed on the model
$T_1$ – On the surface of the hybrid model aft-body
$T_2$ – Inside the hybrid model aft-body massive aluminum body
$T_3$ – Embedded inside the pneumatic boot of the hybrid model leading edge
Description/comments: The deicer was initially cycled after a 1/4 inch of ice had accumulated on the model's leading edge and subsequently cycled three times at intervals of 3 minutes. The intercycle and residual ice 3 minutes after the fourth deicer cycle was characterized by rough glaze ice along the model's leading edge, while the lower leading edge had feathers of roughness greater than a 1/4 inch, and the upper leading edge had columnar feathers of roughness much greater than a 1/4 inch.

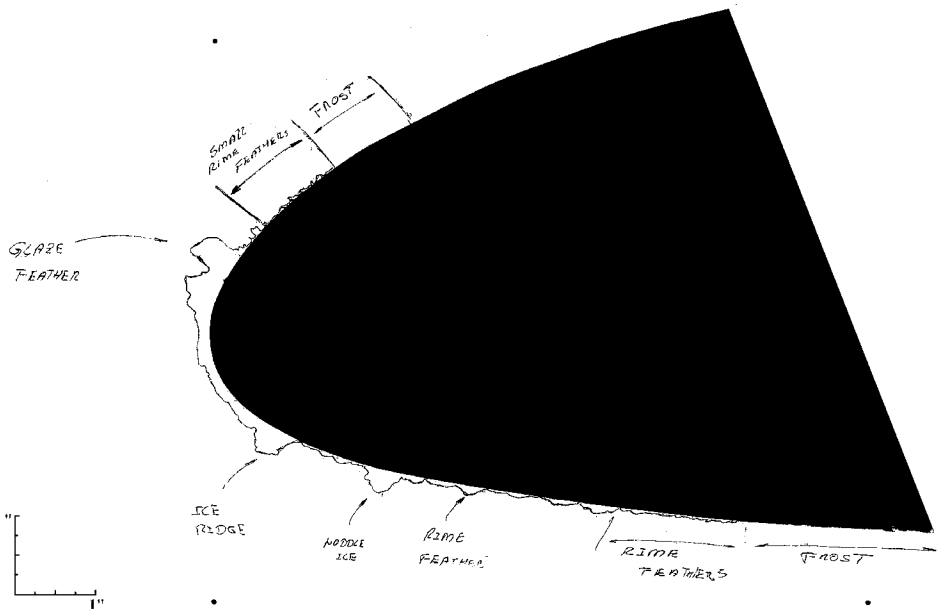


Figure 38. Tracing of Run 3/1

Figure 39. Photograph of Run 3/1 (Upper Surface Leading Edge)

Table 12. Run 2/1A Test Parameters

| Date 3/8/00 | | Run 2/1A | | AOA: +4° | | No Mold | Flap Angle: +0° | | | |
|---|---|---|---|---|---|---|---|---|---|---|
| | | | | | | | Boot Settings | | | |
| $T_{model}$ (°F) | $T_{st}$ (°F) | $T_{tot}$ (°F) | V (mph) | MVD (μm) | LWC ($g/m^3$) | Time (min:sec) | Initial Fire | Cycle | Activation | Spray Off Time |
| 21.9 | 14(21.5) | 19.1 | 195 | 20 | 0.45 | 12:11 | 17:59:30 | 3:00 | ID 0:11* | 18:05:30 |
| 21.9 | | | | | | | | | | |
| 19.4 | | | | | | | | | | |

| Tracing Location |
|---|
| Center |
| Left 4″ |

| Ice Thickness Measurements | |
|---|---|
| Location | Thickness |
| Upper | 0.29 inch |
| Stagnation | 0.19 inch |
| Lower | 0.37 inch |
| Upper | 0.29 inch |
| Stagnation | 0.38 inch |
| Lower | 0.18 inch |

Notes:
$T_{model}$ – The reading of three thermocouples installed on the model
$T_1$ – On the surface of the hybrid model aft-body
$T_2$ – Inside the hybrid model aft-body massive aluminum body
$T_3$ – Embedded inside the pneumatic boot of the hybrid model leading edge
Description/comments: The deicer was initially cycled following an 11-second ice detector response time and then cycled one additional time after a 3-minute rest interval. After 3 minutes of additional exposure to the icing cloud, the testing was interrupted to simulate exposure to a 14 CFR Part 25, Appendix C maximum continuous icing cloud. At this time, the front leading edge had collected rough glaze ice, while the lower leading edge had feathers of a height greater than a 1/4 inch, and the upper leading edge had columnar feathers of a height much greater than a 1/4 inch. There was a region 4 inches left of the center, where a triangular chunk of ice accreted, but it is suspected that this extra accretion was an artifact from the previous tunnel run.

The testing was continued to determine the stable intercycle ice accretion by cycling the deicer immediately with continuation of the icing exposure and cycling the deicer once again following a 3-minute rest interval. Following the final 3-minute rest interval, the test was terminated. Except for the ice triangle, which may be an artifact, the intercycle accretions for the 14 CFR Part 25, Appendix C maximum continuous icing exposure and for an extended icing cloud exposure that produced the stable intercycle ice accretion appeared to be quite similar.

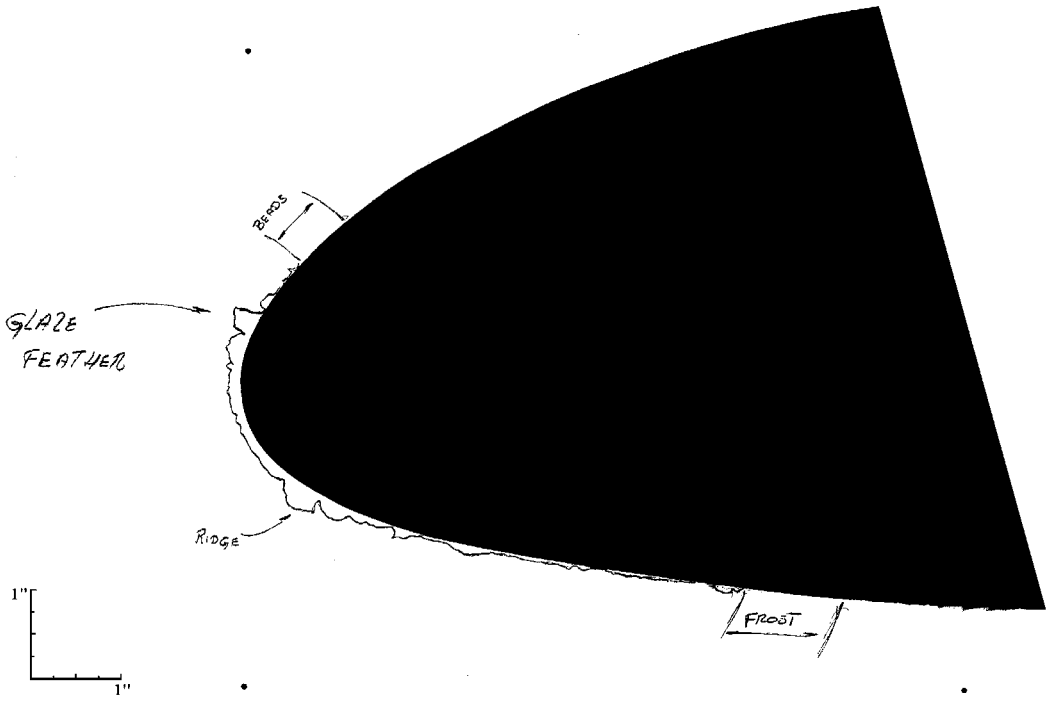


Figure 40. Tracing of Test 2/1A

Figure 41. Photograph of Run 2/1A (Upper Surface Leading Edge)

Table 13. Run 2/1R Test Parameters

| Date 3/8/00 | | Run 2/1R | | AOA: +4° | | No Mold | Flap Angle: +0° | | | |
|---|---|---|---|---|---|---|---|---|---|---|
| | | | | | | | Boot Settings | | | |
| $T_{model}$ (°F) | $T_{st}$ (°F) | $T_{tot}$ (°F) | V (mph) | MVD (μm) | LWC ($g/m^3$) | Time (min:sec) | Initial Fire | Cycle | Activation | Spray Off Time |
| 20.6 | 14(13) | 20.6 | 195 | 20 | 0.45 | 6:11 | 17:20:31 | 3:00 | ID 0:11 | 17:20:20 |
| 20.8 | | | | | | | | | | |
| 19.8 | | | | | | | | | | |

| Tracing Location |
|---|
| Center |

| Ice Thickness Measurements | |
|---|---|
| Location | Thickness |
| Maximum | 0.1 inch |
| Stagnation | 0.12 inch |
| Lower Surface | 0.35 inch |

Notes:
$T_{model}$ – The reading of three thermocouples installed on the model
$T_1$ – On the surface of the hybrid model aft-body
$T_2$ – Inside the hybrid model aft-body massive aluminum body
$T_3$ – Embedded inside the pneumatic boot of the hybrid model leading edge

Description/comments: Run 2/1R repeated the initial testing of run 2/1A to document the intercycle ice accretion following exposure to a 14 CFR Part 25, Appendix C maximum continuous icing cloud. Following an 11-second ice detector response time, the model was exposed 6 minutes to the icing cloud with an initial deicer cycling at 11 seconds and a second deicer cycle 3 minutes later, following a 3-minute rest interval. Testing was terminated following the 3-minute rest interval after the second deicer cycling. The front leading edge collected rough glaze ice, while the lower leading edge had feathers of a height greater than a 1/4 inch, and the upper leading edge had columnar feathers of a height much greater than a 1/4 inch.

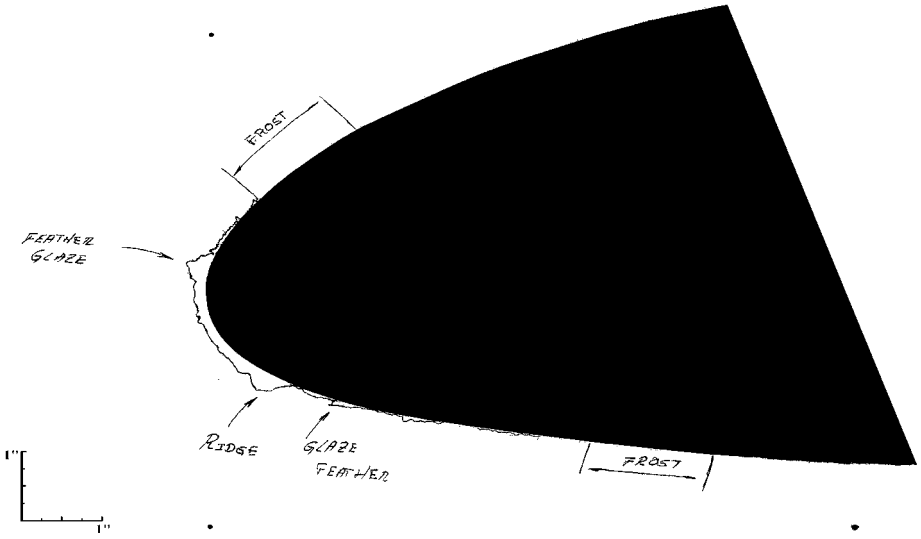


Figure 42. Tracing of Run 2/1R

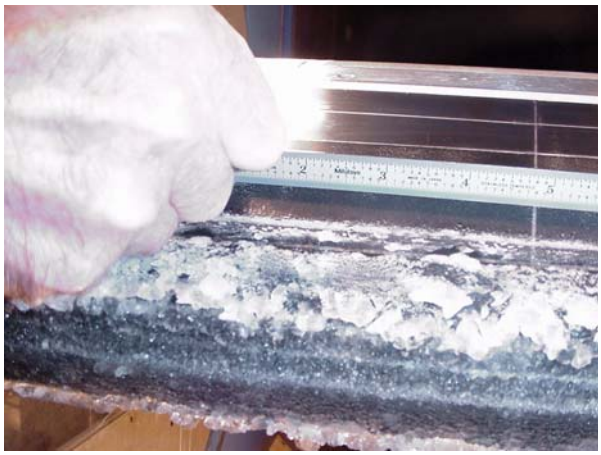

Figure 43. Photograph of Run 2/1R (Upper Surface Leading Edge)

Table 14. Run 2/2 Test parameters

| Date 3/8/00 | | Run 2/2 | | AOA: +4° | | No Mold | Flap Angle: +0° | | | |
|---|---|---|---|---|---|---|---|---|---|---|
| | | | | | | | Boot Settings | | | |
| $T_{model}$ (°F) | $T_{st}$ (°F) | $T_{tot}$ (°F) | V (mph) | MVD (µm) | LWC ($g/m^3$) | Time (min:sec) | Initial Fire | Cycle | Activation | Spray Off Time |
| 21.6 | 14(14.1) | 20.9 | 195 | 20 | 0.45 | 6:11 | 18:55:08 | 1:00 | ID 0:11 | 19:01:08 |
| 21.5 | | | | | | | | | | |
| 20.4 | | | | | | | | | | |

| Tracing Location |
|---|
| |
| Center |

| Ice Thickness Measurements | |
|---|---|
| Location | Thickness |
| Upper | 0.23 inch |
| Lower Surface | 0.20 inch |
| "MidRIDGE" | 0.36 inch |

Notes:
$T_{model}$ – The reading of three thermocouples installed on the model
$T_1$ – On the surface of the hybrid model aft-body
$T_2$ – Inside the hybrid model aft-body massive aluminum body
$T_3$ – Embedded inside the pneumatic boot of the hybrid model leading edge

Description/comments: Run 2/2 repeated run 2/1, except a rest interval of 1 minute was used in an effort to see if a shorter rest interval resulted in less intercycle ice. The 1-minute rest interval corresponds with a heavy ice rest cycle used on some automatically cycled deicer systems. The front leading edge collected rough glaze ice, while the lower leading edge had feathers of a height greater than a 1/4 inch, and the upper leading edge had columnar feathers of a height much greater than a 1/4 inch. A very large ridge formed in the middle of the leading edge, over the stagnation line, where two pneumatic boot tubes meet. This ridge was only attached to the leading edge at the locations where the pneumatic tubes ended at the walls of the tunnel, a region with no pneumatic boot movement. This region with no active boot coverage is artificial, since the particular model used does not represent an actual wing in its length (the model used was less than a third as long as a real wing). Upon attempting to trace the wing, this ridge broke off at the lightest touch, demonstrating that its adhesion to the boot ends was very low and what held this ridge in place during the formation process was aerodynamic forces on this artificially short wing section model.

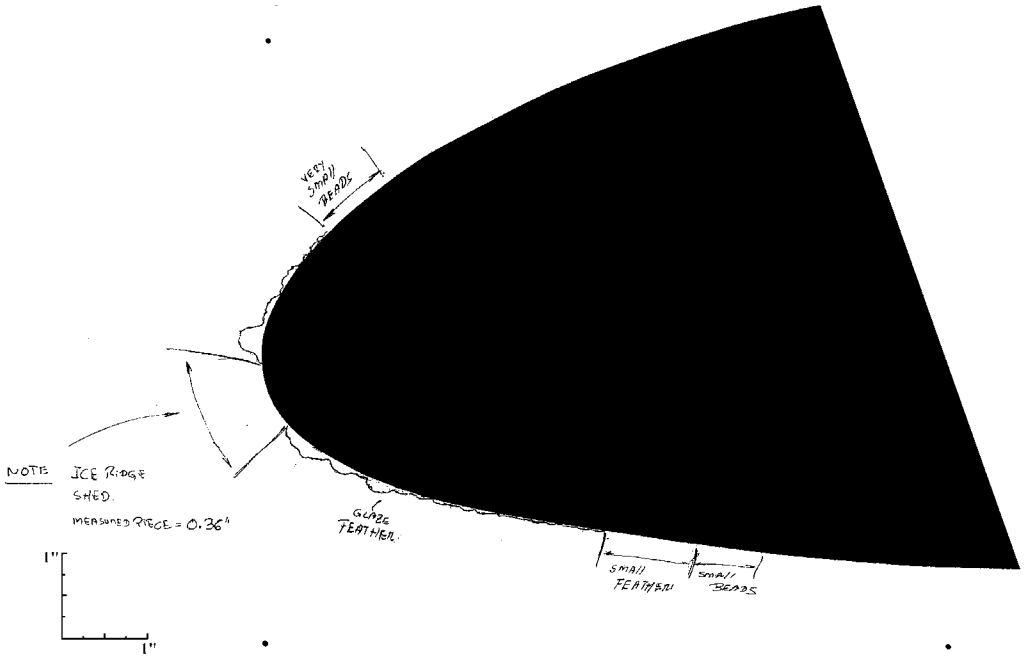


Figure 44. Tracing of Run 2/2

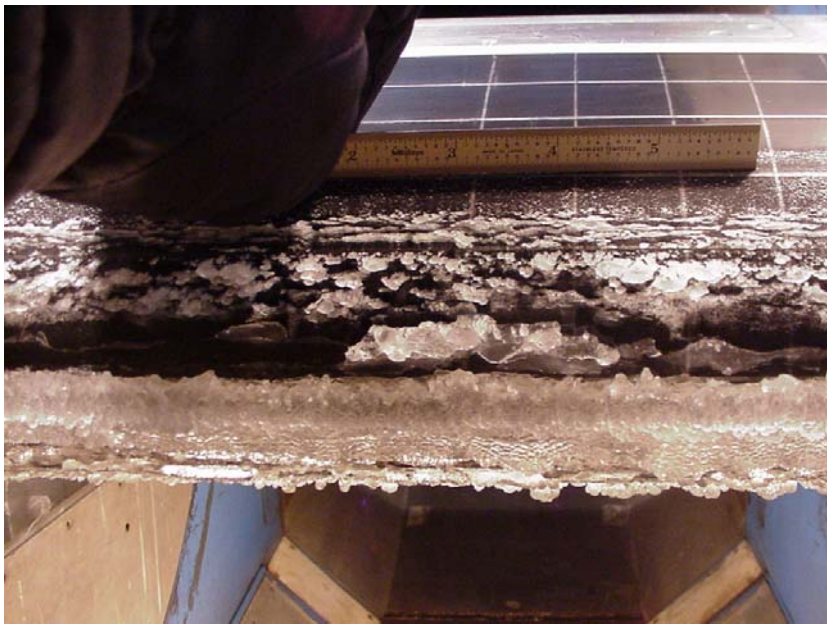

Figure 45. Photograph of Run 2/2 (Upper Surface Leading Edge)

Table 15. Run 4/1 Test Parameters

| Date 3/9/00 | | Run 4/1 | | AOA: +4° | | No Mold | Flap Angle: +2° | | | |
|---|---|---|---|---|---|---|---|---|---|---|
| | | | | | | | Boot Settings | | | Spray Off Time |
| $T_{model}$ (°F) | $T_{st}$ (°F) | $T_{tot}$ (°F) | V (mph) | MVD (μm) | LWC ($g/m^3$) | Time (min:sec) | Initial Fire | Cycle | Activation | |
| 25.4 | 21(21.4) | 27 | 195 | 20 | 0.51 | 6:11 | 15:25:21 | 3:00 | ID 0:11 | 15:31:21 |
| 25.5 | | | | | | | | | | |
| 26.5 | | | | | | | | | | |

| Tracing Location |
|---|
| Center |
| Left 6″ |

| Ice Thickness Measurements | |
|---|---|
| Location | Thickness |
| Upper 2″ | 0.32 inch |
| Stagnation | 0.16 inch |
| Lower 2.25″ | 0.30 inch |
| Upper 2.25″ | 0.42 inch |
| Stagnation | 0.20 inch |
| Lower 2.0″ | 0.27 inch |

Notes:
$T_{model}$ – The reading of three thermocouples installed on the model; (model = 1, 2, or 3)
$T_1$ – On the surface of the hybrid model aft-body
$T_2$ – Inside the hybrid model aft-body massive aluminum body
$T_3$ – Embedded inside the pneumatic boot of the hybrid model leading edge

Description/comments: Following an 11-second ice detector response time, the deicer was cycled twice after a 3-minute rest interval. The testing was terminated after the second rest interval to simulate exposure to a 14 CFR Part 25, Appendix C icing cloud. The front leading edge collected rough glaze ice, while the lower leading edge had columnar feathers of a height greater than a 1/4 inch and the upper leading edge had horn feathers of a height much greater than a 1/4 inch. Icing on the lower surface extended beyond the pneumatic boot coverage area. On the upper surface, there was an appreciable amount of runback ice, but none beyond the boot coverage region.

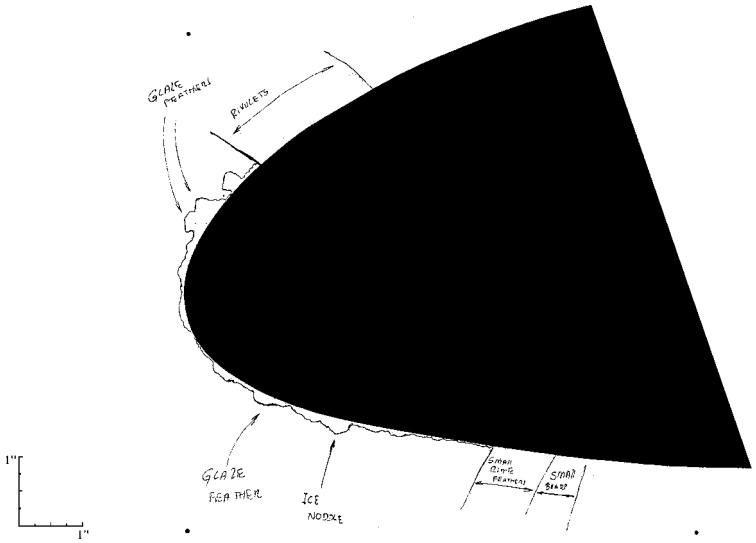


Figure 46. Tracing of Run 4/1

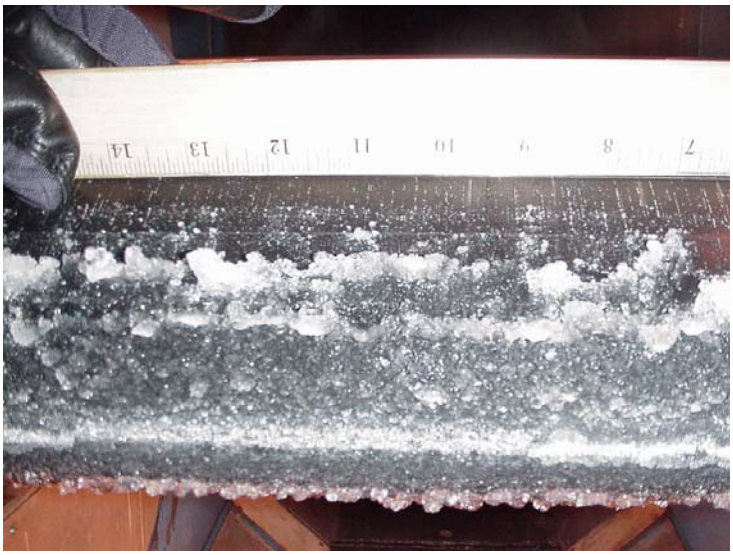

Figure 47. Photograph of Run 4/1 (Upper Surface Leading Edge)

Table 16. Run 4/1.5 Test Parameters

| Date 3/15/00 | | Run 4/1.5 | | AOA: +4° | | No Mold | Flap Angle: +2° | | | |
|---|---|---|---|---|---|---|---|---|---|---|
| | | | | | | | Boot Settings | | | Spray Start and Spray Off Time |
| $T_{model}$ (°F) | $T_{st}$ (°F) | $T_{tot}$ (°F) | V (mph) | MVD (μm) | LWC ($g/m^3$) | Time (min:sec) | Initial Fire | Cycle | Activation | |
| 28.7 | 21 (20.7) | 27.4 | 195 | 20 | 0.51 | 6:11 | 14:13:37 | 1:00 | ID 0:11 | 14:13:26<br>14:19:37 |
| 28.8 | | | | | | | | | | |
| 31.2 | | | | | | | | | | |

| Tracing Location |
|---|
| Center |
| Left 2″ |

| Ice Thickness Measurements | |
|---|---|
| Location | Thickness |
| Upper 2.25″ | 0.16 inch |
| Stagnation | 0.14 inch |
| Lower 1.25″ | 0.11 inch |
| Upper 2.25″ | 0.20 inch |
| Upper 1.25″ | 0.17 inch |
| Stagnation | 0.11 inch |
| Lower 1.25″ | 0.17 inch |

Notes:

$T_{model}$ – The reading of three thermocouples installed on the model

$T_1$ – On the surface of the hybrid model aft-body

$T_2$ – Inside the hybrid model aft-body massive aluminum body

$T_3$ – Embedded inside the pneumatic boot of the hybrid model leading edge

Description/comments: Run 4/1.5 was a repeat of run 4/1, but with 1-minute deicer rest intervals. Ice did not begin to form until after the first boot cycle. There was very little intercycle ice and not a lot of residual ice on this run.

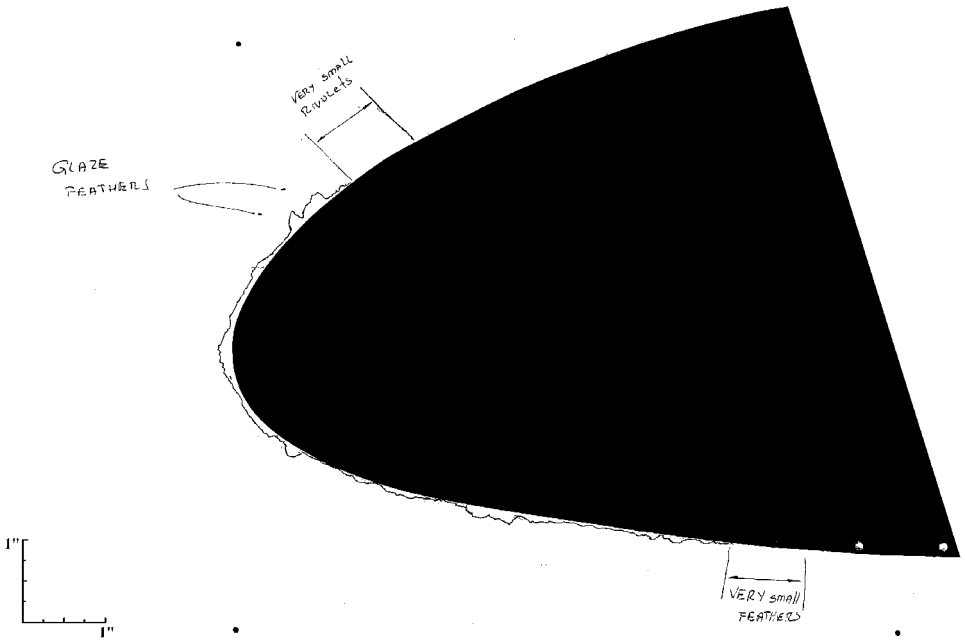


Figure 48. Tracing of Run 4/1.5

Figure 49. Photograph of Run 4/1.5 (Upper Surface Leading Edge)

Table 17. Run 6/1B Test Parameters

| Date 3/13/00 | | Run 6/1B | | AOA: +4° | | No Mold | Flap Angle: +2° | | | |
|---|---|---|---|---|---|---|---|---|---|---|
| | | | | | | | Boot Settings | | | Spray Start and Spray Off Time |
| $T_{model}$ (°F) | $T_{st}$ (°F) | $T_{tot}$ (°F) | V (mph) | MVD (μm) | LWC ($g/m^3$) | Time (min:sec) | Initial Fire | Cycle | Activation | |
| 22.6 | 14 (14.6) | 21.9 | 195 | 20 | 1.87 | 12:03 | 11:44:23 | 3:00 | ID 0:03 | 11:44:20 11:56:23 |
| 22.3 | | | | | | | | | | |
| 24.0 | | | | | | | | | | |

| Tracing Location |
|---|
| Center |
| Left 4.5″ |
| |
| Right 3″ |

| Ice Thickness Measurements | |
|---|---|
| Location | Thickness |
| 2.75″ Up | 0.84 inch |
| Stagnation | 0.35 inch |
| 2.25″ Down | 0.82 inch |
| 2.75″ Up | 0.64 inch |
| Stagnation | 0.38 inch |
| 2.25″ Down | 0.44 inch |
| 2.75″ Up | 0.90 inch |
| Stagnation | 0.39 inch |
| 2.25″ Down | 0.44 inch |

Notes:
$T_{model}$ – The reading of three thermocouples installed on the model
$T_1$ – On the surface of the hybrid model aft-body
$T_2$ – Inside the hybrid model aft-body massive aluminum body
$T_3$ – Embedded inside the pneumatic boot of the hybrid model leading edge

Description/comments: Following a 3-second ice detector response time, the deicer was cycled four times with 3-minute rest intervals, as in 14 CFR Part 25, Appendix C intermittent maximum icing conditions. The wing was clean at the initial boot fire, with considerable ice buildup between boot cycles. However, when the boot fired, there was minimal residual ice on most of the leading edge, but there were small amounts of ice remaining on the aft portion of the boot.

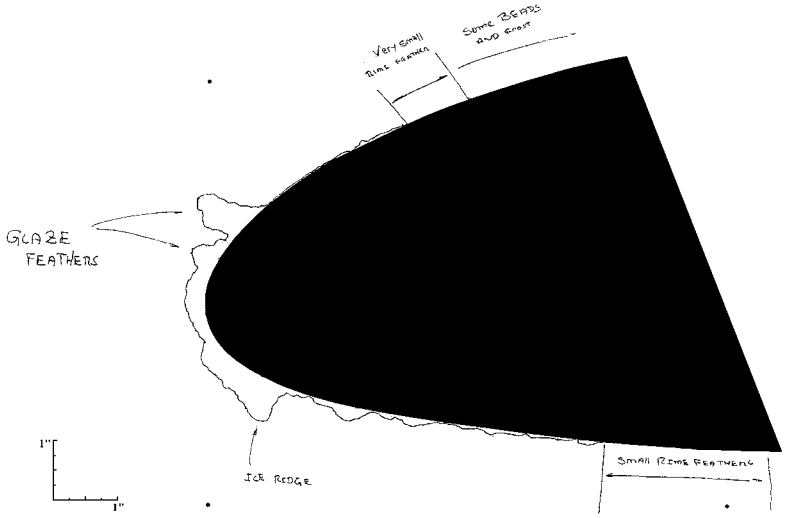


Figure 50. Tracing of Run 6/1B

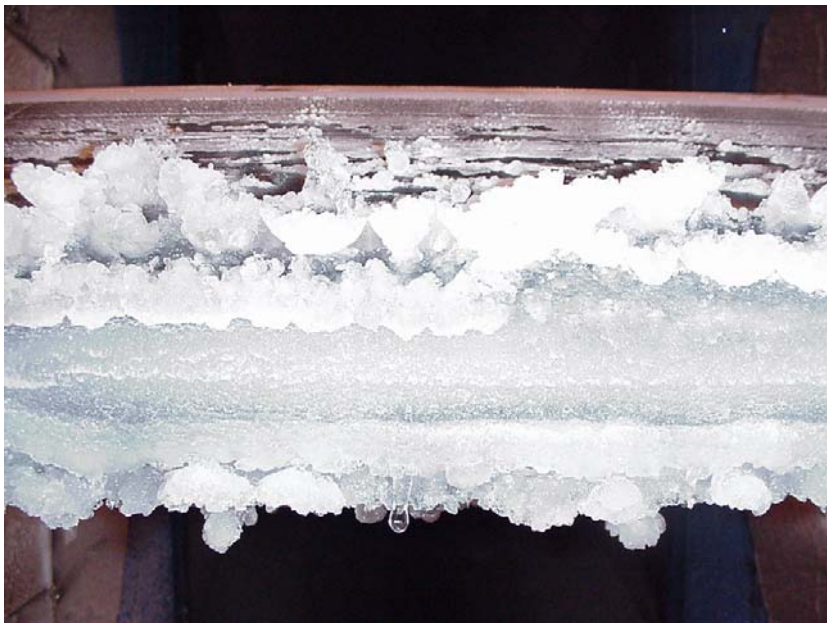

Figure 51. Photograph of Run 6/1B (Upper Surface Leading Edge)

Table 18. Run 6/1A Test Parameters

| Date 3/13/00 | | Run 6/1A | | AOA: +4° | | No Mold | Flap Angle: +2° | | | |
|---|---|---|---|---|---|---|---|---|---|---|
| | | | | | | | Boot Settings | | | Spray Start and Spray Off Time |
| $T_{model}$ (°F) | $T_{st}$ (°F) | $T_{tot}$ (°F) | V (mph) | MVD (μm) | LWC ($g/m^3$) | Time (min:sec) | Initial Fire | Cycle | Activation | |
| 20.6 | 14 (13.7) | 20.8 | 195 | 20 | 1.87 | 2:00 | 10:53:39 | 1:00 | ID 0:00 | 10:53:39<br>10:55:38 |
| 20.7 | | | | | | | | | | |
| 24.9 | | | | | | | | | | |

| Tracing Location | Ice Thickness Measurements | |
|---|---|---|
| | Location | Thickness |
| | 2″ Up | 0.42″ |
| Stagnation | | 0.20″ |
| Center | 1.25″ Down | 0.15″ |

Notes:
$T_{model}$ – The reading of three thermocouples installed on the model
$T_1$ – On the surface of the hybrid model aft-body
$T_2$ – Inside the hybrid model aft-body massive aluminum body
$T_3$ – Embedded inside the pneumatic boot of the hybrid model leading edge

Description/comments: Run 6/1A was a repeat of run 6/1B, but with a deicer rest interval of 1minute and two cycles of the deicer to simulate exposure to 14 CFR Part 25, Appendix C intermittent icing. The ice did not shed from the leading edge on the first boot cycle. The ice shed cleanly on the second boot cycle.

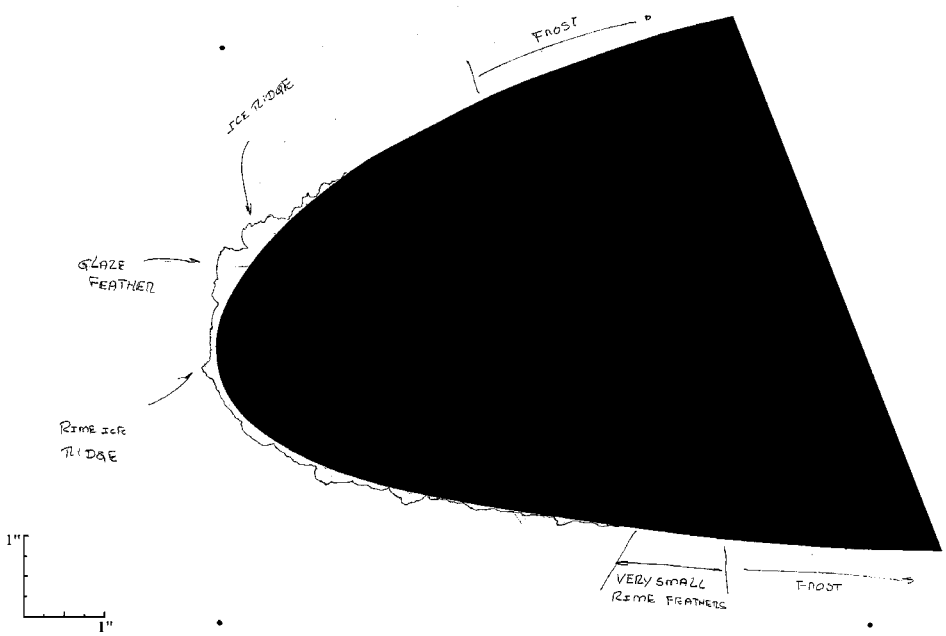


Figure 52. Tracing of Run 6/1A

Figure 53. Photograph of Run 6/1A (Upper Surface Leading Edge)

Table 19. Run 3/4A Test Parameters

| Date 3/9/00 | | Run 3/4A | | AOA: +0° | | No Mold | Flap Angle: +-3.5° | | | |
|---|---|---|---|---|---|---|---|---|---|---|
| | | | | | | | Boot Settings | | | Spray Start and Spray Off Time |
| $T_{model}$ (°F) | $T_{st}$ (°F) | $T_{tot}$ (°F) | V (mph) | MVD (μm) | LWC ($g/m^3$) | Time (min:sec) | Initial Fire | Cycle | Activation | |
| 21.4 | 14(14.4) | 21.4 | 195 | 20 | 0.45 | 12:11 | 11:00:19 | 3:00 | Immediate | 11:12:19 |
| 21.2 | | | | | | | | | | |
| 21.3 | | | | | | | | | | |

| Tracing Location |
|---|
| Center |
| Left 4.5″ |

| Ice Thickness Measurements | |
|---|---|
| Location | Thickness |
| Upper 1.25″ | 0.31 inch |
| Upper 2.25″ | 0.4 inch |
| Stagnation | 0.4 inch |
| Lower 1″ | 0.45 inch |
| Upper 2.25″ | 0.48 inch |
| Stagnation | 0.14 inch |
| Lower 0.75″ | 0.29 inch |

Notes:
$T_{model}$ – The reading of three thermocouples installed on the model
$T_1$ – On the surface of the hybrid model aft-body
$T_2$ – Inside the hybrid model aft-body massive aluminum body
$T_3$ – Embedded inside the pneumatic boot of the hybrid model leading edge

Description/comments: The deicer was initially cycled following an 11-second ice detector response time and then cycled one additional time after a 3-minute rest interval. After 3 minutes of additional exposure to the icing cloud, the testing was interrupted to simulate exposure to a 14 CFR Part 25, Appendix C continuous maximum icing cloud. The front leading edge collected rough glaze ice, while the lower leading edge had columnar feathers of a height greater than a 1/4 inch and the upper leading edge had horn feathers of a height much greater than a 1/4 inch. Icing on the lower leading-edge surface extended to beyond the pneumatic boot coverage area. An area left of center had in some places 1/2-inch-thick ice. This region was thought to be an accretion on top of random residual ice; thus, it is not to be considered representative.

Testing was continued for an additional two cycles of the deicer to achieve a stable intercycle ice accretion. Run 3/4A was a continuation run of the previous run (3/4).

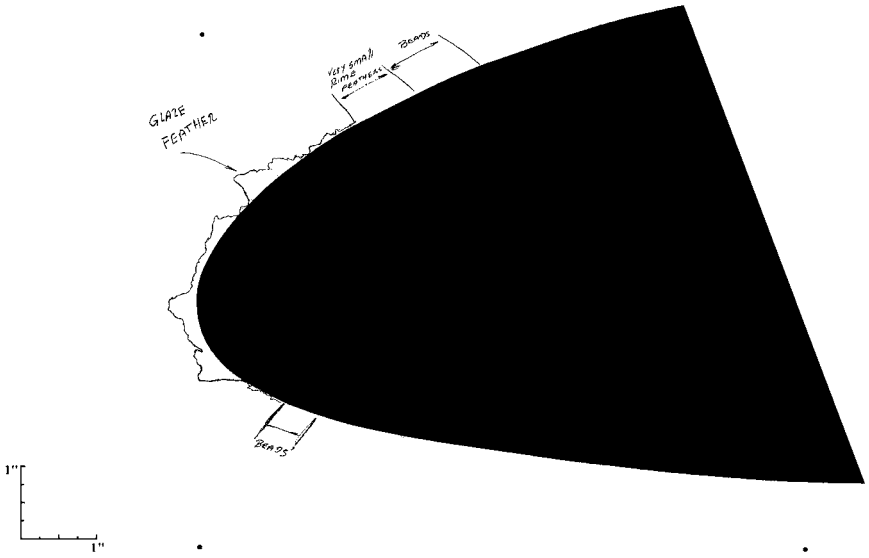


Figure 54. Tracing of Run 3/4A

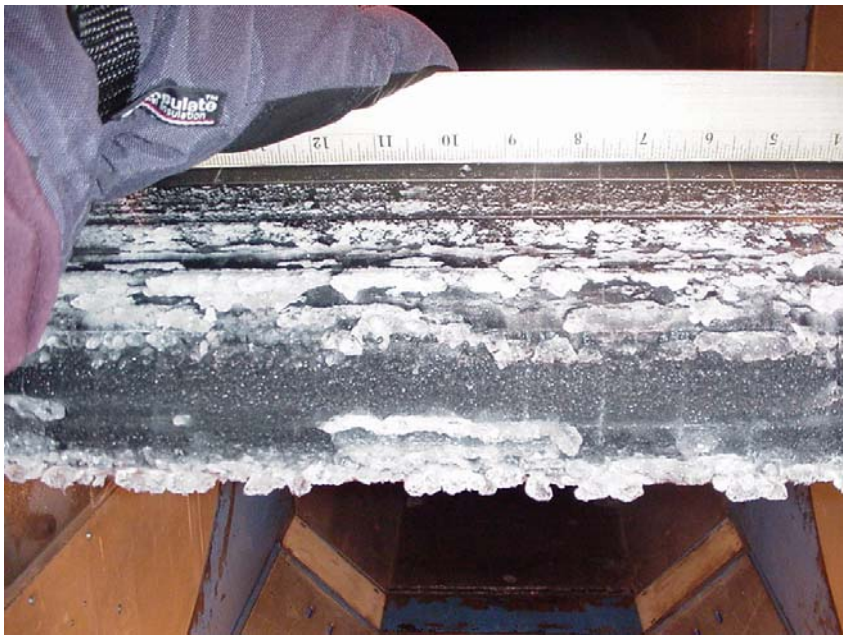

Figure 55. Photograph of Run 3/4A (Upper Surface Leading Edge)

Table 20. Run 3/4.5 Test Parameters

| Date 3/9/00 | | Run 3/4.5 | | AOA: +0° | | No Mold | Flap Angle: -3.5° | | | |
|---|---|---|---|---|---|---|---|---|---|---|
| $T_{model}$ (°F) | $T_{st}$ (°F) | $T_{tot}$ (°F) | V (mph) | MVD (μm) | LWC ($g/m^3$) | Time (min:sec) | Boot Settings | | | Spray Off Time |
| | | | | | | | Initial Fire | Cycle | Activation | |
| 21.7 | 14(13.5) | 20.5 | 195 | 20 | 0.45 | 6:11 | 11:45:02 | 1:00 | ID 0:11 | 11:51:21 |
| 21.3 | | | | | | | | | | |
| 20.6 | | | | | | | | | | |

| Tracing Location |
|---|
| Center |
| Left 5.0″ |

| Ice Thickness Measurements | |
|---|---|
| Location | Thickness |
| Upper 1.25″ | 0.27 inch |
| Stagnation | 0.14 inch |
| Lower 1.25″ | 0.23 inch |
| Upper 2.25″ | 0.15 inch |
| Stagnation | 0.31 inch |
| Lower 1.25″ | 0.15 inch |

Notes:
$T_{model}$ – The reading of three thermocouples installed on the model
$T_1$ – On the surface of the hybrid model aft-body
$T_2$ – Inside the hybrid model aft-body massive aluminum body
$T_3$ – Embedded inside the pneumatic boot of the hybrid model leading edge

Description/comments: Run 3/4.5 was a repeat of run 3/4, but with 1-minute deicer rest intervals. The front leading edge collected rough glaze ice, while the lower leading edge had columnar feathers of a height greater than a 1/4 inch and the upper leading edge had horn feathers of a height slightly less than a 1/4 inch. Jagged ice pieces were left from each boot cycle. Clearly, the boots removed most of the ice, but at the 1-minute cycling rate, some ice pieces remained that later acted like ice collectors.

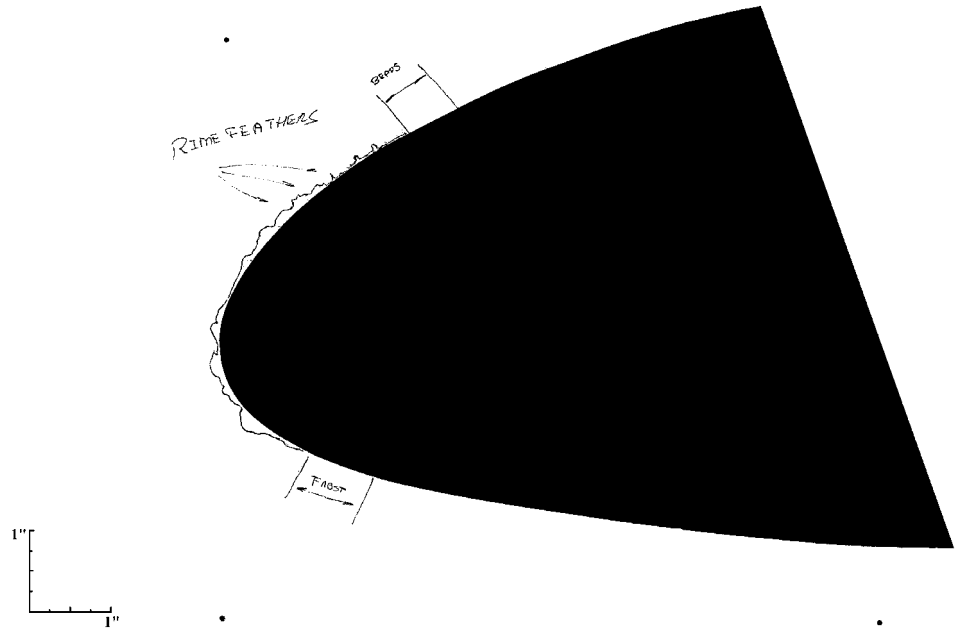


Figure 56. Tracing of Run 3/4.5

Figure 57. Photograph of Test 3/4.5 (Upper Surface Leading Edge)

4.1.2.2 Icing Cloud Horizontal Extent and Number of Deicer Cycles Effects.

In determining the deicer intercycle ice accretion, the question may be asked as to whether or not the intercycle ice accretion should reflect exposure to the 14 CFR Part 25, Appendix C standard icing cloud horizontal extents or to a continuous exposure within a single icing cloud. The 14 CFR Part 25, Appendix C standard horizontal extent for a continuous maximum (stratiform) icing cloud is 17.4 nmi, and 2.6 nmi for a intermittent maximum (cumuliform) icing cloud. At an airspeed of 169.3 kts, a 14 CFR Part 25, Appendix C continuous maximum icing cloud would be traversed in 6.2 minutes, and in 0.9 minute for a 14 CFR Part 25, Appendix C intermittent maximum icing cloud. Alternatively, air traffic control may request that an airplane be flown in a tight flight pattern within a single icing cloud.

For 14 CFR Part 25, Appendix C continuous maximum mixed ice icing conditions, figures 41 and 43 compare intercycle ice accretions that resulted from exposure to a continuous icing cloud and to a 14 CFR Part 25, Appendix C continuous maximum icing cloud standard horizontal extent. The deicer operation for these test runs was a 3-minute automatic cycling of the deicer following initial deicer activation at the first detection of icing when the model AOA was 4°. A similar comparison for 14 CFR Part 25, Appendix C continuous maximum glaze ice icing conditions can be made by comparing figures 59 and 47. For the 0° descent AOA and continuous maximum mixed ice icing conditions, figures 55 and 58 provide the comparison, as the intercycle ice accretions are similar.

For 14 CFR Part 25, Appendix C intermittent maximum icing conditions with a cloud drop MVD of 40 μm, the 0.52 g/m$^3$ LWC was not achieved during the test. To obtain an estimate of the deicer intercycle ice accretion for the 0.9-minute exposure to the 14 CFR Part 25, Appendix C intermittent maximum cloud horizontal extent, the icing exposure was simulated by duplicating the 14 CFR Part 25, Appendix C water catch with only one deicer cycle. The water catch was

accumulated after 2 minute of exposure at an IWT LWC of 0.25 g/m$^3$, compared with a 0.9-minute exposure at the 14 CFR Part 25, Appendix C LWC of 0.52 g/m$^3$. The simulated standard extent 14 CFR Part 25, Appendix C intermittent maximum icing cloud intercycle ice accretion shown in figure 63 can be compared with the continuous intermittent maximum cloud extent (at or near the 14 CFR Part 25, Appendix C LWC of 0.52 g/m$^3$) intercycle ice accretions shown in figure 65 for two cycles of the deicer and in figure 67 for four deicer cycles. Note that this scale technique to achieve 14 CFR Part 25, Appendix C icing conditions that are not within the capability of an icing wind tunnel does not conform with accepted ice accretion scaling practices. Using the 0.25 g/m$^3$ LWC rather than the correct 0.52 g/m$^3$ LWC results in different freezing fractions and probably different ice accretions. Considering the differences in LWC and water catch for this case, the intercycle ice accretions appear similar.

Comparing the following figures indicates that there are minor differences between two and four cycles of the deicer with varying icing conditions and model AOA: figures 43 and 41, 47 and 59, 60 and 51, 65 and 67, 61 and 55, and 71 and 73.

As in the December 1999 IWT test of the 36-inch NACA 23012 model, the intercycle ice accretions achieved a steady-state character after the first few cycles of the deicer.

Table 21. Run 4/1A Test Parameters

| Date 3/9/00 | | Run 4/1A | | AOA: +4° | | No Mold | Flap Angle: +2° | | | |
|---|---|---|---|---|---|---|---|---|---|---|
| $T_{model}$ (°F) | $T_{st}$ (°F) | $T_{tot}$ (°F) | V (mph) | MVD (μm) | LWC (g/m$^3$) | Time (min:sec) | Boot Settings | | | Spray Off Time |
| | | | | | | | Initial Fire | Cycle | Activation | |
| 28.3 | 21(21.5) | 28.4 | 195 | 20 | 0.51 | 12:11 | 16:11:30 | 3:00 | ID 0:11 | 16:20:19 |

| |
|---|
| 28.5 |
| 27.7 |

| Tracing Location |
|---|
| Center |
| Right 3″ |

| Ice Thickness Measurements | |
|---|---|
| Location | Thickness |
| Upper 2″ | 0.29 inch |
| Stagnation | 0.14 inch |
| Lower 3″ | 0.29 inch |
| Upper 2″ | 0.44 inch |
| Stagnation | 0.12 inch |
| Lower 3″ | 0.40 inch |

Notes:
$T_{model}$ – The reading of three thermocouples installed on the model
$T_1$ – On the surface of the hybrid model aft-body
$T_2$ – Inside the hybrid model aft-body massive aluminum body
$T_3$ – Embedded inside the pneumatic boot of the hybrid model leading edge

Description/comments: Following an 11-second ice detector response time, the deicer was cycled four times with 3-minute rest intervals to establish a stable intercycle ice accretion. The front leading edge had rough glaze ice, while the lower leading edge had columnar feathers of a height greater than a 1/4 inch and the upper leading edge had horn feathers of a height much greater than a 1/4 inch. Icing on the lower surface extended beyond the pneumatic boot coverage area. On the upper surface, there was some runback ice, but none beyond the boot coverage region.

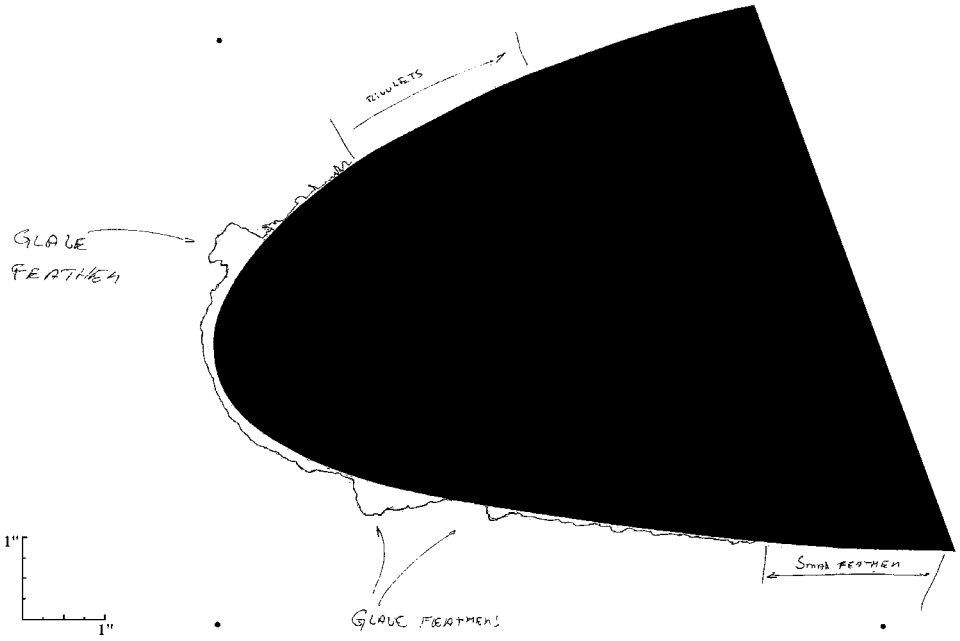


Figure 58. Tracing of Run 4/1A

Figure 59. Photograph of Run 4/1A (Upper Surface Leading Edge)

Table 22. Test Parameters for Run 3/4

| Date 3/9/00 | | Run 3/4 | | AOA: +0° | | No Mold | Flap Angle: -3.5° | | | |
|---|---|---|---|---|---|---|---|---|---|---|
| $T_{model}$ (°F) | $T_{st}$ (°F) | $T_{tot}$ (°F) | V (mph) | MVD (μm) | LWC ($g/m^3$) | Time (min:sec) | Boot Settings | | | Spray Off Time |
| | | | | | | | Initial Fire | Cycle | Activation | |
| 20.1 | 14(13.7) | 20.6 | 195 | 20 | 0.51? | 6:11 | 10:31:21 | 3:00 | ID 0:11 | 10:37:21 |
| 20.0 | | | | | | | | | | |
| 20.4 | | | | | | | | | | |

| Tracing Location |
|---|
| Center |
| Left 4″ |

| Ice Thickness Measurements | |
|---|---|
| Location | Thickness |
| Upper | 0.38 inch |
| Stagnation | 0.20 inch |
| Lower | 0.39 inch |
| Upper | 0.29 inch |
| Stagnation | 0.22 inch |
| Lower | 0.35 inch |

Notes:
$T_{model}$ – The reading of three thermocouples installed on the model
$T_1$ – On the surface of the hybrid model aft-body
$T_2$ – Inside the hybrid model aft-body massive aluminum body
$T_3$ – Embedded inside the pneumatic boot of the hybrid model leading edge

Description/comments: Following an 11-second ice detector response time, the deicer was cycled twice with 3-minute rest intervals to simulate exposure to a 14 CFR Part 25, Appendix C continuous maximum icing cloud. The front leading edge collected rough glaze ice, while the lower leading edge had columnar feathers of roughness greater than a 1/4 inch and the upper leading edge had horn feathers of roughness much greater than a 1/4 inch. No runback ice was observed on either the upper or lower surfaces.

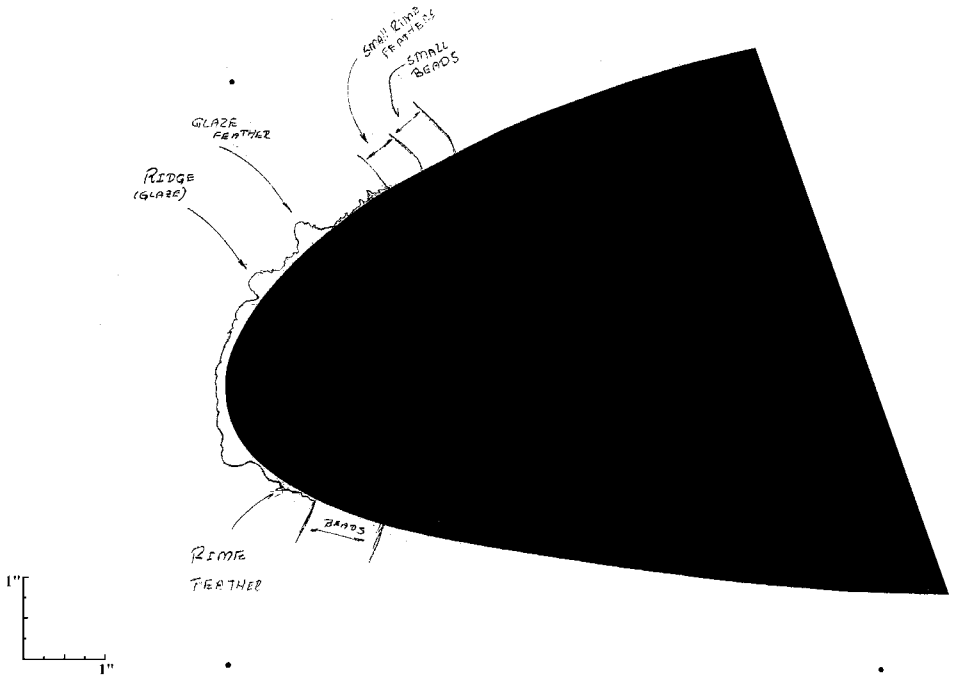


Figure 60. Tracing of Run 3/4

Figure 61. Photograph of Run 3/4 (Upper Surface Leading Edge)

Table 23. Run 3/6 Test Parameters

| Date 3/10/00 | | Run 3/6 | | AOA: +4° | | No Mold | Flap Angle: +2° | | | |
|---|---|---|---|---|---|---|---|---|---|---|
| $T_{model}$ (°F) | $T_{st}$ (°F) | $T_{tot}$ (°F) | V (mph) | MVD (μm) | LWC ($g/m^3$) | Time (min:sec) | Boot Settings | | | Spray Off Time |
| | | | | | | | Initial Fire | Cycle | Activation | |
| 21.3 | 14 (13.6) | 20.7 | 195 | 40 | 0.25 | 2:28 | 13:20:32 | N/A | Man. 0:19 | 13:22:32 |

| $T_1$ (°F) |
|---|
| 21.4 |
| 19.6 |

| Tracing Location |
|---|
| Center |

| Ice Thickness Measurements | |
|---|---|
| Location | Thickness |
| Upper 0.25″ | 0.15 |
| Stagnation | 0.10 |
| Lower 0.25″ | 0.33 |

Notes:
$T_{model}$ – The reading of three thermocouples installed on the model
$T_1$ – On the surface of the hybrid model aft-body
$T_2$ – Inside the hybrid model aft-body massive aluminum body
$T_3$ – Embedded inside the pneumatic boot of the hybrid model leading edge

Description/comments: This run was performed to obtain the intercycle ice for Appendix C by duplicating the water catch. (This procedure is not appropriate since changing the LWC changes the ice accretion freezing fraction, thereby altering the ice shape development.) The water catch for 0.9 minute at the Appendix C LWC of 0.52 $g/m^3$ was simulated by a 2-minute exposure at an IWT LWC of 0.25 $g/m^3$. The same conditions were used as in run 4/4, but at a lower temperature. This could be termed a mixed icing tunnel run for the purpose of gauging ice thickness before boot activation. At this AOA, an ice of height greater than a 1/4 inch was observed only on the lower leading edge.

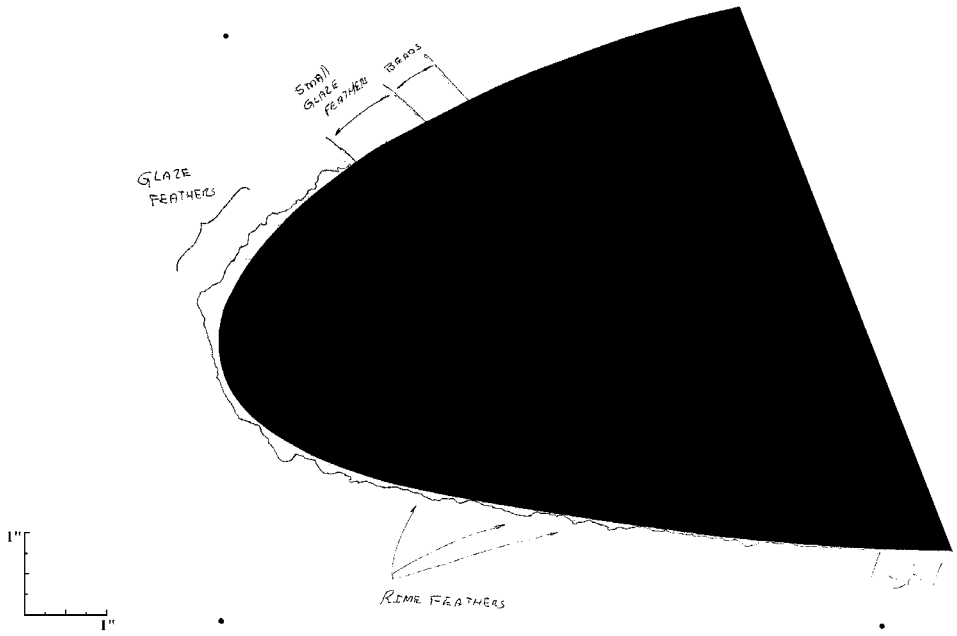


Figure 62. Tracing of Run 3/6

Figure 63. Photograph of Run 3/6 (Upper Surface Leading Edge)

Table 24. Run 6/6 Test Parameters

| Date 3/9/00 | | Run 6/6 | | AOA: +4° | | No Mold | Flap Angle: 2° | | | |
|---|---|---|---|---|---|---|---|---|---|---|
| | | | | | | | Boot Settings | | | Spray Off Time |
| $T_{model}$ (°F) | $T_{st}$ (°F) | $T_{tot}$ (°F) | V (mph) | MVD (µm) | LWC ($g/m^3$) | Time (min:sec) | Initial Fire | Cycle | Activation | |
| 22.1 | 14 (14.7) | 21.7 | 195 | 40 | 0.44 | 2:09 | 13:11:51 | 1:00 | ID 0:09 | 13:13:5 |
| 21.9 | | | | | | | | | | |
| 20.7 | | | | | | | | | | |

| Tracing Location |
|---|
| Center |
| Left 5.0″ |

| Ice Thickness Measurements | |
|---|---|
| Location | Thickness |
| Upper 1.25″ | 0.23 inch |
| Stagnation | 0.09 inch |
| Lower 2.00″ | 0.19 inch |
| Upper 1.25″ | 0.28 inch |
| Stagnation | 0.06 inch |
| Lower 2.00″ | 0.16 inch |

Notes:
$T_{model}$ – The reading of three thermocouples installed on the model
$T_1$ – On the surface of the hybrid model aft-body
$T_2$ – Inside the hybrid model aft-body massive aluminum body
$T_3$ – Embedded inside the pneumatic boot of the hybrid model leading edge

Description/comments: Following a 9-second ice detector response time, the deicer was cycled twice with 1-minute rest intervals to simulate a 14 CFR Part 25, Appendix C intermittent maximum icing cloud exposure. The front leading edge collected rough glaze ice, while the lower leading edge had columnar feathers of a height greater than a 1/4 inch and the upper leading edge had horn feathers of a height of around a 1/4 inch. Jagged ice pieces were left after each boot cycle. There was a substantial amount of ice on the lower boot, with considerable runback. Most of the ice ridges on the lower surface formed along the pneumatic boot stitches.

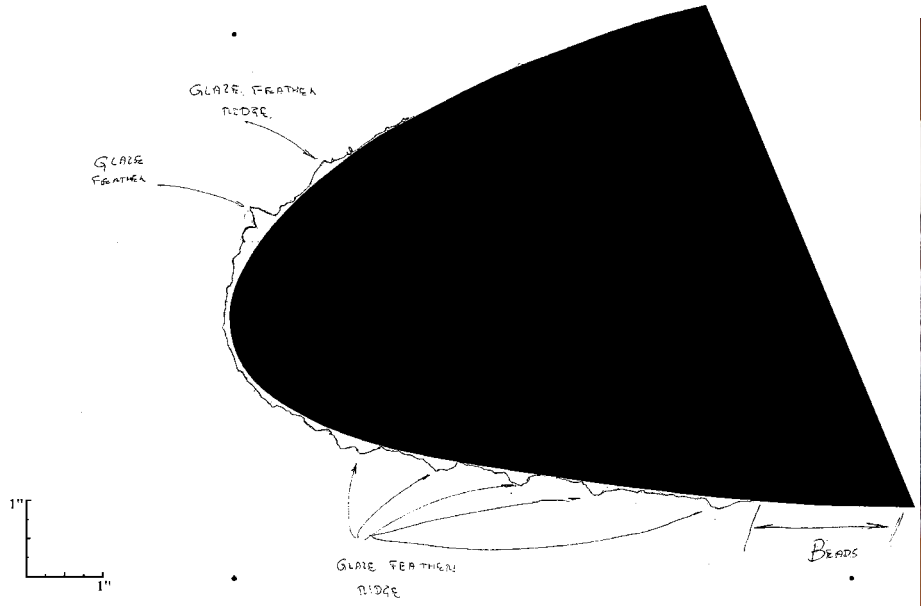


Figure 64. Tracing of Run 6/6

Figure 65. Photograph of Test 6/6 (Upper Surface Leading Edge)

Table 25. Run 6/5 Test Parameters

| Date 3/9/00 | | Run 6/5 | | AOA: +4° | | No Mold | Flap Angle: +2° | | | |
|---|---|---|---|---|---|---|---|---|---|---|
| | | | | | | | Boot Settings | | | Spray Off Time |
| $T_{model}$ (°F) | $T_{st}$ (°F) | $T_{tot}$ (°F) | V (mph) | MVD (μm) | LWC ($g/m^3$) | Time (min:sec) | Initial Fire | Cycle | Activation | |
| 21.7 | 14 (13.5) | 20.5 | 195 | 40 | 0.52 | 4:09 | 12:34:47 | 1:00 | ID 0:09 | 12:38:47 |
| 21.3 | | | | | | | | | | |
| 20.6 | | | | | | | | | | |

| Tracing Location |
|---|
| Center |
| Left 5.0″ |

| Ice Thickness Measurements | |
|---|---|
| Location | Thickness |
| Upper 1.25″ | 0.30 inch |
| Stagnation | 0.05 inch |
| Lower 2.00″ | 0.27 inch |
| Upper 1.25″ | 0.24 inch |
| Stagnation | 0.21 inch |
| Lower 2.00″ | 0.16 inch |

Notes:
$T_{model}$ – The reading of three thermocouples installed on the model
$T_1$ – On the surface of the hybrid model aft-body
$T_2$ – Inside the hybrid model aft-body massive aluminum body
$T_3$ – Embedded inside the pneumatic boot of the hybrid model leading edge
Description/comments: Following the 9-second ice detector response time, the deicer was cycled four times with rest intervals of 1 minute to establish a stable intercycle ice accretion. The front leading edge collected rough glaze ice, while the lower leading edge had columnar feathers of a height greater than a 1/4 inch and the upper leading edge had horn feathers of a height of around a 1/4 inch. Jagged ice pieces were left from each boot cycle. There was a substantial amount of ice on the lower boot and considerable runback.

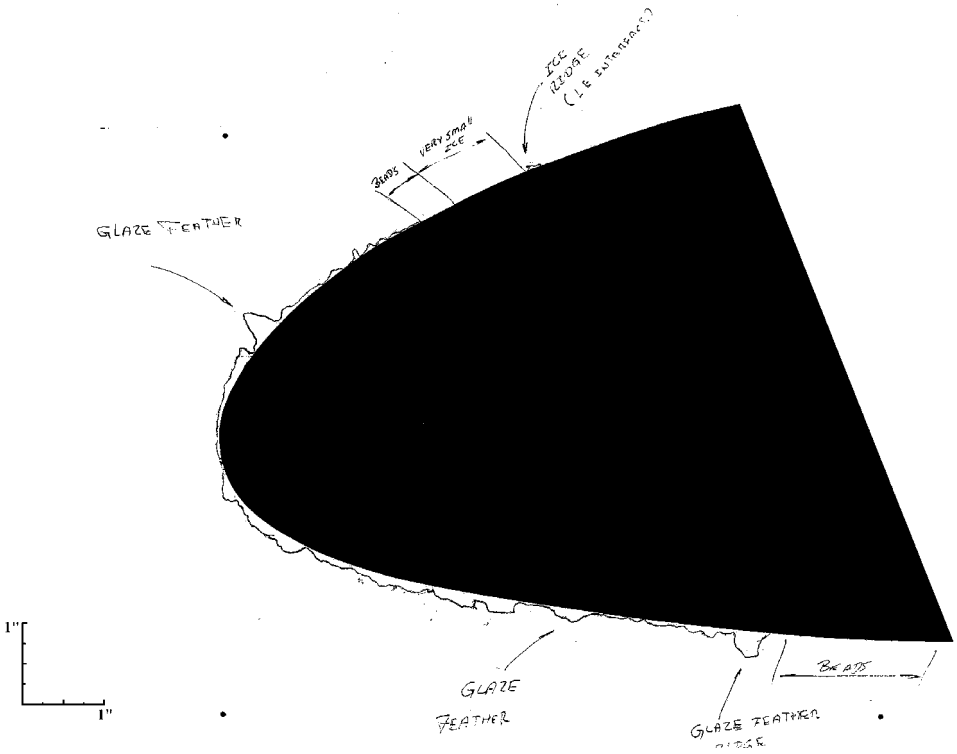


Figure 66. Tracing of Run 6/5

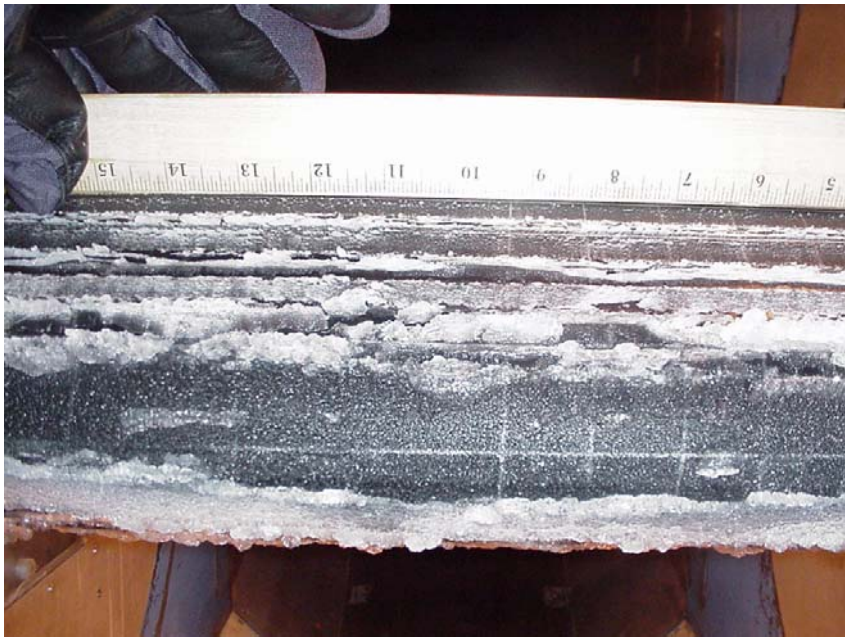

Figure 67. Photograph of Test 6/5 (Upper Surface Leading Edge)

Table 26. Run 6/1 Test Parameters

| Date 3/13/00 | | Run 6/1 | | AOA: +4° | | No Mold | Flap Angle: +2° | | | |
|---|---|---|---|---|---|---|---|---|---|---|
| | | | | | | | Boot Settings | | | Spray Start and Spray Off Time |
| $T_{model}$ (°F) | $T_{st}$ (°F) | $T_{tot}$ (°F) | V (mph) | MVD (µm) | LWC ($g/m^3$) | Time (min:sec) | Initial Fire | Cycle | Activation | |
| 19.6 | 14 (14.5) | 21.6 | 195 | 20 | 1.87 | 2:03 | 10:32;36 | 1:00 | ID 0:03 | 10:32:33 10:34:36 |
| 19.9 | | | | | | | | | | |
| 24.0 | | | | | | | | | | |

| Tracing Location |
|---|
| Center |

| Ice Thickness Measurements | |
|---|---|
| Location | Thickness |
| 2″ Up | 0.22″ |
| Stagnation | 0.23″ |
| 1.5″ Down | 0.20″ |

Notes:
$T_{model}$ – The reading of three thermocouples installed on the model
$T_1$ – On the surface of the hybrid model aft-body
$T_2$ – Inside the hybrid model aft-body massive aluminum body
$T_3$ – Embedded inside the pneumatic boot of the hybrid model leading edge

Description/comments: Following a 3-second ice detector response time, the deicer was cycled twice with 1-minute rest intervals to simulate exposure to a 14 CFR Part 25, Appendix C intermittent maximum icing cloud. The airfoil was clean after the first boot fire. In subsequent boot fires, there was residual ice at the boot stitch lines.

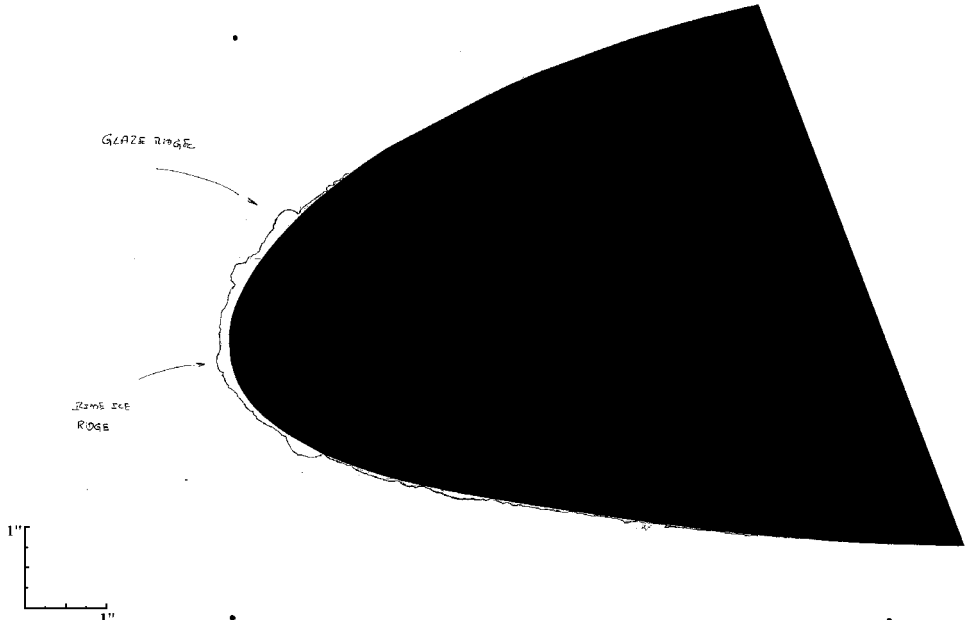


Figure 68. Tracing of Run 6/1

Figure 69. Photograph of Test 6/1 (Upper Surface Leading Edge)

Table 27. Run 6/4 Test Parameters

| Date 3/13/00 | | Run 6/4 | | AOA: 0° | | No Mold | Flap Angle: -3.5° | | | |
|---|---|---|---|---|---|---|---|---|---|---|
| | | | | | | | Boot Settings | | | Spray Start and Spray Off Time |
| $T_{model}$ (°F) | $T_{st}$ (°F) | $T_{tot}$ (°F) | V (mph) | MVD (μm) | LWC ($g/m^3$) | Time (min:sec) | Initial Fire | Cycle | Activation | |
| 21.0 | 14 (14.0) | 21.1 | 195 | 20 | 1.87 | 2:03 | 14:39:28 | 1:00 | ID 0:03 | 14:39:25 14:41:28 |
| 20.4 | | | | | | | | | | |
| 22.7 | | | | | | | | | | |

| Tracing Location |
|---|
| Center |

| Ice Thickness Measurements | |
|---|---|
| Location | Thickness |
| 2″ Up | 0.20 |
| Stagnation | 0.06 |
| 1.25″ Down | 0.23 |

Notes:
$T_{model}$ – The reading of three thermocouples installed on the model
$T_1$ – On the surface of the hybrid model aft-body
$T_2$ – Inside the hybrid model aft-body massive aluminum body
$T_3$ – Embedded inside the pneumatic boot of the hybrid model leading edge

Description/comments: Following a 3-second ice detector response time, the deicer was cycled twice with 1-minute rest intervals to simulate exposure to a 14 CFR Part 25, Appendix C intermittent maximum icing cloud. (Note that the LWC content was less than the Appendix C LWC of 2.21 $g/m^3$. The maximum IWT LWC capability was 1.95 $g/m^3$.) Ice began growing at the boot stitch lines after the initial boot fire. After the boot cycles, the leading edge was clean, but ice did remain in the stitch lines on the aft section of the boot.

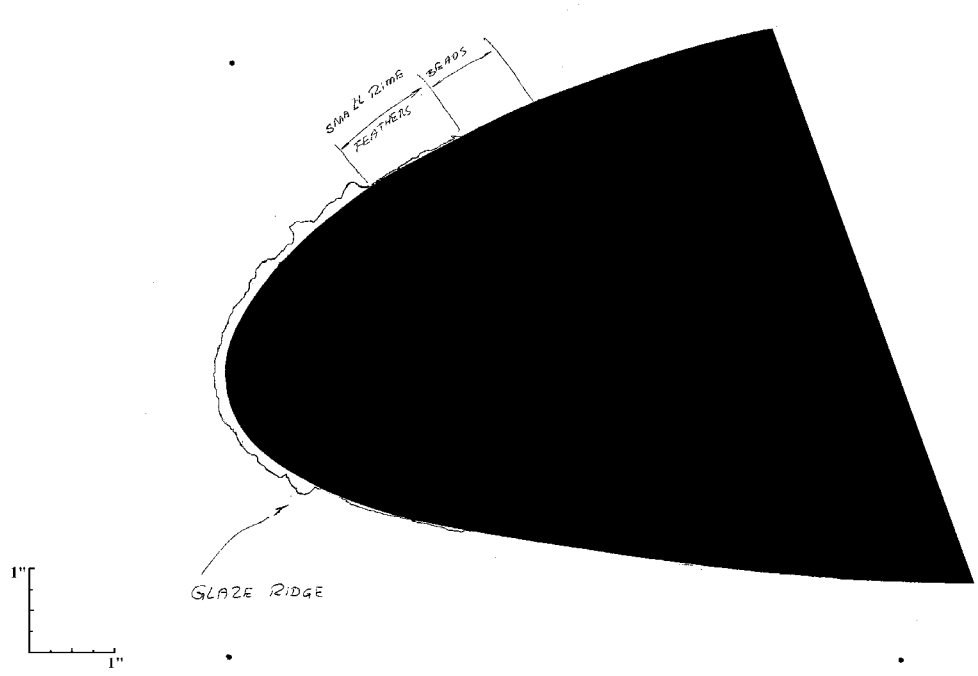


Figure 70. Tracing of Test 6/4

Figure 71. Photograph of Run 6/4 (Upper Surface Leading Edge)

Table 28. Run 6/4A Test Parameters

| Date 3/13/00 | | Run 6/4A | | AOA: 0° | | No Mold | Flap Angle: -3.5° | | | |
|---|---|---|---|---|---|---|---|---|---|---|
| | | | | | | | Boot Settings | | | Spray Start and Spray Off Time |
| $T_{model}$ (°F) | $T_{st}$ (°F) | $T_{tot}$ (°F) | V (mph) | MVD (μm) | LWC ($g/m^3$) | Time (min:sec) | Initial Fire | Cycle | Activation | |
| 20.0 | 14 (13.6) | 20.3 | 195 | 20 | 1.87 | 2:00 | 15:03:06 | 1:00 | ID 0:00 | 15:03:06 15:05:06 |
| 20.2 | | | | | | | | | | |
| 22.9 | | | | | | | | | | |

| Tracing Location |
|---|
| Center |

| Ice Thickness Measurements | |
|---|---|
| Location | Thickness |
| 2″ Up | 0.31″ |
| Stagnation | 0.22″ |
| 1.25″ Down | 0.34″ |

Notes:
$T_{model}$ – The reading of three thermocouples installed on the model
$T_1$ – On the surface of the hybrid model aft-body
$T_2$ – Inside the hybrid model aft-body massive aluminum body
$T_3$ – Embedded inside the pneumatic boot of the hybrid model leading edge

Description/comments: This run is a continuation of the previous run (6/4) to obtain a stable intercycle ice shape. The deicer was cycled twice again with 1-minute rest intervals to establish a stable intercycle ice accretion. (Note that the LWC content was less than the Appendix C LWC of 2.21 $g/m^3$. The maximum IWT LWC capability was 1.95 $g/m^3$.) There was residual ice at the leading edge after the initial boot fire. This ran along the leading edge to the walls of the wind tunnel. At the second boot fire, the leading edge was clean, but there was residual ice in the stitch lines on the rear section of the boot.

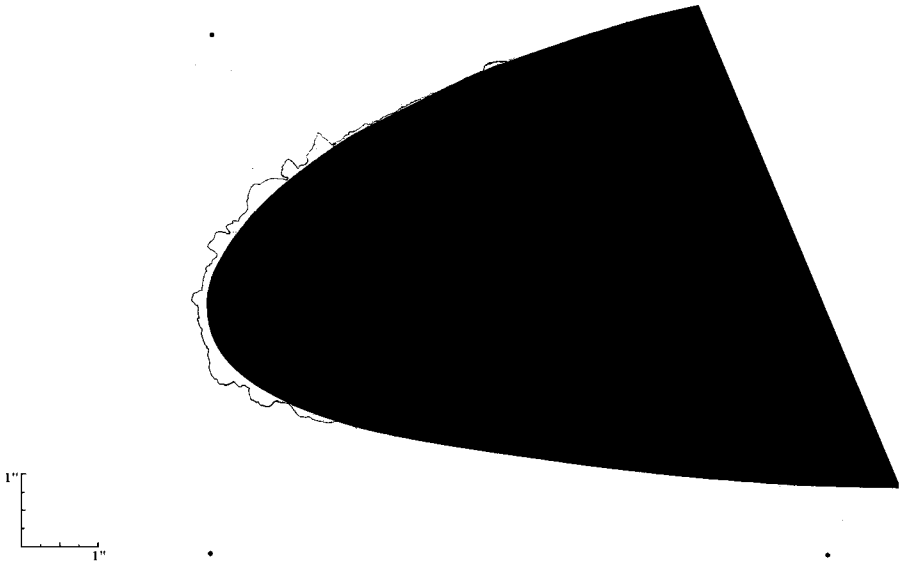


Figure 72. Tracing of Run 6/4A

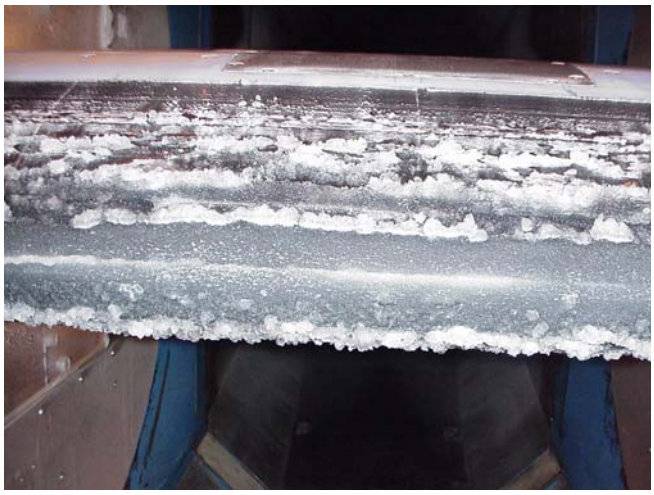

Figure 73. Photograph of Run 6/4A (Upper Surface Leading Edge)

4.1.2.3 Icing Conditions Effects.

As evident in table 3, the deicer intercycle ice accretion investigation included a variety of icing conditions and types of ice. For 14 CFR Part 25, Appendix C continuous maximum and intermittent maximum icing conditions, testing at different temperatures produced mixed, glaze, and rime ice. Data were also obtained with cloud drop MVDs of 20 and 40 μm.

Generally, variations of the deicer intercycle ice accretion characteristics at a cloud drop MVD of 20 μm and 14 CFR Part 25, Appendix C continuous maximum mixed, glaze, and rime icing conditions (model AOA of 4°) can be observed by comparing figures 41, 59, and 75. For 14 CFR Part 25, Appendix C intermittent maximum mixed and rime icing conditions, the variations in intercycle ice accretion characteristics are shown in figures 69 and 77.

The 20-μm intercycle ice accretion characteristic difference between 14 CFR Part 25, Appendix C continuous maximum and intermittent maximum mixed ice icing conditions, assuming the use of 3- and 1-minute cycling periods, respectively, can be seen by comparing figures 41 and 53. For rime ice, figures 75 and 77 provide a similar comparison.

For a cloud drop MVD of 40 μm and a model AOA of 4°, the variation of the deicer intercycle ice accretion characteristics at 14 CFR Part 25, Appendix C continuous maximum and intermittent maximum mixed ice conditions is shown in figures 81 and 67. Deicer intercycle ice accretion variations at 14 CFR Part 25, Appendix C intermittent maximum mixed and glaze icing conditions can be observed by comparing figure 60 with figures 81 and 83. Note that the data shown in figures 81 and 83 were obtained simulating the 14 CFR Part 25, Appendix C intermittent icing conditions LWC by attempting to duplicate the water catch for a standard cloud horizontal extent, similar to the test technique used for the data shown in figure 63.

Similarly, for a model AOA of 0° and a cloud drop MVD of 20 μm, the differences in deicer ice accretion characteristics for 14 CFR Part 25, Appendix C continuous maximum mixed and glaze

icing conditions are shown in figures 61 and 85. The differences between 14 CFR Part 25, Appendix C continuous and intermittent maximum mixed ice intercycle ice accretions can be seen by comparing figures 55 and 73. Figures 87 and 89 illustrate the deicer intercycle ice accretion for exposure to a 14 CFR Part 25, Appendix C intermittent maximum standard icing cloud extent, simulating the Appendix C water catch by extended exposure at a lower LWC than was within the capability of the IWT.

Table 29. Run 5/1 Test Parameters

| Date 3/10/00 | | Run 5/1 | | AOA: +4° | | No Mold | Flap Angle: +2° | | | |
|---|---|---|---|---|---|---|---|---|---|---|
| | | | | | | | Boot Settings | | | |
| $T_{model}$ (°F) | $T_{st}$ (°F) | $T_{tot}$ (°F) | V (mph) | MVD (μm) | LWC ($g/m^3$) | Time (min:sec) | Initial Fire | Cycle | Activation | Spray Off Time |
| -12.3 | -22(-17.5) | -10.6 | 195 | 20 | 0.15 | 12:34 | 16:39:42 | 3.00 | Manual | 16:51:42 |
| -12.2 | | | | | | | | | | |
| -12.1 | | | | | | | | | | |

| Tracing Location |
|---|
| Left 2.75″ |

| Ice Thickness Measurements | |
|---|---|
| Location | Thickness |
| Upper 1.25″ | 0.25 |
| Stagnation | 0.19 |
| Lower 1.0″ | 0.20 |

Notes:
$T_{model}$ – The reading of three thermocouples installed on the model
$T_1$ – On the surface of the hybrid model aft-body
$T_2$ – Inside the hybrid model aft-body massive aluminum body
$T_3$ – Embedded inside the pneumatic boot of the hybrid model leading edge

Description/comments: 14 CFR Part 25, Appendix C continuous maximum rime icing conditions. Considerable ice buildup can be observed. Complete removal of ice for each boot cycle was not observed, and residual ice fragments served as ice collection sites for intercycle ice. Ice accretion on the upper leading edge reached a 1/4 inch.

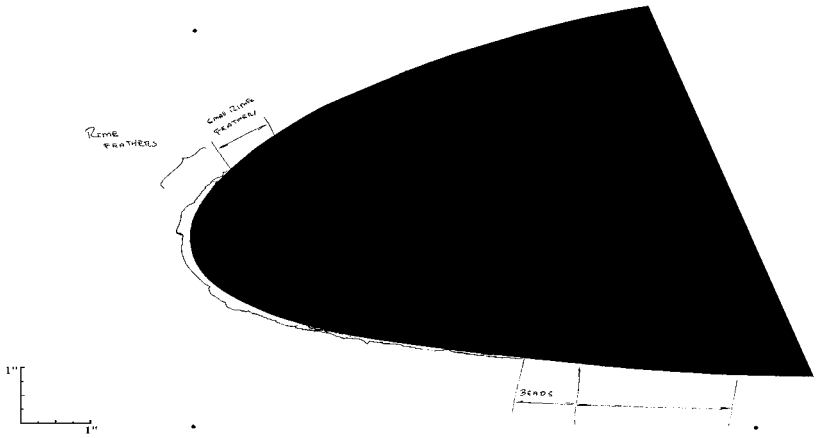


Figure 74. Tracing of Run 5/1

Figure 75. Photograph of Run 5/1 (Upper Surface Leading Edge)

Table 30. Run 5/5 Test Parameters

| Date 3/13/00 | | Run 5/5 | | AOA: +4° | | No Mold | Flap Angle: +2° | | | |
|---|---|---|---|---|---|---|---|---|---|---|
| | | | | | | | Boot Settings | | | Spray Start and Spray Off Time |
| $T_{model}$ (°F) | $T_{st}$ (°F) | $T_{tot}$ (°F) | V (mph) | MVD (µm) | LWC ($g/m^3$) | Time (min:sec) | Initial Fire | Cycle | Activation | |
| -17.7 | -22 (-21.9) | -14.9 | 195 | 20 | 0.85 | 2:06 | 09:25:10 | 1:00 | ID 0:06 | 09:25:04<br>09:27:10 |
| -18.0 | | | | | | | | | | |
| -8.8 | | | | | | | | | | |

| Tracing Location |
|---|
| Center |

| Ice Thickness Measurements | |
|---|---|
| Location | Thickness |
| 1.25″ Up | 0.14″ |
| Stagnation | 0.13″ |
| 0.5″ Down | 0.15″ |

Notes:
$T_{model}$ – The reading of three thermocouples installed on the model
$T_1$ – On the surface of the hybrid model aft-body
$T_2$ – Inside the hybrid model aft-body massive aluminum body
$T_3$ – Embedded inside the pneumatic boot of the hybrid model leading edge

Description/comments: 14 CFR Part 25, Appendix C continuous maximum rime icing conditions, however, Appendix C LWC is 0.99 $g/m^3$. Accretion was entirely rime ice, with a maximum thickness of approximately an 1/8 inch. The ice shed in the first boot fire left some residual ice. The second boot fire had less residual ice.

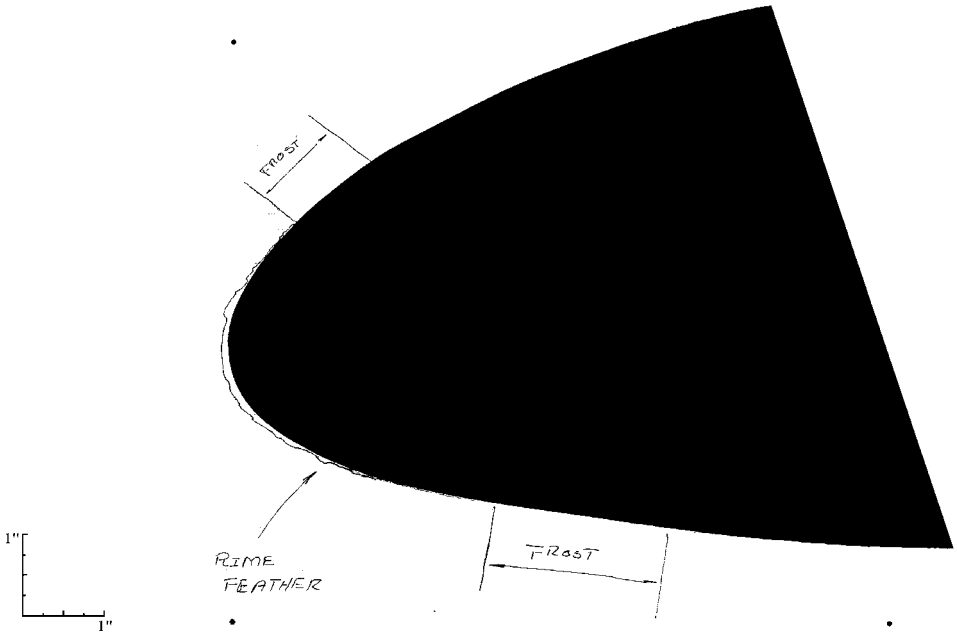


Figure 76. Tracing of Run 5/5

Figure 77. Photograph of Run 5/5 (Upper Surface Leading Edge)

Table 31. Run 3/6A Test Parameters

| Date 3/10/00 | | Run 3/6A | | AOA: +4° | | No Mold | Flap Angle: +2° | | | |
|---|---|---|---|---|---|---|---|---|---|---|
| $T_{model}$ (°F) | $T_{st}$ (°F) | $T_{tot}$ (°F) | V (mph) | MVD (μm) | LWC ($g/m^3$) | Time (min:sec) | Boot Settings | | | Spray Off Time |
| | | | | | | | Initial Fire | Cycle | Activation | |
| 21.3 | 14(14.5) | 21.5 | 195 | 40 | 0.25 | 12:19 | 13:54:08 | 3:00 | Manual 0:51 | 14:03:08 |
| 21.4 | | | | | | | | | | |
| 19.9 | | | | | | | | | | |

| Ice Thickness Measurements | |
|---|---|
| Location | Thickness |
| Maximum | 0.45 inch |
| Stagnation | 0.17 inch |
| Lower Surface | 0.55 inch |

| Tracing Location |
|---|
| Left 2″ |

Notes:
$T_{model}$ – The reading of three thermocouples installed on the model
$T_1$ – On the surface of the hybrid model aft-body
$T_2$ – Inside the hybrid model aft-body massive aluminum body
$T_3$ – Embedded inside the pneumatic boot of the hybrid model leading edge

Description/comments: Attempted to reach 14 CFR Part 25, Appendix C continuous maximum mixed icing conditions with an MVD of 40 μm, but the minimum IWT LWC was 0.25 $g/m^3$, rather than 0.1 $g/m^3$, as defined by Appendix C. The IWT could not achieve the lower LWC. The deicer was cycled following a 19-second exposure of the model to the icing cloud, reflecting the response time of an ice detector. The front leading edge had rough glaze ice, while the lower leading edge had horn feathers of height much greater than a 1/4 inch. The lower surface exhibited many columnar feathers growing between the pneumatic boot tubes, with a height much greater than a 1/4 inch.

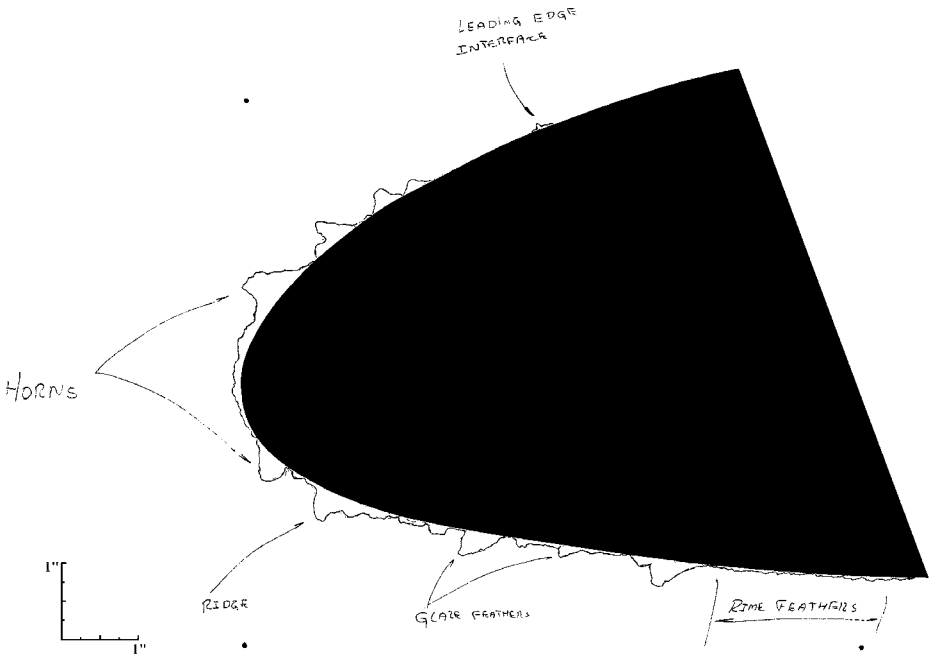


Figure 78. Tracing of Test 3/6A

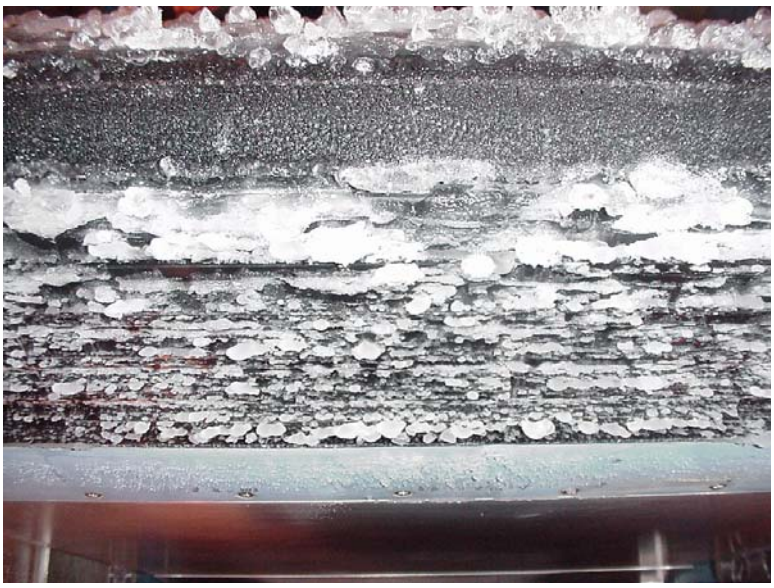

Figure 79. Photograph of Run 3/6A (Upper Surface Leading Edge)

Table 32. Run 4/4 Test Parameters

| Date 3/10/00 | | Run 4/4 | | AOA: +4° | | No Mold | Flap Angle: +2° | | | |
|---|---|---|---|---|---|---|---|---|---|---|
| $T_{model}$ (°F) | $T_{st}$ (°F) | $T_{tot}$ (°F) | V (mph) | MVD (µm) | LWC (g/m$^3$) | Time (min:sec) | Boot Settings | | | Spray Off Time |
| | | | | | | | Initial Fire | Cycle | Activation | |
| 27.7 | 21(21.0) | 28.0 | 195 | 40 | 0.25 | 2:28 | 12:13:12 | N/A | Man. 0:19 | 12:15:20 |
| 28.0 | | | | | | | | | | |
| 27.2 | | | | | | | | | | |

| Tracing Location |
|---|
| Center |

| Ice Thickness Measurements | |
|---|---|
| Location | Thickness |
| Upper 2.0″ | 0.22″ |
| Stagnation | 0.11″ |
| Lower 1.25″ | 0.20″ |

Notes:
$T_{model}$ – The reading of three thermocouples installed on the model
$T_1$ – On the surface of the hybrid model aft-body
$T_2$ – Inside the hybrid model aft-body massive aluminum body
$T_3$ – Embedded inside the pneumatic boot of the hybrid model leading edge

Description/comments: The deicer was activated after 19 seconds of exposure to the icing cloud, simulating the response time of an ice detector. An attempt was made to simulate 14 CFR Part 25, Appendix C intermittent maximum glaze icing conditions with an MVD of 40 µm by accumulating the water catch with an LWC of 0.25 g/m$^3$ over 2 minutes rather than testing at the 0.52 g/m$^3$ of Appendix C. (Note that this is an inappropriate testing procedure since the lower LWC results in a lower ice accretion freezing fraction and, subsequently, an incorrect ice accretion.) The same conditions were as used as in run 4/3, but with the wing at a 4° AOA and a different flap angle. This was a warm temperature run. There were clear ice ridges, typically called ice horns, of slightly below a 1/4 inch in size on the upper and lower leading-edge surfaces. This ice accretion was grainy, but nonetheless, glaze ice.

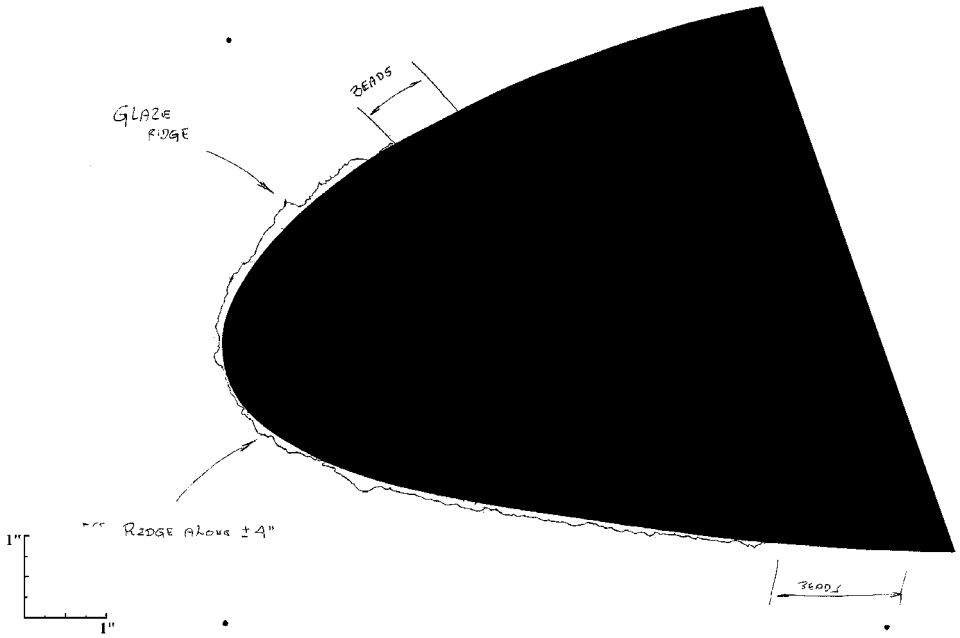


Figure 80. Tracing of Run 4/4

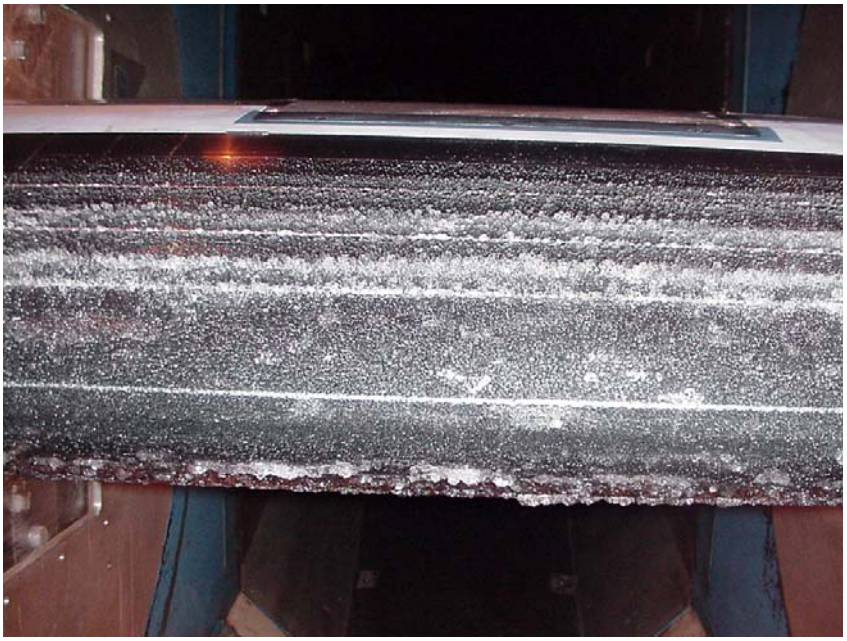

Figure 81. Photograph of Run 4/4 (Upper Surface Leading Edge)

Table 33. Run 4/4.5 Test Parameters

| Date 3/13/00 | | Run 4/4.5 | | AOA: +4° | | No Mold | Flap Angle: +2° | | | |
|---|---|---|---|---|---|---|---|---|---|---|
| | | | | | | | Boot Settings | | | Spray Start and Spray Off Time |
| $T_{model}$ (°F) | $T_{st}$ (°F) | $T_{tot}$ (°F) | V (mph) | MVD (μm) | LWC ($g/m^3$) | Time (min:sec) | Initial Fire | Cycle | Activation | |
| 27.8 | 21 (20.4) | 27.3 | 195 | 40 | 0.25 | 3:19 | 16:35:24 | -* | ID 0:19 | 16:35:04<br>16:38:24 |
| 27.6 | | | | | | | | | | |
| 28.5 | | | | | | | | | | |

| Tracing Location |
|---|
| Center |

| Ice Thickness Measurements | |
|---|---|
| Location | Thickness |
| 2″ Up | 0.33″ |
| Stagnation | 0.13″ |
| 1.25″ Down | 0.15″ |

Notes:
$T_{model}$ – The reading of three thermocouples installed on the model
$T_1$ – On the surface of the hybrid model aft-body
$T_2$ – Inside the hybrid model aft-body massive aluminum body
$T_3$ – Embedded inside the pneumatic boot of the hybrid model leading edge

Description/comments: An attempt was made to simulate 14 CFR Part 25, Appendix C intermittent maximum glaze icing conditions with an MVD of 40 μm, by accumulating the water catch with an LWC of 0.25 $g/m^3$ over 3 minutes rather than testing at the 0.52 $g/m^3$ of Appendix C. (Note that this is an inappropriate testing procedure since the lower LWC results in a lower ice accretion freezing fraction and, subsequently, an incorrect ice accretion.) Glaze ice began forming at the leading edge. Minimal ice was shed during the boot fire that reflected the response time for an ice detector just 19 seconds after the start of the run. A double ridge formed at the first stitch above the stagnation point and a single ridge formed at the second stitch line.

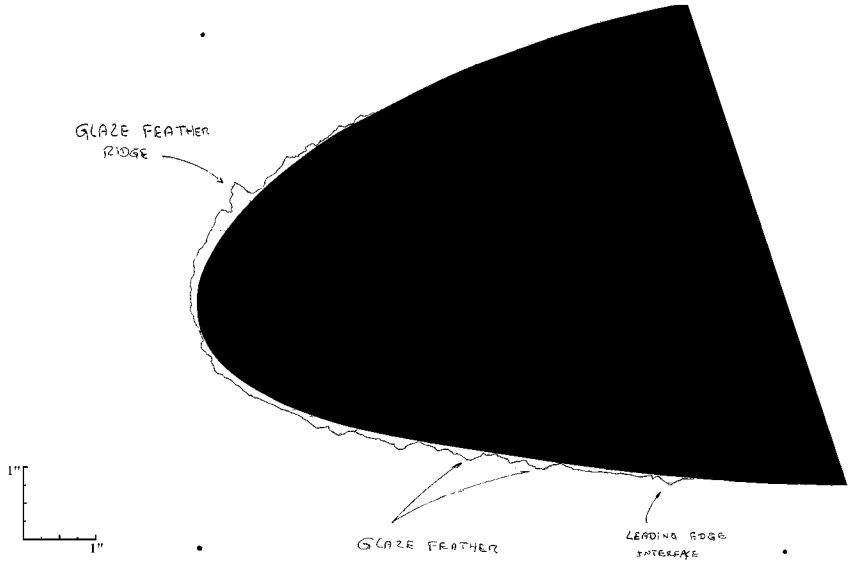


Figure 82. Tracing of Run 4/4.5

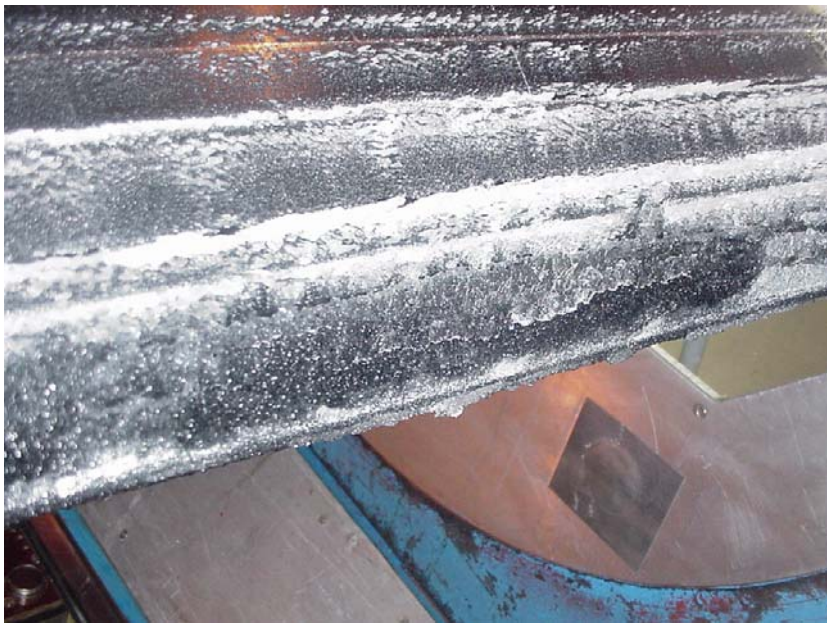

Figure 83. Photograph of Run 4/4.5 (Upper Surface Leading Edge)

Table 34. Run 4/2 Test Parameters

| Date 3/13/00 | | Run 4/2 | | AOA: 0° | | No Mold | Flap Angle: -3.5° | | | |
|---|---|---|---|---|---|---|---|---|---|---|
| | | | | | | | Boot Settings | | | Spray Start and Spray Off Time |
| $T_{model}$ (°F) | $T_{st}$ (°F) | $T_{tot}$ (°F) | V (mph) | MVD (μm) | LWC ($g/m^3$) | Time (min:sec) | Initial Fire | Cycle | Activation | |
| 20.0 | 21 (21.4) | 28.5 | 195 | 20 | 0.51 | 6:11 | 16:00:24 | 3:00 | ID 0:11 | 16:00:13 16:06:24 |
| 27.5 | | | | | | | | | | |
| 29.7 | | | | | | | | | | |

| Tracing Location |
|---|
| 2″ left of center |

| Ice Thickness Measurements | |
|---|---|
| Location | Thickness |
| 2.25″ Up | 0.36″ |
| Stagnation | 0.32″ |
| 2.0″ Down | 0.35″ |

Notes:
$T_{model}$ – The reading of three thermocouples installed on the model
$T_1$ – On the surface of the hybrid model aft-body
$T_2$ – Inside the hybrid model aft-body massive aluminum body
$T_3$ – Embedded inside the pneumatic boot of the hybrid model leading edge

Description/comments: This run was conducted to simulate the response time of an ice detector under 14 CFR Part 25, Appendix C continuous maximum glaze icing conditions with the initial deicer cycling occurring after 11 seconds of exposure to the icing cloud. No visual indications of ice at the first boot fire. Ice began accreting at the stitch lines just after that initial boot fire. The intercycle ice had ridges at the stitch lines. At the second boot fire, the leading edge was clean with the exception of the seam between the leading edge and the aft section of the boot.

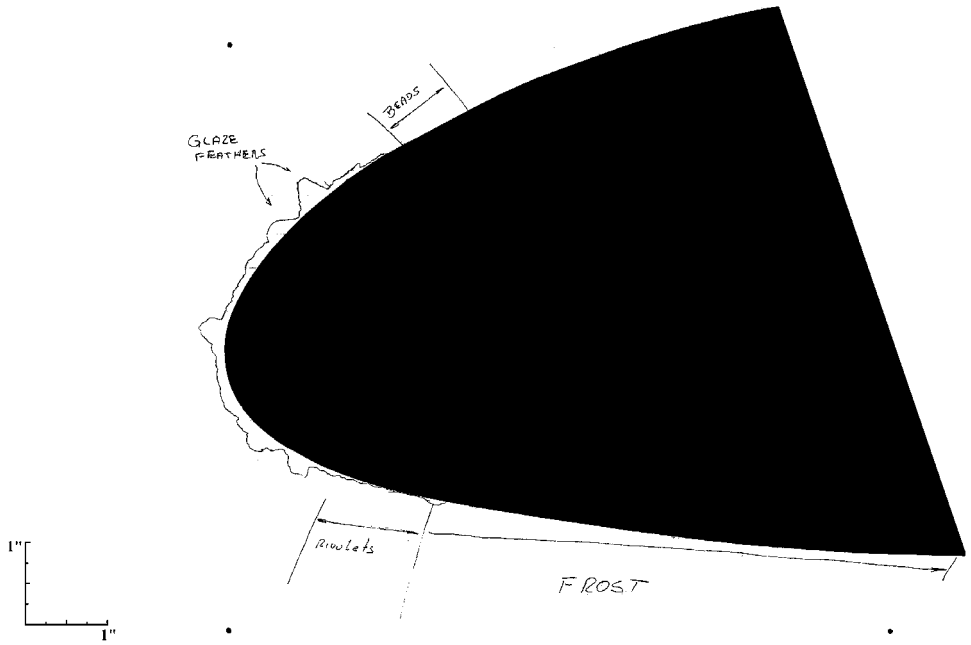


Figure 84. Tracing of Run 4/2

Figure 85. Photograph of Run 4/2 (Upper Surface Leading Edge)

Table 35. Run 3/5 Test Parameters

| Date 3/10/00 | | Run 3/5 | | AOA: +0° | | No Mold | Flap Angle: -3.5° | | | |
|---|---|---|---|---|---|---|---|---|---|---|
| | | | | | | | Boot Settings | | | Spray Off Time |
| $T_{model}$ (°F) | $T_{st}$ (°F) | $T_{tot}$ (°F) | V (mph) | MVD (μm) | LWC ($g/m^3$) | Time (min:sec) | Initial Fire | Cycle | Activation | |
| 27.7 | 14(21.0) | 28.0 | 195 | 40 | 0.25 | 2:28 | 12:46:21 | N/A | Man. 0:19 | 12:48:30 |
| 28.0 | | | | | | | | | | |
| 27.2 | | | | | | | | | | |

| Tracing Location |
|---|
| Center |

| Ice Thickness Measurements | |
|---|---|
| Location | Thickness |
| Upper 2.25″ | 0.21 |
| Stagnation | 0.19 |
| Lower 1.25″ | 0.20 |

Notes:
$T_{model}$ – The reading of three thermocouples installed on the model
$T_1$ – On the surface of the hybrid model aft-body
$T_2$ – Inside the hybrid model aft-body massive aluminum body
$T_3$ – Embedded inside the pneumatic boot of the hybrid model leading edge

Description/comments: 14 CFR Part 25, Appendix C continuous maximum mixed ice icing conditions, but with an LWC of 0.25 $g/m^3$ rather than the 0.52 $g/m^3$ LWC of Appendix C. An attempt was made to accumulate the Appendix C water catch by extending the run to twice the time to traverse an Appendix C intermittent maximum icing cloud. (Note that this is an inappropriate test technique since the lower LWC will result in a different freezing fraction than when at the Appendix C LWC.) This could be termed a mixed icing tunnel run. Compared to run 4/3, where the leading-edge accretion was only 1/10 of an inch thick, the leading-edge accretion for this run was twice as thick.

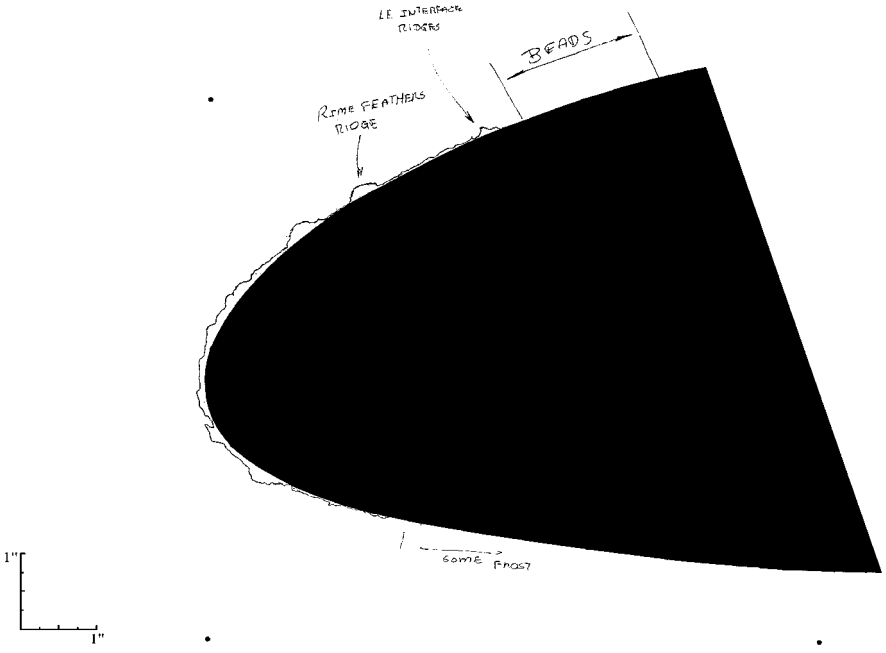


Figure 86. Tracing of Run 3/5

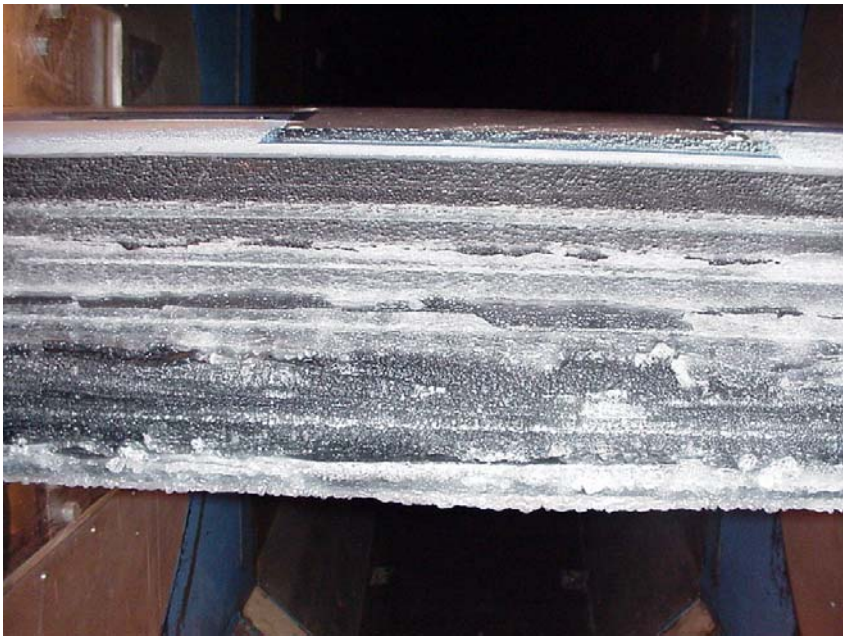

Figure 87. Photograph of Run 3/5 (Upper Surface Leading Edge)

Table 36. Run 4/3 Test Parameters

| Date 3/10/00 | | Run 4/3 | | AOA: +0° | | No Mold | Flap Angle: -3.5° | | | |
|---|---|---|---|---|---|---|---|---|---|---|
| $T_{model}$ (°F) | $T_{st}$ (°F) | $T_{tot}$ (°F) | V (mph) | MVD (μm) | LWC ($g/m^3$) | Time (min:sec) | Boot Settings | | | Spray Off Time |
| | | | | | | | Initial Fire | Cycle | Activation | |
| 26.6 | 21(21.3) | 28.5 | 195 | 40 | 0.25 | 2:28 | 11:19:32 | N/A | Man. 0:19 | 11:21:32 |
| 26.8 | | | | | | | | | | |
| 27.3 | | | | | | | | | | |

| Tracing Location |
|---|
| Center |

| Ice Thickness Measurements | |
|---|---|
| Location | Thickness |
| Upper 2.25″ | 0.27 |
| Stagnation | 0.11 |
| Lower 1.25″ | 0.23 |

Notes:
$T_{model}$ – The reading of three thermocouples installed on the model
$T_1$ – On the surface of the hybrid model aft-body
$T_2$ – Inside the hybrid model aft-body massive aluminum body
$T_3$ – Embedded inside the pneumatic boot of the hybrid model leading edge

Description/comments: This run was an attempt to simulate 14 CFR Part 25, Appendix C intermittent maximum mixed ice icing conditions with an MVD of 40 μm by accumulating the Appendix C water catch (3 minutes with an LWC of 0.25 $g/m^3$ rather than the 1 minute required to traverse the Appendix C intermittent cloud at an LWC of 0.52 $g/m^3$). (Note that this is an inappropriate test technique since the ice accretion freezing fraction is incorrect at the lower LWC.) This was a warm temperature run. There were clear ice ridges, typically called ice horns, about a 1/4 inch in size on the upper and lower leading-edge surfaces. This ice accretion was grainy, but nonetheless, glaze ice.

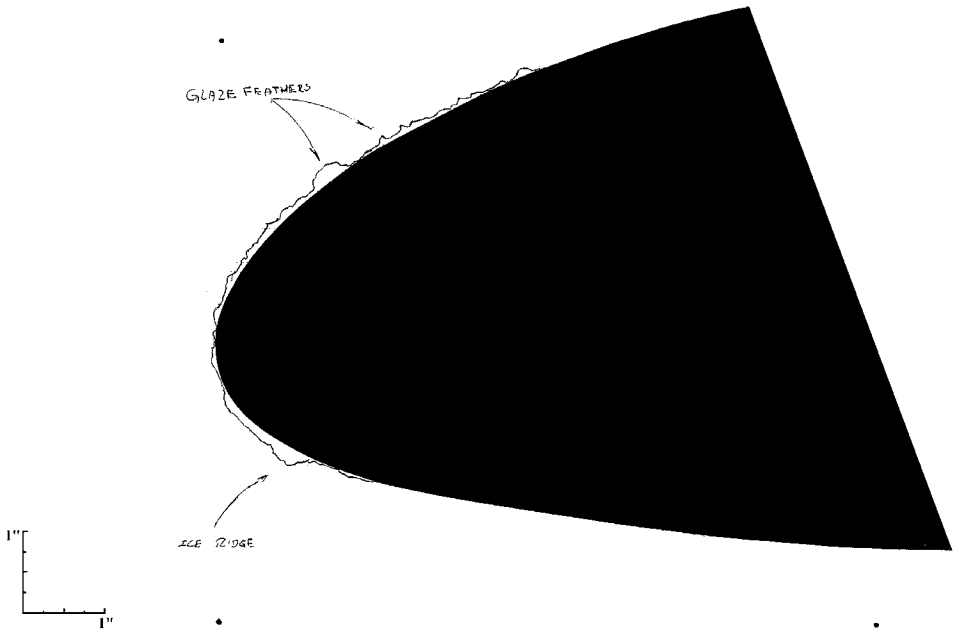


Figure 88. Tracing of Run 4/3

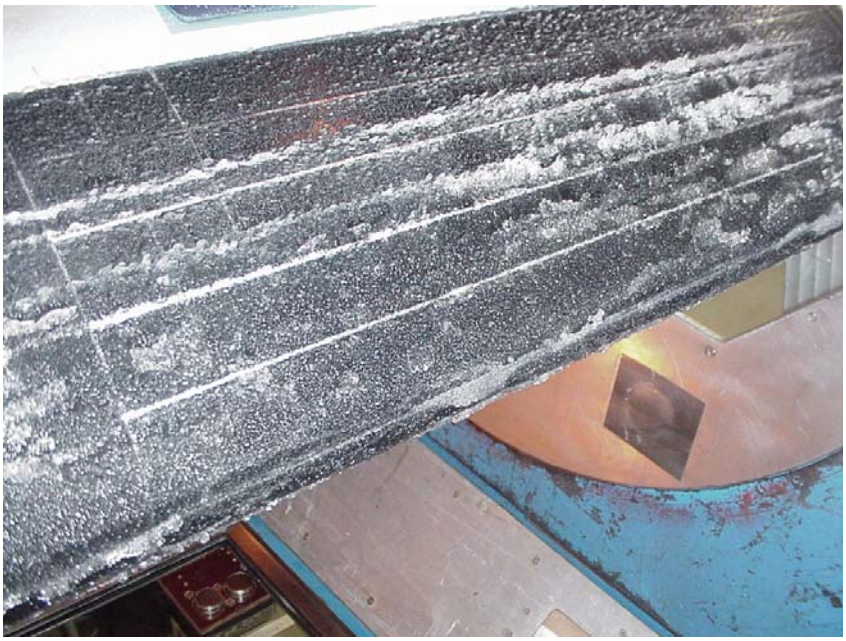

Figure 89. Photograph of Test 4/3 (Upper Surface Leading Edge)

4.1.3 Molds and Test Repeatability.

To document the characteristics of the preactivation and intercycle ice accretions, molds were made for selected icing conditions. Castings from these molds will provide guidance for replicating the surface roughness for flight and aerodynamic wind tunnel tests required to

determine the aerodynamic effects. Table 37 summarizes the icing conditions for which molds were made. Castings of the molds are available at the Flight Safety Branch at the FAA William J. Hughes Technical Center, Atlantic City International Airport, New Jersey 08405.

Table 37. Deicer Mold Runs at 195 MPH (2.82 NMI/MIN) True Airspeed

| | Icing Conditions Description | | | | | Deicer Operation | | | | | | | |
|---|---|---|---|---|---|---|---|---|---|---|---|---|---|
| AOA (deg) | Type Icing Cond. | Type Ice | $T_S$ (°F) | MVD (μm) | LWC ($g/m^3$) | Initial Activ. (sec) | Cycle Period (min.) | No. Cycles | Icing Cloud Extent (nmi) | Comments | Run | Figure | Table |
| 4 | CM | Mixed | 14 | 20 | 0.45 | - | - | - | - | Preact. ice:11 s ID + 30 s Pilot React. | 3/3R | 90 | 39 |
| | IM | Mixed | 14 | 20 | 0.45 | - | - | - | - | Pre-act ice: 3 s ID + 30 s Pilot React. | 6/3R | 91 | 40 |
| | CM | Mixed | 14 | 20 | 0.45 | 11 | 3 | 2 | 14.7 | I/C mold for Run 2/1R | 3/7 | 92 | 41 |
| | CM | | 14 | 20 | 0.45 | 11 | 1 | 5 | 14.7 | I/C mold for Run 2/2 | 4/5 | 93, 94 | 42 |
| 0 | CM | Mixed | 14 | 20 | 0.45 | 11 | 1 | 4 | 14.7 | I/C mold for Run 3/4 | 6/7 | 95 | 43 |
| 4 | CM | Glaze | 21 | 20 | 0.51 | 11 | 3 | 2 | 14.7 | I/C mold for Run 4/1 | 5/6 | 96 | 44 |
| | CM | Glaze | - | 20 | - | 11 | 3 | 2 | 14.7 | Repeat mold for Run 4/1 | 5/6R | 97 | 45 |

Efficient use of the IWT entailed scheduling the mold test runs at the end of each day, repeating an earlier run. These repeated test conditions provided an opportunity to evaluate data repeatability. Table 38 list figures from comparable repeated tests.

Table 38. Figures for Repeated Tests

| Mold Test Results—Figure | Repeated Test Condition Results—Figure |
|---|---|
| 90 | 30 |
| 91 | 32 |
| 92 | 43 |
| 93 | 45 |
| 96 | 47 |

Recognizing the randomness of the intercycle ice accretion process, the test repeatability was considered acceptable.

Table 39. Run 3/3R Test Parameters

| Date 3/15/00 | | Run 3/3R | | AOA: +4° | | Yes Mold | Flap Angle: +2° | | | |
|---|---|---|---|---|---|---|---|---|---|---|
| | | | | | | | Boot Settings | | | Spray Start and Spray Off Time |
| $T_{model}$ (°F) | $T_{st}$ (°F) | $T_{tot}$ (°F) | V (mph) | MVD (µm) | LWC ($g/m^3$) | Time (min:sec) | Initial Fire | Cycle | Activation | |
| 21.63 | 14 (14.2) | 21.19 | 195 | 20 | 0.45 | 0:41 | No boot fire | - | ID 0:* | 16:39:12 16:39:54 |
| 21.61 | | | | | | | | | | |
| 25.43 | | | | | | | | | | |

| Tracing Location |
|---|
| No Tracing |

| Ice Thickness Measurements | |
|---|---|
| Location | Thickness |
| Upper | N/A |
| Stagnation | N/A |
| Lower | N/A |

Notes:
$T_{model}$ – The reading of three thermocouples installed on the model
$T_1$ – On the surface of the hybrid model aft-body
$T_2$ – Inside the hybrid model aft-body massive aluminum body
$T_3$ – Embedded inside the pneumatic boot of the hybrid model leading edge

Description/comments: Mold run. No tracing. No thickness measurements.

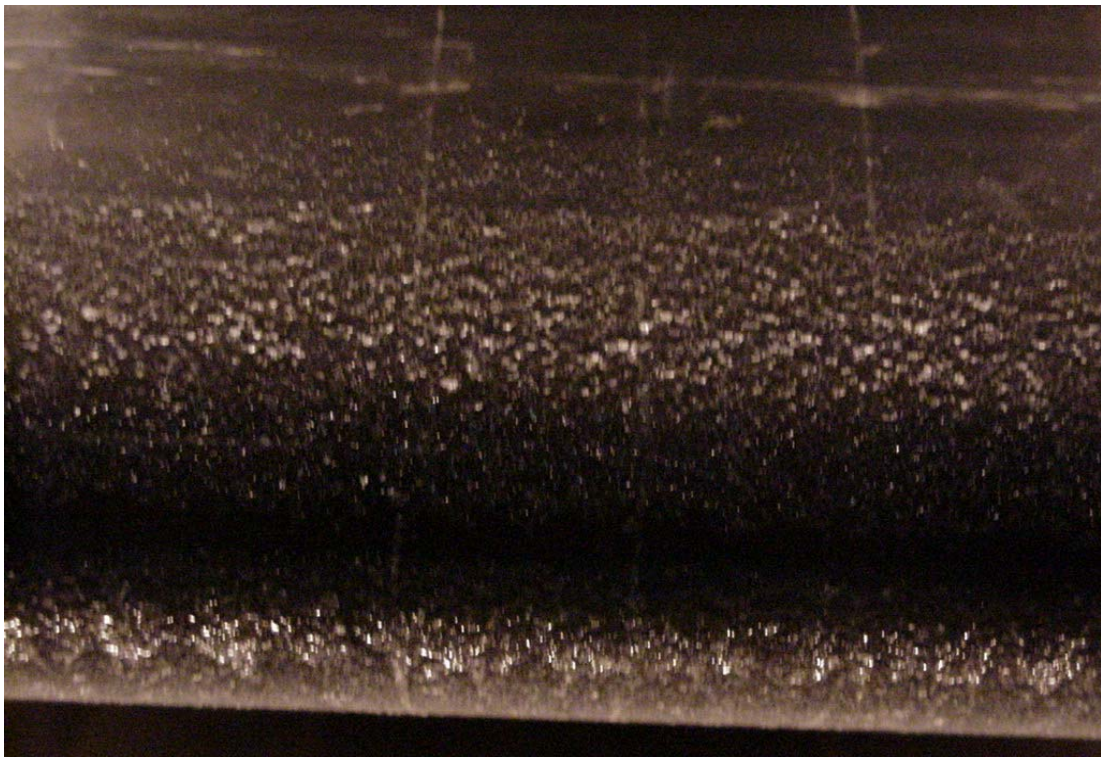

Figure 90. Photograph of Run 3/3R (Upper Surface Leading Edge)

Table 40. Run 6/3R Test Parameters

| Date 3/15/00 | | Run 6/3R | | AOA: +4° | | Yes Mold | Flap Angle: +2° | | | |
|---|---|---|---|---|---|---|---|---|---|---|
| | | | | | | | Boot Settings | | | Spray Start and Spray Off Time |
| $T_{model}$ (°F) | $T_{st}$ (°F) | $T_{tot}$ (°F) | V (mph) | MVD (µm) | LWC ($g/m^3$) | Time (min:sec) | Initial Fire | Cycle | Activation | |
| 23.15 | 14 (13.2) | 20.13 | 195 | 20 | 1.95 | 0:33 | No boot fire | - | - | 09:07:38 09:08:12 |
| 23.42 | | | | | | | | | | |
| 24.98 | | | | | | | | | | |
| 22.10 | | | | | | | | | | |
| 20.03 | | | | | | | | | | |

| Tracing Location |
|---|
| No Tracing |

| Ice Thickness Measurements | |
|---|---|
| Location | Thickness |
| Upper | N/A |
| Stagnation | N/A |
| Lower | N/A |

Notes:
$T_{model}$ – The reading of three thermocouples installed on the model
$T_1$ – After body outside
$T_2$ – After body inside
$T_3$ – IB
$T_4$ – CB
$T_5$ – CT

Description/comments: Preactivation ice. Mold run. No tracing. No thickness measurements. This is one of three preactivation ice accretions (figures 37, 32, and 91) taken at identical tunnel conditions at an AOA of 4°. Figure 32 was also for 33 seconds. Comparison of the photographs suggests a somewhat more substantial accretion for figure 32 than for figure 91. It is not possible to compare tracings or thickness measurements for figures 32 and 91 because there were none for the latter, a mold case. The duration of figure 37 was determined by judging when a 1/4 inch of ice had formed, and then waiting another 30 seconds. This was to simulate pilot recognition of the given thickness, plus some delay in activation that could be due to difficulty in judging thickness, workload, or other reasons. The photographs and tracings indicate a much more substantial and rougher ice accretion for figure 37 than figure 32.

Figure 91. Photograph of Run 6/3R (Upper Surface Leading Edge)

Table 41. Run 3/7 Test Parameters

| Date 3/9/00 | | Run 3/7 | | AOA: +4° | | Yes Mold | Flap Angle: +2° | | | |
|---|---|---|---|---|---|---|---|---|---|---|
| | | | | | | | Boot Settings | | | Spray Off Time |
| $T_{model}$ (°F) | $T_{st}$ (°F) | $T_{tot}$ (°F) | V (mph) | MVD (μm) | LWC ($g/m^3$) | Time (min:sec) | Initial Fire | Cycle | Activation | |
| 23.2 | 14(14.4) | 21.3 | 195 | 20 | 0.45 | 6:11 | 17:02:41 | 3:00 | ID 0:11 | 17:08:41 |
| 23.3 | | | | | | | | | | |
| 21.1 | | | | | | | | | | |

| Tracing Location |
|---|
| Center |

| Ice Thickness Measurements | |
|---|---|
| Location | Thickness |
| Upper | N/A |
| Stagnation | N/A |
| Lower | N/A |

Notes:
$T_{model}$ – The reading of three thermocouples installed on the model
$T_1$ – On the surface of the hybrid model aft-body
$T_2$ – Inside the hybrid model aft-body massive aluminum body
$T_3$ – Embedded inside the pneumatic boot of the hybrid model leading edge

Description/comments: Mold run. No tracing. No thickness measurements.

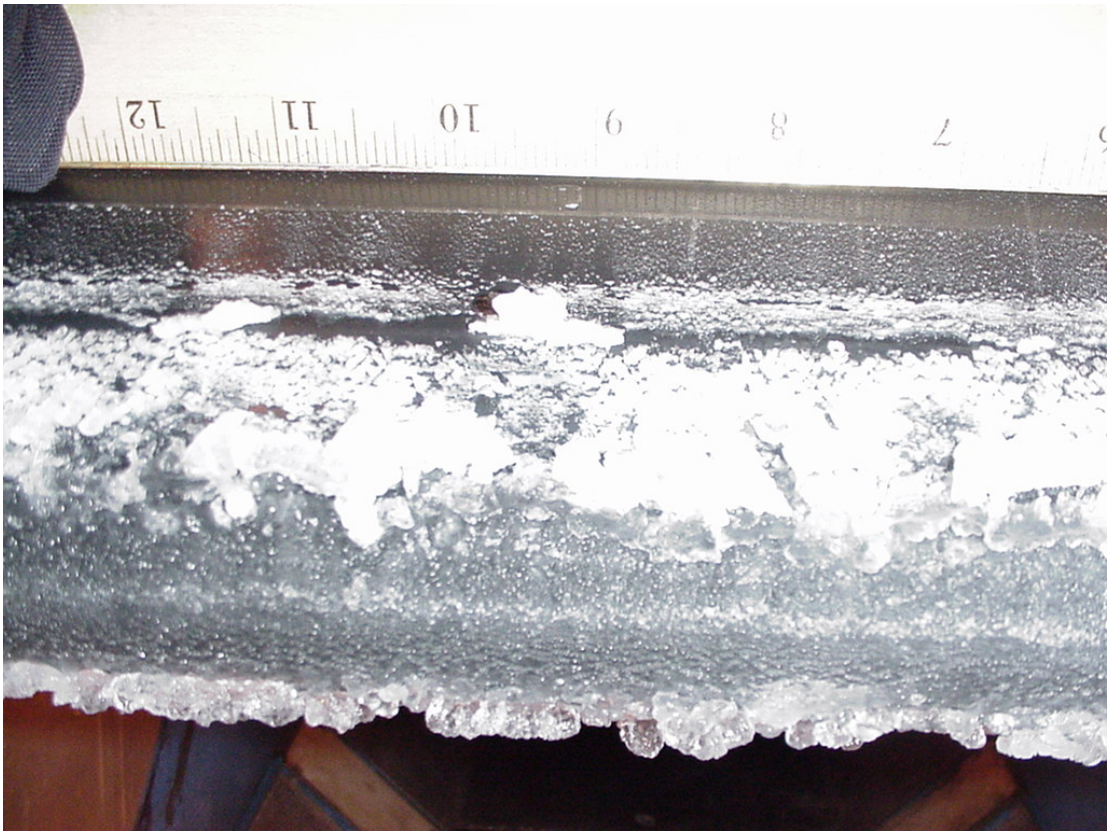

Figure 92. Photograph of Run 3/7 (Upper Surface Leading Edge)

Table 42. Run 4/5 Test Parameters

| Date 3/10/00 | | Run 4/5 | | AOA: +4° | | Yes Mold | Flap Angle: +2° | | | |
|---|---|---|---|---|---|---|---|---|---|---|
| | | | | | | | Boot Settings | | | |
| $T_{model}$ (°F) | $T_{st}$ (°F) | $T_{tot}$ (°F) | V (mph) | MVD (µm) | LWC ($g/m^3$) | Time (min:sec) | Initial Fire | Cycle | Activation | Spray Off Time |
| 19.7 | 14(14.6) | 21.6 | 195 | 20 | 0.45 | 6:11 | 18:14:15 | 1:00 | ID 0:11 | 18:20:15 |
| 20.1 | | | | | | | | | | |
| 20.2 | | | | | | | | | | |

| Tracing Location |
|---|
| Center |

| Ice Thickness Measurements | |
|---|---|
| Location | Thickness |
| Upper | N/A |
| Stagnation | N/A |
| Lower | N/A |

Notes:
$T_{model}$ – The reading of three thermocouples installed on the model
$T_1$ – On the surface of the hybrid model aft-body
$T_2$ – Inside the hybrid model aft-body massive aluminum body
$T_3$ – Embedded inside the pneumatic boot of the hybrid model leading edge

Description/comments: Mold run. No tracing. No thickness measurements. Identical conditions to test run 3/7, but with deicing cycles 1 minute apart. While tunnel run 3/7 had ice ridges on the upper and lower leading-edge surfaces, this test run had chunks of jagged ice at the leading edge at irregular intervals. This was the result of incomplete ice removal at the 1-minute deicing cycle.

Figure 93. Photograph of Run 4/5 (Upper Surface Leading Edge)

Figure 94. Photograph of Test 4/5 (Lower Surface Leading Edge)

Table 43. Run 6/7 Testing Conditions

| Date 3/14/00 | | Run 6/7 | | AOA: 0° | | Yes Mold | Flap Angle: -3.5° | | | |
|---|---|---|---|---|---|---|---|---|---|---|
| | | | | | | | Boot Settings | | | Spray Start and Spray Off Time |
| $T_{model}$ (°F) | $T_{st}$ (°F) | $T_{tot}$ (°F) | V (mph) | MVD (μm) | LWC ($g/m^3$) | Time (min:sec) | Initial Fire | Cycle | Activation | |
| 21.2 | 14 (14.5) | 21.4 | 195 | 20 | 0.45 | 6:11 | 16:30:48 | 1:00 | ID 0:11 | 16:30:37 16:36:48 |
| 20.7 | | | | | | | | | | |
| 25.1 | | | | | | | | | | |

| Tracing Location |
|---|
| No Tracing |

| Ice Thickness Measurements | |
|---|---|
| Location | Thickness |
| Upper | N/A |
| Stagnation | N/A |
| Lower | N/A |

Notes:
$T_{model}$ – The reading of three thermocouples installed on the model
$T_1$ – On the surface of the hybrid model aft-body
$T_2$ – Inside the hybrid model aft-body massive aluminum body
$T_3$ – Embedded inside the pneumatic boot of the hybrid model leading edge

Description/comments: Mold run. No tracing. No thickness measurements. Ice began to be visible just before the initial boot cycle. At the initial cycle, there was considerable residual ice. On the second boot cycle, there was substantial residual ice in the boot stitch area and a section of the leading edge did not clear. On the third and fourth boot cycles, the leading edge was clear with the exception of the stitches. There was also substantial residual ice aft of the leading edge. On the fifth boot cycle, there was substantial residual ice over the entire boot section.

Figure 95. Photograph of Test 6/7 (Upper Surface Leading Edge)

Table 44. Run 5/6 Test Parameters

| Date 3/13/00 | | Run 5/6 | | AOA: +4° | | Yes Mold | Flap Angle: +2° | | | |
|---|---|---|---|---|---|---|---|---|---|---|
| | | | | | | | Boot Settings | | | Spray Start and Spray Off Time |
| $T_{model}$ (°F) | $T_{st}$ (°F) | $T_{tot}$ (°F) | V (mph) | MVD (µm) | LWC ($g/m^3$) | Time (min:sec) | Initial Fire | Cycle | Activation | |
| 26.5 | 21 (20.4) | 27.4 | 195 | 20 | 0.51 | 6:11 | 17:09:10 | 3:00 | ID 0:11 | 17:08:59 17:15:10 |
| 26.0 | | | | | | | | | | |
| 27.5 | | | | | | | | | | |

| Tracing Location |
|---|
| Center |

| Ice Thickness Measurements | |
|---|---|
| Location | Thickness |
| Upper | N/A |
| Stagnation | N/A |
| Lower | N/A |

Notes:
$T_{model}$ – The reading of three thermocouples installed on the model
$T_1$ – On the surface of the hybrid model aft-body
$T_2$ – Inside the hybrid model aft-body massive aluminum body
$T_3$ – Embedded inside the pneumatic boot of the hybrid model leading edge

Description/comments: Mold run. No tracing. No thickness measurements. There was some residual ice at the stitch lines after the initial boot fire. There was residual ice in most of the stitch lines except at the leading edge.

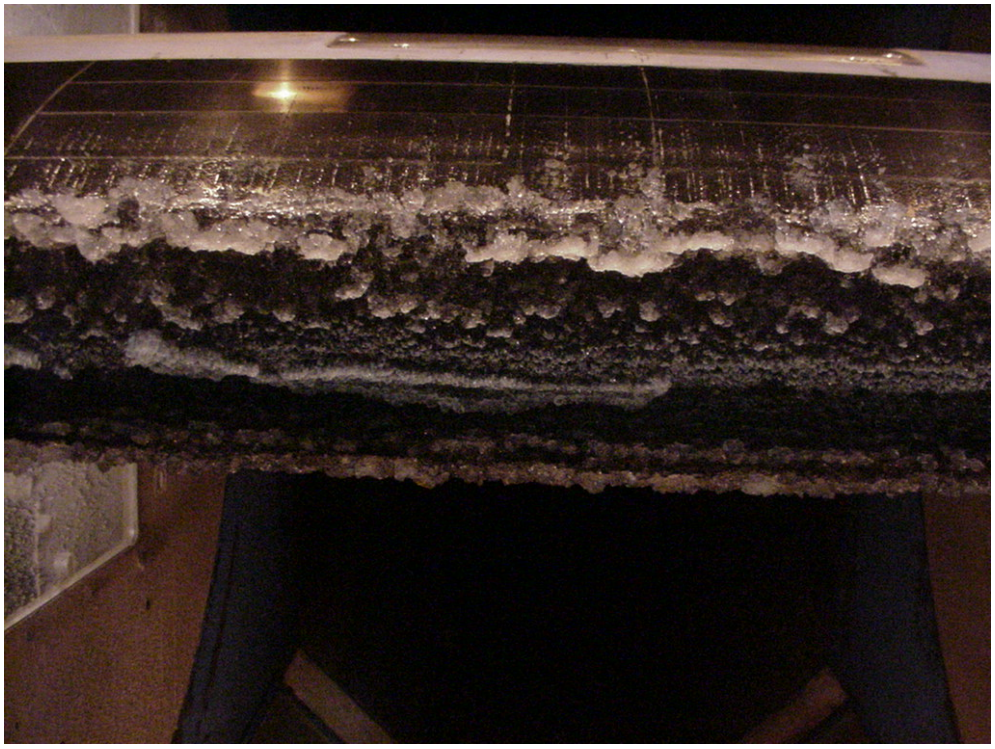

Figure 96. Photograph of Test 5/6 (Upper Surface Leading Edge)

Table 45. Run 5/6R Test Parameters

| Date 3/17/00 | | Run 5/6R | | AOA: +4° | | Yes Mold | Flap Angle: +2° | | | |
|---|---|---|---|---|---|---|---|---|---|---|
| | | | | | | | Boot Settings | | | Spray Start and Spray Off Time |
| $T_{model}$ (°F) | $T_{st}$ (°F) | $T_{tot}$ (°F) | V (mph) | MVD (µm) | LWC ($g/m^3$) | Time (min:sec) | Initial Fire | Cycle | Activation | |
| 26.49 | 21 (21) | 27.36 | 195 | 20 | 0.51 | 6:11 | 14:59:18 | 3:00 | ID 0:11 | 14:59:07 15:05:19 |
| 25.98 | | | | | | | | | | |
| 27.52 | | | | | | | | | | |

| Tracing Location |
|---|
| No Tracing |

| Ice Thickness Measurements | |
|---|---|
| Location | Thickness |
| Upper | N/A |
| Stagnation | N/A |
| Lower | N/A |

Notes:
$T_{model}$ – The reading of three thermocouples installed on the model
$T_1$ – On the surface of the hybrid model aft-body
$T_2$ – Inside the hybrid model aft-body massive aluminum body
$T_3$ – Embedded inside the pneumatic boot of the hybrid model leading edge

Description/comments: Mold run. No tracing. No thickness measurements. On the second boot cycle, there was residual ice in the boot stitch areas.

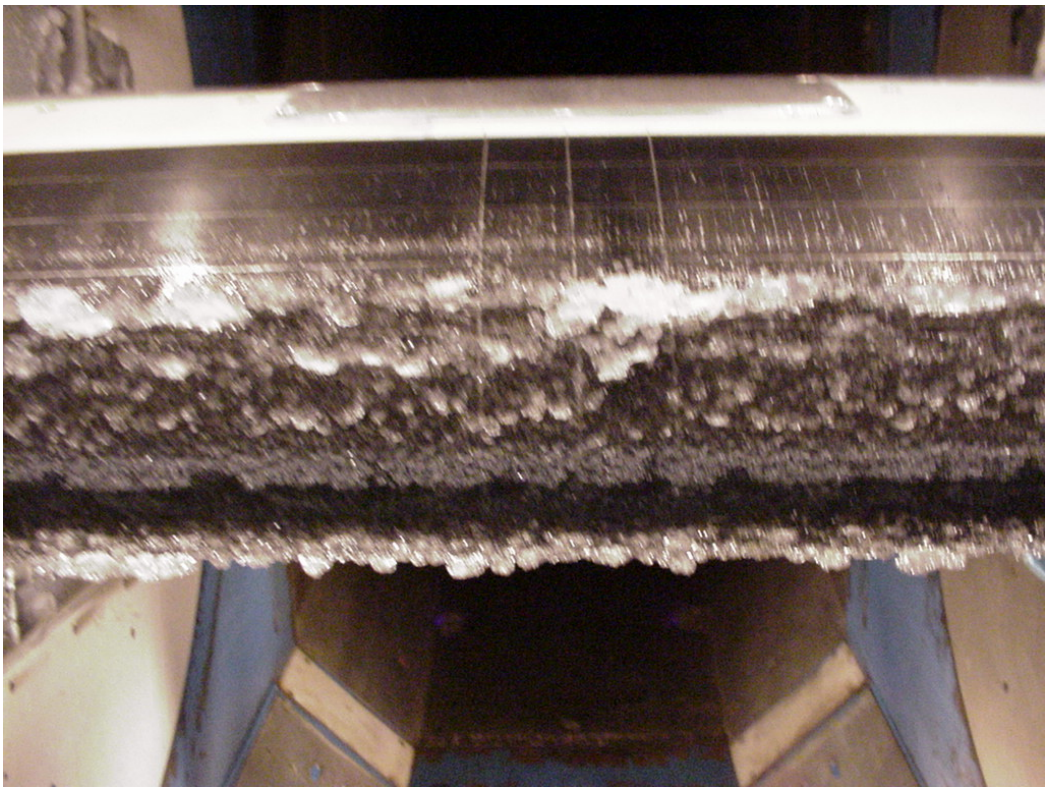

Figure 97. Photograph of Test 5/6R (Upper Surface Leading Edge)

4.1.4 Surface Ice Detectors Evaluations.

Use of local area ice detectors has been proposed as a means to alert flight crews of hazardous ice accretion, such as a ridge of ice, aft of the wing's leading-edge ice protection. A cursory investigation of the capability of three commercially available local area ice detectors to perform this function was made by exposing the detectors to icing conditions by rotating the wind tunnel model to negative AOA. The investigation included rime, mixed, and glaze icing conditions.

The local area surface ice detectors used for the investigation and their installation in the model is described in section 3.1.3.3. Testing performed during the investigation and the test results are summarized in table 46 and detailed in figures 98 through 102 and tables 47 through 51.

The test results indicated that the ice detectors are capable of detecting thin accretions of ice resulting from direct impingement and from run back. The testing performed suggested that the Goodrich local area magnetostrictive ice detector may not sense the presence of slush. The ice detectors are sensitive to installation effects and the acceptability of the detector installation will require a configuration development study. Acceptability of the ice detectors will depend on their ice thickness detection threshold and the acceptability of the resulting aerodynamic effects, the relevance of the specific ice detector's sensor surface area, and the application for which the ice detector is being used.

Table 46. Local Ice Detector Investigation at 195 mph (2.82 nmi/min) True Airspeed

| AOA (Deg) | Icing Condition Description (Type Ice) | $T_S$ (°F) | MVD (µm) | LWC ($g/m^3$) | Deicer Operation Initial Activ. (sec) | Cycle Period (min.) | Comments (Printing problem at bottom of table) | Run | Figure | Table |
|---|---|---|---|---|---|---|---|---|---|---|
| -8 | Rime | -22 | 40 | 0.8 | 6 | 1 | See comments below the tabulated test parameters of table 47. | 9/6A | 98 | 47 |
| | Mixed | 14 | 40 | 3 | 2 | 1 | See comments below the tabulated test parameters of table 48. | 9/1 | 99 | 48 |
| 0 | Glaze | 21 | 40 | 3 | 2 | 1 | See comments below the tabulated test parameters of table 49. | 9/7 | 100 | 49 |
| | Glaze | 21 | 40 | 3 | 2 | 1 | See comments below the tabulated test parameters of table 50. | 9/8 | 101 | 50 |
| | | 23 | 40 | 3 | 2 | 1 | See comments below the tabulated test parameters of table 51. | 9/9 | 102 | 51 |

Table 47. Run 9-6A Test Parameters

| Date 3/16/00 | | Run 9/6A | | AOA: -8° | | No Mold | Flap Angle: 0° | | | |
|---|---|---|---|---|---|---|---|---|---|---|
| | | | | | | | Boot Settings | | | Spray Start and Spray Off Time |
| $T_{model}$ (°F) | $T_{st}$ (°F) | $T_{tot}$ (°F) | V (mph) | MVD (µm) | LWC ($g/m^3$) | Time (min:sec) | Initial Fire | Cycle | Activation | |
| -18.62 | -22 (-30.7) | -18.57 | 195 | 40 | 0.80 | 5:45 | 11:24:49 | 1:00 | ID 0:06 | 11:24:43 11:30:29 |
| -19.66 | | | | | | | | | | |
| -17.55 | | | | | | | | | | |
| -16.02 | | | | | | | | | | |
| -17.79 | | | | | | | | | | |

| Tracing Location |
|---|
| No Tracing |

| Ice Thickness Measurements | |
|---|---|
| Location | Thickness |
| Upper | N/A |
| Stagnation | N/A |
| Lower | N/A |

Notes:
$T_{model}$ – The reading of three thermocouples installed on the model
$T_1$ – After body outside
$T_2$ – After body inside
$T_3$ – IB
$T_4$ – CB
$T_5$ – CT

Description/comments: The magnetostrictive ice detector detected ice within 42 seconds of the beginning of the icing cloud exposure; the SMARTboot ice detector also detected ice, but the time of detection was not recorded. Ice had formed on the undersurface of the ultrasonic ice detector and the detector failed to detect upper surface ice.

The data shown in figure 98 were collected at the end of the test condition, following an icing cloud exposure of 5:45 minutes. An ice thickness of 0.04 inch was measured a 1/4 inch aft of the magnetostrictive ice detector area at the end of the test condition.

Figure 98. Photograph of Run 9/6A (Upper Surface Leading Edge)

Table 48. Run 9/1 Test Parameters

| Date 3/16/00 | | Run 9/1 | | AOA: -8° | | No Mold | Flap Angle: 0° | | | |
|---|---|---|---|---|---|---|---|---|---|---|
| | | | | | | | Boot Settings | | | Spray Start and Spray Off Time |
| $T_{model}$ (°F) | $T_{st}$ (°F) | $T_{tot}$ (°F) | V (mph) | MVD (µm) | LWC ($g/m^3$) | Time (min:sec) | Initial Fire | Cycle | Activation | |
| 22.74 | 14 (14.3) | 21.08 | 195 | 40 | 3.00 | 3:21 | 13:42:59 | 1:00 | ID 0:02 | 13:42:57 13:46:19 |
| 22.15 | | | | | | | | | | |
| 22.06 | | | | | | | | | | |
| 26.37 | | | | | | | | | | |
| 24.24 | | | | | | | | | | |

| Tracing Location |
|---|
| No Tracing |

| Ice Thickness Measurements | |
|---|---|
| Location | Thickness |
| Upper | N/A |
| Stagnation | N/A |
| Lower | N/A |

Notes:
$T_{model}$ – The reading of three thermocouples installed on the model
$T_1$ – After body outside
$T_2$ – After body inside
$T_3$ – IB
$T_4$ – CB
$T_5$ – CT

Description/comments: The magnetostrictive ice detector detected ice within 44 seconds of the beginning of the icing cloud exposure; the SMARTboot ice detector also detected ice, but the time of detection was not recorded. An attempt was made to remove the ice on the undersurface of the ultrasonic ice detector by using hot air; however, the attempt was unsuccessful. Ice thickness detected by the SMARTboot detector was less than 0.015 inch and approximately 0.06 inch by the magnetostrictive ice detector. The data shown in figure 99 were collected at the end of the test condition, following an icing cloud exposure of 3:21 minutes. An ice thickness of 0.45 inch was measured in the middle of the magnetostrictive ice detector area at the end of the test condition.

Figure 99. Photograph of Test 9/1 (Upper Surface Leading Edge)

Table 49. Run 9/7 Test Parameters

| Date 3/16/00 | | Run 9/7 | | AOA: -8° | | No Mold | Flap Angle: 0° | | | |
|---|---|---|---|---|---|---|---|---|---|---|
| | | | | | | | Boot Settings | | | Spray Start and Spray Off Time |
| $T_{model}$ (°F) | $T_{st}$ (°F) | $T_{tot}$ (°F) | V (mph) | MVD (µm) | LWC ($g/m^3$) | Time (min:sec) | Initial Fire | Cycle | Activation | |
| 27.85 | 21 (21.4) | 28.32 | 195 | 40 | 3.00 | 3:15 | 14:08:56 | 1:00 | ID 0:02 | 14:08:54 14:12:09 |
| 27.38 | | | | | | | | | | |
| 28.68 | | | | | | | | | | |
| 32.01 | | | | | | | | | | |
| 30.30 | | | | | | | | | | |

| Tracing Location |
|---|
| No Tracing |

| Ice Thickness Measurements | |
|---|---|
| Location | Thickness |
| Upper | N/A |
| Stagnation | N/A |
| Lower | N/A |

Notes:
$T_{model}$ – The reading of three thermocouples installed on the model
$T_1$ – After body outside
$T_2$ – After body inside
$T_3$ – IB
$T_4$ – CB
$T_5$ – CT

Description/comments: The ultrasonic ice detector detected ice 21 seconds after the beginning of the icing cloud exposure; the SMARTboot ice detector also detected ice, but the time of detection was not recorded. Ice thickness detected by the SMARTboot detector was less than 0.015 inch. The magnetostrictive ice detector did not detect surface icing until after the test condition was terminated, the tunnel airspeed was reduced to the very low airspeed resulting from an idling tunnel fan, and the slush on the magnetostrictive ice detector had frozen solid. The data shown in figure 100 were collected at the end of the test condition, following an icing cloud exposure of 3:15 minutes. An ice thickness of 0.19 inch was measured immediately forward and 0.20 inch at the center of the magnetostrictive ice at the end of the test condition.

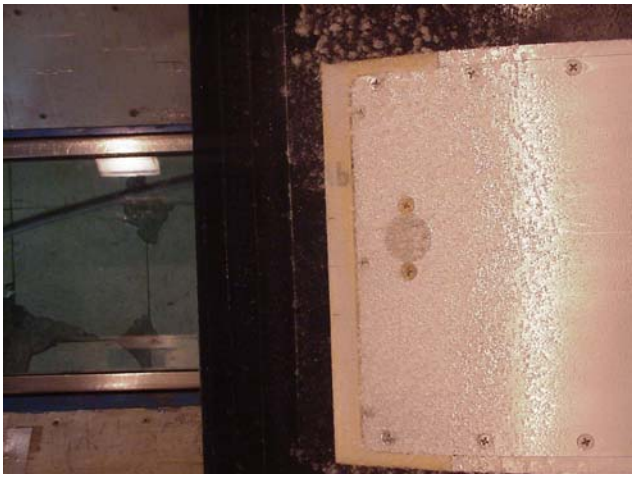

Figure 100. Photograph of Test 9/7 (Upper Surface Leading Edge)

Table 50. Run 9/8 Test Parameters

| Date 3/16/00 | | Run 9/8 | | AOA: 0° | | No Mold | Flap Angle: 0° | | | |
|---|---|---|---|---|---|---|---|---|---|---|
| | | | | | | | Boot Settings | | | Spray Start and Spray Off Time |
| $T_{model}$ (°F) | $T_{st}$ (°F) | $T_{tot}$ (°F) | V (mph) | MVD (μm) | LWC ($g/m^3$) | Time (min:sec) | Initial Fire | Cycle | Activation | |
| 27.70 | 21 (21) | 28.15 | 195 | 40 | 3.00 | 2:25 | 14:26:49 | 1:00 | ID 0:02 | 14:26:47 14:29:13 |
| 27.60 | | | | | | | | | | |
| 29.01 | | | | | | | | | | |
| 31.74 | | | | | | | | | | |
| 29.23 | | | | | | | | | | |

| Tracing Location |
|---|
| No Tracing |

| Ice Thickness Measurements | |
|---|---|
| Location | Thickness |
| Upper | N/A |
| Stagnation | N/A |
| Lower | N/A |

Notes:
$T_{model}$ – The reading of three thermocouples installed on the model
$T_1$ – After body outside
$T_2$ – After body inside
$T_3$ – IB
$T_4$ – CB
$T_5$ – CT

Description/comments: The model AOA was increased to 0° to investigate the ice detector's ability to detect runback ice. The ultrasonic ice detector detected ice 111 seconds after the beginning of the icing cloud exposure. Neither the magnetostrictive nor the SMARTboot ice detectors detected ice, even though the magnetostrictive ice detection threshold frequency was reset to a thinner ice thickness. The data shown in figure 101 were collected at the end of the test condition, following an icing cloud exposure of 2:25 minutes. At the end of the test, an ice thickness of 0.13 inch was measured at the center of the magnetostrictive ice detector. Also, an ice thickness of 0.04 inch was measured on the left SMARTboot and of an ice thickness of 0.05 inch was measured on the right SMARTboot at the chord station of the center of the magnetostrictive ice detector.

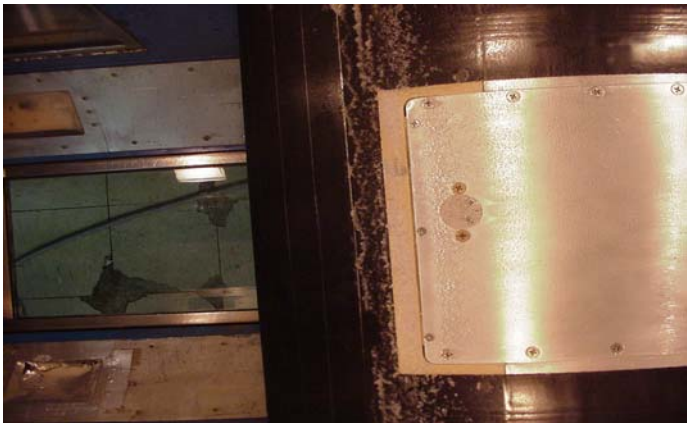

Figure 101. Photograph of Test 9/8 (Upper Surface Leading Edge)

Table 51. Run 9/9 Test Parameters

| Date 3/16/00 | | Run 9/9 | | AOA: 0° | | No Mold | Flap Angle: 0° | | | |
|---|---|---|---|---|---|---|---|---|---|---|
| | | | | | | | Boot Settings | | | Spray Start and Spray Off Time |
| $T_{model}$ (°F) | $T_{st}$ (°F) | $T_{tot}$ (°F) | V (mph) | MVD (μm) | LWC ($g/m^3$) | Time (min:sec) | Initial Fire | Cycle | Activation | |
| 29.29 | 23 (24.8) | 30.40 | 195 | 40 | 3.00 | 3:26 | 14:47:55 | 1:00 | ID 0:02 | 14:47:52<br>14:51:19 |
| 29.12 | | | | | | | | | | |
| 31.31 | | | | | | | | | | |
| 33.16 | | | | | | | | | | |
| 31.11 | | | | | | | | | | |

| Tracing Location |
|---|
| No Tracing |

| Ice Thickness Measurements | |
|---|---|
| Location | Thickness |
| Upper | N/A |
| Stagnation | N/A |
| Lower | N/A |

Notes:
$T_{model}$ – The reading of three thermocouples installed on the model.
$T_1$ – After body outside
$T_2$ – After body inside
$T_3$ – IB
$T_4$ – CB
$T_5$ – CT

Description/comments: The tunnel temperature was increased to 23°F to increase the potential for runback ice. The ultrasonic ice detector detected ice 63 seconds after the beginning of the icing cloud exposure, and the

magnetostrictive ice detector detected ice after 103 seconds. The SMARTboot ice detector detected ice, but the time of detection was not recorded. The data shown in figure 102 were collected at the end of the test condition, following an icing cloud exposure of 3:26 minutes. At the end of the test condition, an ice thickness of 0.19 inch was measured at the center of the magnetostrictive ice detector. Also, an ice thickness of 0.06 inch was measured on the left SMARTboot and an ice thickness of 0.15 inch was measured on the right SMARTboot at the chord station of the center of the magnetostrictive ice detector.

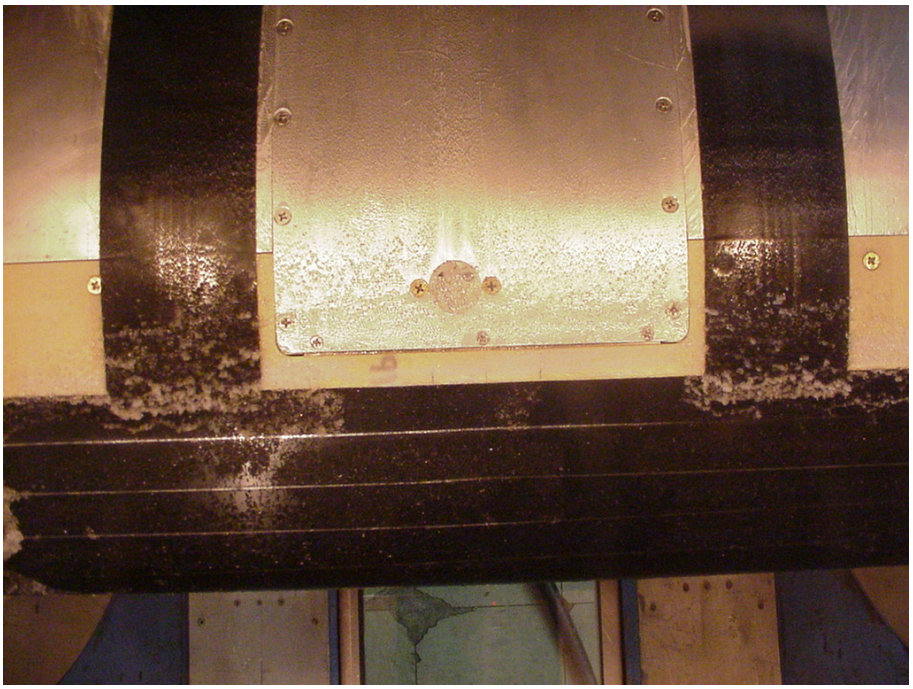

Figure 102. Photograph of Test 9/9 (Upper Surface Leading Edge)

## 4.2 FLIGHT TEST RESULTS.

Using the flight test data recorded by the airplane instrumentation, a data reduction was performed, and the results are presented below. The test airplane weights were influenced by takeoff safety considerations with the simulated ice shapes installed.

### 4.2.1 Lift.

During the flight tests, slowdowns were performed to obtain the $C_L$ × Alpha curves. The aircraft was initially trimmed in wings level flight at a predetermined airspeed, with both engines set to idle and with power for level flight. Then, using the primary longitudinal control only, the airspeed was reduced at a specified deceleration rate until the stick pusher was fired. After that, the aircraft was recovered using normal piloting techniques. Tests were performed in the following configurations: flap up, gear up; flap 15, gear up; and flap 45, gear down.

The tests were performed with weights ranging from 8,980 to 10,920 kg, forward c.g., and altitudes ranging from 7,150 to 17,600 ft.

Before conducting the slowdown tests with ice shapes, tests were performed without ice shapes at the same weight and c.g. conditions used during the tests with intercycle ice. Those tests were intended to establish a baseline to be used as a reference for the tests flown with the intercycle ice shapes.

Table 52 presents the obtained values of $C_{Lmax}$, as defined by the control column pusher AOA, for the baseline and with the intercycle ice for the three tested configurations. A reduction of 25 to 27 percent in $C_{Lmax}$ was observed.

Table 52. $C_{Lmax}$ Values From Flight Test for the Baseline and With Intercycle Ice

| Configuration | $C_{Lmax}$ | | |
|---|---|---|---|
| | Clean (no ice) | With Intercycle Ice | Delta $C_{Lmax}$ |
| Flap Up Gear Up | 1.33 | 0.97 | - 27% |
| Flap 15 Gear Up | 2.00 | 1.49 | - 26% |
| Flap 45 Gear Down | 2.49 | 1.86 | - 25% |

Figures 103 through 105 present the obtained $C_L \times$ Alpha curves, showing the baseline and intercycle curves.

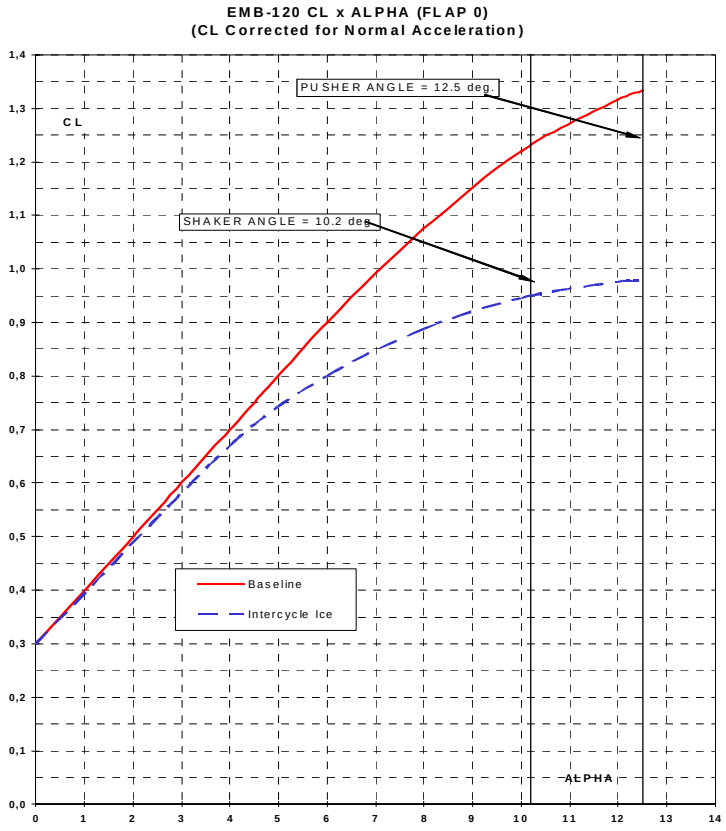


Figure 103. Lift Curve for Flap and Gear Up—Clean and With Intercycle Ice

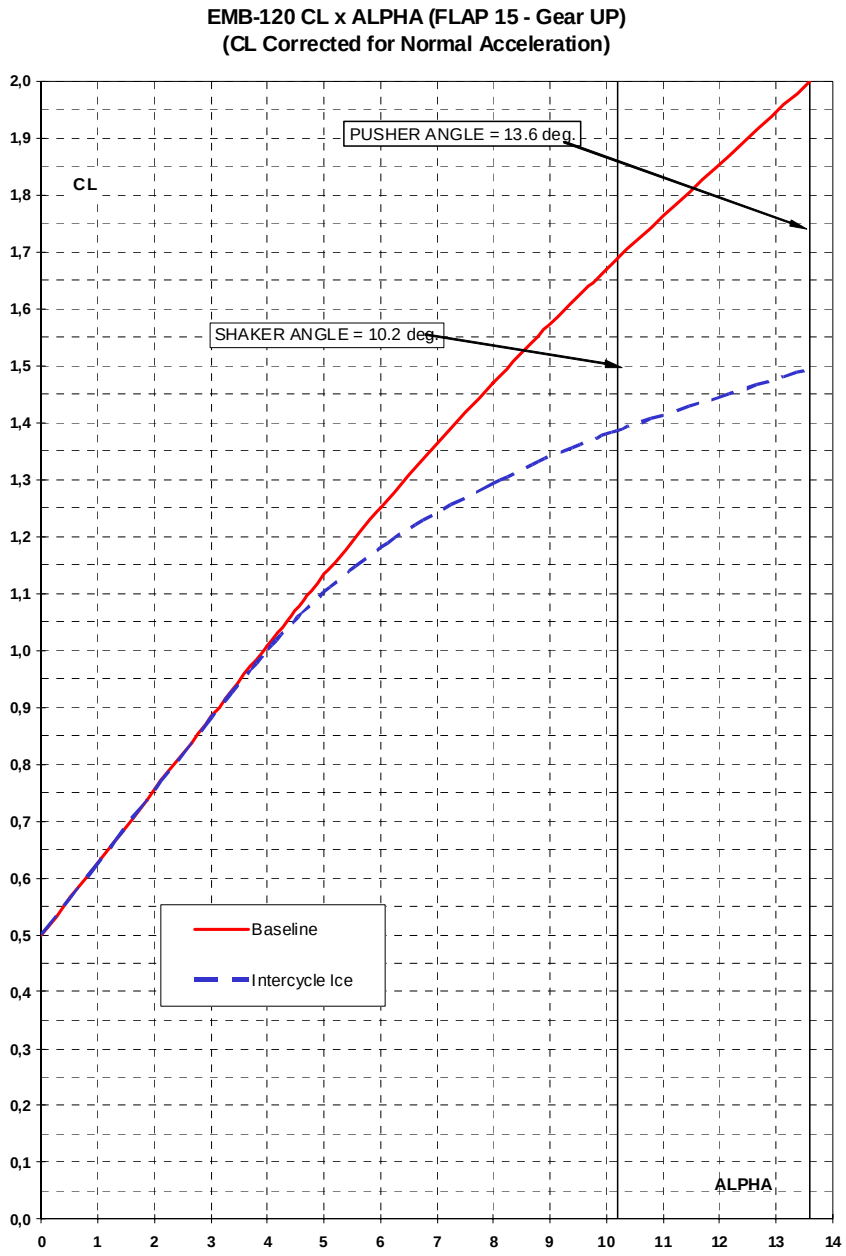


Figure 104. Lift Curve for Flap 15 Gear Up—Clean and With Intercycle Ice

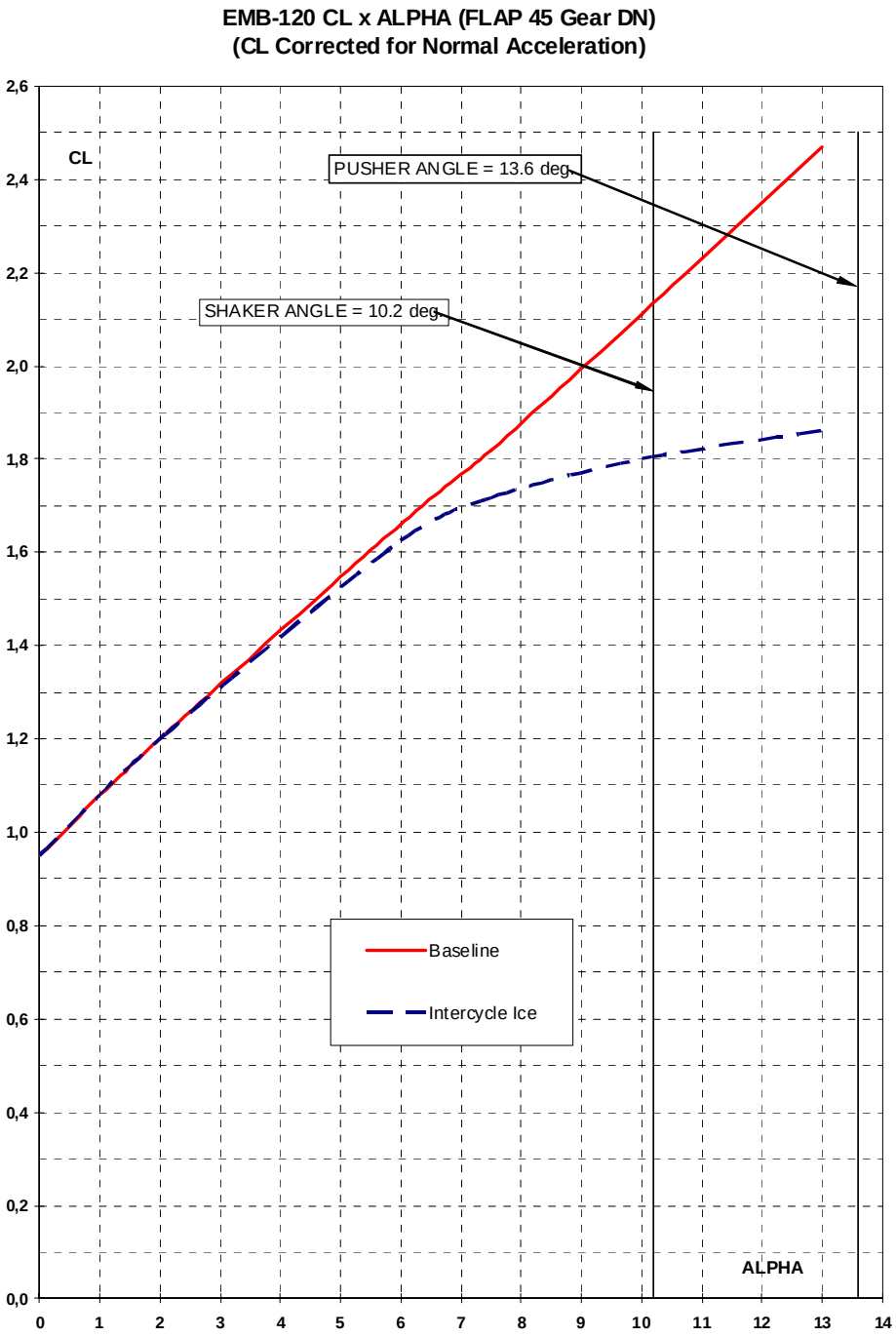


Figure 105. Lift Curve for Flap 45 Gear Down—Clean and With Intercycle Ice

4.2.2 Drag.

Drag polar tests were performed with the intercycle ice shapes, as described in section 3. In addition, a baseline drag polar (aircraft without ice shapes) was also obtained to determine the effect of intercycle ice on the drag polar by comparing the results of those flights.

The aircraft was stabilized at constant speed and altitude, wings level, and cruise configuration for at least 3 minutes. The asymmetric engine power was set as required for keeping the rudder in a neutral position with zero side slip. The propeller speed was set at 100 percent Np. Tests were performed with weights ranging from 10,600 to 10,900 kg, forward c.g., and altitudes ranging from 11,800 to 12,300 ft.

The test points were repeated in the opposite heading for averaging and correcting test results in case of a change in altitude during the tests due to wind gradient effects. Changes in altitude or speed that caused energy variations were also corrected.

For data reduction, engine exhaust thrust was taken from PW118 engine program PW1474/20-F, engine deck PW100/40, basic table 1025, specific table 6001 (May 1985). Propeller efficiency was taken from the following equation:

$$\eta p = 0.8046 - 0.1305 \; x \; C_L{}^2$$

Based on the comparison of two data points for each configuration, the intercycle ice shapes configuration showed more drag than the baseline clean configuration with the landing gear and flaps retracted. For the typical holding condition (approximately 11,250 kilograms force (kgf) and 160 kias), the increase in drag due to ice was as follows:

$$C_{D\_ice} - C_{D\_baseline} = 0.0089$$

Figure 106 presents the drag coefficient measurement results for the clean airplane (baseline) and with the intercycle ice shapes attached.

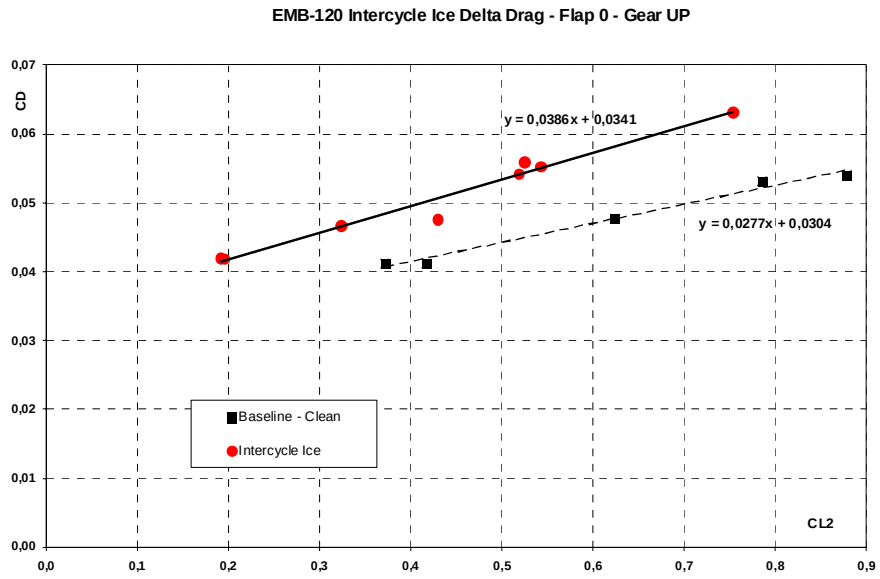


Figure 106. Drag Coefficient for Clean (no ice) and Intercycle Ice—Flap 0

4.2.3 Stability and Control.

In the following sections, the handling qualities of the airplane with the intercycle ice shapes installed are discussed for different test conditions.

4.2.3.1 Stall Speed Determination.

In all configurations, during the approach to the stall, an increasing pull force was always required to reduce the airspeed between the trim speed and the stick pusher firing. The aircraft was easily controlled in all three axes with no tendency to depart in any axis.

In the gear up/flaps up configuration, aerodynamic buffeting was observed to initiate about 10 kias above the stick shaker speed and the buffeting intensity increased as the speed was reduced. A heavy buffeting level was reported by the pilots about 5 kias above the stick shaker speed. The buffet onset was about 10 seconds before stick shaker firing, and the buffeting level was reported by the test pilots to be a clear and distinct indication of the proximity of stall.

In the gear up/flaps 15° and gear down/flaps 25° configurations, the aerodynamic buffet was reported to be initiating at about 2 kias above and 2 seconds before the stick shaker speed.

In the gear down/flaps 15° and gear up/flaps 45° configurations, no buffeting was observed and the stick shaker was, therefore, the only indication to the pilots of the proximity of the stall.

4.2.3.2 Maneuvering Speeds.

The maneuvering speeds published in the Airplane Flight Manual were assessed with the airplane in the intercycle ice configuration. The tests were performed to verify the capability of the aircraft to maneuver with the intercycle ice shapes without the occurrence of stall warning (buffeting or stick shaker).

During the tests, the aircraft was maneuvered at the minimum speeds recommended for icing conditions. In all configurations, except with gear up, flaps 15, and one engine inoperative, banked turns were performed as required to reach a normal acceleration of 1.31 G's, which corresponds to a 40° coordinated banked turn at a constant altitude. Test points performed in the gear up/flaps 15° configuration with the critical engine inoperative were performed up to 1.15 G's, which corresponds to a 30° banked turn.

In the gear up/flaps 0° and gear up/flaps 15° configurations with all engines operating at high power at 160 kias and 140 kias, respectively, the airplane could be maneuvered up to 1.31 G's (corresponding to a 40° banked turn) without any stall warning.

In addition, tests were performed to determine the minimum speeds at which the 1.31-G load factor could be maintained without the occurrence of a stall warning. For the gear up/flaps 0° configuration, the minimum demonstrated speed was $1.13V_{S\_ICE,}$ and in gear up/flaps 15°, the minimum speed was $1.12V_{S\_ICE}$, where $V_{S\_ICE}$ is the determined stall speed. The test pilot reported that the aircraft was fully controllable throughout the maneuvering envelope, and the minimum speeds were defined when light buffeting occurred.

The maneuvering margin was also assessed with the critical engine inoperative in the gear up/flaps 15° configuration. The maneuver was performed with a banked turn of approximately 30° and normal acceleration of 1.15 G's. The test pilot reported that no buffeting occurred and the airplane could be maneuvered down to 105.3 kias, which represented a margin of $1.05V_{S\_ICE}$ at the test weight.

In the gear down/flaps 25° configuration with power on, the airplane was controllable by the test pilot without any buffet or abnormal tendencies. In this configuration, the aircraft could be maneuvered down to 109.6 kias, which represented $1.12V_{S\_ICE}$ at the test weight.

In the gear down/flaps 45° configuration and power on, the airplane could be maneuvered down to 100.3 kias, which represented $1.10V_{S\ ICE}$ with the intercycle ice. The maneuver was performed without any buffet occurrence or abnormal tendencies.

In addition to determining minimum maneuvering speeds as described above, the test pilot reported that 30° bank-to bank-rapid rolls (from 30° left to 30° right and vice-versa) were performed. These rolls were performed to provide a qualitative assessment of the aircraft maneuverability, to confirm that no unusual control responses or noncommanded airplane motions existed, and to confirm buffeting or stall warnings. These tests were performed without rudder to evaluate the influence of sideslip in the roll performance. The aircraft was reported to be fully controllable, with some yaw being exhibited when full ailerons were used. The amount of sideslip generated when using full aileron deflections did not impair the roll maneuver and the aircraft's ability to stop the roll at the opposite bank. The sideslip could be neutralized easily if the pilot made rudder inputs.

4.2.3.3 Stall Characteristics.

Stalls were performed to determine the EMB-120 stall characteristics with intercycle ice shapes. The demonstration included straight flight stalls and turning flight stalls in all operational gear/flap configurations. Tests were performed at high and low weight, with power on, and in flight idle. The maneuvers were performed with aft c.g.

Wings level and turning stalls with 30° bank angles were performed with a trim speed of 1.3Vs and a deceleration rate of 1 kts/sec. The airspeed was reduced using elevator controls only until stick pusher firing. Stall recovery was performed using normal piloting techniques.

4.2.3.3.1 Wings Level Stalls—Flight Idle Power.

During wings level stalls, with the engines in flight idle, a pull force and backward control column displacement was always required to decrease the speed up to stick pusher firing. Lateral and directional control could be easily maintained, and the airplane had no tendency to depart in any axis. Test pilots reported that, except for the gear down/flaps 45° configuration, after the onset of buffeting, its intensity increased from light to moderate as speed was reduced, providing a clear and distinct indication of the approach to stall. Usually, with the gear down and the flaps at 45°, there was no buffeting.

4.2.3.3.2 Wings Level Stalls—Power On.

During the wings level stalls with power on, a pull force and backward control column displacement was always required to decrease the speed up to stick pusher firing. Lateral and directional control could be easily maintained and the airplane had no tendency to depart in any axis. A roll tendency to the left was noticed, which could be easily controlled by the pilot. Test pilots reported that, except for the gear down/flaps 45° configuration, after the onset of buffeting, its intensity increased from light to moderate as speed was reduced, providing a clear and distinct indication of the approach to stall. Usually, with the gear down and the flaps at 45°, there was no buffeting.

4.2.3.3.3 Turning Flight Stalls—Flight Idle Power.

During turning flight stalls (30° of bank) with the engines in flight idle, a pull force and backward control column displacement was always required to decrease speed up to stick pusher firing. Lateral and directional control could be easily maintained and the airplane had no tendency to depart in any axis. The aircraft had a tendency to roll to the wings level attitude. Test pilots reported that, except for the gear down/flaps 45° configuration, after the onset of the buffeting, its intensity increased from light to moderate as speed was reduced, providing a clear and distinct indication of the approach stall. Usually, in the gear down/flaps 45° configuration, there was no buffeting.

4.2.3.3.4 Turning Flight Stalls—Power On.

The stall characteristics of the airplane were similar to the turning flight stalls with idle power. The buffet onset occurred at an average speed of 8.2 kts above the stick shaker and 12 kts above the stick pusher in the UP/UP configuration. In the UP/15 configuration, the onset of buffeting was initiated 5 kts above the stick shaker and 7.8 kts above the stick pusher. With gear down and flaps 15°, the buffet was initiated at an average speed of 4.4 kts above stick shaker and 7.4 kts above stick pusher. With gear down and flaps 25°, the buffet onset was initiated 8.2 kts above the stick shaker and 10.9 kts above the stick pusher. There was no buffeting with gear down and flaps 45°.

In all stall tests, the airplane presented satisfactory handling characteristics. The airplane was controllable in all three axes during deceleration from the trimmed speed to stick pusher. No exceptional piloting skill or strength was required to control the airplane and no misbehavior or mishandling was observed. Decreases in the margins between stick shaker and stick pusher speeds were observed in all configurations; however, aerodynamic buffet and increases in longitudinal control forces as airspeed was reduced were reported by the test pilots as a satisfactory indication of the approach to stall. Only the gear down and flaps 45° configuration did not present aerodynamic buffeting; however, longitudinal control forces and the stick shaker were considered satisfactory to advise the pilot of an approaching stall condition.

4.2.3.4 Autopilot Disconnect Assessment.

The aircraft response to the autopilot disengagement at the stick shaker firing was assessed in both wings level flight and 30° bank turns. The test pilots' report of the aircraft's behavior during the tests is summarized below.

As soon as power was reduced to flight idle at the beginning of the descent, 2° (raw data) of negative sideslip (wind coming from left) developed. The sideslip was eliminated by applying 0.5 unit of left rudder trim, thus centering the ball in the inclinometer.

As the target altitude was reached (10,000 ft), the autopilot held the altitude by trimming the elevator and wings inclination through the aileron servos. The autopilot was automatically disengaged at the shaker speed (125 kts for wings level, 130 kts for $30^o$ left bank, and 132 kts for $30^o$ right bank). At autopilot disengagement, the aircraft was in level flight, with the wings level or with $30^o$ of bank, depending on the test case, and the pitch trim was about 7.5 units nose up. Following the autopilot disengagement, no unusual aircraft behavior was observed. The aircraft attitude in all three axes remained unchanged, with the controls free while the airspeed increased as the altitude was reduced.

The aircraft recovery was conducted by leveling the wings, followed by application of power to increase speed, with the simultaneous use of the electrical pitch trim to reduce push forces. During recovery, the usual EMB-120 left roll tendency with power application was observed.

At one test point, during the recovery, the pilot reported that he waited a few seconds before using the pitch trim. As engine power was increased and airspeed started to increase, a push force was necessary to hold the attitude. It increased from zero at the moment of autopilot disengagement to 15 kgf or 33 lb (pilot's estimate) at about 140 kts. This behavior was as expected (stick force increases as speed increased for an elevator with a constant pitch trim setting). It took approximately 2.5 seconds for the pilot to trim the pitch control force to zero.

Despite the left roll tendency with increasing engine power and untrimmed elevator control forces, the airplane was completely controllable and exhibited no uncommanded movement that could jeopardize the safety of the flight. In all situations, the pilot was able to control the aircraft, stop the roll with opposite aileron, and use elevator inputs to obtain the desired attitude, all without any exceptional piloting skill or strength.

Overall, the tests showed that aircraft recovery could be safely conducted in the case of an uncommanded disengagement of the autopilot without requiring exceptional piloting skills or strength to fly the aircraft.

4.2.3.5 Elevator Deflection and Hinge Moment.

Figure 107 shows the change in the elevator hinge moment due to the presence of intercycle ice shapes on the wing of the airplane, the grit 40 sandpaper on the leading edge of the horizontal tail, and the 45-minute double horn ice shapes on the unprotected areas.

Figures 108 and 109 present the elevator required to trim the airplane for the baseline flight (no ice) and with the intercycle ice for flap 0° (gear up) and for flap 45° (gear down).

What is observed is a reduction of the hinge moment as a function of elevator deflection and an increase in the elevator deflection required to produce the same aircraft AOA. The combination of the two effects produced little effect on the pilot forces to execute the slowdowns. However, a small increase in force was observed, especially for the flaps up configuration.

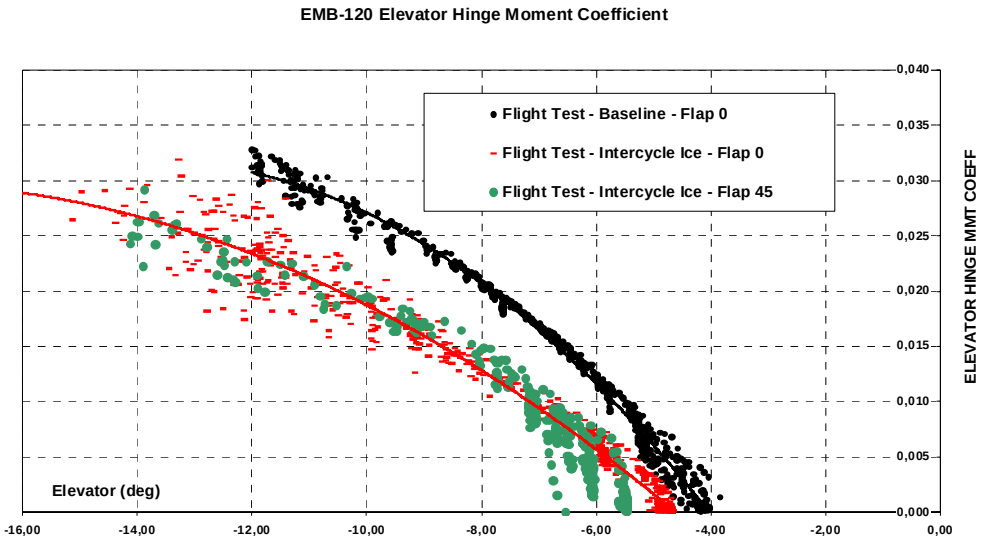


Figure 107. Elevator Hinge Moment—Flaps 0° and 45°—Baseline and With Intercycle Ice

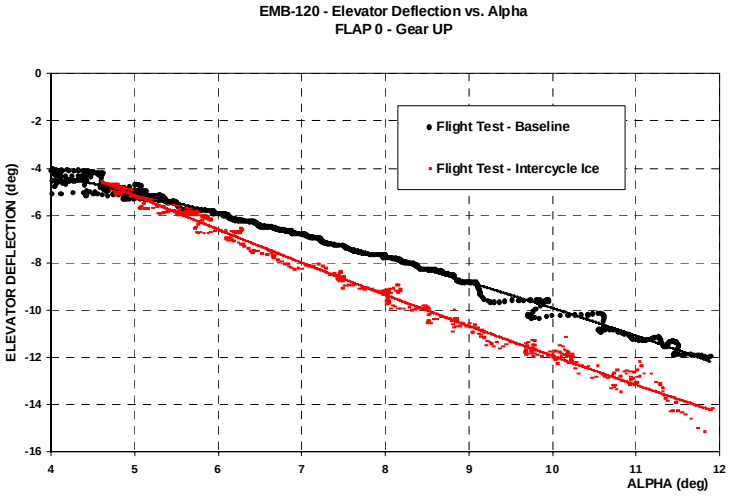


Figure 108. Elevator × Aircraft True AOA—Flap 0°—Baseline and With Intercycle Ice

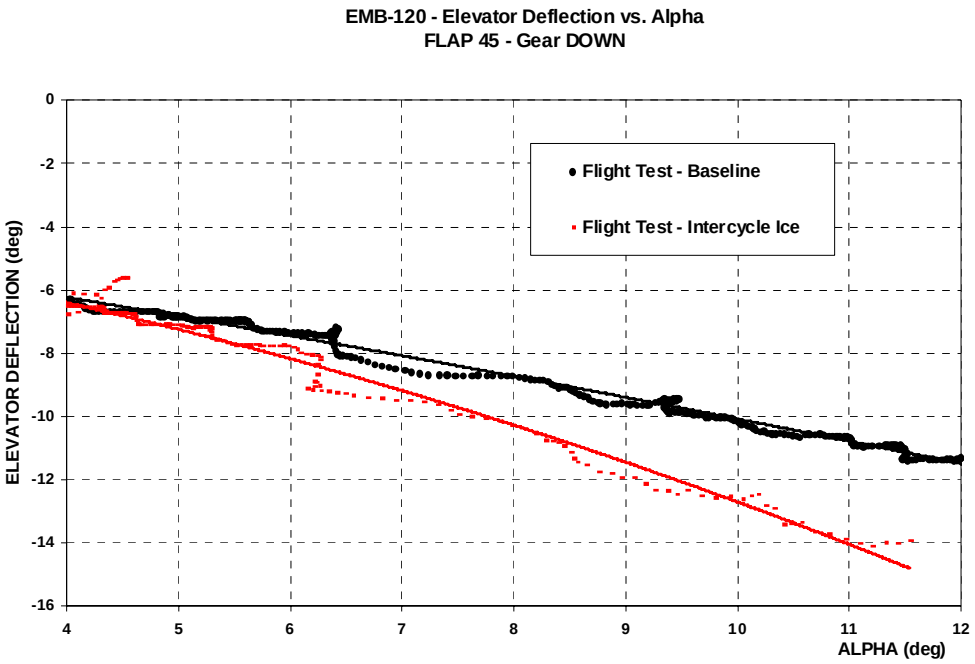


Figure 109. Elevator × Aircraft True AOA—Flap 45°—Baseline and With Intercycle Ice

## 5. CONCLUSIONS.

Photographs of ice that would accumulate before an ice protection system becomes fully effective were taken at 170 knots (kts) in Title 14 Code of Federal Regulations (CFR) Part 25, Appendix C icing conditions. The surface roughness consisted of small, uniformly distributed semihemispheres. The density of the roughness was greater than the 8 to 10 grains per square centimeter previously considered representative of preactivation ice. The data recorded can be used to simulate preactivation ice on flight test airplanes.

Ice shapes remaining after cycling of a deicing boot were documented with photographs, video recordings, tracings, and ice thickness measurements. The character of the intercycle ice varied with the number of cycles, with thin ice being shed during subsequent cycles. Since airplanes can operate in icing clouds that extend beyond the standard cloud extents of 14 CFR Part 25 Appendix C intercycle ice, investigations should consider continuous operation of the deicing boots. The intercycle ice characteristics varied with temperature, liquid water content, and drop size. Selected cases of special interest were documented with molds from which ice castings were made. These castings are available for subsequent aerodynamic testing and other purposes. The intercycle ice roughness was significant and adversely affected the aerodynamic performance of the airfoil. During certification with normal operation of the deicing boots, the protected surfaces of the deicing boots should be characterized by ice roughness found during this investigation. Note that the deicing boot performance found during this investigation are only applicable for airplanes that operate at an indicated airspeed of about 170 kts.

Since the ice shedding performance of pneumatic deicing boots varies with airspeed, the deicing boot performance results from this investigation are questionable for airplanes that operate at lower airspeeds. There are a large number of general aviation and utility airplanes that operate at lower airspeeds. A second test of the model used for this investigation at an airspeed of about 100 kts is recommended. The ice-shedding shearing force at 170 kts is 290 percent higher than at 100 kts. Also, an atmospheric icing wind tunnel was used for this investigation. Testing of the model in a pressurized icing wind tunnel is recommended so that the deicing performance of the deicing boots can be investigated at the ice-shedding shearing forces that occur at operational altitudes and airspeeds.

Flight testing of the deicing boots intercycle ice, using a fully instrumented EMBRAER EMB-120 aircraft, showed lift losses of 25 to 27 percent at the airplane angle of attack (AOA) for the control column pusher. The lift losses were greater at the aerodynamic stall AOA. At the recommended icing conditions maneuvering speed of 160 kts, the increase in drag was 0.0089.

Using the Ruff method for scaling test conditions, intercycle ice roughness obtained on a model that was one-half the scale of the hybrid model compared well with that obtained on the hybrid model. However, the tests with the smaller model tended to produce ice that was less rough than the hybrid model and often did not reproduce the large-scale roughness elements seen during the hybrid model tests. These differences may have occurred because the models' deicers were not scaled from what would have been installed on the full-scale airfoil.

The surface ice detector test results were tenuous. However, the results did show the potential for use of a local surface ice detector for detecting ice accretion aft of a lifting surface's leading-edge ice protection system.

The collaborative research program included a December 1999 icing wind tunnel test of a 36-inch chord NACA 23012 model. Castings of intercycle ice accretions made during that test were used during a subsequent aerodynamic test in the Low Turbulence Pressure Tunnel at the NASA Langley Research Center. An ice shape scaling study was conducted using the results of paired runs from the December 1999 and the hybrid model tests.

The results of these investigations, and from other testing in the collaborative research program, underscore the need to carefully consider the effects of intercycle and preactivation ice accretions during the certification of aircraft that use pneumatic deicing boots. The test results also provide information that supports the activation of lifting surfaces' deicers at the first detection of ice formation on the aircraft's lifting surfaces and for the operation of deicers in the automatic cycling mode.

## 6. REFERENCES.


1. Riley, J.T., Rios, M.A., Anderson, D.N., and Dumont, C.J., "A Study of Intercycle, Residual and Preactivation Ice," AIAA-2001-0089, paper presented at the 39th Aerospace Sciences Meeting, Reno, NV, January 2001.

2. Broeren, A.P. and Bragg, M.B., "Effect of Residual and Intercycle Ice Accretions on Airfoil Performance," FAA report DOT/FAA/AR-02/68, May 2002.

3. Anderson, D.N., Botura, G.C., and Broeren, A.P., "A Study of Scaling for Intercycle Ice Accretion Tests," AIAA-2001-0834, paper presented at the 39th Aerospace Sciences Meeting, Reno, NV, January 2001.

4. Rios, M.A., Botura, G.C., Dumont, C.J., Koosmann, M., and Sweet, D., "Intercycle and Residual Ice—Ice Detector Testing," presented at SAE AC9C Subcommittee Meeting # 33, Portland, Maine, September 2000.

5. Bowden, D.T., "Effect of Pneumatic De-Icers and Ice Formations on Aerodynamic Characteristics of an Airfoil," NACA TN 3564, February 1956.

6. Albright, A.E., Kohlman, D.L., Schweikhard, W.G., and Evanich, P., "Evaluation of a Pneumatic Boot Deicing System on a General Aviation Wing Model," NASA-TM-82363, June 1981.

7. Shin, J. and Bond, T.H., "Surface Roughness Due to Residual Ice in the Use of Low-Power Deicing Systems," NASA TM 105971, AIAA-93-0031, paper presented at the 31st Aerospace Sciences Meeting, Reno, NV, January 1993.

8. Reichold, J.D. and Bragg, M.B., "Residual Ice Characteristics and the Resulting Aerodynamic Performance Penalties," NASA AGATE Task 4.1.1.3.2.1, University of Illinois at Urbana-Champaign, October 1996.

9. Jackson, D.G. and Bragg, M.B., "Effect of Simulated Ice and Residual Ice Roughness on the Performance on a Natural Laminar Flow Airfoil," NASA NCA-3-AGATE-110, University of Illinois at Urbana-Champaign, February 2000.

10. Hill, E.G., "Airplane Deicing Ice Protection Systems, Deicing Boot Ice Bridging, and Airplane Operating Procedures During In-Flight Icing Conditions," Federal Aviation Administration Transportation Airplane Directorate, February 1999.

11. Hill, E.G. and Reehorst, A.L. (eds.), "FAA/NASA Deicing Boot Ice Bridging Workshop Proceedings," Ohio Aerospace Institute, Cleveland, Ohio, November 19, 1997.

# APPENDIX A—THE DESIGN OF A HYBRID AIRFOIL FOR THE NACA 23012 AIRFOIL

## A.1 INTRODUCTION.

This appendix documents the design of a hybrid airfoil to simulate full-scale ice accretions on the National Advisory Committee for Aeronautics (NACA) 23012 airfoil. The first part of this appendix documents the preliminary design of a hybrid airfoil optimized for a 2° angle of attack (AOA). Then, the hybrid airfoil performance and corrections at off-design conditions (0° and 4° AOA) are discussed.

## A.2 DESIGN REQUIREMENTS.

A hybrid airfoil was designed as the icing tunnel model for the NACA 23012. The design requirements and operating conditions were provided as follows:

## A.3 MODEL CONSIDERATIONS.

- Full-scale airfoil: NACA 23012
- Full-scale airfoil chord: 6 ft
- Hybrid airfoil chord: 3 ft
- AOA: 2 degree (0° and 4° off-design)
-

## A.4 ICING TUNNEL CONDITIONS.

- Speed: 200 mph
- Static temperature range: -4º to 21ºF
- Water droplet median volume diameters (MVD): 20 and 40 microns

From the temperature range, the resulting Reynolds number (*Re*) range was calculated and lies between 12.8 $\times 10^6$ and 14.7 $\times 10^6$, based on the full-scale 6-ft chord. Table A-1 lists the coordinates of the full-scale NACA 23012 airfoil [A-1].

Table A-1. Full-Scale Airfoil Coordinates NACA 23012

| x/c | y/c | x/c | y/c | x/c | y/c | x/c | y/c |
|---|---|---|---|---|---|---|---|
| 1.000000 | 0.001260 | 0.280469 | 0.075822 | 0.000909 | -0.002293 | 0.319876 | -0.044912 |
| 0.980454 | 0.004414 | 0.266996 | 0.075942 | 0.002187 | -0.004444 | 0.334429 | -0.045056 |
| 0.960887 | 0.007504 | 0.253805 | 0.075967 | 0.003825 | -0.006456 | 0.349239 | -0.045118 |
| 0.941333 | 0.010529 | 0.240899 | 0.075897 | 0.005816 | -0.008335 | 0.364301 | -0.045098 |
| 0.921801 | 0.013491 | 0.228285 | 0.075732 | 0.008152 | -0.010087 | 0.379610 | -0.044998 |
| 0.902297 | 0.016391 | 0.215967 | 0.075473 | 0.010826 | -0.011719 | 0.395160 | -0.044818 |
| 0.882830 | 0.019230 | 0.203949 | 0.075121 | 0.013829 | -0.013238 | 0.410944 | -0.044558 |
| 0.863407 | 0.022009 | 0.192178 | 0.074674 | 0.017154 | -0.014653 | 0.426957 | -0.044221 |
| 0.844035 | 0.024728 | 0.180601 | 0.074113 | 0.020795 | -0.015974 | 0.443191 | -0.043806 |
| 0.824723 | 0.027388 | 0.169241 | 0.073419 | 0.024747 | -0.017209 | 0.459642 | -0.043316 |
| 0.805477 | 0.029988 | 0.158115 | 0.072573 | 0.029003 | -0.018369 | 0.476302 | -0.042751 |
| 0.786305 | 0.032528 | 0.147244 | 0.071563 | 0.033558 | -0.019463 | 0.493166 | -0.042114 |
| 0.767214 | 0.035009 | 0.136648 | 0.070378 | 0.038409 | -0.020501 | 0.510226 | -0.041405 |
| 0.748212 | 0.037430 | 0.126345 | 0.069011 | 0.043553 | -0.021492 | 0.527476 | -0.040625 |
| 0.729306 | 0.039790 | 0.116354 | 0.067461 | 0.048988 | -0.022447 | 0.544910 | -0.039777 |
| 0.710503 | 0.042089 | 0.106694 | 0.065725 | 0.054713 | -0.023375 | 0.562520 | -0.038862 |
| 0.691811 | 0.044326 | 0.097383 | 0.063809 | 0.060729 | -0.024284 | 0.580300 | -0.037880 |
| 0.673237 | 0.046499 | 0.088435 | 0.061718 | 0.067038 | -0.025183 | 0.598242 | -0.036834 |
| 0.654788 | 0.048608 | 0.079868 | 0.059460 | 0.073642 | -0.026078 | 0.616341 | -0.035724 |
| 0.636470 | 0.050651 | 0.071695 | 0.057047 | 0.080546 | -0.026978 | 0.634589 | -0.034553 |
| 0.618292 | 0.052627 | 0.063928 | 0.054491 | 0.087756 | -0.027887 | 0.652978 | -0.033321 |
| 0.600260 | 0.054534 | 0.056579 | 0.051808 | 0.095278 | -0.028812 | 0.671503 | -0.032028 |
| 0.582381 | 0.056371 | 0.049659 | 0.049012 | 0.103121 | -0.029755 | 0.690155 | -0.030677 |
| 0.564662 | 0.058137 | 0.043174 | 0.046122 | 0.111293 | -0.030720 | 0.708927 | -0.029268 |
| 0.547109 | 0.059829 | 0.037131 | 0.043155 | 0.119803 | -0.031708 | 0.727813 | -0.027802 |
| 0.529730 | 0.061446 | 0.031536 | 0.040128 | 0.128663 | -0.032719 | 0.746805 | -0.026278 |
| 0.512531 | 0.062986 | 0.026393 | 0.037059 | 0.137884 | -0.033749 | 0.765895 | -0.024699 |
| 0.495519 | 0.064448 | 0.021702 | 0.033967 | 0.147475 | -0.034795 | 0.785077 | -0.023063 |
| 0.478700 | 0.065829 | 0.017466 | 0.030868 | 0.157450 | -0.035850 | 0.804343 | -0.021371 |
| 0.462081 | 0.067128 | 0.013683 | 0.027778 | 0.167820 | -0.036903 | 0.823685 | -0.019623 |
| 0.445668 | 0.068344 | 0.010351 | 0.024713 | 0.178596 | -0.037942 | 0.843096 | -0.017819 |
| 0.429467 | 0.069475 | 0.007469 | 0.021686 | 0.189789 | -0.038950 | 0.862568 | -0.015958 |
| 0.413485 | 0.070519 | 0.005033 | 0.018709 | 0.201409 | -0.039905 | 0.882095 | -0.014039 |
| 0.397728 | 0.071475 | 0.003037 | 0.015795 | 0.213399 | -0.040788 | 0.901669 | -0.012062 |
| 0.382202 | 0.072342 | 0.001478 | 0.012951 | 0.225694 | -0.041590 | 0.921281 | -0.010025 |
| 0.366912 | 0.073118 | 0.000349 | 0.010186 | 0.238289 | -0.042311 | 0.940925 | -0.007928 |
| 0.351865 | 0.073803 | -0.000356 | 0.007505 | 0.251179 | -0.042951 | 0.960594 | -0.005770 |
| 0.337067 | 0.074395 | -0.000645 | 0.004913 | 0.264359 | -0.043509 | 0.980278 | -0.003547 |
| 0.322522 | 0.074893 | -0.000523 | 0.002411 | 0.277824 | -0.043984 | 1.000000 | -0.001260 |
| 0.308237 | 0.075297 | 0.000000 | 0.000000 | 0.291568 | -0.044376 | | |
| 0.294218 | 0.075607 | 0.000000 | 0.000000 | 0.305588 | -0.044685 | | |

## A.5 DESIGN METHODOLOGY.

A conceptual illustration of the hybrid airfoil design procedure is shown in figure A-1. The hybrid airfoil was designed using the method of Saeed, et al. [A-2]. First, a droplet impingement code was used to predict the droplet impingement limits. (The droplet code, AIRDROP, is discussed in section A.6.) Once the limits of impingement were known over the leading edge of the full-scale airfoil, that part of the full-scale airfoil geometry was fixed for subsequent hybrid airfoil shapes. For the sake of discussion, this fixed leading-edge section, which is common to both the full-scale and hybrid airfoil, is referred to as the nose section and the remaining hybrid airfoil profile is referred to as the aft section. The aft section of the hybrid airfoil was then designed to provide full-scale flow field and droplet impingement on the nose section of the hybrid airfoil.

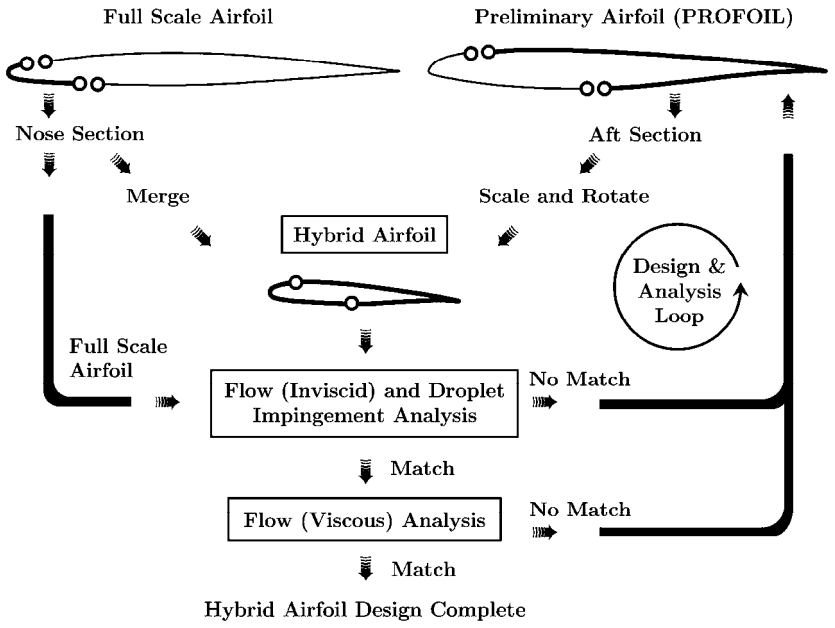


Figure A-1. Conceptual Illustration of the Modified Hybrid Airfoil Design Procedure

An initial geometry for the aft section was obtained through the use of a multipoint inverse airfoil design code (PROFOIL). The design of this intermediate airfoil, from which the aft section of the hybrid airfoil was derived, is governed by several constraints, namely, the scale of the subscale airfoil (i.e., the size relative to full-scale, such as 50 percent, 75 percent, etc.), the upper and lower surface thickness, the slope at the junctions between the nose and the aft sections, and a desired form of pressure recovery characteristics. Once the constraints were satisfied, the aft section was combined with the nose section to form a hybrid airfoil.

The potential flow over both the full-scale and hybrid airfoils was then analyzed using the Eppler code. To have a physically similar flow and, therefore, similar droplet impingement in the vicinity of the nose section of both the hybrid and full-scale airfoils, the analysis was performed at the same AOA relative to the nose section chord of both airfoils. If the desired velocity distribution over the nose section and the stagnation point was not achieved, the aft section of the

hybrid airfoil was redesigned and again merged with the nose section to form a new hybrid airfoil. The flow over the new hybrid airfoil was then analyzed and compared with that over the full-scale airfoil. The process was repeated until the desired inviscid velocity distribution over the nose section and stagnation point location was achieved. The hybrid circulation, water droplet trajectories, and water droplet impingement characteristics were determined. The impingement characteristics of both the full-scale and hybrid airfoils were then compared. If the agreement in the impingement characteristics was poor, the hybrid airfoil was modified and the design process was repeated until good agreement was reached.

The task of simulating full-scale, droplet-impingement characteristics throughout the desired AOA range can be accomplished by introducing a plain flap on the hybrid airfoil [A-3]. The term off-design is being used to indicate off-design angles of attack only. The effects of other important variables, such as varying droplet size or flight conditions, were not considered at this time. It is important to note that this method has been validated experimentally in the NASA Icing Research Tunnel [A-4].

## A.6 DESIGN CODES.

The methods used to design and analyze the hybrid airfoil were XFOIL [A-5], PROFOIL [A-6], XDROP and AIRDROP [A-7], and HYBRID [A-8]. PROFOIL is a multipoint inverse airfoil design method based on conformal mapping, which allows the designer to tailor the inviscid velocity distributions while satisfying several other specifications, such as maximum thickness, camber, pitching moment, trailing-edge shape, and nose droop. The desired inviscid velocity distribution is achieved by dividing the airfoil into several segments, each having a design angle of attack $\alpha^*$. By adjusting the $\alpha^*$ distribution on the upper and lower surfaces, the desired velocity distribution can be precisely controlled, which in turn results in the shape of the airfoil. AIRDROP is a droplet trajectory program used to calculate the impingement of icing cloud-sized water droplets on single-element airfoils. The code uses a Lagrangian method to calculate a series of individual droplet trajectories. From the trajectory information, the local dimensionless impingement efficiency, $\beta$, is determined along with the total collection efficiency and upper- and lower-surface impingement limits.

HYBRID is an integrated program that incorporates PROFOIL for the aft section design and AIRDROP for droplet impingement analysis. XFOIL is a viscous airfoil design and analysis method that couples a panel method with an integral boundary layer method. The viscous and inviscid calculations are coupled using a Newton iteration scheme. XDROP is a modified version of XFOIL, integrating the AIRDROP code into it to enable droplet impingement analysis using a viscous flow field.

In the current design work, HYBRID was used for rapid, interactive design. XDROP was later used for postdesign viscous analysis over the required *Re* range and for design of an optimum flap setting to match the $\beta$-curve at the off-design conditions.

A.7 HYBRID AIRFOIL DESIGN.

A preliminary design of the hybrid airfoil was obtained using HYBRID. The NACA 23012 airfoil was used as a full-scale airfoil input for HYBRID. Since the hybrid airfoil was to be designed for 0°, 2°, and 4° AOA, it was optimized for the 2° case. After several iterations of the design of the hybrid aft section, close agreement between the $\beta$-curves of the full-scale and hybrid airfoils was achieved with a desired pressure distribution. The initial optimal hybrid airfoil shape, designated the SU 1030, is shown in figure A-2 together with the full-scale NACA 23012 airfoil.

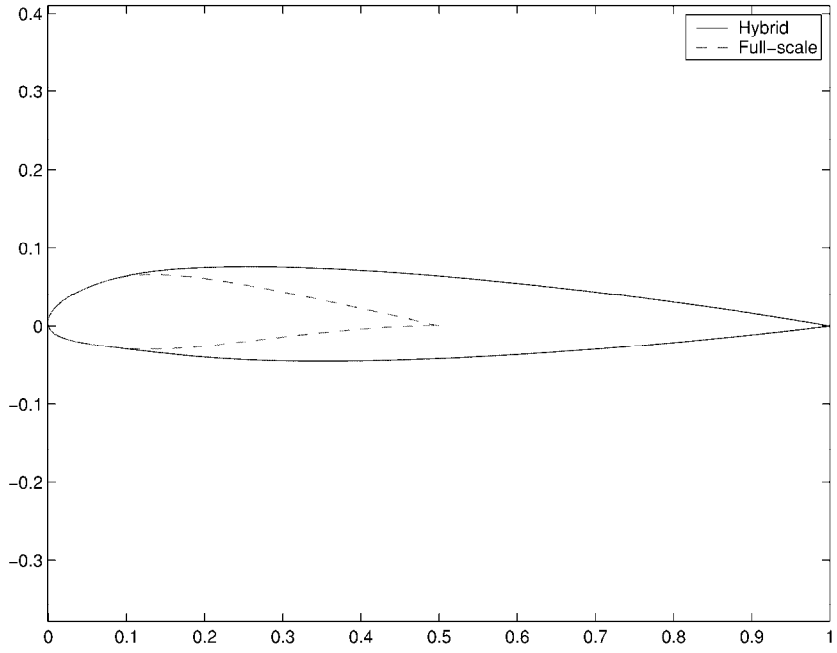


Figure A-2. Full-Scale (NACA 23012) and Optimal Hybrid (SU 1030) Airfoils

Once the preliminary hybrid airfoil was designed, the coordinates of the hybrid airfoil were obtained from HYBRID and a viscous analysis of the hybrid airfoil was performed using XFOIL at $Re = 12.8 \times 10^6$ and $14.2 \times 10^6$. The pressure distribution was then smoothed in an interactive iterative process using the QDES routine in XFOIL. Figure A-3 shows the velocity distribution of the final hybrid airfoil compared to the full-scale NACA 23012. Note that this velocity distribution shown reveals information equivalent to the pressure distribution. Table A-2 lists the coordinates of the final hybrid airfoil. The droplet impingement characteristics of the full-scale and hybrid airfoils were computed again using viscous flow field results from XFOIL. These new results compared very well with the hybrid design obtained using inviscid design methods.

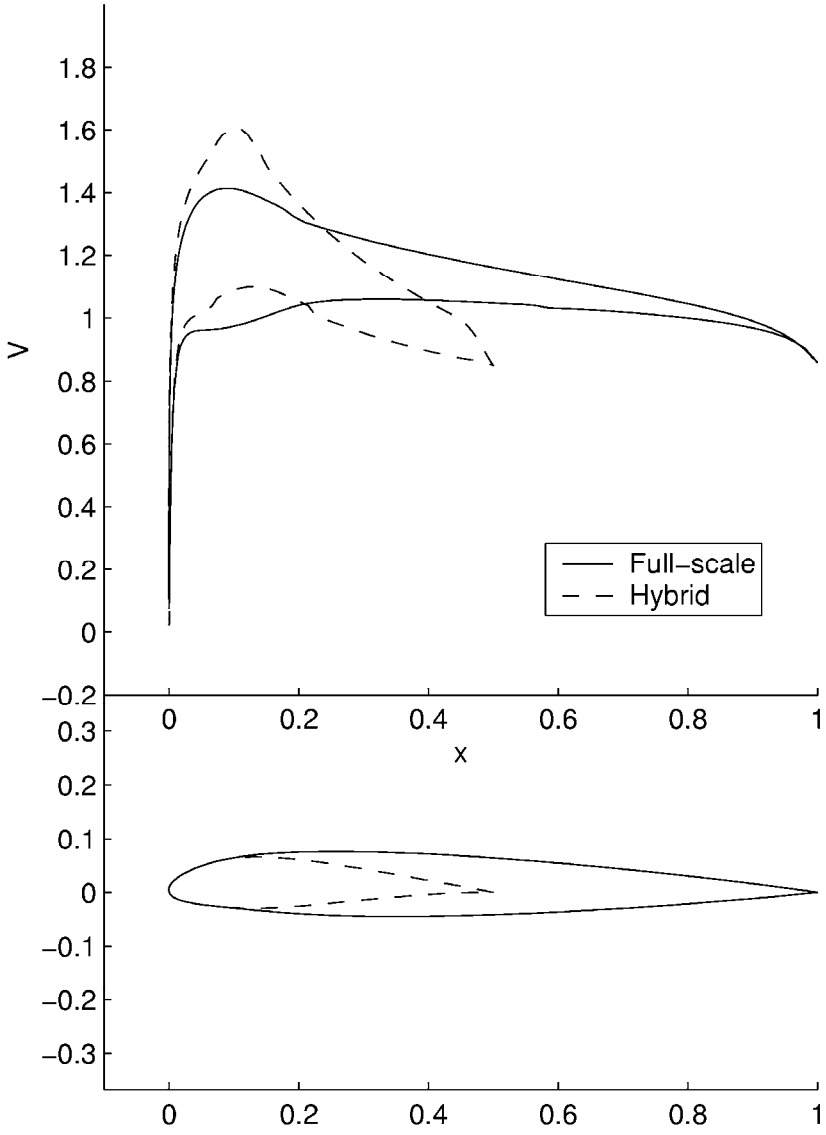


Figure A-3. Full-Scale and Hybrid Airfoils Velocity Distributions for $\alpha = 2°$, $Re = 12.8 \times 10^6$

Table A-2. Hybrid Airfoil Coordinates SU 1030

| x/c | y/c | x/c | y/c | x/c | y/c | x/c | y/c |
|---|---|---|---|---|---|---|---|
| 0.500066 | 0.000620 | 0.119336 | 0.065572 | -0.000628 | 0.003528 | 0.159223 | -0.028826 |
| 0.495649 | 0.001404 | 0.111441 | 0.064992 | -0.000490 | 0.002179 | 0.169751 | -0.028227 |
| 0.488418 | 0.002930 | 0.103762 | 0.064119 | -0.000224 | 0.000814 | 0.180477 | -0.027456 |
| 0.480282 | 0.004783 | 0.096268 | 0.062970 | 0.000181 | -0.000554 | 0.191414 | -0.026523 |
| 0.471279 | 0.006870 | 0.088950 | 0.061560 | 0.000730 | -0.001915 | 0.202580 | -0.025440 |
| 0.461543 | 0.009091 | 0.081814 | 0.059903 | 0.001427 | -0.003258 | 0.214002 | -0.024205 |
| 0.451185 | 0.011368 | 0.074877 | 0.058015 | 0.002277 | -0.004572 | 0.225791 | -0.022853 |
| 0.440233 | 0.013692 | 0.068154 | 0.055924 | 0.003278 | -0.005847 | 0.237826 | -0.021455 |
| 0.428759 | 0.016097 | 0.061684 | 0.053699 | 0.004431 | -0.007079 | 0.250027 | -0.020017 |
| 0.416939 | 0.018579 | 0.055553 | 0.051410 | 0.005733 | -0.008266 | 0.262338 | -0.018558 |
| 0.404915 | 0.021113 | 0.049825 | 0.049083 | 0.007185 | -0.009407 | 0.274688 | -0.017097 |
| 0.392777 | 0.023684 | 0.044525 | 0.046748 | 0.008787 | -0.010505 | 0.287033 | -0.015645 |
| 0.380573 | 0.026279 | 0.039661 | 0.044432 | 0.010545 | -0.011562 | 0.299339 | -0.014214 |
| 0.368344 | 0.028887 | 0.035224 | 0.042155 | 0.012468 | -0.012583 | 0.311591 | -0.012813 |
| 0.356123 | 0.031492 | 0.031194 | 0.039933 | 0.014567 | -0.013573 | 0.323790 | -0.011450 |
| 0.343939 | 0.034082 | 0.027543 | 0.037773 | 0.016858 | -0.014537 | 0.335923 | -0.010129 |
| 0.331813 | 0.036646 | 0.024240 | 0.035679 | 0.019362 | -0.015479 | 0.347988 | -0.008861 |
| 0.319757 | 0.039173 | 0.021252 | 0.033654 | 0.022106 | -0.016403 | 0.359986 | -0.007649 |
| 0.307785 | 0.041654 | 0.018550 | 0.031694 | 0.025123 | -0.017318 | 0.371904 | -0.006499 |
| 0.295902 | 0.044075 | 0.016106 | 0.029798 | 0.028455 | -0.018227 | 0.383735 | -0.005421 |
| 0.284116 | 0.046429 | 0.013894 | 0.027961 | 0.032151 | -0.019138 | 0.395468 | -0.004421 |
| 0.272438 | 0.048704 | 0.011893 | 0.026178 | 0.036271 | -0.020058 | 0.407074 | -0.003505 |
| 0.260869 | 0.050889 | 0.010082 | 0.024446 | 0.040885 | -0.020989 | 0.418523 | -0.002686 |
| 0.249427 | 0.052974 | 0.008445 | 0.022759 | 0.046068 | -0.021945 | 0.429768 | -0.001970 |
| 0.238118 | 0.054946 | 0.006969 | 0.021112 | 0.051894 | -0.022927 | 0.440742 | -0.001368 |
| 0.226954 | 0.056792 | 0.005643 | 0.019503 | 0.058414 | -0.023941 | 0.451359 | -0.000889 |
| 0.215948 | 0.058503 | 0.004457 | 0.017925 | 0.065644 | -0.024988 | 0.461514 | -0.000540 |
| 0.205120 | 0.060064 | 0.003404 | 0.016376 | 0.073454 | -0.026053 | 0.471095 | -0.000321 |
| 0.194485 | 0.061463 | 0.002478 | 0.014853 | 0.081758 | -0.026993 | 0.479985 | -0.000226 |
| 0.184065 | 0.062689 | 0.001675 | 0.013354 | 0.090546 | -0.027810 | 0.488106 | -0.000256 |
| 0.173887 | 0.063730 | 0.000993 | 0.011878 | 0.099705 | -0.028488 | 0.495445 | -0.000423 |
| 0.163972 | 0.064575 | 0.000430 | 0.010423 | 0.109155 | -0.029007 | 0.499934 | -0.000620 |
| 0.154352 | 0.065216 | -0.000014 | 0.008992 | 0.118827 | -0.029350 | | |
| 0.145058 | 0.065642 | -0.000341 | 0.007586 | 0.128681 | -0.029507 | | |
| 0.136102 | 0.065850 | -0.000551 | 0.006207 | 0.138697 | -0.029471 | | |
| 0.127520 | 0.065844 | -0.000646 | 0.004862 | 0.148876 | -0.029242 | | |

Finally, the hybrid airfoil viscous performance and droplet impingement characteristics were analyzed using XDROP at the *Re* of $12.8 \times 10^6$ and $14.5 \times 10^6$. Figure A-4 compares the $\beta$-curves of full-scale and hybrid airfoils at a 2° AOA using the viscous flow field from XDROP at $Re = 12.8 \times 10^6$.

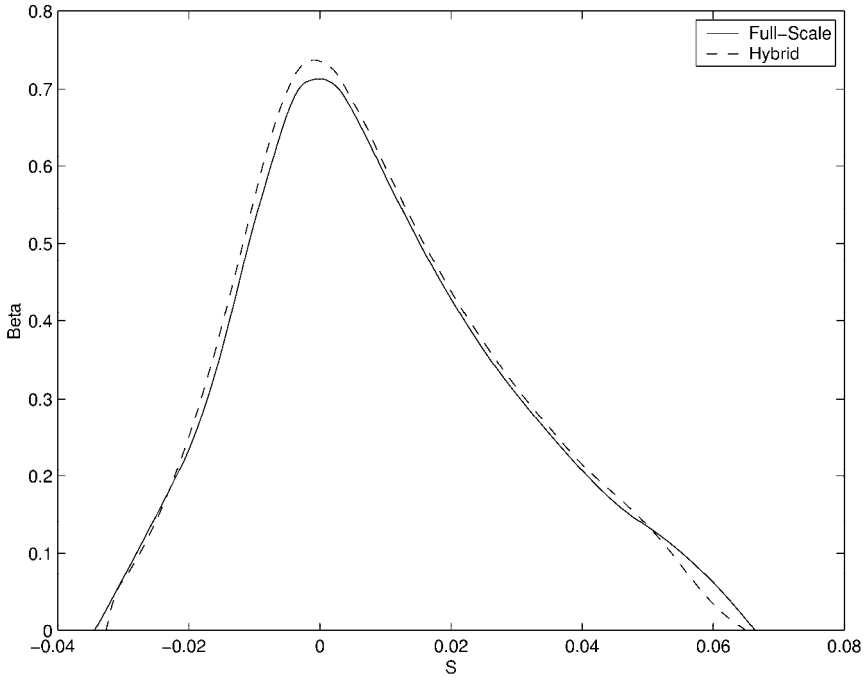


Figure A-4. Full-Scale and Hybrid Airfoil $\beta$-Curves at $\alpha = 2°$, $Re = 12.8 \times 10^6$ (XDROP used for analysis)

A.8 OFF-DESIGN.

If no change in the hybrid airfoil was made when analyzing it at an off-design AOA, then the $\beta$-curves were offset, depending upon how far in AOA the optimized airfoil was from the optimized AOA. This offset in the $\beta$-curves is produced by the difference in the circulation of the full-scale and hybrid airfoils at the particular off-design AOA. Figure A-5 underscores this fact: Point A is the design condition for which the circulation and, hence, the $\beta$-curves of hybrid and full-scale airfoils nearly match. (In the figure, $C_l$ is nondimensionalized by the full-scale chord. Hence, the $C_l$ indicated is proportional to the load on the airfoil and, therefore, the circulation. Stated another way, the hybrid lift coefficient is based on a chord of 0.5, so the lift coefficient is half the value that would be obtained using a chord of 1.0.) When operated at a different AOA, the hybrid airfoil generates less (or more) circulation, depending on whether or not the new AOA is higher (or lower) than the design AOA of 2°. To match the $\beta$-curves for the off-design conditions, a flap is, therefore, needed to control the amount of circulation that drives the droplet impingement.

A 20 percent chord flap was used on the hybrid airfoil to adjust circulation and match the $\beta$-curve at the off-design conditions of 0° and 4° AOA. Figures A-6 and A-7 show the velocity distribution and $\beta$-curves comparison of the hybrid airfoil without any correction at the 4° AOA. It can be seen that the $\beta$- curve peak of the hybrid airfoil is at an offset more toward the upper surface. To move the stagnation point toward the lower surface, the hybrid airfoil circulation has to be increased. Thus, a positive flap deflection was needed.

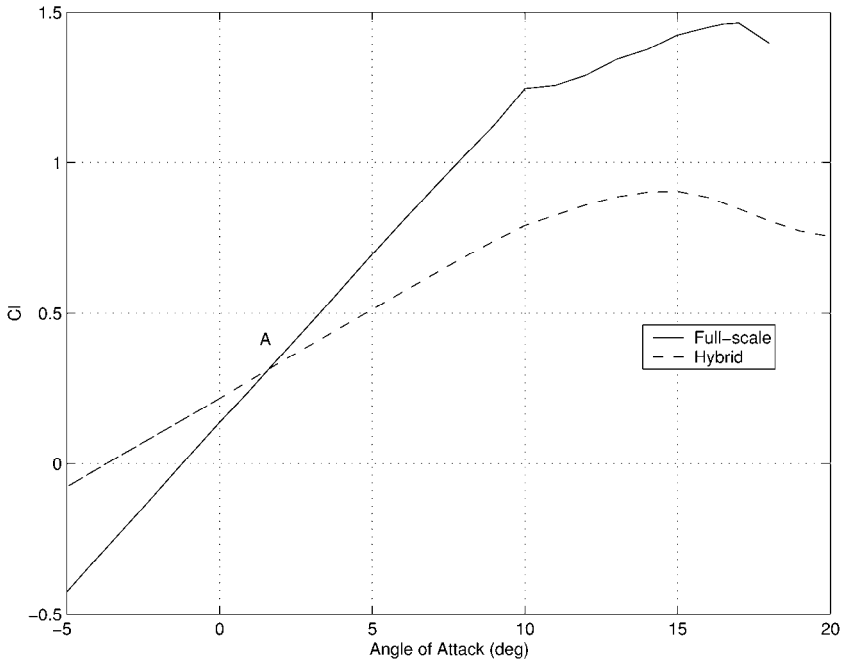


Figure A-5. $C_L$ - $\alpha$ Curves of the Full-Scale (NACA 23012) and Hybrid Airfoils (SU 1030), Indicating the Need for Circulation Adjustment on the Hybrid Airfoil at Off-Design Angles of Attack (Viscous calculations using XFOIL at $Re = 12.8 \times 10^6$)

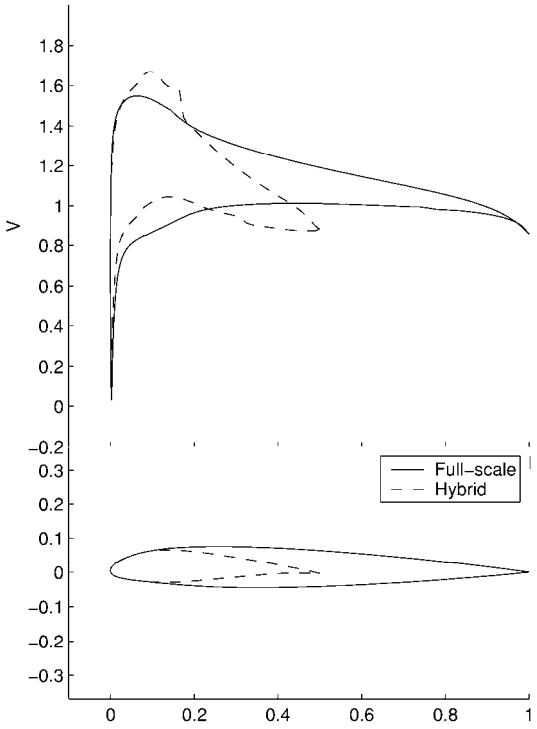


Figure A-6. Full-Scale and Hybrid Airfoil Velocity Distributions at $\alpha = 4°$, $Re = 12.8 \times 10^6$

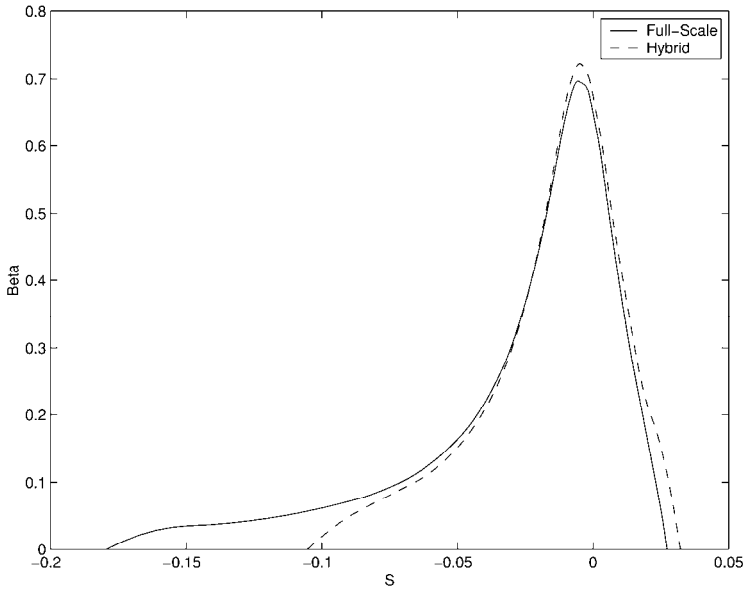


Figure A-7. Full-Scale and Hybrid Airfoil $\beta$-Curves
at $\alpha = 4°$, $Re = 12.8 \times 10^6$

To determine the optimum flap deflection (for which the $\beta$-curves of hybrid and full-scale airfoils agree the best), the flap deflection was increased in steps of 0.5° and a droplet impingement analysis was performed. The optimum flap deflection was found to be 2° (see figure A-8). Figures A-9 and A-10 show the velocity distribution and $\beta$-curves comparison of the hybrid airfoil with a 2° flap deflection at a 4° AOA. Note that the agreement is very good, except at the lower-surface impingement limit. The reason for this disparity is that the lower-surface limit of the nose section was not far enough aft to simulate the full-scale impingement. This limit was chosen for the design point at a 2° AOA. The lower-surface limit of the nose section could have been moved further aft, but this would have resulted in a much thicker airfoil, which was undesirable. The difference in the impingement characteristics shown in figure A-10 is not considered critical since the $\beta$ level is small (less than 0.1).

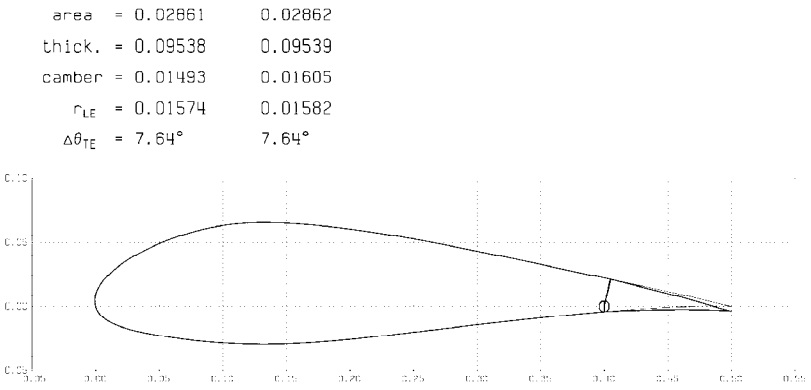


Figure A-8. Required 2° Flap Deflection (20% Chord) to Adjust Circulation of Hybrid Airfoil at $\alpha = 4°$ (Off-Design Condition)

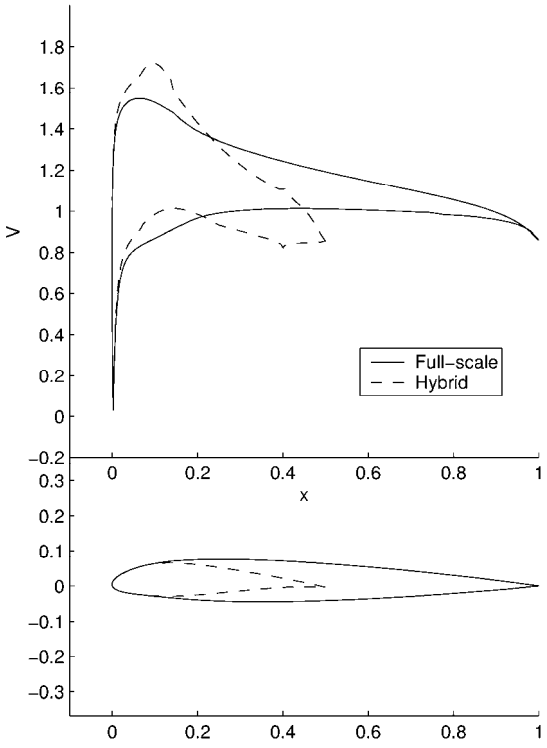


Figure A-9. Full-Scale and Hybrid Airfoil Velocity Distributions at $\alpha = 4°$, $\delta_{FLAP} = 2°$, $Re = 12.8 \times 10^6$

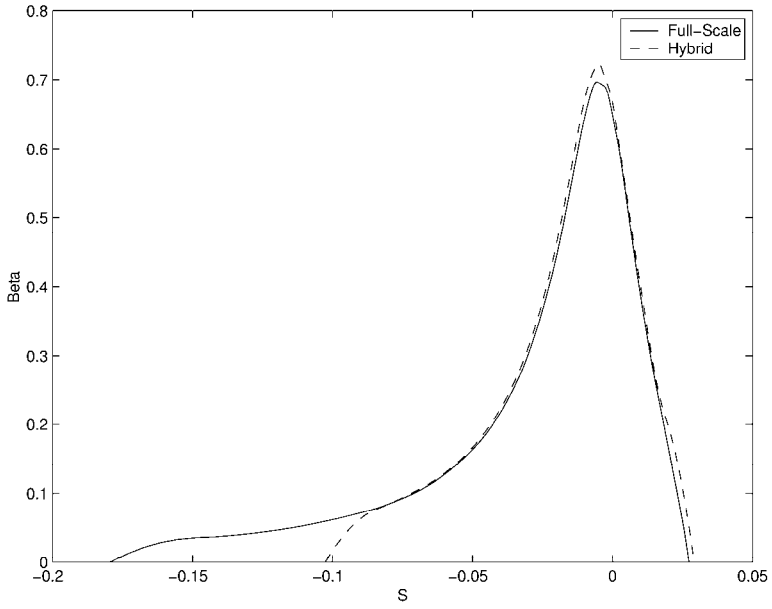


Figure A-10. Full-Scale And Hybrid Airfoil $\beta$-Curves at $\alpha = 4°$, $\delta_{FLAP} = 2°$, $Re = 12.8 \times 10^6$

Figures A-11 and A-12 compare the velocity distribution and the $\beta$-curves without any flap deflection on the hybrid airfoil at 0°AOA. A similar analysis was performed to determine the

optimum flap deflection for which the $\beta$-curves of the hybrid and full-scale airfoils best agree. The analysis yielded the optimum flap deflection for hybrid airfoil to be -3.5° (see figure A-13). Figures A-14 and A-15 show the velocity distribution and $\beta$-curve comparison of the hybrid airfoil with flap deflection.

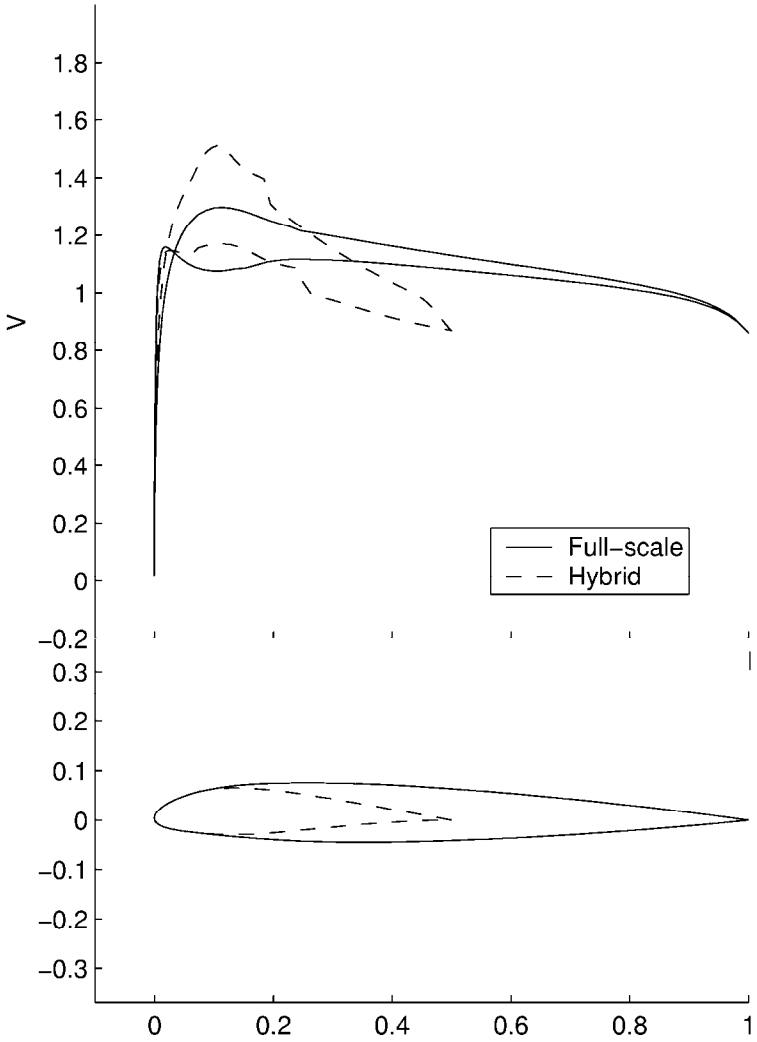


Figure A-11. Full-Scale and Hybrid Airfoil Velocity Distributions at $\alpha = 0°$, $Re = 12.8 \times 10^6$

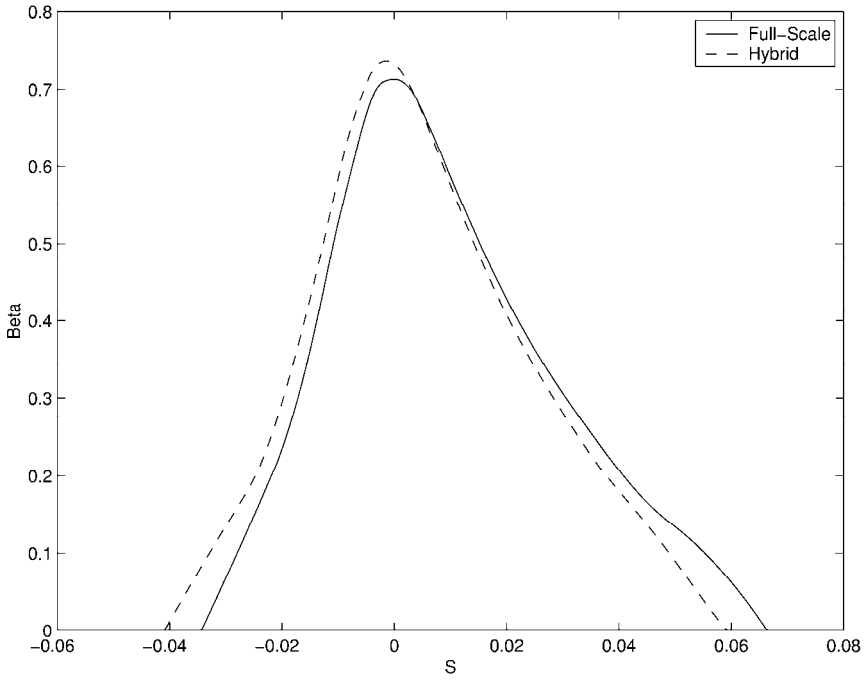


Figure A-12. Full-Scale and Hybrid Airfoil $\beta$-Curves at $\alpha = 0°$, $Re = 12.8 \times 10^6$

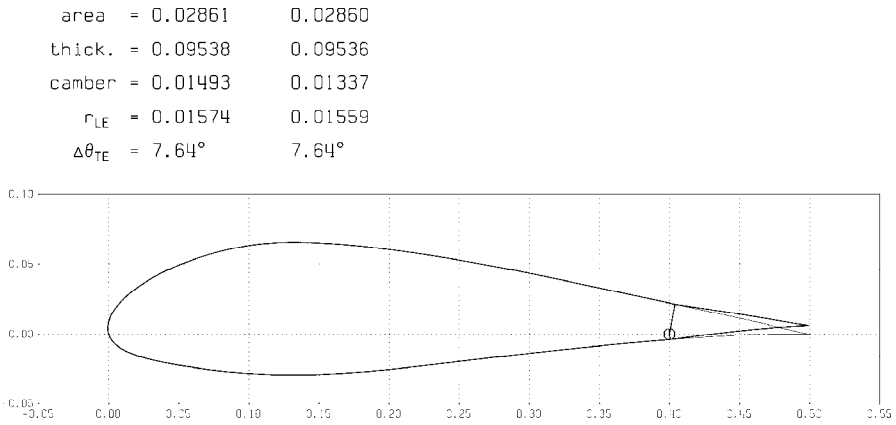


Figure A-13. The Required -3.5° Flap (20% Chord) Deflection to Adjust Circulation at 0° AOA (Off-Design Condition)

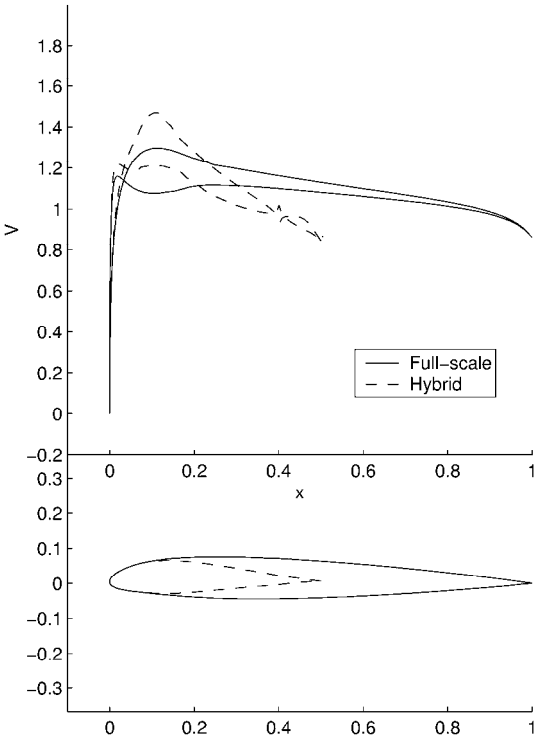


Figure A-14. Full-Scale and Hybrid Airfoil Velocity Distributions at $\alpha = 0°$, $\delta_{FLAP} = -3.5°$, $Re = 12.8 \times 10^6$

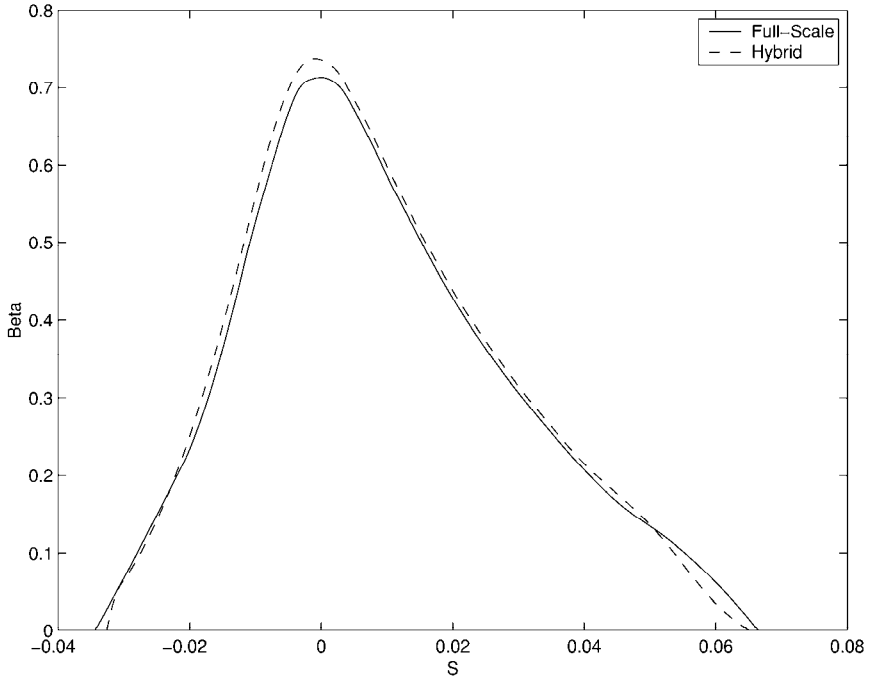


Figure A-15. Full-Scale and Hybrid Airfoil $\beta$-Curves at $\alpha = 0°$, $\delta_{FLAP} = -3.5°$, $Re = 12.8 \times 10^6$

## A.9 SUMMARY.

The SU 1030 hybrid airfoil is designed and optimized for a 2° AOA to yield icing droplet impingement characteristics similar to the NACA 23012 airfoil for the icing conditions previously given.

A 20 percent chord flap is used on the hybrid airfoil to match the $\beta$-curve at off-design conditions.

A flap deflection of -3.5° is required to match the $\beta$-curve for a 0° AOA.

A flap deflection of 2° is required to match the $\beta$-curve for a 4° AOA.

It should be noted that while maintaining the proper flap setting is important to match the droplet impingement, it may not make a critical difference in the final ice shape. This effect is discussed in more detail in reference A-4.

## A.10 REFERENCES.


A-1. Broeren, A. and Bragg, M.B., private communications, October 1999.

A-2. Saeed, F., Selig, M.S., and Bragg, M.B., "Design of Subscale Airfoils With Full-Scale Leading-Edges for Ice Accretion Testing," *Journal of Aircraft*, Vol. 34, No. 1, 1997, pp. 94-100.

A-3. Saeed, F., M.S., Selig, and M.B., Bragg, "Hybrid Airfoil Design Method to Simulate Full-Scale Ice Accretion Throughout a Given $\alpha$ Range," *Journal of Aircraft*, Vol. 35, No. 2, 1998, pp. 233-239.

A-4. Saeed, F., Selig, M.S., and Bragg, M.B., "Hybrid Airfoil Design Procedure Validation for Full-Scale Ice Accretion Simulation," *Journal of Aircraft*, Vol. 36, No. 5, 1999, pp. 769-776.

A-5. Drela, M., "XFOIL: An Analysis and Design System for Low Reynolds Number Airfoils," in *Low Reynolds Number Aerodynamics*, Volume 54 of Lecture Notes in Engineering, T.J. Mueller, ed., Springer-Verlag, New York, June 1989.

A-6. Selig, M.S. and Maughmer, M.D., "Multipoint Inverse Airfoil Design Method Based on Conformal Mapping," *AIAA Journal*, Vol. 30, No. 5, 1992, pp. 1162-1170.

A-7. Bragg, M.B., “Rime Ice Accretion and Its Effect on Airfoil Performance,” Ph.D. Dissertation, Dept. of Aeronautical and Astronautical Engineering, Ohio State University, Columbus, OH, 1981; also NASA CR 16599, March 1982.

A-8. Saeed, F., “Hybrid Airfoil Design Methods for Full-Scale Ice Accretion Simulation,” Ph.D. Dissertation, Dept. of Aeronautical and Astronautical Engineering, Univ. of Illinois at Urbana-Champaign, Urbana, IL, January 1999.

# APPENDIX B—SCALING FOR INTERCYCLE ICING TESTS

## B.1 SIZE SCALING.

### B.1.1 SCALING PARAMETERS.

One goal in testing models with the size reduced from the desired reference dimensions is to produce accreted ice shapes whose coordinates are nondimensionally the same as would have been obtained with the reference test. When the model has been geometrically scaled using the same airfoil section as the reference, the physical parameters that define ice accretion shapes for the scale test have to satisfy similarity with those for the reference test. These parameters represent the flow fields around the models, the droplet trajectories, the total water catch on the models, and for glaze ice, the heat balance on the surface of the models.

The flow field can be simulated by using a model that is dimensionally similar to the full-scale (reference) article by using the same angle of attack and by matching scale and reference values of Reynolds number (*Re*) and *M*. For icing encounters, the speeds involved are usually low enough that *M* should have little effect and is neglected. *Re* is usually ignored as well by arguing that any ice accretion will trip the boundary layer and the flow will then be independent of *Re*. A recent study [B-1] looked at including *Re* by matching its scale to the reference value, but to do this requires very high-scale velocities. Consequently, this approach is not always practical.

Similarity of droplet trajectories and, therefore, droplet collection efficiencies, can be obtained by matching the modified inertia parameter, $K_0$, of Langmuir and Blodgett [B-2]. An exact determination of $K_0$ is somewhat involved and is not discussed here, but $K_0$ can be approximated using the following expression:

$$K_0 = (\text{constant})\frac{\delta^{2-\kappa} V^{1-\kappa}}{2 r_{le}\, p^{\kappa}} \tag{B-1}$$

where $\kappa$ is a constant and $r_{le}$ is the leading-edge radius of the model. For the NACA 23012, $r_{le} = 0.0158c$, $c$ is the chord. The use of $2r_{le}$ as the length scale instead of chord provides consistency between airfoil and cylinder studies. Another advantage of using $r_{le}$ instead of $c$ is that models with the same chords but different airfoil sections will be differentiated in $K_0$, according to the size of the leading edge. Equation B-1 results from approximating the droplet drag versus the droplet *Re* curve by a straight line over a portion of the droplet *Re* range. This approximation has been used at least since 1955 [B-3] to simplify the development of scaling equations. Over a range of interest to typical icing encounters, a value of $\kappa = 0.38$ provides modified inertia parameters sufficiently close to values found in more involved procedures. Equating the scale and reference values of $K_0$ gives a practical expression that relates scaled conditions to reference conditions to satisfy droplet trajectory similarity:

$$\frac{\delta_S}{\delta_R} = \left(\frac{r_{le,S}}{r_{le,R}}\right)^{\frac{1}{2-\kappa}} \left(\frac{p_S}{p_R}\right)^{\frac{\kappa}{2-\kappa}} \left(\frac{V_S}{V_R}\right)^{\frac{\kappa-1}{2-\kappa}} \tag{B-2}$$

The collection efficiency at the leading edge, $\beta_0$, is directly related to $K_0$ by the following expression given by Langmuir and Blodgett:

$$\beta_0 = \frac{1.4\left(K_0 - \frac{1}{8}\right)^{0.84}}{1 + 1.4\left(K_0 - \frac{1}{8}\right)^{0.84}} \tag{B-3}$$

Similarity of ice accumulation results from a match of the accumulation parameter, $A_c$

$$A_c = \frac{LWC\, V\, \tau}{2\, r_{le}\, \rho_i} \tag{B-4}$$

Finally, the energy balance at the surface can be written following Messinger [B-4] in the following form:

$$n = \frac{c_{p,ws}}{\Lambda_f}\left(\phi + \frac{\theta}{b}\right) \tag{B-5}$$

where $n$ is the freezing fraction; $\phi$, is the water energy transfer parameter; $\theta$ is the air energy transfer parameter; and $b$ is the relative heat factor of Tribus, et al. [B-5], $c_{p,ws}$ is specific heat of water on model surface, Btu/lbm R, and $\Lambda_f$ is latent heat of freezing, Btu/lbm. Equation B-5 thus provides four additional parameters, with three of the four independent. The parameters $\phi$, $\theta$, and $b$ are defined in the following equations:

$$\phi = t_f - t_{st} - \frac{V^2}{2c_{p,ws}} \tag{B-6}$$

$$\theta = \left(t_s - t_{st} - r\frac{V^2}{2c_p}\right) + \frac{h_G}{h_c}\left(\frac{p_{ww} - p_w}{p}\right)\Lambda_v \tag{B-7}$$

$r$ is recovery factor, dimensionless and $h_G$ is the gas-phase mass transfer coefficient, lbm/hr Ft$^2$

$$b = \frac{LWC\, V\, \beta_0 c_{p,ws}}{h_c} \tag{B-8}$$

The convective heat transfer coefficient, $h_c$, in equation B-8 is found from

$$h_c = \frac{1.14\,\mathrm{Re}^{.5}\,\mathrm{Pr}^{.4}\,k}{2r_{le}} \tag{B-9}$$

Here, *Re* is based on air properties, free-stream velocity, $V$, and a length of twice the leading-edge radius, $r_{le}$.

B.1.1.1 Ruff Scaling Method.

Using combinations of the parameters $K_0$, $A_c$, $n$, $\phi$, and $\theta$, Ruff [B-6] performed scaling tests in the AEDC R-1D icing tunnel. He found that the scaled ice shapes agreed best with reference shapes when all five of these scaling parameters were matched to the reference values. This approach to scaling is known as the Ruff (or AEDC) method. Because the R-1D allows altitude simulation, Ruff's work included the calculation of the scale test section pressure, in addition to temperature, droplet size, liquid water content (LWC), and time. With only five scaling parameters to establish these five test conditions, the sixth test condition, scale velocity, was selected arbitrarily. The Ruff method has also been used in sea level tunnels in a modified form in which $\theta$ is ignored and just $K_0$, $A_c$, $n$, and $\phi$ are matched, with the scale velocity chosen by the user.

In Ruff's experiments, the scale velocity was often simply equated with the reference value. This is a practical approach, and it coincidentally ensures that the scale and reference $M$ will match. Note also from equation B-6 that if scale and reference $V$ are matched, so is the static temperature, $t_{st}$. For sea level tunnels, when velocity is matched, the static pressure will also match, and equation B-2 reduces to the following:

$$\delta_S = \delta_R \left( \frac{r_{le,S}}{r_{le,R}} \right)^{\frac{1}{2-\kappa}} \tag{B-10}$$

Tests with glaze ice conditions showed [B-7] that when the Ruff method with a constant scale velocity was used to determine scale test conditions, the quantity of ice accreted and accretion limits were properly simulated, but features such as horn angle and location were not exactly the same as for the reference ice shape. Scaling studies at NASA [B-7 and B-8] demonstrated that the best similarity of scaled and reference ice shapes was achieved when the Ruff method was used with an additional similarity parameter, such as the *Re* or Weber number (*We*), to determine the scale velocity. The use of either of these parameters results in a scale velocity higher than the reference value. For the present study of intercycle ice, the short times between boot firings resulted in small accretions for which features like horns did not have time to develop. For this situation, the use of a scale velocity that matches the reference should be valid.

With the scale airspeed set equal to the reference, the scale static temperature was also equated to the reference to satisfy $\phi_S = \phi_R$, using the definition of $\phi$ from equation B-6. The droplet size, $\delta_S$, medium volume diameter (MVD) was determined from equation B-9, and then the scale and reference collection efficiency, $\beta_0$, was calculated from equation B-3. Next, the scaled liquid water content, $LWC_S$, was found by solving $n_S = n_R$ using equations (B-5 through B-9). Finally, the value for scale accretion time was calculated by matching $A_{cS}$ and $A_{cR}$ from equation B-4.

B.2 HYBRID SCALING.

Hybrid scaling [B-9 and B-10] uses a full-size, leading-edge section attached to a smaller after body. The aft section is designed so that the flow field around the leading edge and droplet impingement on the leading edge are the same as for the full-size wing section. This approach to scaling requires that the aft section coordinates be established using fairly sophisticated

analytical models. Furthermore, the aft section design is limited to a single airspeed and droplet size or to a small range of conditions. The flow field can be matched to the full-size case over a series of angles of attack through the use of an adjustable trailing-edge flap. Limited testing of this method [B-10] has shown that full-size ice accretions can be successfully reproduced with the hybrid model over a range of angles of attack.

Figure B-1 shows the collection efficiency curves for both the hybrid model designed for these tests and a full-size (72-inch chord) NACA 23012. The design condition included a droplet size of 40 μm MVD and a 2° angle of attack (AOA). Figure B-1(a) shows that the two collection efficiency curves were, for all practical purposes, identical at this condition. The collection efficiencies for an AOA of 4° are given in figure B-1(b). While $\beta$ is the same over much of the two surfaces, aft of $s/c$ = -0.10 (on the lower surface), $\beta$ for the hybrid model falls to zero while the full-size airfoil is approximately 0.05 until $s/c$ = -0.16. Assuming that the 36-inch chord hybrid airfoil accurately reproduces the collection efficiency of the full-size airfoil NACA 23012, figure B-1(b) would suggest that the lower-surface icing limit for the hybrid model would be near the boot edge, while the geometrically scaled model might show ice beyond this position.

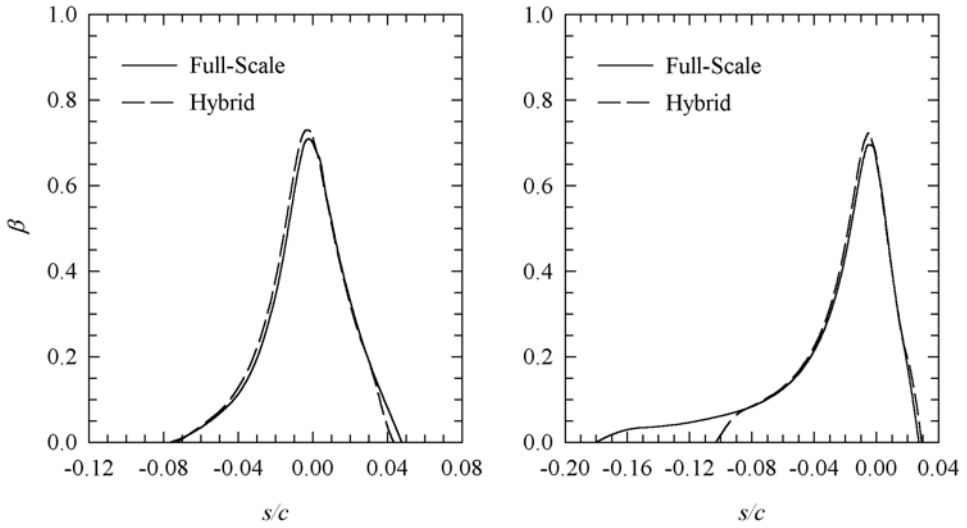


(a) 2°AOA (b) 4°AOA

Figure B-1. Collection Efficiency Over Model Surfaces (MVD = 40 μm)

At the leading edge, because the hybrid-scaled flow and droplet trajectories are identical to the full-size airfoil N 23012, all similarity parameters will be matched if hybrid icing conditions are the same as the full-size airfoil NACA 23012. The hybrid-scale tests were, therefore, performed at the reference values of temperature, airspeed, droplet size, LWC, and icing time. Because no separate tests were made with a full-size model, the hybrid tests represented the reference case for these scaling studies.

Two series of tests were performed in the Goodrich Icing Wind Tunnel to evaluate scaling for intercycle icing. In the first, a 36-inch chord NACA 23012 airfoil was used to represent a half-size model. The Ruff scaling method was applied for these tests to scale the test conditions from

reference values. The second series of tests used a hybrid-scaled model to provide icing results representing those for a 72-inch chord NACA 23012 wing section.

B.3 TEST CONDITIONS.

Table B-1 lists the reference and scale conditions for these tests. AOAs were 0° and 4° and static temperatures ranged from -4° to 21°F. Except for two pairs of tests at 175 mph, all tests were conducted with an airspeed of 200 mph. Reference water droplet sizes were just under 20 and slightly more than 30 μm MVD. A range of reference LWC covered 0.25 to 1.56 g/m$^3$. The total spray times for the reference case were 8.6 to 34.5 minutes. Boot cycle times for the reference case were 170 to 509 seconds. These cycle times were scaled along with the total spray time for the scale tests. The static pressure for all tests was one atmosphere. Along with the test conditions, the corresponding similarity parameters are given in table B-1. The accumulation parameter given is based on the boot cycle time. Most tests were performed at glaze ice conditions, with freezing fractions varying from 0.13 to 0.6. One set of reference and scale tests was made with rime ice.

Table B-1. IWT Intercycle Ice Tests Scaling Conditions and Similarity Parameters

| Run | Date | $c$, (in.) | $\alpha$, (deg) | $t_{st}$, (°F) | $t_{tot}$, (°F) | $V$, (mph) | $\delta$, (μm) | LWC, (g/m$^3$) | $\tau$, (min) | Boot Cycle, (sec) | $K_0$ | $\beta_0$ | $A_c$ | $n$ | $b$ | $\phi$, (°F) | $\theta$, (°F) |
|---|---|---|---|---|---|---|---|---|---|---|---|---|---|---|---|---|---|
| 7/5R | 3-17-00 | 72 | 0 | 14.0 | 21.2 | 200 | 20 | 0.45 | 12.4 | 181 | 0.73 | 0.48 | 0.14 | 0.56 | 0.32 | 16.3 | 20.5 |
| 8/2 | 3-17-00 | 72 | 0 | 14.0 | 21.2 | 200 | 20 | 0.45 | 12.4 | 181 | 0.73 | 0.48 | 0.14 | 0.56 | 0.32 | 16.3 | 20.5 |
| 54/4S | 12-9-99 | 36 | 0 | 14.0 | 21.2 | 200 | 13 | 0.64 | 4.4 | 64 | 0.74 | 0.48 | 0.14 | 0.56 | 0.32 | 16.3 | 20.5 |
| 55/5S* | 12-9-99 | 36 | 0 | 14.0 | 21.2 | 200 | 13 | 0.64 | 4.4 | 64 | 0.74 | 0.48 | 0.14 | 0.56 | 0.32 | 16.3 | 20.5 |
| 8/4 | 3-15-00 | 72 | 0 | 14.0 | 21.2 | 200 | 31 | 0.32 | 34.5 | 509 | 1.40 | 0.63 | 0.27 | 0.60 | 0.30 | 16.3 | 20.6 |
| 1/2 | 11-30-99 | 36 | 0 | 14.0 | 21.2 | 200 | 20 | 0.45 | 12.2 | 180 | 1.41 | 0.63 | 0.27 | 0.60 | 0.30 | 16.3 | 20.6 |
| RE2* | 11-30-99 | 36 | 0 | 14.0 | 21.2 | 200 | 20 | 0.45 | 12.2 | 180 | 1.41 | 0.63 | 0.27 | 0.60 | 0.30 | 16.3 | 20.6 |
| 8/5 | 3-17-00 | 72 | 0 | 21.0 | 28.2 | 200 | 31 | 0.46 | 34.3 | 509 | 1.40 | 0.63 | 0.39 | 0.23 | 0.43 | 9.3 | 10.3 |
| 6/4 | 12-1-99 | 36 | 0 | 21.0 | 28.2 | 200 | 20 | 0.65 | 12.1 | 180 | 1.41 | 0.63 | 0.39 | 0.23 | 0.44 | 9.3 | 10.4 |
| 9/4* | 12-1-99 | 36 | 0 | 21.0 | 28.2 | 200 | 20 | 0.65 | 12.1 | 180 | 1.41 | 0.63 | 0.39 | 0.23 | 0.44 | 9.3 | 10.4 |
| 7/2 | 3-15-00 | 72 | 0 | 21.0 | 26.5 | 175 | 31 | 1.56 | 8.6 | 170 | 1.29 | 0.61 | 0.39 | 0.13 | 1.32 | 9.7 | 12.0 |
| 45/46 | 12-8-99 | 36 | 0 | 21.0 | 26.5 | 175 | 20 | 2.20 | 3.0 | 60 | 1.29 | 0.61 | 0.39 | 0.13 | 1.32 | 9.7 | 12.1 |
| 7/4 | 3-14-00 | 72 | 4 | -4.0 | 3.2 | 200 | 20 | 0.25 | 12.6 | 181 | 0.74 | 0.48 | 0.08 | 1.00 | 0.18 | 34.3 | 43.6 |
| 49/2S | 12-9-99 | 36 | 4 | -4.0 | 3.2 | 200 | 13 | 0.35 | 4.5 | 64 | 0.74 | 0.48 | 0.08 | 1.00 | 0.18 | 34.3 | 43.6 |
| 50/3S* | 12-9-99 | 36 | 4 | -4.0 | 3.2 | 200 | 13 | 0.35 | 4.5 | 64 | 0.74 | 0.48 | 0.08 | 1.00 | 0.18 | 34.3 | 43.6 |
| 7/3 | 3-15-00 | 72 | 4 | 14.0 | 21.2 | 200 | 31 | 1.38 | 8.6 | 170 | 1.39 | 0.63 | 0.39 | 0.23 | 1.29 | 16.3 | 20.5 |
| 42/44 | 12-8-99 | 36 | 4 | 14.0 | 21.2 | 200 | 20 | 1.95 | 3.1 | 60 | 1.40 | 0.63 | 0.39 | 0.23 | 1.29 | 16.3 | 20.5 |
| 43/44B* | 12-8-99 | 36 | 4 | 14.0 | 21.2 | 200 | 20 | 1.95 | 3.1 | 60 | 1.40 | 0.63 | 0.39 | 0.23 | 1.29 | 16.3 | 20.5 |
| 8/3 | 3-14-00 | 72 | 4 | 21.0 | 28.2 | 200 | 31 | 0.46 | 34.3 | 509 | 1.39 | 0.63 | 0.40 | 0.23 | 0.43 | 9.3 | 10.3 |
| 7/5 | 12-1-99 | 36 | 4 | 21.0 | 28.2 | 200 | 20 | 0.65 | 12.1 | 180 | 1.40 | 0.63 | 0.39 | 0.23 | 0.43 | 9.3 | 10.3 |
| 7/1 | 3-15-00 | 72 | 4 | 21.0 | 26.5 | 175 | 31 | 1.56 | 8.6 | 170 | 1.30 | 0.62 | 0.39 | 0.13 | 1.33 | 9.7 | 12.1 |
| 44/47 | 12-8-99 | 36 | 4 | 21.0 | 26.5 | 175 | 20 | 2.20 | 3.0 | 60 | 1.28 | 0.61 | 0.39 | 0.13 | 1.31 | 9.7 | 12.0 |

*Runs for which molds were taken. No midspan tracings were obtained for mold runs.

B.4 RESULTS.

At the completion of each boot inflation/deflation cycle, ice immediately began to accrete. Behind the main ice shape over the leading edge, small feather growths were observed to start along any horizontal (spanwise) mark on the surface. One consistent location for feather growth, for example, was along the stitch lines between the inflatable tubes of the boot. Thus, the feathers grew in nearly straight lines along the span of the model. As the feather height became great enough, small portions of these lines of feathers would sometimes shed with new growth starting from the same location as the just-shed feathers. Because of this random shedding, the final appearance of the model aft of the main ice shape was that of a series of more-or-less straight lines of feathers stretching spanwise with random heights of feathers along each line.

An example of this structure can be seen in figures B-2a and B-2b, which shows the appearance of the reference (hybrid) model at the end of an intercycle icing test. The photographs were taken before the ice was cut for tracing. The view in figure B-2a is from the bottom of the tunnel with the model's leading edge at the top of the picture. Lines were drawn chordwise on the model at midspan and 1 inch on either side of the midspan position for reference purposes. These markings are visible in the photograph. In addition, the spanwise stitch lines between active deicing tubes were marked so that their location could be seen. Several rows containing large feathers can be seen immediately aft of the main ice. Because this test was made with 0°AOA, little ice accreted on the lower surface. The feathers beyond about 2 inches from the main ice are very small, but clearly grow at or near the stitch lines between the tubes.

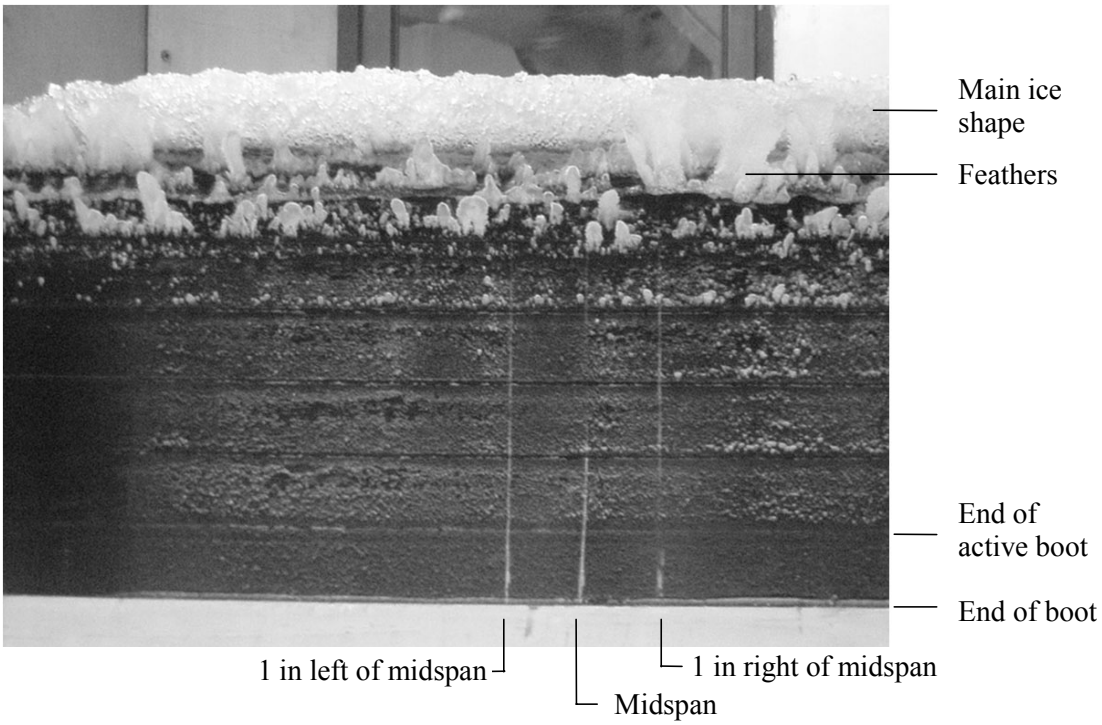


Figure B-2a. Deicing Boot With Intercycle Ice
(Reference Model, Run 8/4, 3-15-00—Lower Surface)

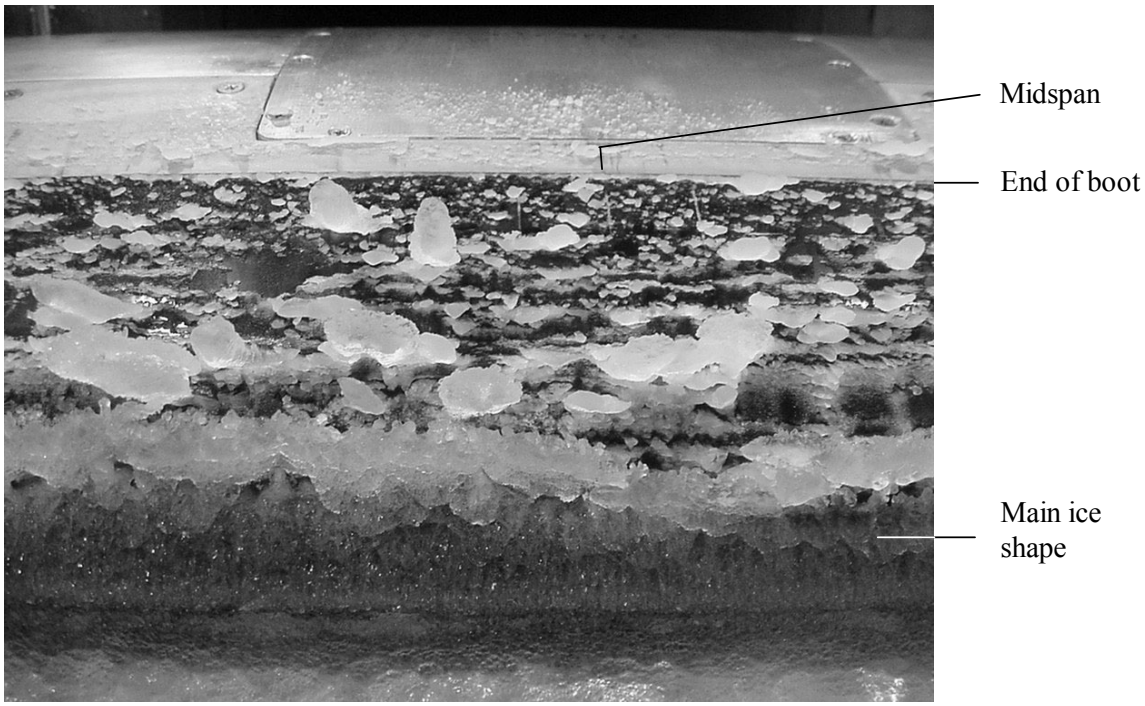


Figure B-2b. DeIcing Boot with Intercycle Ice
(Reference Model, Run 8/4, 3-15-00—Upper Surface)

The upper surface for the same test is shown in figure B-2b. The leading edge of the model is at the bottom of this photograph and the trailing edge at the top. On this surface, ice feathers of significant size grew into the flow from the horizontal joint between the trailing edge of the boot and the model skin. Because these feathers lay close to the surface, it was difficult or impossible to maneuver the tracing pencil between the feather and the model skin; therefore, in the tracings, the distinctive appearance of feathers, with a long, thin structure growing from a small area on the surface, was usually lost. It is apparent from figures B-2a and B-2b that the main ice shape might look nearly the same in tracings taken at the midspan and any other location along the span, but the feather features aft of the main ice cannot be expected to be duplicated everywhere. Furthermore, because the feathers grew from surface imperfections whose nondimensional size and position were not the same for both test models, the scale test could not be expected to reproduce the position of feathers observed in the reference tests.

B.4.1 SPANWISE VARIABILITY.

For the reference tests, an ice tracing was usually taken both at the midspan position (tunnel center) and one other spanwise location. The off-center locations were selected to record the more prominent features; therefore, they do not always show the random nature of the ice shedding. Nevertheless, it is helpful to get some sense of how much variation there is in the ice profile along the span by comparing tracings at different locations. Two examples from the tests with the reference model at 0°AOA are given in figures B-3a and B-3b.

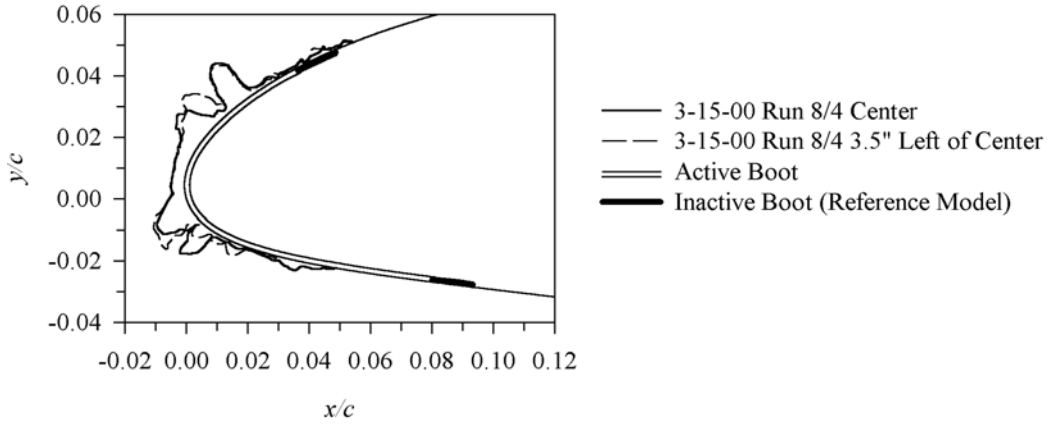


Figure B-3a. SpanWise Variability at 0°AOA With Reference Model
(Run 8/4 center tracing compared with tracing at 3.5 inches left of center)

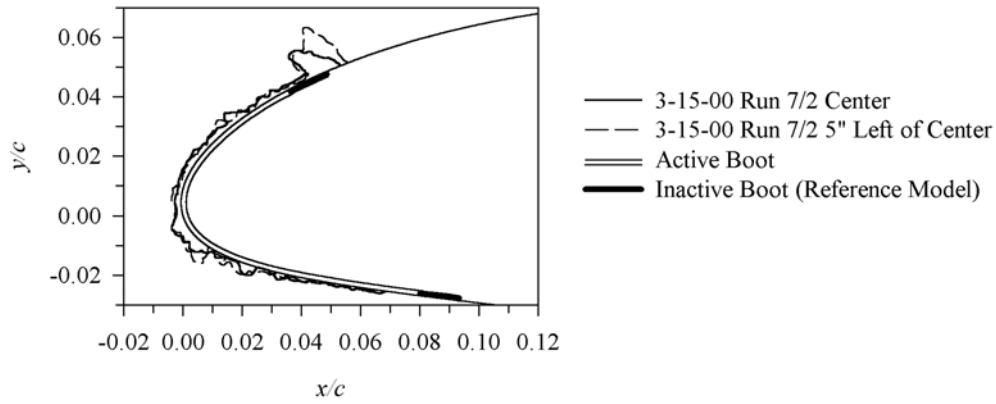


Figure B-3b. SpanWise Variability at 0°AOA With Reference Model
(Run 7/2 center tracing compared with tracing at 5 inches left of center)

The active part of the boot is indicated on the figure with a line parallel to the airfoil surface contour but within the model cross section. Aft of the active region on both the upper and lower surfaces is the inactive portion of the boot, shown with the solid black bands below the model surface outline. Figure B-3a presents ice profiles taken at the midspan (center) of the model and at a position 3.5 inches left of center for run 8/4. Photographs of this ice before the tracings were taken are shown in figures B-2a and B-2b. This run had one of the largest accumulation parameters tested. The accumulation was sufficient for significant features of the ice to begin to show. The thickness and general shape of the main ice cap is the same at both tracing locations, and the large upper surface feather structure just aft of the main ice shape appears in both tracings with near perfect agreement. Figures B-2a and B-2b showed that other locations along the span would not necessarily have shown this same feather location or size. On the lower surface, the large feather seen in the midspan tracing just aft of the main shape is absent from the left-of-center tracing.

Figure B-3b shows the results for run 7/2, which had one of the shortest intercycle times. For this run, tracings were taken at the midspan and 5 inches to the left of midspan. The main ice thickness and the size of the features along the upper and lower surfaces were reproduced at both locations. At the position at which the boot butts against the skin of the model's upper surface, a large feather structure had grown. This feature appeared in both tracings. Note that at this location, any ice that formed would not have been subject to periodic boot activation, and the full 8.6-minute spray time was available for accretion. As with the large feather structures seen in figure B-3a, these prominent features do not represent continuous ridges, but rather local feather growths existing in both locations.

Additional tracing comparisons for the reference model from 4° AOA tests are discussed in section B.4.3. When comparing reference and scale tracings, it is important to keep in mind that aft of the main ice shape, the features shown in two-dimensional profile are probably local and randomly located.

B.4.2 REPEATABILITY.

Features of the accreted ice that are random in size or location are typically not repeatable. Scaling success with nonrepeatable characteristics cannot be expected to be good. Thus, to establish typical run-to-run variations in intercycle ice, some sets of conditions were tested on more than one occasion. Figure B-4 gives a comparison of two such tests, runs 7/5R and 8/2, both made with the reference model. Because no midspan tracing had been made for run 8/2, the center tracing for run 7/5R was compared with the 2-inch-left-of-center tracing for run 8/2. The two tracings compared well, exhibiting features of similar size and chordwise location. This result suggests that main ice shapes for these tests were fairly repeatable, even though feather size and location may not be.

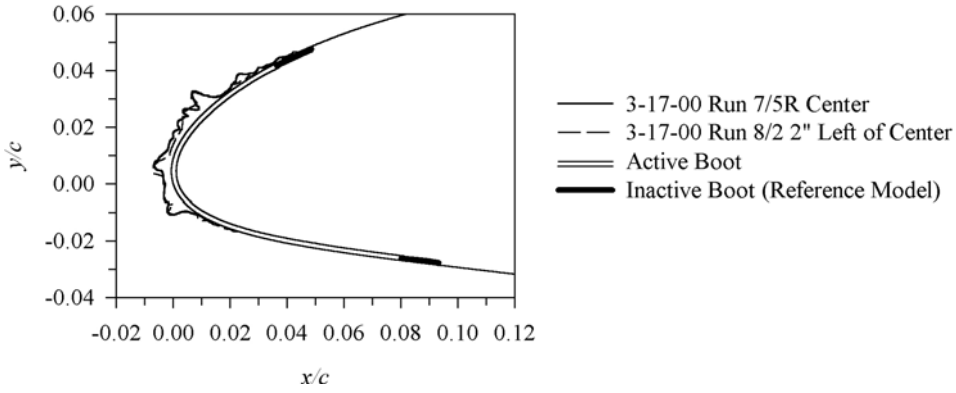


Figure B-4. Repeatability of Ice Shapes
(Reference (hybrid) model)

B.4.3 SCALING RESULTS.

Figures B-5a through B-5d compares the scale and reference ice shapes for each of the scaling tests made at 0° AOA, while figures B-6a through B-6c gives the results for 4° AOA. For these figures, the active deicing boot region for both models and the inactive portion of the reference

boot are shown as described in figures B-3a and B-3b. The inactive boot for the scale model extends (nondimensionally) beyond that of the reference and is shown as a dashed line parallel to and within the airfoil cross section. Remember that the active boots for both scale and reference models extended to the same nondimensional position; thus, the inactive part of the scale boot included, but extended farther aft than the inactive region of the reference boot. Except for run 8/3, shown in figure B-6c, all reference and scale ice profiles shown in figures in this section were traced at the tunnel center, i.e., the model midspan. Run 8/3 was traced 1 inch to the right of midspan. In most cases, the scale test accurately simulated the thickness of the leading-edge ice. Success in simulating the main ice shape indicates that the accumulation parameter, $A_c$, and the modified inertia parameter, $K_0$, (which determines the stagnation collection efficiency, $\beta_0$), were properly matched in determining the scaled conditions. Accretion limits, which are also dependent on $K_0$, were difficult to establish. Agreement between scale and reference shapes also tends to validate the design of the hybrid model with respect to reproducing the correct droplet trajectories around the leading-edge portion of the model.

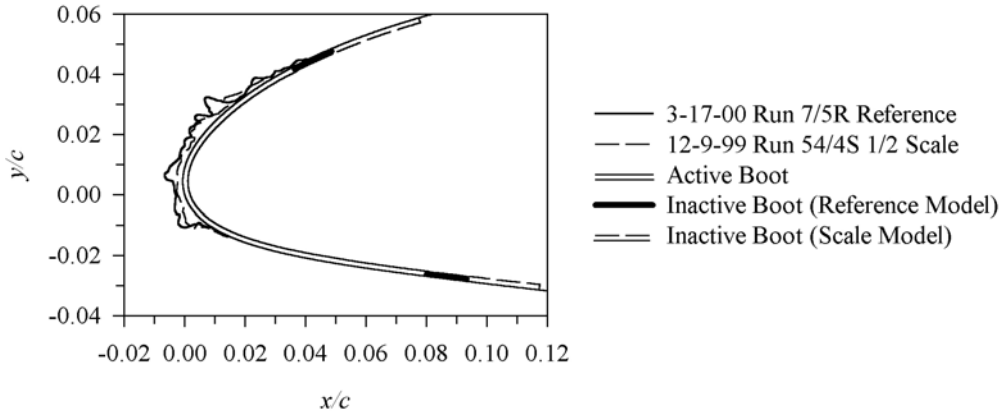


Figure B-5a. Scaling at 0°AOA (Runs 7/5R and 54/44S)

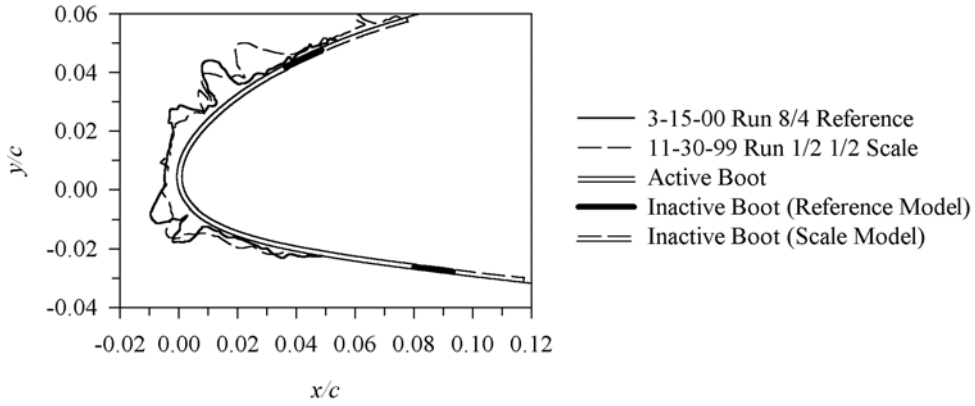


Figure B-5b. Scaling at 0°AOA (Runs 8/4R and 1/2)

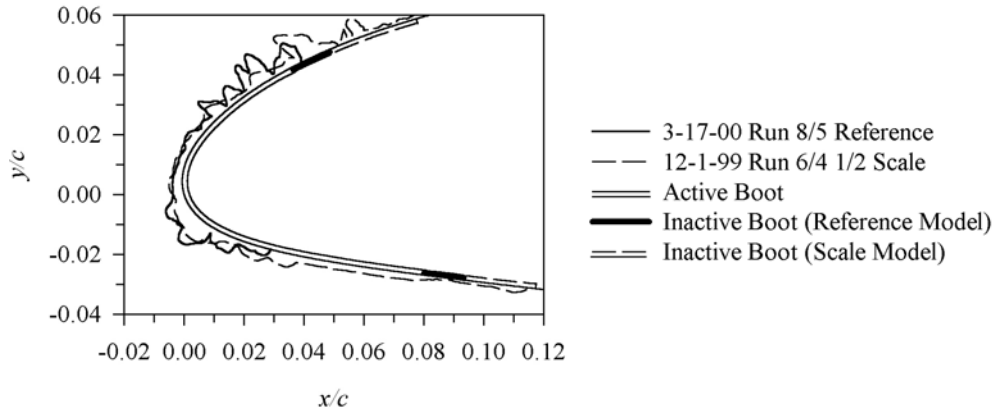


Figure B-5c. Scaling at 0°AOA (Runs 7/5R and 6/4)

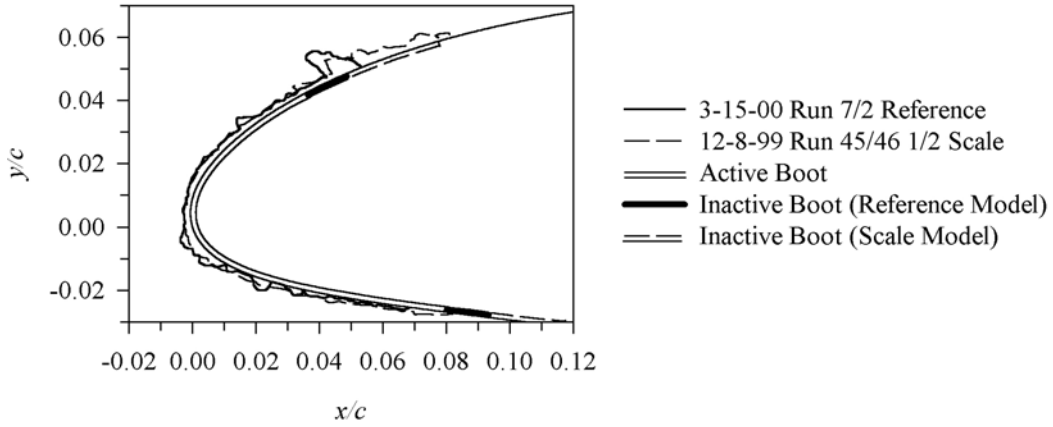


Figure B-5d. Scaling at 0°AOA (Runs 7/5R and 45/46)

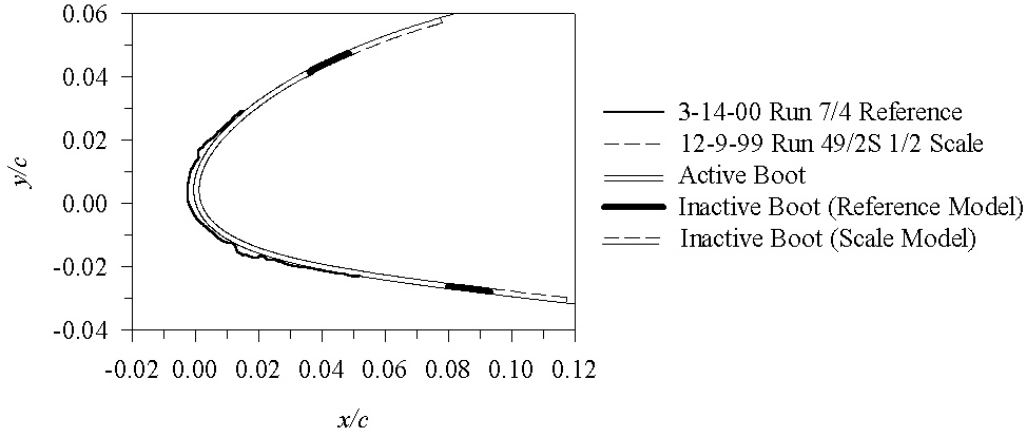


Figure B-6a. Scaling at 4°AOA (Tracings at Midspan, Reference Test 7/4 versus Scale Test 49/2S)

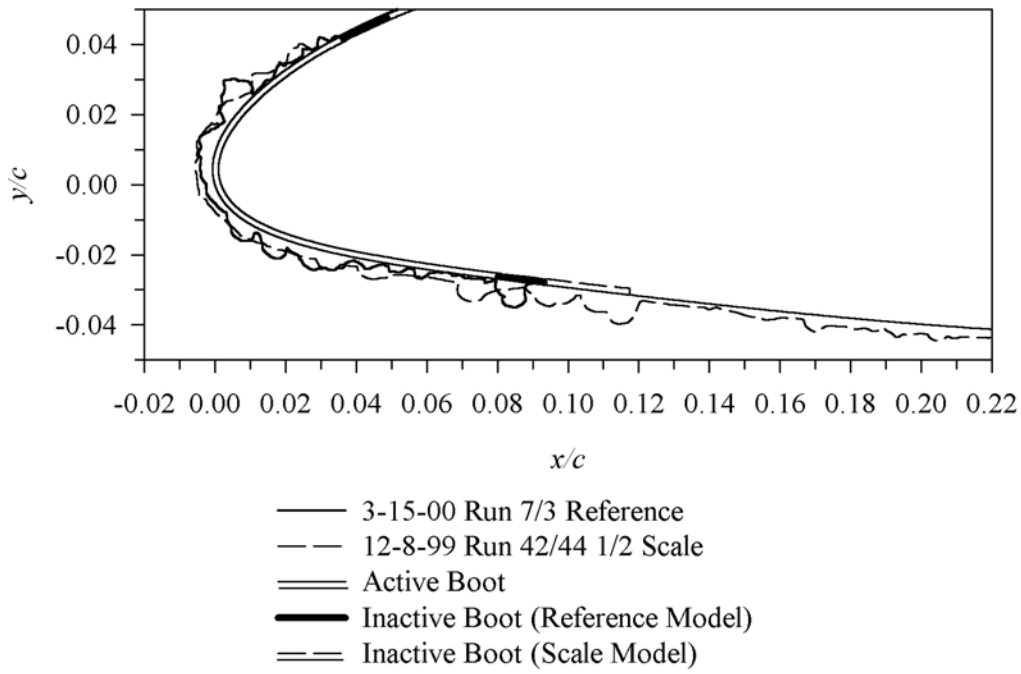


Figure B-6b. Scaling at 4°AOA (Reference Test 7/3 versus Scale Test 42/44)

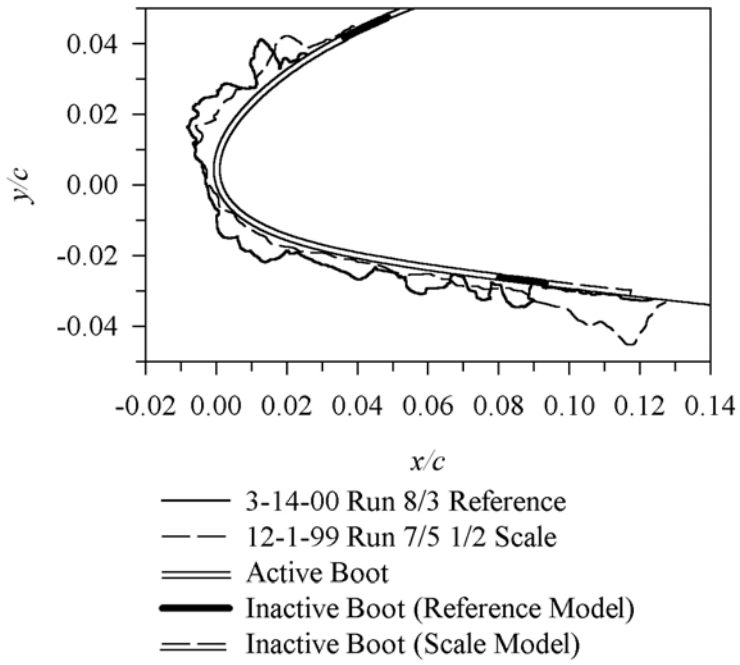


Figure B-6c. Scaling at 4°AOA (Reference Test 8/3 versus Scale Test 7/5, Test 8/3 was Traced at 1 inch Right of Midspan)

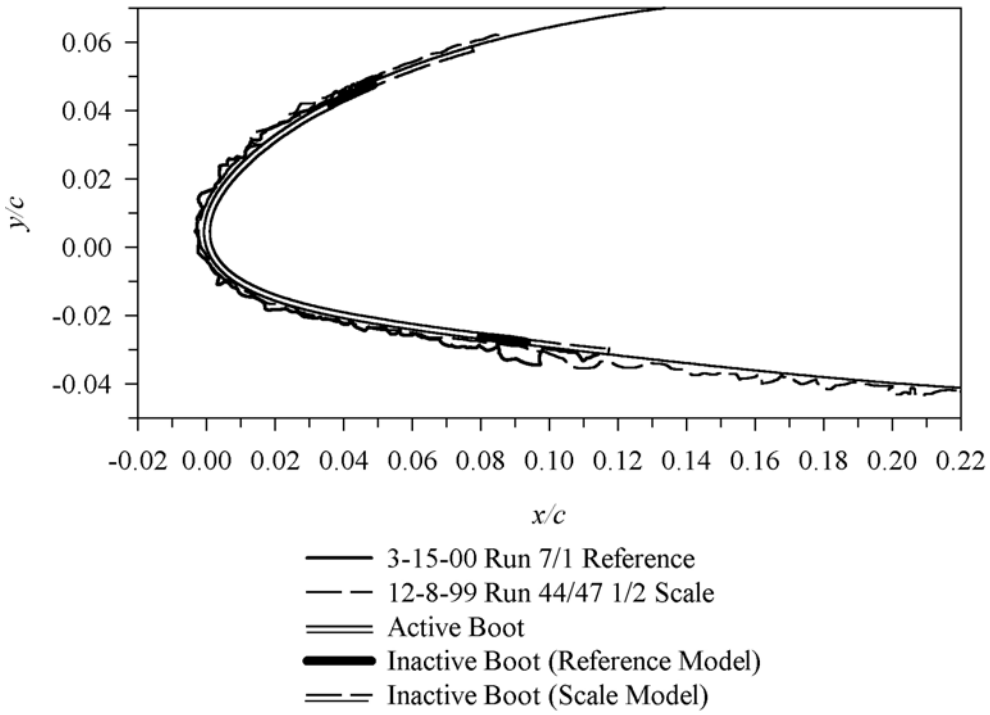


Figure B-6d. Scaling at 4°AOA (Reference Test 7/1 Versus Scale Test 44/47)

For the reference tests, the cardboard template on which the ice profile was traced was not a perfect fit to the model surface aft of the leading edge. Consequently, it is estimated that whenever the nondimensional ice thickness was less than 0.001 inch, it would not have been recorded on the reference tracings.

The ice thickness at the leading edge depends primarily on $A_c$ and $\beta_0$. Consistent with this expectation, less ice was accreted at the leading edge for the tests shown in figure B-5a ($A_c\beta_0 = 0.07$) than for those shown in figure B-5b ($A_c\beta_0 = 0.17$). The quantity of leading-edge ice decreased for the results given in figure B-5c and decreased still further for those of figure B-5d, although the latter two sets of tests had products $A_c\beta_0$ of about 0.24. The reason for these differences is the change in freezing fraction. For both sets of tests, whose results are shown in figures B-5a and B-5b, $n$ was about 0.6. For the tests of figure B-5c, however, $n$ was only 0.23, and for B-5d it was 0.13. The freezing fraction is defined as the ratio of the amount of water that freezes in the zone of impact to the total water entering that zone. Thus, at very low freezing fractions, water impinging at the leading edge will not freeze there but will tend to flow aft before freezing.

The reference test results shown in figure B-5a exhibited more protuberances than the corresponding scale tests. The scale tests did, however, simulate correctly the leading-edge ice thickness and icing limits. The reason for the smoother ice for the scale tests is not understood, but may be related to the use of larger (relative to the representative chord) inflatable tubes and relatively longer inflation and deflation times for the scale test. Further study of the effect of these characteristics is needed.

In the results reported in figure B-5b, the scale test simulated the leading-edge ice thickness and the approximate shape of the main ice cap. The small horns developing on the edges of the main ice did not appear in the scale shape, however. While the scale and reference tests did not agree on the exact locations of the large feather structures aft of the main ice, the scale tests did correctly simulate the size of those feathers. The ice for the reference test accreted just beyond the inactive portion of the boot on the upper surface. For the scale test, some upper-surface ice was recorded beyond the end of the reference boot, ending near the end of the inactive scale boot. These differences appear to be minor.

In figure B-5c, it is apparent that the scale test again simulated the leading-edge ice thickness and the size of the feathers formed downstream. The feather location was different for the scale and reference tests, however, and some of the near leading-edge protuberances seen in the reference ice were less pronounced in the scale tracing. The most noticeable difference between the two tests was the scale test, ice formed significantly farther aft than for the reference test on both the upper and lower surfaces. A review of the photographs of the ice accreted for the reference test for figure B-5c shows that upper-surface ice on either side of the midspan included large features here and there aft of what is shown in the midspan tracing. Similarly, some small ice roughness appears to be present on the lower surface farther aft of that shown in the tracings. This thin ice layer was probably not captured in the tracings for the reference tests because of the small template surface gap. It is not likely that the collection efficiency differences noted in figure B-1(b) had an effect on the ice appearance. All of these observations suggest that scale and reference test differences shown in figure B-5c are probably not significant.

Figure B-5d shows the results for the lowest freezing fraction tested, $n = 0.13$. The ice around the active portion of the boot was fairly thin, with agreement between the scale and reference ice thickness. The largest ice features were seen beyond the active boot. In this region, ice had several boot cycles to accumulate. The scale tests again appeared to result in somewhat smoother ice over much of the active boot.

Figure B-6a shows the results with rime ice conditions at 4° AOA. Because of the very low accumulation parameter, only a small accretion was obtained for either the scale or reference test. Good agreement in ice thickness and the upper-surface accretion limit appears to have been achieved. Any extended lower-surface ice in the reference tests may have been too thin to be recorded due to the small gap between the model surface and the cardboard template.

Figure B-6b shows icing characteristics like those seen previously in the 0° AOA results. The scale tests correctly simulated both the thickness of the ice around the leading edge and the size of randomly located protuberances. Both models had feathers on the lower surface growing at or near the end of the active portion of the boot as well as at the joint at which the inactive boot met the model surface. The ice for the half-scale NACA 23012 test extended aft of the boot and well beyond the chordwise icing limit suggested by the full-scale, collection efficiency curve of figure B-1(b). The lower-surface ice is probably runback resulting from the low freezing fraction ($n = 0.23$) for this test. Photographs (not included) suggest that ice aft of the boot may have also been present in the reference tests, although it was not recorded in the tracings for run 7/3.

The greatest differences between scale and reference tests were shown in figure B-6c. Note again that the ice for the reference test, run 8/3, was traced at 1 inch to the right of midspan.

However, the photographs of the ice for this run show little variation along the span, particularly at and near the leading edge. Furthermore, tracings taken at 1 inch to the right and 2 inches to the left of midspan show good agreement (see figure B-3c.) Therefore, this tracing is probably a good representation of the midspan profile. The test conditions for the reference and scale runs given in figure B-6c were respectively the same as figure B-5c, but for figure B-6c, the models were at an AOA of 4° instead of 0° for figure B-5c. The thickness of the reference ice at the leading edge was consistent for the two figures. In figure B-6c, however, although the scale test did simulate the size of the upper-surface feather aft of the main ice shape, the thickness of the scale ice over much of the surface was significantly less than the reference test. The freezing fraction for these tests was again 0.23, but of greater significance was the relatively high total temperature, 28°F. Previous studies [B-7 and [B-8] have raised concerns about the repeatability of icing tests at such high temperatures. Because the ice shape is very sensitive to temperature at conditions near freezing, small variations in temperature from run to run can produce large differences in ice shape. If the scale test was performed at a slightly higher temperature than the reference test, the scale freezing fraction would have been lower and less water would have frozen near the leading edge. This scenario is consistent with the ice shapes shown in figure B-6c.

The comparison in figure B-6d shows characteristics similar to those of previous figures. The reference and scale test conditions for the results given in this figure were the same as figure B-5d, but the models were at an AOA of 4° for figure B-6d and 0° for figure B-5d. The freezing fraction for these tests was 0.13, and extensive runback ice was apparent in the scale profile. The scale ice simulated the ice thickness over much of the boot surface, but appeared to be smoother than the reference ice.

## B.5 SUMMARY AND CONCLUSIONS.

The Ruff method with matched scale and reference velocity was used to determine appropriate half scale test conditions to simulate a full-size icing encounter for a NACA 23012 wing section protected with a pneumatic boot. Intercycle ice accretions were recorded on a 36-inch chord 23012 representing a half-scale model and compared with a hybrid model (full size, leading edge, and truncated aft section) representing a 72-inch chord airfoil.

The scaling tests generally simulated the ice thickness of the reference tests near the leading edge. In addition, the maximum feather size, although not the location of feathers, was simulated well. Feather location depended on the location of such features of the model as the interface between active boot tubes, junctions between the boot surface and model skin, and imperfections in the model surface. Because these physical features were not scaled, the feather locations could not be accurately predicted by the scale tests. In many cases, the approximate accretion limits were also simulated when runback was not present.

The effect of any residual ice left after boot activation is not clear from these tests. It is possible that the smoother scale shapes, especially for short intercycle times, was due to differences in the residual ice left after boot activation. Because of the possible importance of residual ice on the subsequent accretion of intercycle ice, rigorous scaling would require that the shedding process be scaled as well as the ice accretion. This study did not take this rigorous approach, and the same pneumatic boot operating characteristics were used for both the hybrid and the half-size

model. It is not presently known how such design features as pneumatic boot tube size and inflation time relate to ice shedding characteristics for different size models. A more extensive study is needed regarding whether or not pneumatic boot design might need to be tailored to model size for more accurate scaling.

Within the limitations of the test, the scaling applied was sufficiently successful to draw a preliminary conclusion that either the Ruff method with constant velocity applied to a half-scale model or the hybrid method can be used to scale intercycle icing tests. Further tests comparing the results of both models to a 72-inch chord, full-size NACA 23012 airfoil would be helpful to better assess intercycle ice scaling.

B.6 REFERENCES.


B-1. Anderson, David N. and Ruff, G.A., "Evaluation of Methods to Select Scale Velocities in Icing Scaling Tests," AIAA-99-0244, January 1999.

B-2. Langmuir, Irving and Blodgett, Katharine B., "A Mathematical Investigation of Water Droplet Trajectories," Army Air Forces Technical Report No. 5418, February 1946.

B-3. Sibley, E.J. and Smith, R.E., "Model Testing in an Icing Wind Tunnel," Lockheed Aircraft Corporation, California Division, Report LR10981, October 1955.

B-4. Messinger, B.L., "Equilibrium Temperature of an Unheated Icing Surface as a Function of Airspeed," *J. Aeron. Sci*. Vol. 20 No. 1, January 1953, pp. 29-42.

B-5. Tribus, Myron, Young, G.B.W., and Boelter, L.M.K., "Analysis of Heat Transfer Over a Small Cylinder in Icing Conditions on Mount Washington," *Trans. ASME* Vol. 70, November 1948, pp. 971-976.

B-6. Ruff, G.A., "Analysis and Verification of the Icing Scaling Equations," AEDC-TR-85-30, Vol. 1 (Rev), March 1986.

B-7. Anderson, David N. and Ruff, Gary A., "Evaluation of Methods to Select Scale Velocity in Icing Scaling Tests," AIAA-99-0244, January 1999.

B-8. Anderson, David N., "Effect of Velocity in Icing Scaling Tests," AIAA-2000-0236, January 2000.

B-9. Saeed, Farooq, Selig, Michael S., and Bragg, Michael B., "Hybrid Airfoil Design Method to Simulate Full-Scale Ice Accretion Throughout a Given $\alpha$ Range," *J. Aircraft*, Vol. 35, No. 2, March-April 1998.

B-10. Saeed, Farooq, Selig, Michael S., and Bragg, Michael B., "Experimental Validation of the Hybrid Airfoil Design Procedure for Full-Scale Ice Accretion Simulation," AIAA-98-0199, January 1998.